รายงานสุดท้ายโครงการ

(รายงานในช่วงตั้งแต่วันที่ 1 ธ.ค. 2555 ถึงวันที่ 31 พ.ค. 2556)

โครงการ การประยุกต์ใช้หลักความสมมูล AdS/CFT จากทฤษฎีสตริง (String Theory)

ปิยบุตร บุรีคำ จุฬาลงกรณ์มหาวิทยาลัย

สนับสนุนโดยสำนักงานคณะกรรมการการอุดมศึกษา และสำนักงานกองทุนสนับสนุนการวิจัย และคณะวิทยาศาสตร์ จุฬาลงกรณ์มหาวิทยาลัย

(งานวิจัยยังไม่เสร็จสมบูรณ์ โปรดอย่านำไปใช้อ้างอิง)

1. สำหรับหัวหน้าโครงการวิจัยผู้รับทุน รายงานความก้าวหน้าประกอบด้วย

1.1 การดำเนินงาน

ดำเนินการไปได้เรียบร้อยโดยปัจจุบันกำลังดำเนินการต่อยอดงานวิจัยต่อไปในทิศทางของ glueball physics และ deconfinement และความเป็นไปได้ของควาร์กกลูออนพลาสม่าที่มีความจุความร้อนเป็นลบ เรายังพบว่าก๊าซของเฟอร์มิออนในสองมิติก็สามารถมีความจุความร้อนเป็นลบได้เช่นเดียวกัน นอกจากนี้ยังกำลังทำการคำนวณ effective action ในแบบจำลอง nonlocal Nambu-Jona-Lasinio model ที่มาจาก Sakai-Sugimoto model อีกด้วย งาน nonlocal NJL ส่วนหนึ่งสำเร็จเป็นผลงานเขียนเป็นบทความส่งตีพิมพ์แล้ว ส่วนงานการศึกษาควาร์กกลูออนพลาสม่าที่ความจุความร้อนเป็นลบกำลังดำเนินการ เรายังขยายการศึกษา nonlocal NJL model ไปสู่กรณีที่ความหนาแน่นและอุณหภูมิมีค่ามากด้วย เพื่อใช้ศึกษาแผนภาพเฟส

.....

1.2 รายละเอียดผลการดำเนินงานของโครงการ

สรุปย่อ (summary) ประกอบด้วยวัตถุประสงค์และการดำเนินงานวิจัย รวมทั้งผลงานวิจัยที่ได้รับ

<u>วัตถุประสงค์ของโครงการ</u>

1.) ประยุกต์ใช้ความสมมูล AdS/CFT ในการศึกษาสมบัติของควาร์ก-กลูออน พลาสม่าที่อุณหภูมิสูงกว่า 175 MeV ซึ่งเป็นอุณหภูมิการเปลี่ยนสถานะจากสภาพที่ควาร์กและกลูออนถูกกักขังในฮาดรอนไปสู่สถานะที่มันกลายเป็นพลาสม่าร้อนที่ควาร์กและกลูออนเป็นอิสระ ศึกษาปริมาณ transport coefficients ในพลาสม่านี้โดยใช้ dual string theory ในอวกาศโค้งชนิดต่าง ๆ

2.) ศึกษาสมบัติของสสารนิวเคลียร์ที่สภาวะสุดโต่งอื่น ๆ เช่น เมื่อความหนาแน่นสูงมาก ๆ เช่น ภายในดาวนิวตรอนโดยใช้สมมูล AdS/CFT

3.) ศึกษาสมบัติของทฤษฎีเกจและทฤษฎีความโน้มถ่วงจากมุมมองของความสมมูล AdS/CFT ศึกษาอันตรกิริยาใหม่ ๆที่อาจจะมีได้จากสมมูลของอันตรกิริยาของสตริงแบบเปิดและแบบปิด (open-closed string duality) [8]

4.) ศึกษาสมบัติของโพเมอรอน (pomeron) [9,12]ในอันตรกิริยาแบบเข้มโดยใช้มุมมองของทฤษฎีสตริงเปรียบเทียบผลกับผลที่ได้จากทฤษฎี S-matrix [13]และที่ได้จากการคำนวณใน Quantum Chromodynamics (QCD)

5.) ศึกษา quasi-normal modes ของหลุมดำและประยุกต์ใช้สมมูลAdS/CFT เพื่อทำนายพฤติกรรมของสสารนิวเคลียร์ในควาร์กกลูออนพลาสม่าจากข้อมูลของ quasi-normal modes ที่มี

6.) ศึกษาการประยุกต์ใช้สมมูล AdS/CFT ใน condensed matter physics

<u>การดำเนินการวิจัย</u> **ในที่ผ่านมาได้**

1. **พิจารณามัลติควาร์กในแบบจำลอง Sakai-Sugimoto ที่สมมูลกับมัลติควาร์กและฮาดรอน (hadronic bound state) ในทฤษฎีแบบเกจ ศึกษาสมบัติของมันใน deconfined phase ของควาร์กกลูออนพลาสม่า ศึกษา magnetic and electric responses ผ่านทาง Dirac-Born-Infeld action ที่เป็น nonlinear generalization ของทฤษฎีที่บรรยาย gauge theory ภายใต้อิทธิพลของสนามแม่เหล็กไฟฟ้า**
2. **วาดแผนภาพสถานะของสสารนิวเคลียร์แบบมัลติควาร์กภายใต้สนามแม่เหล็กและอุณหภูมิสูง ๆ**

ภายใต้สภาวะความหนาแน่นต่าง ๆกัน

3.) ศึกษาสมบัติของสสารนิวเคลียร์แบบ pure pion gradient ซึ่งเกิดจาก response ต่อสนามแม่เหล็กภายนอกของ chiral condensate

4.) ศึกษาดาวภายใต้สนามแม่เหล็กสูง ๆใน AdS space 5 มิติที่อุณหภูมิค่าใด ๆ เป็นงานวิทยาพนธ์ปริญญาโทของผู้ช่วยวิจัย Tossaporn Chullaphan ค่า mass limit ของดาวเช่นนี้จะมี dual object เป็นสสารนิวเคลียร์อุณหภูมิสูงภายใต้อิทธิพลของสนามแม่เหล็กซึ่งน่าจะเป็นรูปแบบของสสารภายในแก่นของดาวนิวตรอนสนามแม่เหล็กสูงที่เรียกว่า magnetar

5.) ศึกษาความเป็นไปได้ของสถานะควาร์กกลูออนพลาสม่าที่มีความร้อนจำเพาะเป็นลบ และความสัมพันธ์กับความหนาแน่นของ glueball ในควาร์กกลูออนพลาสม่านั้น ๆ

6.) คำนวณ effective action ใน nonlocal Nambu-Jona-Lasinio model ที่มาจาก Sakai-Sugimoto model ทั้งในระดับหนึ่งและสองลูปอีกด้วย เราพบว่า chiral symmetry breaking ยังคงเกิดขึ้นแม้เมื่อ 't Hooft coupling มีค่าน้อย ๆมาก ๆ

2. ผลงานวิจัยที่ทำในหกเดือนที่ผ่านมา ประกอบด้วย

ศึกษาเพิ่มเติมความเป็นไปได้ของควาร์กลูออนพลาสม่าที่มีมีความร้อนจำเพาะเป็นลบสำหรับอิเลคตรอนหรือนิวตรอนในสองมิติเราพบเช่นกันว่าสามารถมีสถานะที่มีความจุความร้อนเป็นลบได้ด้วย ในกรณีที่ความหนาแน่นพลังงานของก๊าซมีค่าไม่มากนัก ณ จุดเปลี่ยนสถานะเป็นก๊าซ แต่ยังต้องพิจารณาความหมายทางกายภาพของผลที่ได้ต่อไปว่าในสองมิตินั้นเป็นการเปลี่ยนสถานะของอะไรไปสู่ก๊าซของอิเลคตรอน

ศึกษาการประยุกต์ใช้หลักการ holographic duality กับระบบ condensed matter ศึกษาหลุมดำใน 1+3 มิติที่ coupled กับสนาม scalar ที่มีโครงสร้างเป็นโครงผลึก งานแบบนี้มีคนใช้ในการศึกษา high temperature superconductivity cuprates และพบกฎ power law scaling ของ optical conductivity ที่ตรงกับการทดลอง

คำนวณ effective action ใน nonlocal Nambu-Jona-Lasinio model ที่มาจาก Sakai-Sugimoto model ที่ระดับหนึ่งและสองลูป กำลังขยายผลไปสู่กรณีความหนาแน่นและอุณหภูมิสูง ๆ

3. ผลงานวิจัยที่ตีพิมพ์ในวารสารวิชาการระดับนานาชาติ (หากยังไม่มี ให้ระบุชื่อเรื่องและชื่อวารสารนานาชาติที่คาดจะตีพิมพ์ได้ และจะตีพิมพ์ได้เมื่อใด)

มีผลงานเป็นบทความหนึ่งฉบับ กำลังส่งพิจารณาเพื่อตีพิมพ์ในวารสารนานาชาติต่อไป ได้แก่

Chiral symmetry breaking from two-loop effective potential of the holographic non-local NJL model, Piyabut Burikham, Daris Samart, Suppiya Siranan, [arXiv:1302.4994].

อนึ่ง ในรายงานสุดท้ายของโครงการฉบับนี้ได้แนบผลงานทั้งหมด 5 บทความมาด้วย 4 บทความได้รับการตีพิมพ์เรียบร้อยแล้วใน Journal of High Energy Physics 3 บทความ ใน Advances in High Energy Physics 1 บทความ เป็น invited review article

4. กิจกรรมอื่น ๆที่เกี่ยวข้อง ได้แก่

(1) มีการพูดคุยกับนักวิจัยที่มหาวิทยาลัยเทคโนโลยี่สุรนารีและมหาวิทยาลัยราชมงคลอีสาน

เกี่ยวกับความเป็นไปได้ในการขยายผลไปบรรยาย scattering ของอนุภาคนิวเคลียร์ที่พลังงานประมาณ 1-10 GeV เป็นไปได้หรือไม่ที่จะตรวจจับควาร์กกลูออนพลาสม่าที่มีความจุความร้อนเป็นลบที่ heavy ion collision experiment อย่างเช่น LHC ของ CERN และในเรื่องการศึกษาแผนภาพสถานะของสสารนิวเคลียร์โดยใช้ nonlocal NJL model

(2) ไปเสนอผลงานและอภิปรายแลกเปลี่ยนกับนักฟิสิกส์จากญี่ปุ่นในสาขาเอกภพวิทยาในงาน TJ2012: Japan-Thai Workshop in Cosmology รายละเอียดดังเวบไซต์ http://www.if.nu.ac.th/act/tj2012 จึงเบิกค่าใช้จ่ายในการเดินทางจากทุนด้วย

(3) ได้รับเชิญไปเสนอผลงานที่ SPC2013 โรงแรมเชียงใหม่แกรนด์วิว จังหวัดเชียงใหม่ รายละเอียดดังเวบไซต์ http://www.physics.science.cmu.ac.th/physics/index.php/news/news/130-spc2013 จึงเบิกค่าใช้จ่ายในการเดินทางส่วนหนึ่งจากทุนด้วย

5. ปัญหาและอุปสรรค (ถ้ามี)

-ความล่าช้าจากระเบียบการเบิกจ่ายของคณะวิทยาศาสตร์และของ จุฬาลงกรณ์มหาวิทยาลัย จะมีประโยชน์อะไรที่จะออกนอกระบบแต่ประสิทธิภาพการทำงานยังล่าช้าเหมือนอยู่ในระบบราชการ ระเบียบจุกจิกไร้ประโยชน์ที่ทำให้ล่าช้ายังมีอยู่เหมือนเดิมเป็นตัวการทำให้การดำเนินการล่าช้าและซับซ้อนยุ่งยากอย่างไร้เหตุอันควร

-หัวหน้าโครงการต้องสำรองจ่ายเงินเดือนผู้ช่วยวิจัยไปก่อนเพราะเงินในบัญชีทุนวิจัยมีไม่พอ ทั้งนี้มาจากระบบการจ่ายเงินที่ล่าช้าของระบบราชการ นอกจากนี้ยังค้างเงินเดือนผู้ช่วยวิจัยอีกหลายเดือนเพราะหัวหน้าโครงการเองก็มีเงินไม่พอสำรองจ่ายได้หมด

6. ความเห็นและข้อเสนอแนะ

การเขียนส่งรายงานวิจัยต่อสกว. นี้หากลดจำนวนครั้งให้เหลือรายปีจะดีกว่าเป็นอย่างมากเพราะเอกสารรายงานเหล่านี้ไม่สำคัญเท่าการทำวิจัยและผลงานวิจัยที่ได้ตีพิมพ์ไปแล้ว การทำเอกสารมากเกินไปยังทำลายทรัพยากรต้นไม้โดยไม่จำเป็นซึ่งนำไปสู่ภาวะโลกร้อนอันเป็นวิกฤตระดับโลกที่สำแดงผลมาครั้งแล้วครั้งเล่าในไม่กี่ปีที่ผ่านมาและหากเราไม่เริ่มปรับเปลี่ยนวิธีการทำงานและการใช้ชีวิตของเราตั้งแต่ตอนนี้ เราก็อาจต้องประสบภัยที่หนักหนาสาหัสเพิ่มขึ้น ๆเรื่อย ๆ

ได้รับทราบจากเพื่อนร่วมวงการฟิสิกส์ทฤษฎีว่าหลาย ๆคนที่มีผลงานโดดเด่น (ตีพิมพ์ในวารสารที่มี IF 5-7 ต่อเนื่องหลายเปเปอร์) ไม่ได้รับทุนสกว. ทั้งแบบต่อเนื่องในรุ่นกลาง รุ่นใหญ่และรุ่นใหม่รวมถึงตัวของหัวหน้าโครงการนี้เองที่แม้จะได้รับรางวัลผลงานดีเด่น TRF-CHE Researcher Award แต่กลับไม่ได้รับทุนสกว. ต่อเนื่องต่อไป ชีวิตของนักทฤษฎีฟิสิกส์ที่ลำบากอยู่แล้วก็ยิ่งลำบากขึ้นไปอีก ผมจึงขอเสนอความคิดเห็นว่าหากนี่เป็นนโยบายของสกว.สกอ. ที่จะตัดทุนสนับสนุนงานวิจัยทางฟิสิกส์ทฤษฎีที่ไม่มีประโยชน์ในการนำไปประยุกต์ใช้เชิงอุตสาหกรรมแล้ว เป็นนโยบายที่ผิดมหันต์ครับ ผมทราบดีว่าสกว. มีนโยบายเพิ่มทุนไปทางวิจัยเพื่อการเกษตรและอุตสาหกรรมซึ่งเป็นนโยบายที่ถูกต้องอย่างยิ่ง แต่การเพิ่มทุนที่ควรให้แต่ไปตัดทุนที่มีอยู่แล้วโดยเฉพาะทุนวิจัยด้านพื้นฐานคือสิ่งผิด เป็นวิสัยทัศน์ที่ผิดแสดงถึงความไม่เข้าใจในธรรมชาติของวิทยาศาสตร์และการวิจัยโดยแท้จริง การจะรีบต่อยอดโดยไปลดพื้นฐานคือนโยบายที่ผิด

สิ่งที่สกว. ควรทำและต้องรีบดำเนินการคือการเพิ่มทุนวิจัยในทุกด้าน หากจะเพิ่มทุนทางอุตสาหกรรมและเทคโนโลยี่ก็ต้องเพิ่มทุนวิจัยพื้นฐานให้มากขึ้นไปด้วย อย่างน้อยจำนวนนักวิจัย

พื้นฐานจะต้องมีไม่น้อยกว่านักวิจัยทางด้านประยุกต์ นักวิจัยนักวิชาการทางวิทยาศาสตร์บริสุทธิ์และทางพื้นฐานเป็นรากฐานของนักวิจัยในระดับประยุกต์และระดับสูงขึ้นไป หากเราไม่มีพื้นฐานและรากฐานที่แข็งแรง มั่นคงและแน่นหนาแล้ว การวิจัยเพื่อประยุกต์ใช้ใด ๆย่อมทำไม่ได้ผลดี การจะวิจัยนำองค์ความรู้ใดไปใช้ประโยชน์ในทางเทคโนโลยี่ ไปประยุกต์ในด้านต่าง ๆได้เราต้องมีความรู้ความเข้าใจในองค์ความรู้พื้นฐานแต่ละด้านเป็นอย่างดีเสียก่อนเท่านั้น หากไม่มีความรู้ทางฟิสิกส์พื้นฐานของสสารดีพอ ไม่มีความรู้ทางคณิตศาสตร์ชั้นสูงดีพอ ไม่มีความรู้ทางการคำนวณโดยใช้คอมพิวเตอร์ดีพอ ย่อมไม่สามารถนำความรู้พื้นฐานเหล่านี้ไปประยุกต์ใช้อะไรได้ ตัวอย่างที่เห็นชัดที่สุดคือการออกแบบโครงสร้างหรือเครื่องยนต์ใด ๆหรือแม้กระทั่งวงจรอิเลกทรอนิกส์ต่าง ๆในปัจจุบันต้องใช้คอมพิวเตอร์และการสร้างแบบจำลองทางคณิตศาสตร์ของระบบนั้น ๆ สมบัติพื้นฐานต่าง ๆของวัสดุทั้งทางเคมีและฟิสิกส์ต้องเป็นที่เข้าใจเป็นอย่างดีและป้อนเข้าในแบบจำลองอย่างถูกต้อง คณิตศาสตร์ที่ใช้คำนวณในแบบจำลองก็เป็นคณิตศาสตร์ชั้นสูงที่พบเจอกันในงานวิจัยฟิสิกส์และคณิตศาสตร์พื้นฐานทั้งสิ้น กว่าจะมาถึงขั้นวิจัยเพื่อประยุกต์ใช้ในระดับเหล่านี้ องค์ความรู้พื้นฐานเหล่านี้ย่อมต้องถูกวิจัยศึกษาโดนนักฟิสิกส์ทฤษฎีและนักคณิตศาสตร์มาก่อน โจทย์ปัญหาที่นักวิจัยด้านประยุกต์พบเจอก็สามารถนำมาปรึกษาหาคำตอบที่เหมาะกับกับนักวิจัยพื้นฐานทางฟิสิกส์ เคมีและคณิตศาสตร์ได้

อีกตัวอย่างหนึ่งคือการใช้โปรแกรม molecular dynamics ออกแบบยาในปัจจุบัน ตัวโปรแกรมถูกเขียนขึ้นจากความรู้ทางกลศาสตร์ควอนตัม ทางเทอร์โมไดนามิกส์พื้นฐานของสารเคมีทางชีวภาพต่าง ๆซึ่งองค์ความรู้พื้นฐานเหล่านี้ต้องเป็นศึกษาจนเข้าใจกันเป็นอย่างดี ไม่ว่าจะเรื่องกลศาสตร์ควอนตัมของพันธะทางเคมีต่าง ๆ พลังงาน free energy ของโครงสร้างเช่น โปรตีนในการ fold และ unfold ที่สำคัญที่สุดคือการศึกษาโครงสร้างโดยใช้ Xray diffraction analysis ซึ่งถูกค้นคว้าโดยนักฟิสิกส์พื้นฐานตั้งแต่ร้อยปีก่อนหน้า คนที่อ่านข้อมูลจาก Xray diffraction ของ DNA และสรุปว่าต้องเป็นโครงสร้างเกลียวคู่ก็เป็นนักฟิสิกส์พื้นฐานที่มีความรู้ความเข้าใจในหลักการและฟิสิกส์พื้นฐานของ Xray diffraction เป็นอย่างดีเยี่ยม (Francis Crick) ยังมีตัวอย่างอีกหลายหลากมากมายถึงความเชื่อมโยงโดยตรงของงานวิจัยพื้นฐานไปสู่งานวิจัยประยุกต์ ที่จริงแล้วงานวิจัยประยุกต์เกือบทุกอันล้วนวางอยู่บนพื้นฐานขององค์ความรู้พื้นฐานทั้งสิ้น บางอย่างใช้เวลาเป็นร้อยปี บางอย่างใช้เวลาชั่วข้ามคืนในการแปรองค์ความรู้ไปสู่การประยุกต์ใช้ เครื่องสแกนช่วยวินิจฉัยโรค เครื่อง Xray ต่าง ๆในโรงพยาบาลเป็นหลักฐานโดดเด่นชัดเจนว่าแม้กระทั่งงานวิจัยพื้นฐานทางฟิสิกส์อนุภาคและนิวเคลียร์ก็นำไปประยุกต์ใช้ประโยชน์ได้อเนกอนันต์ เราเพียงไม่รู้เท่านั้นเองว่าจะประยุกต์ใช้อะไรกับอะไรในเมื่อเรายังไม่ศึกษาค้นคว้าจนรู้ว่าความรู้พื้นฐานนั้น ๆคืออะไรกันแน่ โลกแห่งการสื่อสารด้วยคลื่นแม่เหล็กไฟฟ้าคงไม่เป็นอย่างในปัจจุบัน โลกไซเบอร์แห่งอินเตอร์เนทคงไม่มีในปัจจุบัน หากไม่มีงานวิจัยพื้นฐานทางฟิสิกส์และคณิตศาสตร์โดยแมกซ์เวลล์ หากเราไม่มี CERN และนักฟิสิกส์อนุภาคที่เขียนโปรแกรมสคริปต์และวางโครงสร้างพื้นฐานของ world wide web และไม่มีนักฟิสิกส์ทฤษฎีที่คำนวณการใช้สายใย fibre optic ส่งผ่านข้อมูลด้วยแสง

ผมขอให้ทางสกว. สกอ. และผู้ที่เกี่ยวข้องพิจารณาปรับแก้นโยบายใด ๆที่เข้าใจผิดว่าการตัดงบวิจัยพื้นฐานไปโปะให้งานวิจัยประยุกต์เป็นสิ่งถูก การสนับสนุนการวิจัยต้องทำตั้งแต่ฐานไปสู่ยอด ส่วนที่เป็นฐานในปัจจุบันจะขึ้นหิ้งแค่ไหนก็ต้องทำ เพราะนั่นคือธรรมชาติขององค์ความรู้และการวิจัย ทัศนคติที่ว่า “วิจัยไปใช้ประโยชน์อะไร?” เป็นทัศนคติที่ผิดธรรมชาติของงานวิจัย เพราะเราต้องศึกษาค้นคว้าให้รู้ก่อนว่าองค์ความรู้นั้นคืออะไร ก่อนที่จะสามารถตั้งคำถามได้ว่ามันจะเอาไปประยุกต์ใช้อะไรได้

7. งานที่จะทำในปีต่อไป

-ศึกษาสมบัติเชิง hydrodynamics ของมัลติควาร์กโดยพยายามสรุปผลและส่งตีพิมพ์ผลงานทุก ๆหก เดือน

-ศึกษา Nambu-JonaLasinio model จากทฤษฎีสตริงและความเป็นไปได้ที่จะต่อยอดต่อไป

-ศึกษาสถานะความร้อนจำเพาะเป็นลบของควาร์กกลูออนพลาสม่าและความสัมพันธ์กับความหนาแน่น Glueball

8. รายละเอียดผู้ช่วยวิจัย

ค่าตอบแทนผู้ช่วยวิจัยจะให้ 5,000 บาทต่อคนต่อเดือน แต่ละเดือนจะให้ไม่เกินหนึ่งหมื่นบาท

- **นายทศพร จุลพันธ์ 36 เดือนเป็นเงิน 200,000 บาทโดยมี 4 เดือนที่รับเดือนละหนึ่งหมื่นบาท ยังจ่ายเงินเดือนไม่หมด**
- **นายฉัตรชัย พรหมสิริ 25 เดือนเป็นเงิน 125,000 บาทยังจ่ายเงินเดือนไม่หมด**
- **นายสมเกียรติ สุนทรสวัสดิ์ 2 เดือนเป็นเงิน 10,000 บาท จ่ายเงินเดือนหมดแล้ว**

เงินเดือนดังกล่าวบางส่วนจ่ายโดยทุนวิจัยบางส่วนหัวหน้าโครงการสำรองจ่ายไปก่อน และบางส่วนยังไม่ได้จ่ายให้ผู้ช่วยวิจัยเพราะเงินในบัญชีทุนไม่พอ

Prepared for submission to JHEP

Chiral symmetry breaking from two-loop effective potential of the holographic non-local NJL model

Piyabut Burikham,[a,c] **Daris Samart**[b,c] **and Suppiya Siranan**[b]

[a] *Department of Physics, Faculty of Science, Chulalongkorn University, Phyathai Road, Bangkok 10330, Thailand*

[b] *Department of Applied Physics, Faculty of Sciences and Liberal arts, Rajamangala University of Technology Isan, Nakhon Ratchasima, 30000, Thailand*

[c] *Thailand Center of Excellence in Physics (ThEP), Commission on Higher Education, Bangkok 10400, Thailand*

E-mail: piyabut@gmail.com, daris.sa@rmuti.ac.th, suppiya.si@rmuti.ac.th

Abstract: We calculate the two-loop effective potential of the non-local NJL model derived from the Sakai-Sugimoto model in string theory. In contrast to conventional NJL with 4-fermion contact interaction, the chiral symmetry was previously found to be dynamically broken for arbitrary weak coupling at the one-loop level. We calculate the one and two-loop contribution to the effective potential of the non-local NJL model and found that the two-loop contribution is negative. The two-loop potential for the chirally symmetric vacuum is also negative but larger than the combined effective potential of the chirally broken vacuum at the two-loop level. The chiral symmetry breaking thus persists for arbitrary weak coupling.

Keywords: non-local NJL model, Sakai-Sugimoto model, chiral symmetry breaking

Contents

1 Introduction

Spontaneous Symmetry breaking (SSB) plays an important role in modern particle physics theory. Higgs mechanism in the standard model, for example, can be used to generate masses of elementary particles, leptons and quarks. The generation of quark masses by spontaneous symmetry breaking inevitably breaks the chiral symmetry of the QCD. Chiral symmetry breaking (χSB) could also be generated *dynamically* by the vacuum expectation value (vev) of chiral condensate $\psi(x)\overline{\psi}(y)$. Dynamical χSB can explain masses of mesons and hadrons which are responsible for most of the visible mass in the universe. It can also explain hadronic particle generation in strong interaction at low energies. The key idea of SSB is that any theory whose Lagrangian is invariant under some associated symmetry where vacuum state of such theory is not invariant and hence its vacuum carries non-trivial quantum number associated with the symmetry. In the spontaneous broken phase, there is an existence of Nambu-Goldstone (NG)-boson [1]. One can classify NG-boson into 2 cases i.e. on one hand, NG-boson is massless elementary particle and on the other hand, such boson could be a composite particle. Dynamical symmetry breaking (DSB) usually

occurs as a result of the interaction between constituent particles in the theory and yields a composite NG boson.

For chiral symmetry breaking of the QCD, the NG boson is usually identified with e.g. the three pions from the breaking of $SU(2)_L \times SU(2)_R$ to $SU(2)_V$ or the eight light mesons from the breaking of $SU(3)_L \times SU(3)_R$ to $SU(3)_V$ flavour diagonal. This symmetry breaking pattern [2] was successfully used to explore properties of the light hadrons and gives precise predictions of light hadronic spectra [3]. Early stage of χSB in the strong interaction was demonstrated by the linear-sigma model [4] and the current-algebra approach [5, 6]. At the present, there is an incorporation between χSB and principle of effective field theory which gives a systematic framework to study QCD at low-energies, the so-called chiral perturbation theory [7]. The theory starts with an effective theory of hadrons with chiral symmetry in the action and use the SSB to generate a chiral symmetry breaking vacuum. The observed meson spectra shows good agreement with the prediction of the chiral perturbation theory [8, 9].

To address the chiral symmetry breaking/restoration phase transition, ones need to work with the action of quarks instead of hadrons. Nambu-Jona-Lasinio (NJL) model [10] is a model of quarks with four-fermion interaction which is employed to demonstrate the dynamical chiral symmetry breaking in the strong interaction independent of the confinement. Originally, NJL was formulated to explain mass of the nucleon as a consequence of the χSB. NJL model has been widely used as a description of low-energy effective model of hadrons in QCD with zero or finite-temperature [11–14] and electroweak symmetry breaking by top-quark condensation or other fermions within or beyond the standard model [15–17]. NJL model is a very successful effective model to describe many hadronic properties in low-energy QCD, for example, the mesons and baryons mass spectra, the pion decay constant, and the pion form factor (see [11–13] for review).

Despite the success of the NJL as a low-energy phenomenological model approach to low-energy QCD, the original NJL model does not address confinement. There are extensions of the NJL where inclusions of non-local interactions have been proposed in the literature (see [18] and references therein). One can simply reproduce the non-local NJL interaction from the QCD Lagrangian by integrating out the gluon field from the one-gluon exchanging diagram [15, 18].

In the non-local NJL approach, interaction depends on the momenta carried by the quarks leading to a momentum-dependent quark mass, generated by the spontaneous χSB. It has been shown that a non-local NJL model could lead to quark confinement with acceptable values of the parameters [19]. This phenomenon originates from the fact the quark propagator has no real poles and consequently quarks have no asymptotic states. There are several other advantages of the non-local NJL approach over the original (local) NJL model i.e. the nonlocality regularizes the model in a manner that anomalies [20] and gauge invariance [21] are preserved and the momentum-dependent regulator makes the theory finite to all orders in the $1/N_c$ expansion. Finally the dynamical quark mass is momentum dependent in contrast to the original NJL model and consistent with lattice simulations of QCD [22]. As a result, one can see that the non-local NJL model may have more predictive power and be more realistic. There are two major applications of

the non-local NJL model in the strong interaction. Firstly, it is incorporated in the quark model to give mass spectra of excited mesons in good agreement with the experimental data [23]. Secondly, the thermodynamics of nuclear matter and QCD phase diagram could be explained quantitatively well by using non-local NJL model (with Polyakov-loop) [24].

A non-local NJL model can also be constructed from certain intersecting-branes configurations in string theory. The Sakai-Sugimoto model (SS) [25, 26] is a D8-$\overline{\text{D8}}$-D4 intersecting-branes model in type IIA string theory. The background spacetime is generated from a stack of N_c D4-branes. An x^4 coordinate is compactified into a circle with radius R and the D4-branes wrap around the x^4. On the boundary of the 10-dimensional space, a stack of N_f D8 and $\overline{\text{D8}}$ are located at $x^4 = -L/2$ and $L/2$ respectively. The left (right)-handed quarks live on the D8 ($\overline{\text{D8}}$)-D4 intersection in the form of open-string excitations. They are thus separated by distance L on the boundary and there is a $U(N_f)_L \times U(N_f)_R$ chiral symmetry. Geometrically, when the D8 and $\overline{\text{D8}}$ merge at certain radial coordinate, the chiral symmetry breaking $U(N_f)_L \times U(N_f)_R \to U(N_f)_V$ occurs.

We will not be considering the SS model in its full details in the present work but would rather focus on the low-energy effective 5-dimensional field theory limit of the model. In contrast to the strong coupling regime where the supergravity picture of intersecting branes provide simple geometrical interpretation of the theory, the weak coupling limit has its own unique picture of chiral symmetry breaking in terms of non-local NJL model in 5 dimensions.

In such intersecting branes setting there are two crucial parameters i.e. the 5-dimensional 't Hooft coupling, λ and the length scale of separation between D8-$\overline{\text{D8}}$ flavor branes, L. One can consider the hierarchy of those parameter as $\lambda \ll L$ which is the weak coupling regime. In such limit, we can treat left- and right-handed quarks as weakly interacting by single (five dimensional) gluon exchange process. The non-local NJL interaction is reproduced by integrating out gluon fields in bulk spacetime from such D-branes configuration. In terms of effective potential in holographic non-local NJL, the nonzero solution of chiral quark condensate exists at arbitrary weak coupling [27, 28]. In contrast, if one considers the SS model in compactified case i.e. R is finite, and includes the KK tower of states. The χSB will happen only above a certain value of 't Hooft coupling [29]. In any cases, the analysis has been done on the effective potential of the non-local NJL at the one-loop level. It is interesting to investigate whether the two-loop contribution would change the profile of the effective potential in any significant way.

We will start by reviewing the method of effective action in 5 dimensions when gauge fields propagate in 5 dimensions and fermions are localized in 4 dimensional subspace. By integrating out heavy gauge fields, we will obtain the effective fermionic action of the SS NJL model. Subsequently, by using auxiliary field approach, we integrate out the residual fermionic fields to obtain the effective scalar action of the SS NJL model. One-loop and two-loop contributions of the action are then calculated and discussed. Chiral symmetry breaking is demonstrated at both one and two-loop levels.

2 The effective Lagrangian

We start with the effective action of the single-intersection model where left-handed quarks are located at a single intersection of N_c D4 and N_f D8 branes [27],

$$\mathscr{S} = \int d^5\, x \left\{ -\frac{1}{4\, g_5^2}\, F_{MN}\, F^{MN} + \delta\,(x^4)\, q_L^\dagger\, \bar{\sigma}^\mu\, (i\,\partial_\mu + A_\mu)\, q_L \right\}, \tag{2.1}$$

where $M, N, \cdots = 0, 1, 2, 3, 4$ and $\mu\ \nu\,, \cdots = 0, 1, 2, 3$. Integrating by part and fix the gauge, the action can be rewritten in the following form,

$$\mathscr{S} = \frac{1}{g_5^2} \int d^5\, x \left\{ \frac{1}{2}\, A_M \,\Box\, A^M + \delta\,(x^4)\, J^M\, A_M \right\} + \int d^4x\, q_L^\dagger\, \bar{\sigma}^\mu\, i\,\partial_\mu\, q_L, \tag{2.2}$$

where we have defined $J^\mu = g_5^2\, q_L^\dagger\, \bar{\sigma}^\mu\, q_L$ and set $J^{(4)} = 0$.

The gauge fields live in 5 dimensions and it is natural to integrate them out to obtain 4-dimensional effective action of the fermions. For consideration of the chiral symmetry breaking, we can bosonize the fermion bilinear and integrate out the fermions subsequently. In order to integrate out the heavy-gauge field A_M. We recall the procedure from [30], start with

$$e^{i\int d^4x\, \mathscr{L}_{\text{eff}}} = \int [d\, H]\, e^{i\ \int d^4x\, \mathscr{L}\left(H(x), l(x)\right)} \Big/ \int [d\, H]\, e^{i\ \int d^4x\, \mathscr{L}\left(H(x), 0\right)}, \tag{2.3}$$

where $H(x)$ and $l(x)$ are heavy and light fields respectively. In our case, A_M is the heavy field and $q_{L,R}$ are the light fields. The actions with and without the light fields are given by

$$\begin{aligned} \int d^5\, x\, \mathscr{L}\left(A_M, q_L\right) &= \frac{1}{g_5^2} \int d^5\, x \left\{ \frac{1}{2}\, A_M \,\Box\, A^M + \delta\,(x^4)\, J^M\, A_M \right\} \\ &\quad + \int d^4x\, q_L^\dagger\, \bar{\sigma}^\mu\, i\,\partial_\mu\, q_L\,, \end{aligned} \tag{2.4}$$

$$\int d^5\, x\, \mathscr{L}\left(A_M, 0\right) = \frac{1}{g_5^2} \int d^5\, x\, \frac{1}{2}\, A_M \,\Box\, A^M\,. \tag{2.5}$$

By using functional path integral as demonstrated in appendix A, the effective action after integrating out the heavy gauge field can be read off from eq. (A.3),

$$\begin{aligned} \mathscr{S}_{\text{eff}} &= i \int d^4x\, q_L^\dagger\, \bar{\sigma}^\mu\, \partial_\mu\, q_L \\ &\quad - \frac{g_5^2}{16\,\pi^2} \int d^4x\ d^4y\, G(x-y\,,\,0) \left[q_L^\dagger(x)\, \bar{\sigma}^\mu\, q_L(y) \right] \left[q_L^\dagger(y)\, \bar{\sigma}_\mu\, q_L(x) \right]. \end{aligned} \tag{2.6}$$

Next, we extend the Lagrangian (2.1) to the the left and right-handed quark fields located at different intersections, D4-D8 and D4-$\overline{\text{D8}}$ respectively [27] , this is the low-energy field

theory limit of the SS model,

$$\begin{aligned}\mathscr{S} &= \int d^5\,x \Bigg\{ -\frac{1}{4\,g_5^2}\,F_{MN}\,F^{MN} + \delta\left(x^4+\frac{L}{2}\right)\,q_L^\dagger\,\bar\sigma^\mu\,(i\,\partial_\mu + A_\mu)\,q_L \\ &\qquad\qquad + \delta\left(x^4-\frac{L}{2}\right)\,q_R^\dagger\,\sigma^\mu\,(i\,\partial_\mu + A_\mu)\,q_R\Bigg\}, \\ &= \frac{1}{g_5^2}\int d^5\,x\left\{A_M^{(L)}\,g^{MN}\,\Box\,A_N^{(R)} + \delta\left(x^4+\frac{L}{2}\right)\,J^M_{(L)}\,A_M^{(L)} + \delta\left(x^4-\frac{L}{2}\right)\,J^M_{(R)}\,A_M^{(R)}\right\} \\ &\qquad + \int d^4x\,q_L^\dagger\,\bar\sigma^\mu\,i\,\partial_\mu\,q_L + \int d^4x\,q_R^\dagger\,\sigma^\mu\,i\,\partial_\mu\,q_R \end{aligned} \tag{2.7}$$

where we define $J^M_{(L)} \equiv g_5^2\,q_L^\dagger\,\bar\sigma^M\,q_L\,,\ J^M_{(R)} \equiv g_5^2\,q_R^\dagger\,\sigma^M\,q_R$ and $A_M^{(L)}\,,\ A_M^{(R)}$ are the gauge fields in 5-dimensional spacetime which are located on the D4-D8 and D4-$\overline{\text{D8}}$ intersections respectively.

Then the generating functional of the above action is given by

$$\begin{aligned}&\int [d\,A_M^{(L)}\,d\,A_M^{(R)}]\,\Delta_{FP}\,\exp\left\{i\,\mathscr{S}\big(A_M^{(L)},A_M^{(R)},q_L,q_R\big)\right\} \\ &= \int [d\,A_M^{(L)}\,d\,A_M^{(R)}]\,\Delta_{FP} \\ &\times \exp\Bigg\{\frac{i}{g_5^2}\int d^5x\,A_M^{(L)}\,g^{MN}\,\Box\,A_N^{(R)} \\ &\qquad -\frac{i}{g_5^2}\int d^5x\;d^5y\,\delta\left(x^4+\frac{L}{2}\right)\delta\left(y^4-\frac{L}{2}\right)J^M_{(L)}(x)\,G_{MN}(x-y\,,\,x^4-y^4)\,J^N_{(R)}(y) \\ &\qquad\qquad + i\int d^4x\,q_L^\dagger\,\bar\sigma^\mu\,i\,\partial_\mu\,q_L + i\int d^4x\,q_R^\dagger\,\sigma^\mu\,i\,\partial_\mu\,q_R\Bigg\}. \end{aligned} \tag{2.8}$$

Using eq. (2.8), the effective action in the integrating out procedure is written by

$$\begin{aligned}e^{i\,\mathscr{S}_{\rm eff}} &= \frac{\int [d\,A_M^{(L)}\,d\,A_M^{(R)}]\,\Delta_{FP}\,\exp\left\{i\,\mathscr{S}\big(A_M^{(L)},A_M^{(R)},q_L,q_R\big)\right\}}{\int [d\,A_M^{(L)}\,d\,A_M^{(R)}]\,\Delta_{FP}\,\exp\left\{i\,\mathscr{S}\big(A_M^{(L)},A_M^{(R)},0,0\big)\right\}}\,, \\ &= \exp\Bigg\{i\int d^4x\,(q_L^\dagger\,\bar\sigma^\mu\,i\,\partial_\mu\,q_L + q_R^\dagger\,\sigma^\mu\,i\,\partial_\mu\,q_R) \\ &\qquad -i\,g_5^2\int d^4x\;d^4y\,q_L^\dagger(x)\,\bar\sigma^\mu\,q_L(x)\,G_{\mu\nu}\,(x-y\,,\,L)\;q_R^\dagger(y)\,\sigma^\nu\,q_R(y)\Bigg\}. \end{aligned} \tag{2.9}$$

Finally, we obtain the effective non-local Lagrangian in the Feynman gauge as

$$\begin{aligned}\mathscr{S}_{\rm eff} &= \int d^4x\,(q_L^\dagger\,\bar\sigma^\mu\,i\,\partial_\mu\,q_L + q_R^\dagger\,\sigma^\mu\,i\,\partial_\mu\,q_R) \\ &\qquad -g_5^2\int d^4x\;d^4y\,\frac{1}{8\,\pi^2}\,g_{\mu\nu}\,G\,(x-y\,,\,L)\,q_L^\dagger(x)\,\bar\sigma^\mu\,q_L(x)\;q_R^\dagger(y)\,\sigma^\nu\,q_R(y),\end{aligned}$$

$$= \int d^4x \, (q_L^\dagger \, \bar{\sigma}^\mu \, i \, \partial_\mu \, q_L + q_R^\dagger \, \sigma^\mu \, i \, \partial_\mu \, q_R)$$
$$+ \frac{g_5^2}{4\,\pi^2} \int d^4x \; d^4y \, G\,(x-y\,,\,L)\,[\,q_L^\dagger(x)\cdot\,q_R(y)]\,[\,q_R^\dagger(y)\cdot\,q_L(x)], \tag{2.10}$$

where we used the Fierz identity $\left(q_L^\dagger(x)\,\bar{\sigma}^\mu\,q_L(x)\right)\left(q_R^\dagger(y)\,\sigma_\mu\,q_R(y)\right) = -\,2\left(q_L^\dagger(x)\cdot q_R(y)\right)\left(q_R^\dagger(y)\cdot q_L(x)\right)$. The dot in the right-hand side is the contraction in the colour indices, therefore each fermion bilinear in the final expression of the effective interaction Lagrangian is a colour singlet. There is a non-local interaction between two colour singlet operators in the theory.

3 Effective potential at one-loop : Auxiliary field approach

In this section, we will calculate the effective potential from the effective action eq. (2.10). Actually, there are many ways to perform this kind of calculation. We will use the standard method of effective field theory i.e. bosonize the fermion bilinear which would become the chiral condensate and integrate out the heavy-residual fields (in our case is the fermion fields) and then we can automatically obtain the effective potential with one-loop radiative correction from the effective Lagrangian.

Following ref. [27], we start with the auxiliary field method. This method is used to study the symmetry breaking of the model by introducing the auxiliary field to the effective Lagrangian. In our case is the bosonized complex fields i.e.

$$\begin{aligned} T(x,y) &= \frac{\lambda}{N_c}\,G(x-y,L)\,q_L^\dagger(x)\cdot\,q_R(y), \\ \bar{T}(y,x) &= T^\dagger(x,y) = \frac{\lambda}{N_c}\,G(x-y,L)\,q_R^\dagger(y)\cdot\,q_L(x), \end{aligned} \tag{3.1}$$

where the coupling λ/N_c is related to the g_5^2 coupling in the effective Lagrangian by the relation $\lambda = \frac{g_5^2}{4\,\pi^2}\,N_c\,.$

Substituting auxiliary fields from eq. (3.1) into the effective action eq. (2.10), we obtain

$$\mathscr{S}_{\rm eff} = \int d^4x \, (q_L^\dagger \, \bar{\sigma}^\mu \, i \, \partial_\mu \, q_L + q_R^\dagger \, \sigma^\mu \, i \, \partial_\mu \, q_R) \tag{3.2}$$
$$+ \int d^4x \; d^4y \left(-\frac{N_c}{\lambda}\,\frac{T(x,y)\,\bar{T}(x,y)}{G\,(x-y\,,\,L)} + \bar{T}(y,x)\,q_L^\dagger(x)\cdot\,q_R(y) + T(x,y)\,q_R^\dagger(y)\cdot\,q_L(x)\right).$$

In the chiral (Weyl) basis, one can rewrite the Lagrangian as

$$\mathscr{S}_{\rm eff} = \int d^4x\,\bar{q}(x)\left(i\,\partial\!\!\!/ + T(x)\,P_L + \bar{T}(x)\,P_R\right)q(x) - \int d^4x\,\frac{N_c}{\lambda}\,\frac{T(x)\,\bar{T}(x)}{G\,(x,\,L)}, \tag{3.3}$$

where we imposed the simplifying ansatz $T(x,y) = T(|x-y|)$ consistent with the Poincare symmetry of the expectation value of the operator. This is justified since we are considering expectation value of $T(x,y)$ in the vacuum to study the chiral symmetry breaking.

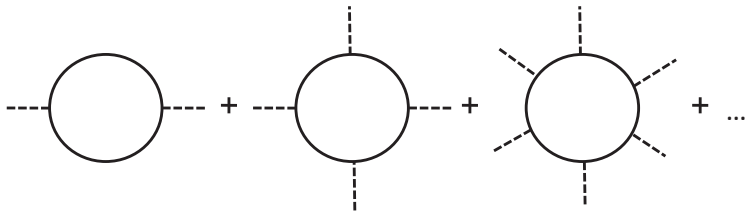

Figure 1. One-loop expansion of fermion fields.

We are ready to integrate out the fermion fields in eq. (3.3), it reads

$$\begin{aligned} e^{i\,\mathscr{S}_{\rm eff}} &= \int [d\bar{q}\,dq]\,\exp\left\{i\,\mathscr{S}\left(\bar{q},q,T,\bar{T}\right)\right\} \Big/ \int [d\bar{q}\,dq]\,\exp\left\{i\,\mathscr{S}\left(\bar{q},q,0,0\right)\right\}, \\ &= \exp\left\{\mathrm{Tr}\,\ln\left(1+\frac{T(x)\,P_L+\bar{T}(x)\,P_R}{i\,\partial\!\!\!/}\right) - i\int d^4x\,\frac{N_c}{\lambda}\,\frac{T(x)\,\bar{T}(x)}{G\,(x,\,L)}\right\}. \end{aligned} \tag{3.4}$$

The identities $\int [d\bar{q}\,dq]\,\exp\left\{i\int d^4x\,\bar{q}(x)\,\mathcal{A}\,q(x)\right\} = \det\mathcal{A} = \exp(\mathrm{Tr}\,\ln\mathcal{A})$ are used above. Then the effective potential with one-loop expansion can be determined from the effective action,

$$\begin{aligned} V_{\rm eff} &= -\,\mathscr{S}_{\rm eff} \\ &= \int d^4x\,\frac{N_c}{\lambda}\,\frac{T(x)\,\bar{T}(x)}{G\,(x,\,L)} + i\,\mathrm{Tr}\,\ln\left(1+\frac{T(x)\,P_L+\bar{T}(x)\,P_R}{i\,\partial\!\!\!/}\right), \end{aligned} \tag{3.5}$$

where $\mathrm{Tr}\equiv\mathrm{Tr}_{\rm spinor}\,\mathrm{Tr}_{\rm colour}\,\mathrm{Tr}_{\rm flavor}\,\mathrm{Tr}_{\rm spacetime}$ is the trace over all indices (i.e. spinor, color, flavor, spacetime). The physical meaning of this procedure is depicted by figure 1.

The second term in the effective potential can be calculated by expansion

$$\begin{aligned} \mathrm{Tr}\,\ln\left(1+\frac{(T\,P_L+\bar{T}\,P_R)}{i\,\partial\!\!\!/}\right) &= \mathrm{Tr}_{\rm spinor}\,\mathrm{Tr}_{\rm color}\,\mathrm{Tr}_{\rm flavor}\,\mathrm{Tr}_{\rm spacetime} \\ &\quad\times\sum_{n=1}^{\infty}\frac{(-1)^{n-1}}{n}\left[\frac{(T\,P_L+\bar{T}\,P_R)}{i\,\partial\!\!\!/}\right]^n, \\ &= i\,N_c\,N_f\,V\int\frac{d^4k_E}{(2\,\pi)^4}\,\ln\left(1+\frac{T(k_E)\,\bar{T}(k_E)}{k_E^2}\right), \end{aligned} \tag{3.6}$$

where we used the following relations;

$$\begin{aligned} &\mathrm{Tr}_{\rm spinor}\,\mathbf{1}_{\rm spinor} = 2\ \text{(in chiral basis)}\,, \quad \mathrm{Tr}_{\rm color}\,\mathbf{1}_{\rm color} = N_c\,, \\ &\mathrm{Tr}_{\rm flavor}\,\mathbf{1}_{\rm flavor} = N_f\,, \quad \mathrm{Tr}_{\rm spacetime} = \int d^4x = V\,, \\ &\frac{1}{\partial\!\!\!/} = \int\frac{d^4k}{(2\,\pi)^4}\,\frac{k\!\!\!/}{k^2}\,e^{i\,k\cdot\,(x-y)}\,, \qquad (T\,k\!\!\!/\,P_L+\bar{T}\,k\!\!\!/\,P_R)^2 = T\,\bar{T}\,k^2. \end{aligned} \tag{3.7}$$

The momentum has been Euclideanized and henceforth we will drop the subscript.

Finally, the effective potential at one-loop is given by (scaled by factor N_f)

$$V_{1-\text{loop}} = N_c \left[\int d^4x\, T(x)\, \bar{T}(x)\, \frac{(x^2+L^2)^{\frac{3}{2}}}{\lambda} - \int \frac{d^4k}{(2\,\pi)^4}\, \ln\left(1 + \frac{T(k)\,\bar{T}(k)}{k^2}\right)\right]. \quad (3.8)$$

The equation of motion (the gap equation) of the scalar $T(x)$ from the effective action, eq. (3.8), is

$$\int d^4x\, T(x)\, e^{-ikx}\, \frac{(x^2+L^2)^{\frac{3}{2}}}{\lambda} = \frac{T(k)}{k^2 + T(k)\,\bar{T}(k)}. \quad (3.9)$$

Apart from the trivial solution $T = 0$ for the chiral-symmetric vacuum, the general solution to the gap equation $\delta V_{\text{eff}}/\delta\bar{T}(k) = 0$ can be solved perturbatively either analytically or numerically (see appendix C). Non-vanishing T solution corresponds to chiral symmetry breaking vacuum which has lower energy and thus represents a true vacuum. We can obtain approximate solution by solving the gap equation in 2 regions of momentum, small and large k (i.e. $T(k)\bar{T}(k) \gg k^2$ and $T(k)\bar{T}(k) \ll k^2$ respectively). The two solutions then can be matched to determine the unknown constants. An approximate solution from such method is in the following form [27]

$$T(k) = \bar{T}(k) = \begin{cases} T_0 = k_* \equiv \sqrt{\frac{\lambda}{L^3}} & ,\ 0 < k \le k_*\,, \\ \\ T_0^2\, \frac{e^{-L\,k}}{k} \equiv \frac{\lambda}{L^3}\, \frac{e^{-L\,k}}{k} & ,\ k_* < k < \Lambda\,. \end{cases} \quad (3.10)$$

Generically by using the gap equation, the one-loop potential can be rewritten to be

$$V_{1-\text{loop}} = N_c \int \frac{d^4k_E}{(2\,\pi)^4} \left[\frac{T(k)\bar{T}(k)}{k^2 + T(k)\bar{T}(k)} - \ln\left(1 + \frac{T(k)\,\bar{T}(k)}{k^2}\right)\right]. \quad (3.11)$$

By substituting approximate propagator eq. (3.10) into eq. (3.11), we can demonstrate that there is chiral symmetry breaking vacuum induced by small momentum contribution to the one-loop potential. The details are discussed in section 5. Essentially, since the integrand in eq. (3.11) is a negative-definite function of variable $k^2/T(k)\bar{T}(k)$, the one-loop potential is always negative for nonzero T regardless of the exact form of the solution of the gap equation. It is obvious that the solution with nonzero T gives the lower potential than the chiral symmetric solution $T = 0$.

It is remarkable that the chiral symmetry breaking of the one-loop potential occurs at any weak coupling. The reasons are the boundness of the positive classical term (the first term in the right-hand side of eq. (3.11)) whilst the negative loop term (the second term in the right-hand side of eq. (3.11)) is not bounded for low momentum. The solution of the gap equation, eq. (3.10), is a constant for the low momentum, resulting in $\ln(1/k^2)$-divergence of the loop term as $k \to 0$, regardless of λ.

4 Effective potential at two-loop level

Even though the one-loop potential demonstrates the possibility of chiral symmetry breaking solution, higher loops contribution could likewise be significant. In this section, we will calculate the effective potential at two-loop level by following Jackiw's functional effective action method [31]. The two-loop contribution can be calculated from the vacuum expectation value of the interaction Lagrangian $\mathscr{L}_I(x)$

$$V_{2-\text{loop}} = i\,\langle\,0\,|\,\mathcal{T}\,e^{i\int d^4x\,\mathscr{L}_I(x)}\,|\,0\,\rangle, \tag{4.1}$$

where $\mathcal{T}$ is the time-ordering operator. In order to obtain the two-loop contribution, we simply use the conventional Feynman rules to calculate all possible two-loop diagrams exist in the effective theory of fermion and auxiliary scalar. The propagator $\mathcal{G}$ of the field ϕ to be used in the evaluation of the 2-loop diagrams is defined by the inverse of the functional operator, namely

$$i\,\mathcal{G}^{-1}(x,y) = \frac{\delta^2}{\delta\phi(x)\,\delta\phi(y)}\int d^4x\,\mathscr{L}_{\text{eff}}(x). \tag{4.2}$$

In the previous section, we recall the effective Lagrangian

$$\begin{aligned}
\mathscr{S}_{\text{eff}} &= \int d^4x\left[i\,\bar{q}(x)\,\partial\!\!\!/\,q(x) + \bar{q}(x)\,T(x)\,P_L\,q(x) + \bar{q}(x)\,\bar{T}(x)\,P_R\,q(x) - \frac{N_c}{\lambda}\,\frac{T(x)\,\bar{T}(x)}{G\,(x,\,L)}\right],\\
\mathscr{S}_I &= \int d^4x\,\mathscr{L}_I(x) = \int d^4x\left[\,\bar{q}(x)\,T(x)\,P_L\,q(x) + \bar{q}(x)\,\bar{T}(x)\,P_R\,q(x)\,\right].
\end{aligned} \tag{4.3}$$

The functional operator $\mathcal{S}^{-1}$ of the quark fields and $\mathcal{D}^{-1}$ of the complex scalar fields from the effective Lagrangian therefore can be written as

$$\begin{aligned}
i\,\mathcal{S}^{-1}(k) &= \int d^4x\,e^{-\,i\,k\cdot(x-y)}\,\frac{\delta^2\mathscr{S}_{\text{eff}}}{\delta q(x)\,\delta\bar{q}(y)},\\
&= \not{k} + T(k)\,P_L + \bar{T}(k)\,P_R\,,\\
i\,\mathcal{D}^{-1}(k) &= \int d^4x\,e^{-\,i\,k\cdot(x-y)}\,\frac{\delta^2\mathscr{S}_{\text{eff}}}{\delta T(x)\,\delta\bar{T}(y)},\\
&= -\,\frac{N_c}{\lambda\,G\,(k,\,L)}.
\end{aligned} \tag{4.4}$$

Noting that, $\mathcal{D}^{-1}$ has no kinetic term for the scalars $T, \bar{T}$. The vertices of the interaction in the effective action are given by [31, 32]

$$\begin{aligned}
\Gamma_L &= \int d^4x\,e^{-\,i\,k\cdot(x-y-z)}\,\frac{(-i)^3\delta^3\mathscr{S}_{\text{eff}}}{\delta q(x)\,\delta\bar{q}(y)\,T(z)},\\
&= iP_L,
\end{aligned} \tag{4.5}$$

$$\begin{aligned}
\Gamma_R &= \int d^4x\,e^{-\,i\,k\cdot(x-y-z)}\,\frac{(-i)^3\delta^3\mathscr{S}_{\text{eff}}}{\delta q(x)\,\delta\bar{q}(y)\,\bar{T}(z)},\\
&= iP_R\,.
\end{aligned} \tag{4.6}$$

Putting everything together, the two-loop contribution is (see figure 2 for the corresponding diagram)

$$\begin{aligned} V_{2-\text{loop}} &= -i\,\text{Tr}\int\frac{d^4k}{(2\,\pi)^4}\,\frac{d^4p}{(2\,\pi)^4}\,\Gamma_L\,\mathcal{S}(p)\,\Gamma_R\,\mathcal{S}(k)\,\mathcal{D}(p-k), \\ &= -\frac{\lambda}{N_c}\,N_f\,N_c\int\frac{d^4k}{(2\,\pi)^4}\,\frac{d^4p}{(2\,\pi)^4}\,\frac{2\,p\cdot k\,G\,(p-k,\,L)}{\left[p^2-T(p)\,\bar{T}(p)\,\right]\left[k^2-T(k)\,\bar{T}(k)\,\right]}, \end{aligned} \tag{4.7}$$

where we have used

$$\frac{\not{k}-\bar{T}\,P_L-T\,P_R}{\left(\not{k}+T\,P_L+\bar{T}\,P_R\right)\left(\not{k}-\bar{T}\,P_L-T\,P_R\right)}=\frac{\not{k}-\bar{T}\,P_L-T\,P_R}{k^2-\bar{T}\,T}, \tag{4.8}$$

and

$$\text{Tr}\left\{P_L\,(\not{p}-\bar{T}\,P_L-T\,P_R)\,P_R\,(\not{k}-\bar{T}\,P_L-T\,P_R)\right\}=\,2\,p\cdot k. \tag{4.9}$$

Using Wick rotation i.e. $k\to i\,k_E$, $d^4k\to i\,d^4k_E$, we obtain the two-loop contribution in Euclidean space

$$\begin{aligned} V_{2-\text{loop}} = -4\pi^2\lambda\,N_f\int\frac{d^4k_E}{(2\,\pi)^4}\frac{1}{\left[\,k_E^2+T(k_E)\,\bar{T}(k_E)\,\right]} \\ \times\int\frac{d^4p_E}{(2\,\pi)^4}\,\frac{2\,p_E\cdot k_E\,e^{-\,L\left|\,p_E-k_E\,\right|}}{\left[p_E^2+T(p_E)\,\bar{T}(p_E)\right]\left|\,p_E-k_E\,\right|}\,. \end{aligned} \tag{4.10}$$

The angle integration can be evaluated as shown in appendix D to be

$$\begin{aligned} V_{2-\text{loop}} = -\frac{\lambda\,N_f}{4\,L^5\pi^3}\int_0^{L\,\Lambda}d\tilde{k}_E\,\frac{\tilde{k}_E^4}{\left[\,\tilde{k}_E^2+L^2\,T(k_E)\,\bar{T}(k_E)\,\right]}\int_0^{L\,\Lambda}d\tilde{p}_E\,\frac{\tilde{p}_E^4}{\left[\tilde{p}_E^2+L^2\,T(p_E)\,\bar{T}(p_E)\,\right]} \\ \times\sum_{n=0}^{\infty}\frac{(-1)^n}{n\,!}\left\{-\frac{\pi\,(n-1)\,A^{\frac{n-3}{2}}}{(n+3)\,(n+5)\,B}\right. \\ \times\left[2\,(A^2-B^2)\;{}_2F_1\Big(\frac{3-n}{4},\frac{5-n}{4};1;\frac{B^2}{A^2}\Big)\right. \\ \left.\left.+\left(B^2\,(n+2)-2\,A^2\right)\;{}_2F_1\Big(\frac{3-n}{4},\frac{5-n}{4};2;\frac{B^2}{A^2}\Big)\right]\right\}, \end{aligned} \tag{4.11}$$

where $\tilde{k}_E\equiv L\,k_E$, $\tilde{p}_E\equiv L\;p_E$, $A\equiv\tilde{p}_E^2+\tilde{k}_E^2$, $B\equiv 2\,\tilde{p}_E\,\tilde{k}_E$. Henceforth, for convenience we will simply write the Euclidean momentum without a subscript.

5 Results and Discussions

Adding all of the one-loop and two-loop contributions, the total effective potential becomes

$$\begin{aligned} V_{\text{eff}} &= V_{1-\text{loop}}+V_{2-\text{loop}}, \\ &= N_c\int\frac{d^4k_E}{(2\,\pi)^4}\left[\frac{T(k)\bar{T}(k)}{k^2+T(k)\bar{T}(k)}-\ln\left(1+\frac{T(k)\,\bar{T}(k)}{k^2}\right)\right]+V_{2-\text{loop}}. \end{aligned} \tag{5.1}$$

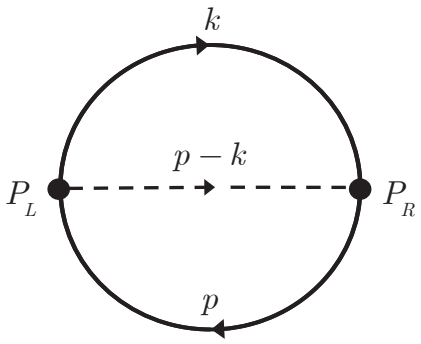

Figure 2. Two-loop vacuum diagram for $V_{2-\text{loop}}$, solid line is the fermion and dash line is the scalar.

The resulting effective potential of the scalar shows the possibility of chiral symmetry breaking at nontrivial $T(k) \neq 0$ since the sign of the one-loop contribution is opposite to the classical action of the scalar. The 2-loop effect as given in the form of eq. (4.11) could be either positive or negative depending on the relative sizes of each n-term. A closer investigation reveals that the $n = 0$ term is the largest and it is negative. The odd-n terms are positive with smaller values than the preceding even-n terms. Consequently, the entire two-loop potential is negative. Since the chiral symmetric solution $T = \bar{T} = 0$ gives larger negative two-loop contribution than the chirally broken case (with smaller denominator of the integrand in eq. (4.11)). It is thus possible that the difference of 2-loop contributions would compensate the one-loop effect and alter the true vacuum of the theory in a significant way. We will demonstrate that the two-loop contribution is small comparing to the leading one-loop and the chiral symmetry breaking persists. In evaluation of the momentum integrals, we will apply a UV-cutoff Λ required in non-renormalizable effective field theory. The cutoff will be taken to be larger than T_0 and smaller than $1/L$.

5.1 1-loop

Since both one-loop and two-loop contributions scale with the number of flavour N_f, we will simply suppress the N_f factor henceforth. First, we will consider 1-loop contribution of the scalar to the effective potential and demonstrate that the potential has nontrivial minima when using the ansatz solution of the gap equation as given in eq. (3.10). The 1-loop integrations, eq. (3.11), can be performed in two separate momentum regions and rewritten as the following

$$\begin{aligned}\frac{V_{\text{eff}}}{N_c} &= \int \frac{d^4k}{(2\,\pi)^4}\left[\frac{T(k)\bar{T}(k)}{k^2+T(k)\bar{T}(k)} - \ln\left(1+\frac{T(k)\,\bar{T}(k)}{k^2}\right)\right], \\ &= \left(\int_0^{T_0} + \int_{T_0}^{\Lambda}\right)\frac{d^4k}{(2\,\pi)^4}\left[\frac{T(k)\bar{T}(k)}{k^2+T(k)\bar{T}(k)} - \ln\left(1+\frac{T(k)\,\bar{T}(k)}{k^2}\right)\right],\end{aligned}$$

$$= -\frac{T_0^4}{16\pi^2}\left(\ln 2 - \frac{1}{2} + 2\sum_{n=1}^{\infty}\frac{(-1)^{n-1}(1-n)}{n}F_{4n-3}(LT_0, L\Lambda; n)\right). \tag{5.2}$$

where we define the function

$$F_{4n-3}(LT_0, L\Lambda; n) \equiv E_{4n-3}(2nLT_0) - E_{4n-3}(2nL\Lambda)\left(\frac{T_0}{\Lambda}\right)^{4n-4},$$
$$E_m(z) \equiv \int_1^{\infty}\frac{e^{-zt}}{t^m}\,dt.$$

The function $F_{4n-3}(LT_0, L\Lambda; n)$ decreases very rapidly with n, therefore the sum in the one-loop potential, eq. (5.2), can be approximated by truncating at finite n with a high precision.

The one-loop contribution will be explored by fixing one and two of the 3 parameters, λ, L, Λ and numerically plot the effective potential with respect to the remaining parameters. The physically-valid region of the parameter space for our SS NJL model is $T_0 = \sqrt{\lambda/L^3} < \Lambda < 1/L$. As shown in figure 3, the one-loop potential is negative at any nonzero values of Λ, λ, L corresponding to nonzero values of $T_0 = \sqrt{\lambda/L^3}$. Since when $T = 0$, the potential is zero and less preferred than negative potential occuring at any coupling λ, chiral symmetry breaking thus naturally occurs for any weak coupling (i.e. $T_0 < 1/L$). In figure 3(a), the potential approaches negative constant for $\Lambda \gtrsim 0.7 - 0.8$ for $\lambda = 0.1, L = 1$. If we instead fix the UV-cutoff scale $\Lambda = 0.5$, the potential will be a decreasing function with λ as demonstrated in figure 3(b). Figure 3(c) also shows the one-loop potential at fixed $\lambda = 0.3, \Lambda = 0.5$ as a function of L. It is important that we restrict ourselves to the physical region $T_0 < \Lambda < 1/L$ in our consideration of the effective potential in the nonlocal NJL model.

We also plot the potential landscape in the physical region at fixed $L = 1$, as is shown in figure 4.

5.2 2-loop

In this section, we investigate the 2-loop contribution to the effective potential. Using the one-loop approximate scalar ansatz, eq. (3.10), the two loop integration given by eq. (4.11) can be separated into 3 terms,

$$\begin{aligned}
V_{2-\text{loop}} = \frac{\lambda}{4\pi^3 L^5}&\left[\int_0^{T_0L} d\tilde{k}\int_0^{T_0L} d\tilde{p} + \int_{T_0L}^{\Lambda L} d\tilde{k}\int_{T_0L}^{\Lambda L} d\tilde{p} + 2\int_0^{T_0L} d\tilde{k}\int_{T_0L}^{\Lambda L} d\tilde{p}\right] \\
&\times \frac{\tilde{k}^4}{\left[\tilde{k}^2 + L^2\,T(\tilde{k}/L)\,\bar{T}(\tilde{k}/L)\right]}\frac{\tilde{p}^4}{\left[\tilde{p}^2 + L^2\,T(\tilde{p}/L)\,\bar{T}(\tilde{p}/L)\right]} \\
&\times \sum_{n=0}^{\infty}\frac{(-1)^n}{n\,!}\left\{\frac{\pi\,(n-1)\,A^{\frac{n-3}{2}}}{(n+3)\,(n+5)\,B}\right. \\
&\quad\times\left[2\,(A^2 - B^2)\;{}_2F_1\Big(\frac{3-n}{4}, \frac{5-n}{4}; 1; \frac{B^2}{A^2}\Big)\right. \\
&\qquad\left.\left. + \left(B^2\,(n+2) - 2\,A^2\right)\;{}_2F_1\Big(\frac{3-n}{4}, \frac{5-n}{4}; 2; \frac{B^2}{A^2}\Big)\right]\right\}.
\end{aligned} \tag{5.3}$$

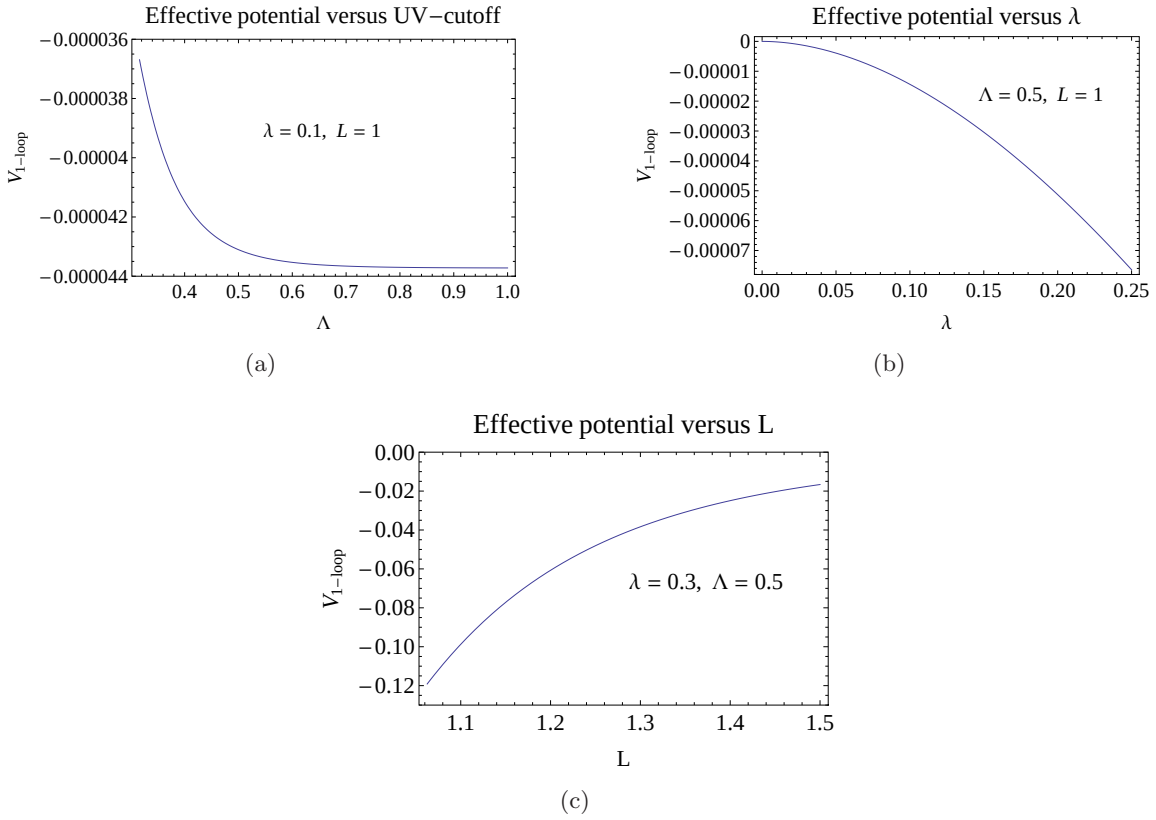

Figure 3. One-loop effective potential per colour as a function of Λ, λ, L.

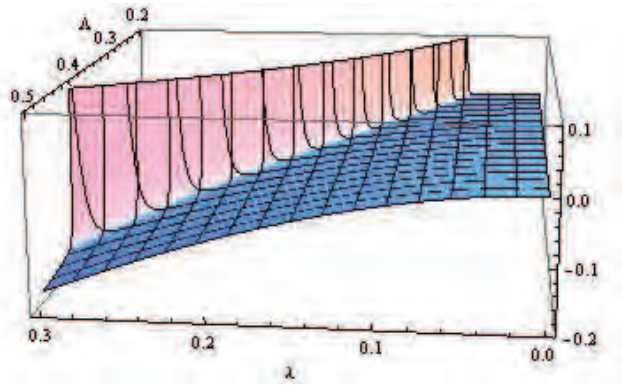

Figure 4. One-loop effective potential per colour as a function of Λ, λ for $L = 1$.

The overall 2-loop contribution scales with λ/L^5. The integration in the low momentum region has additional $(T_0 L)^6 \times (T_0 L)^{n-1}$ factor for each n-term in the sum. The integration in the high momentum region, on the other hand, has additional $(\Lambda L)^6 \times (\Lambda L)^{n-1}$ dependence for each n-term. The cross term integration has additional overall scaling factor $(T_0 L)^3 (\Lambda L)^3$ for all n. We perform numerical integration on each n-term and add them up. Since the integrand for each n is a smooth and well-behave function with no singularities and abrupt changes, numerical integration yield very precise results. The value of the

integration for each n-term decreases rapidly with n and the error is less than 10^{-6} if we truncate the sum at $n = 10$.

Figure 5 shows the effect of 2-loop contribution to the effective potential. Similar to the one-loop case, the chiral-symmetry broken vacuum solution has lower energy than the chiral symmetric one ($T = \bar{T} = 0$). However, there is one crucial difference between one and two-loop potential. The magnitude of 2-loop contribution could increase with the cutoff in contrast to the 1-loop which saturates to negative constant. This is originated from the ΛL dependence of the potential in eq. (5.3) getting larger with increasing Λ resulting in the decreasing function of the effective potential with the cutoff.

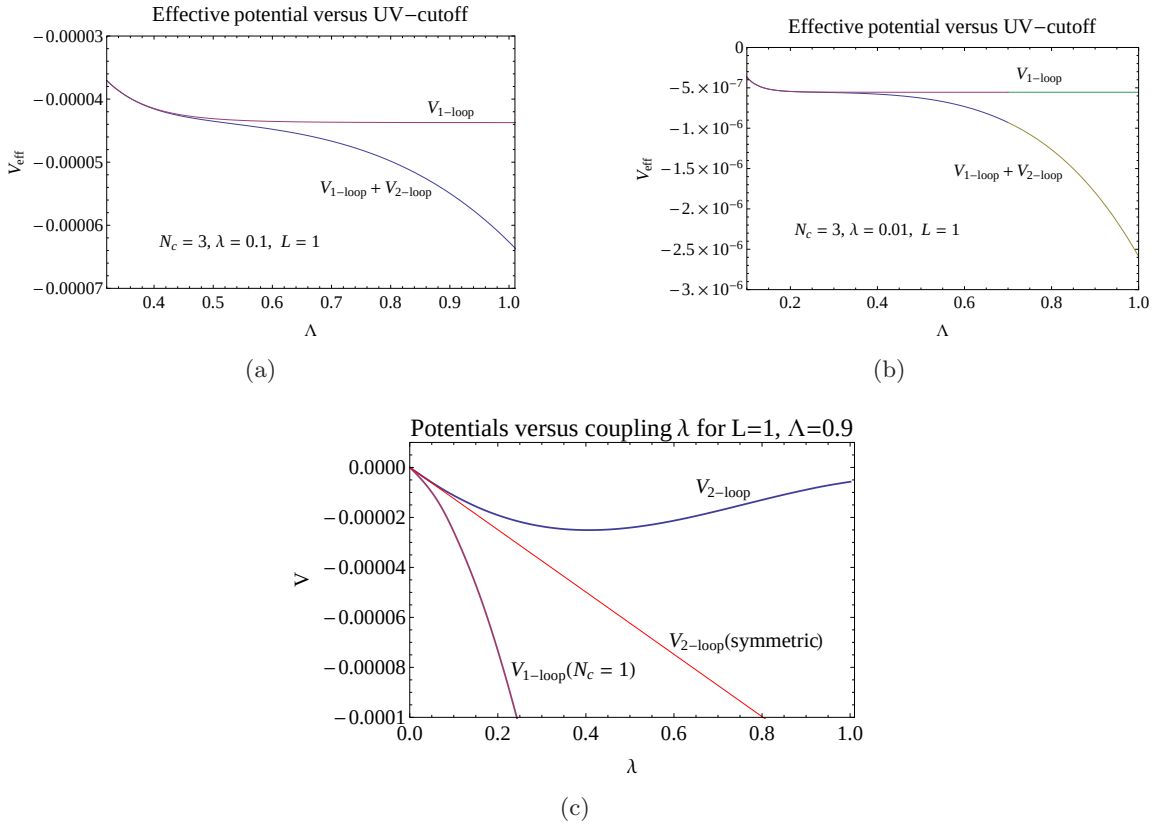

Figure 5. Effective potential up to 2-loop as a function of Λ for $N_c = 3, \lambda = 0.1$ (a), 0.01 (b); $L = 1$. The 2-loop contributions for both chirally broken and symmetric solutions are shown in (c) in comparison to the chirally broken 1-loop.

When the 't Hooft coupling is very small, $\lambda \lesssim 0.08$, interesting phenomenon occurs. As we can see from figure 6 (a), the ratio (magnitude) of the 2-loop to 1-loop increases sharply as $\lambda \to 0$. From eq. (5.2) and (5.3), since $V_{1-\text{loop}} \sim \lambda^2 N_c$ while $V_{2-\text{loop}} \sim \lambda$, the ratio of the 2-loop to 1-loop potential will scale as $(\lambda N_c)^{-1}$ and the 2-loop contribution will be dominant for sufficiently small λ. However, since both one and two loop contributions are negative and together they are larger in magnitude than the two-loop potential of the chirally symmetric solution (figure 5 (c)), the chirally broken vacuum always has lower potential as is demonstrated in Figure 5 (c) and 6 (b). Chiral symmetry breaking therefore persists for

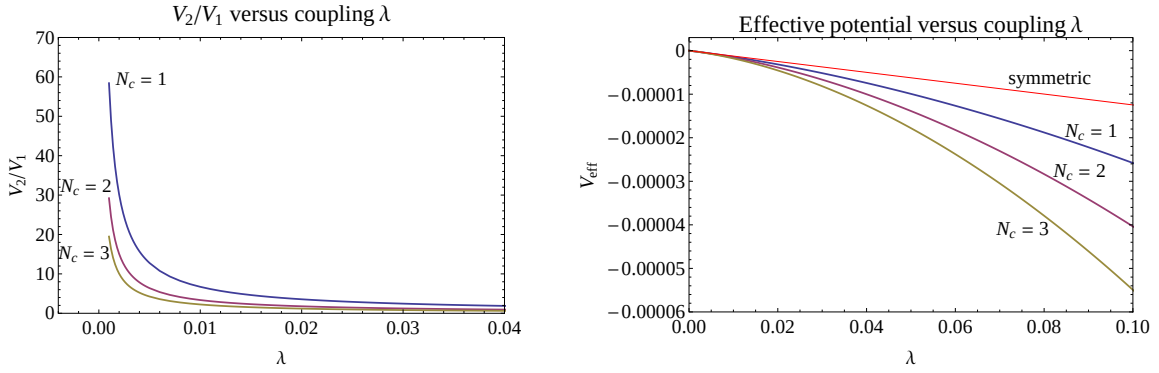

(a) (b)

Figure 6. The ratio of $V_{2-\text{loop}}/V_{1-\text{loop}}$ decreases rapidly with increasing λ (a). In (b), the effective potential for small λ remains negative (and smaller than the chirally symmetric case), chiral symmetry breaking thus persists. The cutoff Λ is set to 0.9 and $L = 1$ for these plots.

arbitrary weak coupling. One might anticipate the chirally symmetric potential to become more negative than the chirally broken one as $\lambda \to 0$ since $V_{2-\text{loop}}(\text{sym}) < \text{V}_{2-\text{loop}}(\chi\text{SB})$ and $V_{2-\text{loop}}/V_{1-\text{loop}} \sim (N_c\lambda)^{-1}$. However, a closer investigation reveals that the difference $V_{2-\text{loop}}(\text{sym}) - \text{V}_{2-\text{loop}}(\chi\text{SB}) \simeq \lambda \text{V}_{2-\text{loop}}(\text{sym})$ for very small λ and $V_{1-\text{loop}}(\chi SB)$ is actually larger in magnitude (i.e. more negative) than $\lambda V_{2-\text{loop}}(\text{sym})$. Consequently, the chirally broken solution still has lower potential than the chirally symmetric one even for extremely small coupling.

6 Conclusions

SS intersecting-branes model provides a geometrized model of chiral symmetry breaking and confinement in both weak and strong coupling regimes. The effective field theory at low energy ($E < 1/L$) from the SS model is a type of NJL model with non-local 4-fermion interaction. In constrast to conventional NJL with 4-fermion contact interaction which requires sufficiently large coupling to break chiral symmetry, the holographic non-local NJL model prefers chirally broken phase for arbitrarily weak coupling at the 1-loop level. In this work, we found that the 2-loop effect does NOT change this feature of the model and the chiral symmetry breaking persists for arbitrary weak coupling. The 2-loop effect can be understood as the antiscreening of the non-local 4-fermion interaction induced from the coupling of fermion with the cloud of scalar condensate. The 2-loop contribution in our model is suppressed below the 1-loop contribution for $\lambda \gtrsim 0.08$. One of the suppression factor is the number of colour degrees of freedom $N_c = 3$ when the coupling λ is fixed. Bosonization of the fermion bilinear into a colour-singlet scalar naturally matches the loop expansion of the effective potential with the $1/N_c$ expansion. The large-N_c expansion makes it manifest that the 1-loop contribution scales as $(N_c)^1$ and the 2-loop scales as $(N_c)^0$. The higher-order loops are therefore suppressed by negative power of N_c and so on.

The solution to the gap equation in our model gives fermion condensate proportional to $\sqrt{\lambda/L^3}$ resulting in λ^2-dependence of the one-loop potential while the two-loop scales as

λ. Therefore the two-loop contribution becomes dominant to the one-loop for very small coupling. However, since the difference between the two-loop contribution of the chirally symmetric and broken solutions is smaller than the size of the one-loop potential of the chirally broken solution, chiral symmetry remains broken for arbitrary small coupling.

Acknowledgments

We would like to thank Yupeng Yan, Janos Polonyi and Sanjin Benic for helpful discussions. P.B. is supported in part by the Thailand Research Fund (TRF) and Commission on Higher Education (CHE) under grant RMU5380048. D.S. is supported in part by the Thailand Center of Excellence in Physics (ThEP).

A Integrating out heavy gauge field for single intersection model

According to the standard technique of path integral (see [30], or textbooks in QFT), the generating function of the action in eq. (2.4) is written by

$$\begin{aligned}
&\int [d\,A_M]\,\Delta_{FP}\,\exp\left\{i\,\mathscr{S}\big(A_M, q_L\big)\right\},\\
&= \int [d\,A_M]\,\Delta_{FP}\,\exp\Big\{i\int d^5x\,\frac{1}{g_5^2}\left[\frac{1}{2}\,A_M\,\Box\,A^M + \delta\,(x^4)\,J^M\,A_M\right] + i\int d^4x\,q_L^\dagger\,\bar\sigma^\mu\,i\,\partial_\mu\,q_L\Big\},\\
&= \int [d\,A_M]\,\Delta_{FP}\\
&\qquad \times \exp\Big\{\frac{i}{g_5^2}\int d^5x\,\frac{1}{2}\,A_M\,\Box\,A^M\\
&\qquad\qquad -\frac{i}{g_5^2}\int d^5x\;d^5y\,\delta\,(x^4)\,\delta\,(y^4)\,\frac{1}{2}\,J^M(x)\,G_{MN}(x-y\,,\,x^4-y^4)\,J^N(y)\\
&\qquad\qquad + i\int d^4x\,q_L^\dagger\,\bar\sigma^\mu\,i\,\partial_\mu\,q_L\Big\},
\end{aligned}\tag{A.1}$$

where Δ_{FP} is the Faddeev-Popov's determinant. In the Feynman-gauge, the propagator, $G_{MN}(x, x^4)$ of the gauge field A_M can be written as

$$\begin{aligned}
G_{MN}\left(x\,,\,x^4\right) &= \frac{1}{8\,\pi^2}\,g_{MN}\,G\left(x\,,\,x^4\right),\\
&= \frac{1}{8\,\pi^2}\,\frac{g_{MN}}{((x^4)^2-x^2)^{3/2}}.
\end{aligned}\tag{A.2}$$

Using eq. (2.5,A.1) in eq. (2.3), we obtain

$$
\begin{aligned}
e^{i\,\mathscr{S}_{\rm eff}} &= \int [d\,A_M]\,\Delta_{FP}\,e^{i\int d^4x\,\mathscr{L}\left(A_M(x),q_L(x)\right)} \Big/ \int [d\,A_M]\,\Delta_{FP}\,e^{i\int d^4x\,\mathscr{L}\left(A_M(x),0\right)} \\
&= \int [d\,A_M]\,\Delta_{FP} \\
&\qquad \times \exp\Big\{\frac{i}{g_5^2}\int d^5x\,\frac{1}{2}\,A_M\,\Box\,A^M \\
&\qquad\qquad -\frac{i}{g_5^2}\int d^5x\;d^5y\,\delta\,(x^4)\,\delta\,(y^4)\,\frac{1}{2}\,J^M(x)\,G_{MN}(x-y\,,\,x^4-y^4)\,J^N(y) \\
&\qquad\qquad\qquad +i\int d^4x\,q_L^\dagger\,\bar\sigma^\mu\,i\,\partial_\mu\,q_L\Big\} \\
&\qquad \Big/ \int [d\,A_M]\,\Delta_{FP}\,\exp\Big\{\frac{i}{g_5^2}\int d^5x\,\frac{1}{2}\,A_M\,\Box\,A^M\Big\}, \\
&= \exp\Big\{-\frac{i}{g_5^2}\int d^4x\;d^4y\,\frac{1}{16\,\pi^2}\,g_5^2\,q_L^\dagger(x)\,\bar\sigma^\mu\,q_L(x)\,G(x-y\,,\,0)\,g_5^2\,q_L^\dagger(y)\,\bar\sigma_\mu\,q_L(y) \\
&\qquad\qquad +i\int d^4x\,q_L^\dagger\,\bar\sigma^\mu\,i\,\partial_\mu\,q_L\Big\}, \\
&= \exp\Big\{-i\int d^4x\;d^4y\,\frac{g_5^2}{16\,\pi^2}\,G(x-y\,,\,0)\,\Big[q_L^\dagger(x)\,\bar\sigma^\mu\,q_L(y)\Big]\,\Big[q_L^\dagger(y)\,\bar\sigma_\mu\,q_L(x)\Big] \\
&\qquad\qquad +i\int d^4x\,q_L^\dagger\,\bar\sigma^\mu\,i\,\partial_\mu\,q_L\Big\}, \quad \text{(A.3)}
\end{aligned}
$$

where we used $J^{(4)}=0$ and Fierz identity $(q_{L,1}^\dagger\,\bar\sigma^\mu\,q_{L,2})\,(q_{L,3}^\dagger\,\bar\sigma_\mu\,q_{L,4}) = (q_{L,1}^\dagger\,\bar\sigma^\mu\,q_{L,4})\,(q_{L,3}^\dagger\,\bar\sigma_\mu\,q_{L,2})$.

B Fourier transform in Euclidean 5-dimensions

The coordinates of a d dimensional Euclidean space are given by

$$
\begin{aligned}
x_1 &= x\,\cos\theta_1\,, \\
x_2 &= x\,\sin\theta_1\,\cos\theta_2\,, \\
x_3 &= x\,\sin\theta_1\,\sin\theta_2\,\cos\theta_3\,, \\
x_4 &= x\,\sin\theta_1\,\sin\theta_2\,\sin\theta_3\,\cos\theta_4\,, \\
x_5 &= x\,\sin\theta_1\,\sin\theta_2\,\sin\theta_3\,\sin\theta_4\,\cos\theta_5, \\
&\;\;\vdots \\
x_n &= x\,\sin\theta_1\,\sin\theta_2\,\sin\theta_3\,\cdots\sin\theta_{n-1}\,\cos\theta_n \\
x_{n+1} &= x\,\sin\theta_1\,\sin\theta_2\,\sin\theta_3\,\cdots\sin\theta_{n-1}\,\sin\theta_n, \qquad \text{(B.1)}
\end{aligned}
$$

where only $\theta_n \in [0, 2\pi)$ (so that $x_{n+1} \in [-x, +x,]$) and other angles range from 0 to π. For Euclidean momentum in 5 dimensions, the components are

$$
\begin{aligned}
k_1 &= k\,\cos\theta_1\,, \\
k_2 &= k\,\sin\theta_1\,\cos\theta_2\,,
\end{aligned}
$$

$$
\begin{aligned}
k_3 &= k\,\sin\theta_1\,\sin\theta_2\,\cos\theta_3\,,\\
k_4 &= k\,\sin\theta_1\,\sin\theta_2\,\sin\theta_3\,\cos\theta_4\,,\\
k_5 &= k\,\sin\theta_1\,\sin\theta_2\,\sin\theta_3\,\sin\theta_4\,.
\end{aligned}
\tag{B.2}
$$

The volume element in 5-dimension is thus

$$
d^5k = k^4\,\sin^3\theta_1\,\sin^2\theta_2\,\sin\theta_3\,dk\,d\theta_1\,d\theta_2\,d\theta_3\,d\theta_4. \tag{B.3}
$$

With this measure, the Fourier transform in 5 dimensional Euclidean space can be performed as the following

$$
\begin{aligned}
F(x) &= \int \frac{d^5\,k}{(2\,\pi)^5}\,\tilde{F}(k)\,e^{i\,k\cdot x} = \int \frac{d^5\,k}{(2\,\pi)^5}\,\tilde{F}(k)\,e^{i\,k\,x\,\cos\theta_1},\\
&= \frac{1}{(2\,\pi)^5}\int dk\,d\theta_1\,d\theta_2\,d\theta_3\,d\theta_4\,k^4\,\sin^3\theta_1\,\sin^2\theta_2\,\sin\theta_3\,\tilde{F}(k)\,e^{i\,k\,x\,\cos\theta_1},\\
&= \frac{1}{(2\,\pi)^5}\int_0^\infty \tilde{F}(k)\,k^4\,dk\int_0^\pi e^{i\,k\,x\,\cos\theta_1}\,\sin^3\theta_1\,d\theta_1\int_0^\pi \sin^2\theta_2\,d\theta_2\int_0^\pi \sin\theta_3\,d\theta_3\int_0^{2\,\pi} d\theta_4,\\
&= \frac{1}{4\,\pi^3}\int_0^\infty dk\,\tilde{F}(k)\,k^4\left[\frac{\sin(k\,x)}{(k\,x)^3} - \frac{\cos(k\,x)}{(k\,x)^2}\right].
\end{aligned}
\tag{B.4}
$$

Given an explicit functional form $\tilde{F}(k)$, the transform can be completed.

However, in the situation where the quarks are localized at particular x^4 and the gauge fields in 5 dimensions are integrated out to obtain the effective 4-dimensional action, we will need to perform the Fourier transform of the propagator given in eq. (A.2) under the condition that the gauge fields are propagating at a fixed distance in x^4 direction. The Fourier integration will split into a delta function in x^4 coordinate and the Fourier transform in the Euclidean 4 dimensions.

For example, in our model, the Fourier transform becomes

$$
\begin{aligned}
G(k\,,k_4) &= \int d^5\,x\,G(x\,,L)\,e^{i\,k\cdot x} = \int_{-\infty}^{\infty} d\,x_4\,e^{i\,k_4\,x_4}\int d^4\,x\,G(x\,,L)\,e^{-\,i\,k\cdot\,x},\\
&= \delta(k_4)\int dx\,d\theta_1\,d\theta_2\,d\theta_3\;x^3\,\sin^2\theta_1\,\sin\theta_2\,G(x\,,L)\,e^{i\,k\,x\,\cos\theta_1},\\
&= \delta(k_4)\int_0^\infty \frac{1}{\left(L^2+\tilde{x}^2\right)^{\frac{3}{2}}}\,x^3\,dx\,\frac{\pi\,J_1(k\,x)}{k\,x}\,(2)\,(2\,\pi),\\
&= \frac{4\,\pi^2}{k}\,\delta(k_4)\int_0^\infty \frac{(k\,x)^2\,J_1(k\,x)}{\left((k\,L)^2+(k\,x)^2\right)^{\frac{3}{2}}}\,d(k\,x),\\
&= \delta(k_4)\,4\,\pi^2\,\frac{e^{-\,L\,k}}{k},
\end{aligned}
\tag{B.5}
$$

where $J_n(x)$, is Bessel function. If we neglect the momentum in bulk spacetime say, $k_4 = 0$, we obtain

$$
G(k\,,0) = 4\,\pi^2\,\frac{e^{-\,L\,k}}{k}. \tag{B.6}
$$

C Gap equation at two-loop

In this section, we will derive the gap equation at the two-loop level. Start with the two-loop effective potential

$$
\begin{aligned}
V_{\rm eff} \,=\, & N_c \left[\int d^4x\, T(x)\, \bar{T}(x)\, \frac{(x^2+L^2)^{\frac{3}{2}}}{\lambda} - \int \frac{d^4k}{(2\,\pi)^4}\, \ln\left(1+\frac{T(k)\,\bar{T}(k)}{k^2}\right)\right] \\
& - \lambda \int \frac{d^4k}{(2\,\pi)^4} \int \frac{d^4p}{(2\,\pi)^4} \frac{G(p-k,\,L)}{\Big[\,k^2+T(k)\,\bar{T}(k)\,\Big]}\, \frac{2\,p\cdot k}{\Big[p^2+T(p)\,\bar{T}(p)\,\Big]}\,. \qquad \text{(C.1)}
\end{aligned}
$$

The functional derivative of $V_{\rm eff}$ with respect to $\bar{T}(q)$ gives the gap equation

$$
\begin{aligned}
\frac{\delta\, V_{\rm eff}}{\delta\,\bar{T}(q)} \,=\, & \frac{\delta}{\delta\,\bar{T}(q)} \Bigg\{ N_c \int d^4x\, T(x) \int \frac{d^4k}{(2\,\pi)^4}\, e^{-ik\cdot x}\, \bar{T}(k)\, \frac{(x^2+L^2)^{\frac{3}{2}}}{\lambda} \\
& - N_c \int \frac{d^4k}{(2\,\pi)^4}\, \ln\left(1+\frac{T(k)\,\bar{T}(k)}{k^2}\right) \\
& - \lambda \int \frac{d^4k}{(2\,\pi)^4} \int \frac{d^4p}{(2\,\pi)^4} \frac{G(p-k,\,L)}{\Big[\,k^2+T(k)\,\bar{T}(k)\,\Big]}\, \frac{2\,p\cdot k}{\Big[p^2+T(p)\,\bar{T}(p)\,\Big]} \Bigg\}, \\
= \, & \frac{N_c}{\lambda} \int d^4x\, T(x) \int \frac{d^4k}{(2\,\pi)^4}\, e^{-ik\cdot x}\, \delta^{(4)}(k-q)\, (x^2+L^2)^{\frac{3}{2}} \\
& - N_c \int \frac{d^4k}{(2\,\pi)^4}\, \frac{T(k)}{k^2+T(k)\,\bar{T}(k)}\, \delta^{(4)}(k-q) \\
& - \lambda \int \frac{d^4k}{(2\,\pi)^4} \int \frac{d^4p}{(2\,\pi)^4}\, 2\,p\cdot k\, G(p-k,\,L) \\
& \times \Bigg(- \frac{k^2\, T(p)\, \delta^{(4)}(p-q)}{\big[k^2+T(k)\,\bar{T}(k)\big]^2\, \big[p^2+T(p)\,\bar{T}(p)\big]^2} - \frac{T(k)\,\bar{T}(k)\,T(p)\,\delta^{(4)}(p-q)}{\big[k^2+T(k)\,\bar{T}(k)\big]^2\, \big[p^2+T(p)\,\bar{T}(p)\big]^2} \\
& \quad - \frac{T(p)\,\bar{T}(p)\,T(k)\,\delta^{(4)}(k-q)}{\big[k^2+T(k)\,\bar{T}(k)\big]^2\, \big[p^2+T(p)\,\bar{T}(p)\big]^2} - \frac{p^2\,T(k)\,\delta^{(4)}(k-q)}{\big[k^2+T(k)\,\bar{T}(k)\big]^2\, \big[p^2+T(p)\,\bar{T}(p)\big]^2} \Bigg), \\
= \, & \frac{N_c}{\lambda\,(2\,\pi)^4} \int d^4x\, e^{-iq\cdot x}\, \frac{T(x)}{G(x,L)} - \frac{N_c}{(2\,\pi)^4}\, \frac{T(q)}{q^2+T(q)\,\bar{T}(q)} \\
& + 2\,\frac{\lambda}{(2\,\pi)^4} \int \frac{d^4k}{(2\,\pi)^4}\, \frac{2\,q\cdot k\; G(q-k,\,L)\, k^2\, T(q)}{\big[k^2+T(k)\,\bar{T}(k)\big]^2\, \big[q^2+T(q)\,\bar{T}(q)\big]^2} \\
& + 2\,\frac{\lambda}{(2\,\pi)^4} \int \frac{d^4k}{(2\,\pi)^4}\, \frac{2\,q\cdot k\; G(q-k,\,L)\, T(k)\,\bar{T}(k)\,T(q)}{\big[k^2+T(k)\,\bar{T}(k)\big]^2\, \big[q^2+T(q)\,\bar{T}(q)\big]^2}\,, \qquad \text{(C.2)}
\end{aligned}
$$

where we have used the symmetric property of the propagator $G(k,L)$ i.e. $G(k-p,L) = G(|k-p|\,,L) = G(|p-k|\,,L)$. One then obtains the E.O.M. $(\delta\, V_{\rm eff}/\delta\,\bar{T}(q)=0)$ as

$$
\begin{aligned}
& \frac{N_c}{\lambda} \int d^4x\, e^{-iq\cdot x}\, \frac{T(x)}{G(x,L)} - N_c\, \frac{T(q)}{q^2+T(q)\,\bar{T}(q)} \\
& \quad + 2\,\lambda \int \frac{d^4k}{(2\,\pi)^4}\, 2\,q\cdot k\, G(q-k,\,L)\, \frac{k^2\,T(q)}{\big[k^2+T(k)\,\bar{T}(k)\big]^2\, \big[q^2+T(q)\,\bar{T}(q)\big]^2}
\end{aligned}
$$

$$+2\,\lambda\int\frac{d^4k}{(2\,\pi)^4}\,2\,q\cdot k\,G(q-k,\,L)\,\frac{T(k)\,\bar{T}(k)\,T(q)}{\left[k^2+T(k)\,\bar{T}(k)\right]^2\left[q^2+T(q)\,\bar{T}(q)\right]^2}=0\,. \quad \text{(C.3)}$$

C.1 The $k^2 \gg T(k)\,\bar{T}(k)$ approximation

We will approximate the gap equation in two regimes. First when $k^2 \gg T(k)\,\bar{T}(k)$, eq. (C.3) becomes

$$\begin{aligned}\frac{N_c}{\lambda}\int d^4x\,e^{-iq\cdot x}\,\frac{T(x)}{G(x,L)}-\,N_c\,\frac{T(q)}{q^2}\\ +2\,\lambda\int\frac{d^4k}{(2\,\pi)^4}\,2\,q\cdot k\,G(q-k,\,L)\,\frac{k^2\,T(q)}{k^4\,q^4}\\ +2\,\lambda\int\frac{d^4k}{(2\,\pi)^4}\,2\,q\cdot k\,G(q-k,\,L)\,\frac{T(k)\,\bar{T}(k)\,T(q)}{k^4\,q^4}=0. \quad \text{(C.4)}\end{aligned}$$

Multiply by q^4 and neglect the last term in the left-hand side, we obtain

$$\frac{N_c\,q^4}{\lambda}\int d^4x\,e^{-iq\cdot x}\,\frac{T(x)}{G(x,L)}-\,N_c\,q^2T(q)+\,2\,\lambda\int\frac{d^4k}{(2\,\pi)^4}\,2\,q\cdot k\,G(q-k,\,L)\,\frac{T(q)}{k^2}=0 \quad \text{(C.5)}$$

The last term represents the non-local screening effect of the scalar which is N_c-suppressed comparing to the other terms. If we neglect the screening effect and Fourier transform the rest, the one-loop gap equation is recovered,

$$\nabla^2\left(\frac{T(x)}{G(x,L)}\right)+\lambda T(x)=0, \quad \text{(C.6)}$$

where ∇^2 is the Euclidean Laplacian in 4 dimensions.

C.2 The $T(k)\,\bar{T}(k) \gg k^2$ approximation

Next, we consider to the low momentum regime i.e. $T(k)\,\bar{T}(k) \gg k^2$, the E.O.M. in this limit is given by

$$\begin{aligned}\frac{N_c}{\lambda}\int d^4x\,e^{-iq\cdot x}\,\frac{T(x)}{G(x,L)}-\,N_c\,\frac{T(q)}{T(q)\,\bar{T}(q)}\\ +2\,\lambda\int\frac{d^4k}{(2\,\pi)^4}\,2\,q\cdot k\,G(q-k,\,L)\,\frac{k^2\,T(q)}{\left[T(k)\,\bar{T}(k)\right]^2\left[T(q)\,\bar{T}(q)\right]^2}\\ +2\,\lambda\int\frac{d^4k}{(2\,\pi)^4}\,2\,q\cdot k\,G(q-k,\,L)\,\frac{T(k)\,\bar{T}(k)\,T(q)}{\left[T(k)\,\bar{T}(k)\right]^2\left[T(q)\,\bar{T}(q)\right]^2}=0. \quad \text{(C.7)}\end{aligned}$$

Neglecting the third term in the left-hand side, the gap equation becomes

$$\frac{N_c}{\lambda}\int d^4x\,e^{-iq\cdot x}\,\frac{T(x)}{G(x,L)}=\,N_c\,\frac{1}{\bar{T}(q)}-\,2\,\lambda\int\frac{d^4k}{(2\,\pi)^4}\,\frac{2\,q\cdot k\,G(q-k,\,L)}{T(k)\,\bar{T}(k)\,T(q)\,\bar{T}(q)}\,\frac{1}{\bar{T}(q)}\,. \quad \text{(C.8)}$$

The last term on the right-hand side represents the non-local screening effect of the scalar which is N_c-suppressed. Again, the one-loop gap equation is recovered when the screening effect is neglected.

The gap equation at one-loop level is solved in ref. [27] as given in eq. (3.10). We use this approximate solution in the evaluation of the effective potential.

D Evaluation of the 2-loop angle integration

We will integrate out the internal angle of Euclidean 4-dimension, we start with the two-loop effective potential,

$$
\begin{aligned}
V_{2-\rm loop} &= -4\pi^2\lambda\, N_f \int \frac{d^4k_E}{(2\,\pi)^4}\,\frac{1}{\Big[\,k_E^2 + T(k_E)\,\bar{T}(k_E)\,\Big]} \int \frac{d^4p_E}{(2\,\pi)^4}\,\frac{2\,p_E\cdot k_E}{\Big[p_E^2 + T(p_E)\,\bar{T}(p_E)\,\Big]}\,\frac{e^{-\,L\,\Big|\,p_E - k_E\,\Big|}}{\Big|\,p_E - k_E\,\Big|} \\
&= -\frac{4\pi^2\lambda\, N_f}{(2\,\pi)^8}\int_0^{\Lambda} dk_E\,\frac{(2\,\pi^2)\,k_E^4}{\Big[\,k_E^2 + T(k_E)\,\bar{T}(k_E)\,\Big]} \\
&\qquad \int_0^{\Lambda} dp_E \int_0^{\pi} d\theta\,\frac{2\,(4\,\pi)\,p_E^4\,\sin^2\theta\,\cos\theta}{\Big[p_E^2 + T(p_E)\,\bar{T}(p_E)\,\Big]}\,\frac{e^{-\,L\,\sqrt{p_E^2 - 2\,p_E\,k_E\,\cos\theta + k_E^2}}}{\sqrt{p_E^2 - 2\,p_E\,k_E\,\cos\theta + k_E^2}} \\
&= -\frac{\lambda\, N_f}{4\,L^5\,\pi^3}\int_0^{L\,\Lambda} d(L\,k_E)\,\frac{(L\,k_E)^4}{\Big[\,(L\,k_E)^2 + L^2\,T(k_E)\,\bar{T}(k_E)\,\Big]} \\
&\quad \times \int_0^{L\,\Lambda} d(L\,p_E)\,\frac{(L\,p_E)^4}{\Big[(L\,p_E)^2 + L^2\,T(p_E)\,\bar{T}(p_E)\,\Big]} \\
&\qquad \times \int_{-1}^{1} d(\cos\theta)\;\cos\theta\,\sqrt{1-\cos^2\theta}\,\frac{e^{-\,\sqrt{(L\,p_E)^2 - 2\,(L\,p_E)\,(L\,k_E)\,\cos\theta + (L\,k_E)^2}}}{\sqrt{(L\,p_E)^2 - 2\,(L\,p_E)\,(L\,k_E)\,\cos\theta + (L\,k_E)^2}} \\
&= -\frac{\lambda\, N_f}{4\,L^5\pi^3}\int_0^{L\,\Lambda} d\tilde{k}_E\,\frac{\tilde{k}_E^4}{\Big[\,\tilde{k}_E^2 + L^2\,T(k_E)\,\bar{T}(k_E)\,\Big]} \int_0^{L\,\Lambda} d\tilde{p}_E\,\frac{\tilde{p}_E^4}{\Big[\tilde{p}_E^2 + L^2\,T(p_E)\,\bar{T}(p_E)\,\Big]} \\
&\qquad \times \int_{-1}^{1} dx\;x\,\sqrt{1-x^2}\,\frac{e^{-\,\sqrt{A - B\,x}}}{\sqrt{A - B\,x}}\,, \qquad\qquad (D.1)
\end{aligned}
$$

where $\tilde{k}_E \equiv L\,k_E\,,\ \tilde{p}_E \equiv L\ p_E\,,\ A \equiv \tilde{p}_E^2 + \tilde{k}_E^2\,,\ B \equiv 2\,\tilde{p}_E\,\tilde{k}_E\,.$

Expanding function $\frac{e^u}{u} = \frac{1}{u}\,\sum_{n=0}^{\infty}\frac{u^n}{n!}$ gives

$$
\begin{aligned}
V_{2-\rm loop} &= -\frac{\lambda\, N_f}{4\,L^5\pi^3}\int_0^{L\,\Lambda} d\tilde{k}_E\,\frac{\tilde{k}_E^4}{\Big[\,\tilde{k}_E^2 + L^2\,T(k_E)\,\bar{T}(k_E)\,\Big]} \int_0^{L\,\Lambda} d\tilde{p}_E\,\frac{\tilde{p}_E^4}{\Big[\tilde{p}_E^2 + L^2\,T(p_E)\,\bar{T}(p_E)\,\Big]} \\
&\qquad \times \int_{-1}^{1} dx\;x\,\sqrt{1-x^2}\;\frac{1}{\sqrt{A - B\,x}}\,\sum_{n=0}^{\infty}\frac{(-1)^n}{n\,!}\,\Big(\sqrt{A - B\,x}\Big)^n\,, \\
&= -\frac{\lambda\, N_f}{4\,L^5\pi^3}\int_0^{L\,\Lambda} d\tilde{k}_E\,\frac{\tilde{k}_E^4}{\Big[\,\tilde{k}_E^2 + L^2\,T(k_E)\,\bar{T}(k_E)\,\Big]} \int_0^{L\,\Lambda} d\tilde{p}_E\,\frac{\tilde{p}_E^4}{\Big[\tilde{p}_E^2 + L^2\,T(p_E)\,\bar{T}(p_E)\,\Big]} \\
&\qquad \times \sum_{n=0}^{\infty}\frac{(-1)^n}{n\,!}\int_{-1}^{1} dx\;x\,\sqrt{1-x^2}\;(A - B\,x)^{\frac{n-1}{2}}\,, \\
&= -\frac{\lambda\, N_f}{4\,L^5\pi^3}\int_0^{L\,\Lambda} d\tilde{k}_E\,\frac{\tilde{k}_E^4}{\Big[\,\tilde{k}_E^2 + L^2\,T(k_E)\,\bar{T}(k_E)\,\Big]} \int_0^{L\,\Lambda} d\tilde{p}_E\,\frac{\tilde{p}_E^4}{\Big[\tilde{p}_E^2 + L^2\,T(p_E)\,\bar{T}(p_E)\,\Big]}
\end{aligned}
$$

$$\times \sum_{n=0}^{\infty} \frac{(-1)^n}{n\,!} \Bigg\{ -\frac{\pi\,(n-1)\,A^{\frac{n-3}{2}}}{(n+3)\,(n+5)\,B} \times \Bigg[2\,(A^2-B^2)\;{}_2F_1\Big(\frac{3-n}{4},\frac{5-n}{4};1;\frac{B^2}{A^2}\Big) + \big(B^2\,(n+2)-2\,A^2\big)\;{}_2F_1\Big(\frac{3-n}{4},\frac{5-n}{4};2;\frac{B^2}{A^2}\Big)\Bigg]\Bigg\}, \tag{D.2}$$

where ${}_2F_1(a,b;c;z)$ is the hypergeometric function.

References

[1] J. Goldstone, *Field Theories with Superconductor Solutions*, *Nuovo Cim.* **19**, 154 (1961).

[2] C. Vafa and E. Witten, *Restrictions on Symmetry Breaking in Vector-Like Gauge Theories*, *Nucl. Phys. B* **234**, 173 (1984).

[3] J. Beringer *et al.* [Particle Data Group Collaboration], *Review of Particle Physics (RPP)*, *Phys. Rev. D* **86**, 010001 (2012).

[4] M. Gell-Mann and MLevy, *The axial vector current in beta decay*, *Nuovo Cim.* **16**, 705 (1960).

[5] M. L. Goldberger and S. B. Treiman, *Decay of the pi meson*, *Phys. Rev.* **110**, 1178 (1958).

[6] M. Gell-Mann, R. J. Oakes and B. Renner, *Behavior of current divergences under SU(3) x SU(3)*, *Phys. Rev.* **175**, 2195 (1968).

[7] J. Gasser and H. Leutwyler, *Chiral Perturbation Theory to One Loop*, *Annals Phys.* **158**, 142 (1984).

[8] S. Scherer, *Introduction to chiral perturbation theory*, *Adv. Nucl. Phys.* **27**, 277 (2003) [hep-ph/0210398].

[9] H. Leutwyler, *On the foundations of chiral perturbation theory*, *Annals Phys.* **235**, 165 (1994) [hep-ph/9311274].

[10] Y. Nambu and G. Jona-Lasinio, *Dynamical Model of Elementary Particles Based on an Analogy with Superconductivity. 1.*, *Phys. Rev.* **122**, 345 (1961).

[11] U. Vogl and W. Weise, *The Nambu and Jona Lasinio model: Its implications for hadrons and nuclei*, *Prog. Part. Nucl. Phys.* **27**, 195 (1991).

[12] S. P. Klevansky, *The Nambu-Jona-Lasinio model of quantum chromodynamics*, *Rev. Mod. Phys.* **64**, 649 (1992).

[13] T. Hatsuda and T. Kunihiro, *QCD phenomenology based on a chiral effective Lagrangian*, *Phys. Rept.* **247**, 221 (1994) [hep-ph/9401310].

[14] M. Buballa, *NJL model analysis of quark matter at large density*, *Phys. Rept.* **407**, 205 (2005) [hep-ph/0402234].

[15] V. A. Miransky, *Dynamical symmetry breaking in quantum field theories*, World Scientific, Singapore (1993).

[16] W. A. Bardeen, C. T. Hill and M. Lindner, *Minimal Dynamical Symmetry Breaking of the Standard Model*, *Phys. Rev. D* **41**, 1647 (1990).

[17] C. T. Hill and E. H. Simmons, *Strong dynamics and electroweak symmetry breaking*, *Phys. Rept.* **381**, 235 (2003) [Erratum-ibid. **390**, 553 (2004)] [hep-ph/0203079].

[18] G. Ripka, *Quarks bound by chiral fields*, Oxford University Press, (1997).

[19] R. D. Bowler and M. C. Birse, *A Nonlocal, covariant generalization of the NJL model*, *Nucl. Phys. A* **582**, 655 (1995) [hep-ph/9407336].

[20] E. Ruiz Arriola and L. L. Salcedo, *Chiral and scale anomalies of nonlocal Dirac operators*, *Phys. Lett. B* **450** (1999) 225 [hep-th/9811073].

[21] B. Golli, W. Broniowski and G. Ripka, *Solitons in a chiral quark model with nonlocal interactions*, *Phys. Lett. B* **437**, 24 (1998) [hep-ph/9807261].

[22] M. B. Parappilly, P. O. Bowman, U. M. Heller, D. B. Leinweber, A. G. Williams and J. B. Zhang, *Scaling behavior of quark propagator in full QCD*, *Phys. Rev. D* **73**, 054504 (2006) [hep-lat/0511007].

[23] R. S. Plant and M. C. Birse, *Meson properties in an extended nonlocal NJL model*, *Nucl. Phys. A* **628** (1998) 607 [hep-ph/9705372];

[24] I. General, D. Gomez Dumm and N. N. Scoccola, *Chiral phase transition in a covariant nonlocal NJL model*, *Phys. Lett. B* **506**, 267 (2001) [hep-ph/0010034];

[25] T. Sakai and S. Sugimoto, *Low energy hadron physics in holographic QCD*, *Prog. Theor. Phys.* **113**, 843 (2005) [hep-th/0412141].

[26] T. Sakai and S. Sugimoto, *More on a holographic dual of QCD*, *Prog. Theor. Phys.* **114**, 1083 (2005) [hep-th/0507073].

[27] E. Antonyan, J. A. Harvey, S. Jensen and D. Kutasov, *NJL and QCD from string theory*, arXiv:hep-th/0604017.

[28] J. A. Harvey, *Chiral symmetry breaking and intersecting D-brane systems*, *Nucl. Phys. Proc. Suppl.* **171**, 243 (2007).

[29] A. Dhar and P. Nag, *Intersecting branes and Nambu−Jona-Lasinio model*, *Phys. Rev. D* **79**, 125013 (2009) [arXiv:0901.4942 [hep-th]].

[30] J. F. Donoghue, E. Golowich and B. R. Holstein, *Dynamics of the standard model*, Cambridge Universe Press (1992).

[31] R. Jackiw, *Functional evaluation of the effective potential*, *Phys. Rev. D* **9**, 1686 (1974).

[32] H. Kleinert, *Particles and Quantum Fields (chapter 15)*, http://users.physik.fu-berlin.de/ kleinert/b6/psfiles/Chapter-15-direffac.pdf.

Hindawi Publishing Corporation
Advances in High Energy Physics
Volume 2011, Article ID 123184, 40 pages
doi:10.1155/2011/123184

Review Article

Holographic Multiquarks in the Quark-Gluon Plasma: A Review

Piyabut Burikham[1,2] and Ekapong Hirunsirisawat[1]

[1] *Theoretical High-Energy Physics and Cosmology Group, Department of Physics, Faculty of Science, Chulalongkorn University, Bangkok 10330, Thailand*
[2] *Thailand Center of Excellence in Physics, CHE, Ministry of Education, Bangkok 10400, Thailand*

Correspondence should be addressed to Piyabut Burikham, piyabut@gmail.com

Received 1 July 2011; Accepted 23 September 2011

Academic Editor: Ian Jack

We review the holographic multiquark states in the deconfined quark-gluon plasma. Nuclear matter can become deconfined by extremely high temperature and/or density. In the deconfined nuclear medium, bound states with colour degrees of freedom are allowed to exist. Using holographic approach, the binding energy and the screening length of the multiquarks can be calculated. Using the deconfined Sakai-Sugimoto model, the phase diagram of the multiquark phase, the vacuum phase, and the chiral-symmetric quark-gluon plasma can be obtained. Then we review the magnetic properties of the multiquarks and their phase diagrams. The multiquark phase is compared with the pure pion gradient, the magnetized vacuum, and the chiral-symmetric quark-gluon plasma phases. For moderate temperature and sufficiently large density at a fixed magnetic field, the mixed phase of multiquark and pion gradient is the most energetically preferred phase.

1. Introduction

At low energy, only hadrons can be observed. Due to the large coupling of the strong interaction on large distance scale, the genuine constituents of the nuclear matter are confined within the baryons and mesons. They can be explored only with a high energy probe, for example, in the deep inelastic scattering (DIS) experiments. When the energy scale involved is sufficiently large, roughly few hundred MeVs, the interaction among quarks and gluons become perturbatively weak, the phenomenon known as the asymptotic freedom. The quarks and gluons subsequently become "deconfined" from the confinement of the strong interaction.

For effectively free quarks and gluons, perturbative treatment of the Quantum Chromodynamics (QCD) has been proven very successful in making verifiable quantitative and reliable predictions. The QCD background calculations of the scattering of quarks

and gluons at the Tevatron give accurate and vital results, which are crucial in providing the benchmark for the search of New Physics beyond the Standard Model. Nevertheless, unexpected ridge-like signals related to the strong interaction are already observed from the collision of proton and proton at the Large Hadron Collider (LHC) [1]. Further investigations are required in order to determine whether this ridge structure could be explained by the perturbative QCD or if it is nonperturbative in nature.

A general picture of the deconfinement process of the quarks and gluons within hadrons is currently incomplete at the most. Naively, from argument of the RGE (Renormalization Group Equation) running of the beta function, effectively free quarks and gluons are expected to appear at high energies and/or temperatures. Transition from nonperturbative phase of nuclear matter to the perturbative regime, where the perturbative QCD is reliable, is explored most successfully in the lattice approach. Lattice studies of the QCD predicts the deconfinement temperature around 175 MeV [2]. Nuclear matter at such temperature would undergo a phase transition into a deconfined phase called the quark-gluon plasma (QGP). Most bound states of light quarks would melt down at this temperature leaving free quarks and gluons in the plasma. Remarkably, the mesonic states of heavy quarks (e.g., charmonium) in the nuclear matter at such high temperature tend to persist melting at least until $1.5T_c$ [3–5] due to the remaining screened Coulomb-type binding potential between quark and antiquark. Multiquark states such as baryons can also exist in the QGP up to certain temperatures provided that the baryonic charge density is sufficiently large.

In the confined phase, only colour singlet states can exist as free particle due to the confinement. Above the deconfinement, quarks and gluons with colour charges can propagate with more freedom in the plasma. It is therefore possible that the coloured multiquark states such as diquarks could also exist in the deconfined nuclear medium. Similar to the mesonic states of the heavy quarks, these multiquarks could persist melting up to relatively high temperature above the deconfinement. We can expect the multiquarks to be abundant in the nuclear matter when the density is large up to temperature well above the deconfinement temperature. Consequently, it is interesting to investigate the physical properties of the multiquarks as well as their thermodynamical phase diagram in details. Unfortunately, perturbative QCD based on quarks and gluons is not reliable during the deconfinement phase transition. Lattice QCD is applicable only when the baryon density is small.

An alternative approach to study the strongly coupled gauge theory is the holographic model based on the AdS/CFT correspondence [6, 7]. A string theory in the curved background generated by D-branes source is conjectured to be dual to the gauge theory on the branes. The duality suggests a correspondence between the strongly coupled gauge theory on the branes and the weakly coupled string theory in the bulk. Extension of the duality to the finite temperature gauge theory can be done by adding a black hole horizon to the near-horizon limit of the background spacetime [8]. Baryons and multiquarks can be holographically constructed using the baryon vertex and strings [9–12].

In this paper, we will review the physics of the holographic multiquarks in the quark-gluon plasma using mainly the Sakai-Sugimoto (SS) model [13, 14]. The SS model and the holographic setup of the multiquarks is discussed in Section 2. Section 3 describes the thermodynamical properties and the phase diagram of the multiquark nuclear phase. Magnetic properties of the multiquark phase and the corresponding phase diagram are discussed in Sections 4 and 5, respectively. Section 6 concludes our paper. To present the main results of this paper, a summary table of the deconfined nuclear phase in the SS model is given in Table 1.

Table 1: Summary table of the phases in the deconfined Sakai-Sugimoto model, B represents the external magnetic field.

$B = 0$	vacuum	Multiquark (MQ)		χS-QGP
Region in parameter space	$d = 0$ (i.e., $\mu < \mu_{\text{source}}$)	$d > 0$ (i.e., $\mu \geq \mu_{\text{source}}$) $0 \leq n_s \lesssim 0.3$		$d > 0$
Preferred at	low μ, low T	High μ, low T		high T
Important properties	Mixing of different n_s-multiquarks			
$B \neq 0$	magnetized vacuum	$\nabla\varphi$	MQ-$\nabla\varphi$	χS-QGP
Region in parameter space	$\mu_{\text{source}} = 0$ $\nabla\varphi = 0$ $d = 0$ $j_A = 0$	$\mu_{\text{source}} = 0$ $\nabla\varphi > 0$ $d = (3/2)B\nabla\varphi$ $j_A = 0$	$\mu_{\text{source}} > 0$ $\nabla\varphi > 0$ $d > 0$ ($\mu \geq \mu_{\text{source}}$) $j_A = 0$ $0 \leq n_s \lesssim 0.3$	$\mu_{\text{source}} = 0$ $\nabla\varphi = 0$ $d > 0$ $j_A = (3/2)B\mu$
Preferred at	none	Low μ, low T	High μ, low T	High T
Important properties			Configuration **A**, **B** merging at high T and/or high B	

2. Multiquark States and the Holographic Models

In addition to baryons and mesons, the possibility of multiquark states were recognized by Gell-Mann since the proposal of the quark model. $Q^m\overline{Q}^n$-multiquark ($n + m > 3$) such as the tetraquark and dibaryon were proposed since 1977 by Jaffe [15–17] using the MIT bag model. There are theoretical models of colour-singlet multiquarks using interactions of various origins, for example, chromomagnetism, flux tube confinement, and hadronic molecules. Despite the theoretical possibilities, conclusive discovery of the multiquarks has yet to be confirmed experimentally (see [18] and references therein).

Series of experimental results from RHIC suggests that the produced QGP is strongly coupled (sQGP) [19–22]. The fact that the QGP is strongly coupled near-and-above the deconfinement temperature T_c suggests the possibility of the existence of exotic bound states with colour degrees of freedom in the deconfined QGP. Recall that an interaction between two heavy quarks in the confined phase at $0 < T < T_c$ can be described empirically by the screened Cornell potential

$$V_{Q\overline{Q}}(r,T) = \sigma r\left[\frac{1-e^{-M_D(T)r}}{M_D(T)r}\right] - \frac{\alpha}{r}\left[e^{-M_D(T)r}\right], \tag{2.1}$$

where M_D is the Debye screening mass depending on T and α is the effective coupling. The first part represents the (colour-screened) confining force due to QCD string with the effective string tension σ; it is around $0.20\,(\text{GeV})^2$ as suggested by the lattice studies. The second part represents the effective (colour-screened) Coulomb potential due to transverse string oscillation. By definition, the effective string tension σ vanishes at $T > T_c$. As a result, only the screened Coulomb part contributes to the interaction between quarks but within the range of screening length M_D^{-1}. Yet, as suggested by [23], a short string-like configuration of

colour fields at low T becomes longer strings at-and-near T_c which contribute to the binding between quarks and gluons. Therefore, the bound states of gluons and quarks can exist in both colour-singlet and colour-nonsinglet forms in the sQGP.

The studies of the multibody bound states in the sQGP were initiated by Shuryak and colleagues [23–25]. Based on the studies in [23], three proposed multibody bound states: (i) diquark or "polymer-chain" ($\bar{q}gg\cdots gq$); (ii) baryons (qqq); (iii) closed (3-)chains of gluons (ggg) seem to exist only for $T = (1\text{–}1.5)T_c$. Importantly, the existence of these bound states could affect the thermodynamical and hydrodynamical properties of the sQGP.

The holographic models of colour-singlet baryon was originally investigated by Witten et al. [9, 10]. In the $AdS_5 \times S^5$ background, a D5-brane wrapping the subspace S^5 with N_c strings attached is proposed to be a dual description of a baryon. A holographic dual of a k-quark ($k < N_c$) with colour degrees of freedom is discussed in [11] (see also [26]) for the supersymmetric background. There is a number of interesting articles investigating various possibilities of the multiquarks in both confined and deconfined medium, some of them consider deformed baryon vertex [12, 27–33]. Notably, [12] uses a simplified configuration with only one point-like baryon vertex to describe a variety of classes of the multiquarks with and without the colour degrees of freedom. We will focus our attention to such multiquark model in this paper.

In recent years, the AdS/CFT correspondence has attracted interests in its applicability to the phenomenological studies of non-perturbative QCD. However, this correspondence cannot provide the gravity dual of the large N_c QCD. As its name suggests, the AdS/CFT have the gauge theory side, which is conformal, differing from the confining behaviour of the real-world QCD. There has been many attempts to engineer the holographic model whose the confining feature is taken into account [8, 34–36].

One natural way is to consider a stack of N_c D4-branes, in Type IIA string theory, whose the world volume possesses one compact spatial direction [8]. In the near-horizon metric of a near-extremal D4-brane, the compactified spatial circle shrinks to zero size at some finite value of the radial direction representing a smooth cutoff of the spacetime. This feature can provide us with the confining spacetime background in which the potential between a holographic quark-antiquark bound state is mainly contributed by the tension of string lying along the "hard-wall." Consequently, the potential is linearly proportional to the separation between two ends of the string resulting in the confinement of quarks and antiquarks in the dual gauge theory.

At finite temperature, the time coordinate becomes Wick-rotated, and the asymptotic circumference of the time circle equals to the inverse of the temperature, T^{-1}. Consequently, the confining spacetime background at finite temperature has two compact directions. The metric of the geometry then can be written as

$$ds^2 = \left(\frac{u}{R_{\mathrm{D4}}}\right)^{3/2}\left[\delta_{ij}\,dx^i dx^j + d\theta_1^2 + f(u)d\theta_2^2\right] + \left(\frac{R_{\mathrm{D4}}}{u}\right)^{3/2}\left[\frac{du^2}{f(u)} + u^2 d\Omega_4\right], \tag{2.2}$$

where θ_1 is the Euclidean time with temperature dependent period $\delta\theta_1 = \beta \equiv T^{-1}$, θ_2 is the compact spatial circle with period $\delta\theta_2 \equiv (4\pi/3)(R^{3/2}/u_\Lambda^{1/2})$, and $f(u) \equiv 1 - (u_\Lambda/u)^3$. Notice that $f(u)$ equals zero for $u = u_\Lambda$ but equals one as u approaches infinity. This $f(u)$ factor renders the $\theta_2 - u$ subspace a cigar-like shape, while the $\theta_1 - u$ subspace has a cylindrical shape. However, there is an alternative supergravity solution whose the time and the compact spatial coordinates exchange the role. That is, θ_1 is the compact spatial coordinate with fixed

Table 2: Brane configuration of the Sakai-Sugimoto model.

	0	1	2	3	4	5	6	7	8	9
N_c D4	o	x	x	x	o					
N_f D8($\overline{\text{D8}}$)	o	x	x	x		x	x	x	x	x

circumference, θ_2 is the Euclidean time with period $\delta\theta_2 = \beta = (4\pi/3)(R^{3/2}/u_T^{1/2})$, and $f(u) \equiv 1 - (u_T/u)^3$. In other words, there are two geometries which can be the supergravity solution. The comparison of the free energy between these two competing geometries tells us about the deconfinement phase transition in the gauge theory side. It is important to emphasize that the asymptotic circumference of the time circle can be variable depending on the temperature, namely, $\delta\theta_1 = T^{-1}$, while the θ_2-circle has a fixed circumference. As a result, the phase transition occurs once the asymptotic circumferences of the two circles become the same in both geometries such that they have the same value of free energy. This gives rise to the deconfinement transition line in the $T - \mu$ phase diagram of the holographic nuclear matter [8, 37]. For a concise review, see [38].

2.1. The Sakai-Sugimoto Model

More realistic holographic dual of the large N_c QCD is the Sakai-Sugimoto (SS) model [13, 14]. The brane construction of the SS model is a stack of N_c D4 branes intersecting with N_f D8- and N_f anti-D8-branes, where $N_f \ll N_c$ such that the presence of the probe branes D8/anti-D8-branes does not affect the D4 background. This is called the probe limit, corresponding to the quenched approximation in the lattice QCD.

Stack of N_f D8 and $\overline{\text{D8}}$ branes are introduced as the flavour branes. They are located at separation distance L_0 along the compactified x_4 direction at the boundary $u \to \infty$. Open-string excitation with one end on the flavour branes behave like a chiral "quark." In the setup where D8 and $\overline{\text{D8}}$ are parallel in the (x_4, u) projection, each chiral excitation on each stack of branes transform independently, therefore the theory has a chiral symmetry. For the setup where D8 and $\overline{\text{D8}}$ connect, forming a U-shape or a V-shape configuration in the (x_4, u) projection, chiral symmetry is broken.

To obtain a SUSY broken QCD at low energy, the boundary conditions of the superpartners in the x_4 direction are chosen so that the zeroth modes vanish (Scherk-Schwarz mechanism). For energies below the first KK modes, the gauge theory therefore contains only gluons and chiral quarks. If the number of the stack of D4-branes source N_c is chosen to be 3, this low-energy gauge theory will look exactly like QCD. The brane configuration of the SS model is shown in Table 2.

Note that the "x" sign signifies that the coordinate is occupied by an infinite extending direction of the D-brane world volume and the "o" sign means that the coordinate is occupied by a compact direction of the D-brane world volume. This holographic model is a QCD-like theory in many aspects. (i) It is nonsupersymmetric resulting from the antiperiodicity for superpartners around the x^4 circle. (ii) It has the confining behaviour and the deconfinement phase transition in the same way as mentioned above. In the confined phase, the x^4 coordinate is the cigar-like compact direction and x^0 (the Euclidean time) is the cylindrical compact direction. In the deconfined phase, the two coordinates exchange their roles. To summarize, the coordinates θ_1 and θ_2 in (2.2) can be specified in the confined and deconfined phase as shown in Table 3.

Table 3: Geometric assignment of the compactified bulk coordinates in the Sakai-Sugimoto model.

	Confined phase ($T < T_{\text{deconf}}$)	Deconfined phase ($T > T_{\text{deconf}}$)
θ_1	x^0	x^4
θ_2	x^4	x^0
$f(u)$	$1-(u_\Lambda/u)^3$	$1-(u_T/u)^3$

(iii) It has dynamical quarks resulting from the presence of the flavour branes. (iv) The phases of chiral symmetry breaking and chiral symmetric quark-gluon plasma (χS-QGP) can be realized. There exist two configurations of the flavour D8- and anti-D8-branes, both satisfy the equation of motion. One is the connected configuration of the D8- and anti-D8-branes representing the chiral symmetry breaking phase. Another is the parallel configuration of the D8- and anti-D8-branes lying along the radial direction of the bulk spacetime representing the chiral symmetric phase. Note that $T_{\text{chiral}} = T_{\text{deconf}}$ when the separation between the D8- and anti-D8-branes $L_0 \gtrsim 0.97R$; $R \equiv$ the radius of the x_4 circle, while $T_{\text{deconf}} < T_{\text{chiral}}$ when $L_0 \lesssim 0.97R$ [37].

Since the SS model is the holographic model which gives exactly the particle content of the QCD at low energy, we will consider the holographic multiquarks in the deconfined SS model. The idea is to construct a gravity dual of the 5-dimensional gauge theory with chiral fermions which gives approximately the 4-dimensional QCD at low energy. The inevitable supersymmetry of the dual gauge theory in the string construction is broken at the position of the flavour branes used to introduce the chiral fermions. To construct the SS model, stack of D4-branes is used as the source to generate a curved background of the type IIA string theory. After taking the near-horizon limit and adding a black hole horizon, we arrive at the following background metric:

$$ds^2 = \left(\frac{u}{R_{\text{D4}}}\right)^{3/2}\left(f(u)dt^2 + \delta_{ij}\,dx^i dx^j + {dx_4}^2\right) + \left(\frac{R_{\text{D4}}}{u}\right)^{3/2}\left(u^2 d\Omega_4^2 + \frac{du^2}{f(u)}\right) \tag{2.3}$$

$$F_{(4)} = \frac{2\pi N_c}{V_4}\epsilon_4, \qquad e^{\phi} = g_s\left(\frac{u}{R_{\text{D4}}}\right)^{3/4}, \qquad R_{\text{D4}}^3 \equiv \pi g_s N_c l_s^3, \tag{2.4}$$

where $f(u) \equiv 1 - u_T^3/u^3$, $u_T = 16\pi^2 R_{\text{D4}}^3 T^2/9$. Note that the compact x_4 coordinate (x_4 transverse to the probe D8-branes), with arbitrary periodicity $2\pi R$, never shrinks to zero. The volume of the unit four-sphere Ω_4 is denoted by V_4 and the corresponding volume 4-form by ϵ_4. $F_{(4)}$ is the 4-form field strength, l_s is the string length, and g_s is the string coupling. The dilaton in this background has u-dependence, and its value changes along the radial direction u. This is a crucial difference in comparison to the AdS-Schwarzschild metric case where dilaton contribution is constant.

In the Sakai-Sugimoto model of D4-D8-branes construction, the D4-brane wrapping the S^4 is used as the baryon vertex. Remarkably, it was found that the baryon can also be realized as an instanton in the bulk of N_c D4-brane-induced background spacetime, corresponding to baryon in the Skyrme model on the gauge theory side. This instanton can be described in terms of the Chern-Simons action in the bulk. Therefore, these two pictures of baryon are equivalent.

A Dn-brane wrapping an internal subspace S^n accommodate a $U(1)$ which will couple to certain n-form field of the string background and becomes charged under the $U(1)$. To

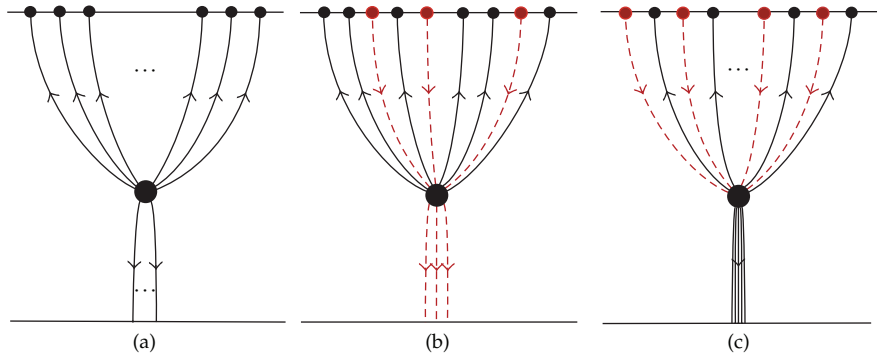

Figure 1: An illustration of the holographic multiquark states (a) k-baryon with $k_h = k < N_c$ and $k_r = N_c - k$, (b) $(N_c + \overline{k})$-baryon with $k_h = N_c + \overline{k}$ and $k_r = \overline{k}$, and (c) j-mesonance with $k_h = 2j$ and $k_r = N_c$.

cancel this charge for the entire background, a number of N_c strings emerging from the vertex is required. While a string emerging from the vertex contributes a negative $U(1)$ charge, a string entering the vertex in the opposite orientation contributes a positive unit of $U(1)$ charge. Therefore, as long as the number of strings emerging from the vertex subtracting the number of strings entering the vertex is N_c, the configuration is allowed to exist since the total charge of the background is still zero.

Based on the charge cancelation at the vertex, three classes of exotic multiquarks are proposed in [12]. Namely, they are k-baryons, $(N_c + \overline{k})$-baryon, and j-mesonance (strongly coupled bunch of mesons), corresponding to diquark, some exotic baryons such as pentaquark and a bunch of mesons, respectively. We parameterize k_h as the number of hanging strings which extends from the vertex to the boundary and k_r as the number of radial strings extending from the vertex to the horizon. Figure 1 shows 3 classes of the holographic multiquarks. Their conditions are summarized as the following.

For k-baryon,

$$k_h + k_r = N_c, \qquad k_h = k. \tag{2.5}$$

For $(N_c + \overline{k})$-baryon,

$$k_h - k_r = N_c, \qquad k_h = N_c + \overline{k}. \tag{2.6}$$

For j-mesonance,

$$k_h = 2j, \qquad k_r = N_c. \tag{2.7}$$

Note that the values of $\overline{k}$ and j can be as large as $N_c \times N_f$.

2.2. Force Balance Condition

Using the field background shown in the last section, the total action of these exotic multiquark states can be generally written as

$$S = S_{\mathrm{D4}} + k_h S_{\mathrm{F1}} + k_r \widetilde{S}_{\mathrm{F1}}. \tag{2.8}$$

The DBI action of D4-brane

$$S_{\mathrm{DBI}} = \int dx^0 d\xi^p T_p, \quad T_p = \left(e^{-\phi}(2\pi)^p \alpha'^{(p+1)/2}\right)^{-1} \sqrt{-\det(g)}, \tag{2.9}$$

and the Nambu-Goto action of k_h hanging strings and k_r radial strings can be written as

$$S_{\mathrm{D4}} = \frac{\tau N_c u_c \sqrt{f(u_c)}}{6\pi\alpha'}, \qquad S_{\mathrm{F1}} = \frac{\tau}{2\pi\alpha'} \int_0^L d\sigma \sqrt{u'^2 + f(u)\left(\frac{u}{R}\right)^3}, \qquad \widetilde{S}_{\mathrm{F1}} = \frac{\tau}{2\pi\alpha'}(u_c - u_{\mathrm{T}}), \tag{2.10}$$

respectively. Note that τ is the total time over which we evaluate the action and u_c is the position where the D4-brane vertex is located.

Now let us write the force condition. As will be seen later, this is the equilibrium condition for the existence of the multiquark states. Assume the vertex to be a point at the cusp position u_c that does not receive any distortion from the attached strings. The distortion of the baryon vertex due to the attached strings is discussed in details in [39, 40]. Because of the spherical symmetry of the configuration in the (x_1, x_2, x_3) subspace, the action is sensitive to only the variation in the holographic direction u. The variation of the action gives the volume term as well as the surface term. The equation of motion is obtained by requiring that the volume term and surface term vanishes separately. The volume term gives the Euler-Lagrange equation which determines the shape of the hanging strings. On the other hand, the surface term provides the equilibrium condition of the configuration at the tip u_c under the variation in the u direction, that is, the force balance condition at the cusp. It can be written as [12]

$$\frac{N_c}{3} G_0(x) - k_h B + k_r = 0, \tag{2.11}$$

where

$$G_0(x) \equiv \frac{1 + x^3/2}{\sqrt{1 - x^3}}, \qquad x \equiv \frac{u_T}{u_c} < 1, \qquad B \equiv \frac{u_c'}{\sqrt{u_c'^2 + f(u_c)(u_c/R_{\mathrm{D4}})^3}}. \tag{2.12}$$

Obviously, B is always less than one, thus we obtain the equilibrium condition

$$k_h > \frac{N_c}{3} G_0(x) + k_r. \tag{2.13}$$

Together with (2.5), (2.6), and (2.7), we obtain the lower bound of the hanging string parameter for each multiquark configuration as

for *k-baryon*,

$$k_h = k > \frac{N_c}{6}(G_0(x) + 3), \tag{2.14}$$

for $(N_c + \overline{k})$-*baryon*,

$$k_h = N_c + \overline{k} > \frac{N_c}{3} G_0(x) + \overline{k}, \tag{2.15}$$

for *j-mesonance*,

$$j > \frac{N_c}{6}(G_0(x) + 3). \tag{2.16}$$

Note that $G_0(x) = 1$ at $T = 0$ and it is an increasing function of the temperature.

2.3. Binding Energy and Screening Length

Theoretically, all of these bound states are allowed to exist. But a question arises which multiquark state is more stable than another. This can be addressed by considering the binding energies of each class of the multiquarks. Naturally, the binding energy of each of these holographic bound states is the total energy of the configuration subtracted by the energy of the free quarks. Similar to the calculation of Wilson loop in [41], the binding energy in the large N_c limit could be estimated to be the total classical action divided by τ.

The solution or the shape of the hanging strings can be obtained by using the Nambu-Goto action from (2.10), the regulated energy of the hanging strings (subtracted by energy of the free quarks) is

$$E_{\mathrm{F1}} = \frac{1}{2\pi}\int_0^L d\sigma \sqrt{u'^2 + \left(\frac{u}{R_{\mathrm{D4}}}\right)^3 f(u)} - \frac{1}{2\pi}\int_{u_T}^{\infty} du. \tag{2.17}$$

From the equilibrium condition corresponding to the surface term, that is, (2.11) and (2.12), we obtain

$$u_c'^2 = \frac{f(u_c)B^2}{1-B^2}\left(\frac{u_c}{R_{\mathrm{D4}}}\right)^3, \tag{2.18}$$

where

$$B = B(k_h, k_r, x) = \frac{N_c}{3k_h}G_0(x) + \frac{k_r}{k_h}. \tag{2.19}$$

Consider S_{F1} in (2.10), the Lagrangian,

$$\mathcal{L} = \sqrt{u'^2 + f(u)\left(\frac{u}{R}\right)^3}, \tag{2.20}$$

does not explicitly depend on σ, such that we can define the constant of motion

$$\mathcal{H} \equiv \mathcal{L} - u'\frac{\partial \mathcal{L}}{\partial u'} = \text{const.} \tag{2.21}$$

This leads to

$$\frac{f(u_c)(u_c/R_{\mathrm{D4}})^3}{\sqrt{u_c'^2 + f(u_c)(u_c/R_{\mathrm{D4}})^3}} = \frac{f(u)(u/R_{\mathrm{D4}})^3}{\sqrt{u'^2 + f(u)(u/R_{\mathrm{D4}})^3}}. \tag{2.22}$$

Eliminating u_c' using (2.18) and (2.22), we have the relation

$$u'^2 = \frac{f(u)^2(u/R_{\mathrm{D4}})^6}{f(u_c)(u_c/R_{\mathrm{D4}})^3(1-B^2)} - f(u)(u/R_{\mathrm{D4}})^3. \tag{2.23}$$

Using the above equation, we obtain the size of the radius of the multiquark state as

$$L = \frac{R_{\mathrm{D4}}^{3/2}}{u_c^{1/2}} \int_1^\infty dy \sqrt{\frac{(1-x^3)(1-B^2)}{(y^3-x^3)(y^3-x^3-(1-x^3)(1-B^2))}}, \tag{2.24}$$

and together with (2.17), we also have

$$E_{\mathrm{F1}} = \frac{u_c}{2\pi}\left\{\int_1^\infty dy \left[\sqrt{\frac{y^3-x^3}{(y^3-x^3)-(1-x^3)(1-B^2)}}-1\right]-(1-x)\right\}. \tag{2.25}$$

Therefore, the total energy of the vertex D-brane and the radial strings are

$$\begin{aligned} E &= \frac{N_c u_T}{2\pi}\left(\frac{\sqrt{1-x^3}}{3x}+\left(\frac{k_h}{N_c}\right)\frac{\mathcal{E}}{x}+\left(\frac{k_r}{N_c}\right)\frac{1-x}{x}\right) \\ &\sim \frac{N_c^2}{L^2}, \end{aligned} \tag{2.26}$$

where $\mathcal{E}$ represents the terms within the brace of (2.25).

By numerical calculations, we compare the E/N_c (the energy per degrees of freedom) versus L (the size of radius of the bound states) of the 3 classes of the multiquark as in Figure 2. The deeper the binding energy is, the harder the multiquark will melt in the thermal bath. From Figure 2, the colour singlet N_c-baryon has deeper binding well than the $(k < N_c)$-baryon and $(N_c + \overline{k})$-baryon. As expected, the $(k < N_c)$-multiquark is bound more tightly as k gets larger. For $(N_c + \overline{k})$-baryon, the bound state is less tightly bound, as $\overline{k}$ increases. Similarly, a j-mesonance has the binding energy less than j mesonic states. It becomes closer to j mesons as j grows.

The screening length L^* can also be numerically calculated. It is defined to be the value at which the binding energies become zero from negative values at small distances. The numerical results, as shown in Figure 3, indicate that the multiquark states of all classes have smaller screening lengths as the temperature increases, with approximately $L^* \sim 1/T$ for a fixed k, $\overline{k}$, and j. Furthermore, L^* is larger as k and j increases for k-baryon and j-mesonance, respectively, while it is smaller as $\overline{k}$ increases for $(N_c+\overline{k})$-baryon. Interestingly, the saturation of j-mesonance's screening length occurs as $j \to \infty$, where $L^*_{j\text{-mesonance}}$ approaches the screening length of a meson L^*_{meson}.

3. Thermodynamic Properties of Holographic Multiquark

In the non-antipodal SS model, the holographic plasma can have two distinctive phase transitions; a deconfinement and the chiral symmetry restoration [37]. The deconfinement could occur at lower temperature than the chiral symmetry restoration. For the temperature in between the two transitions, quarks and gluons are deconfined from the confining flux tube but still interact strongly among each other through the remaining screened Coulomb-type $SU(N_c)$ potential. Therefore, it is possible to have the multiquark phase in the temperature

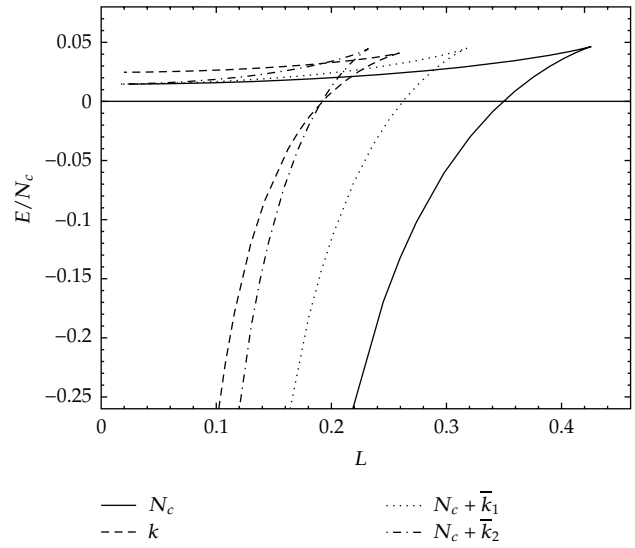

Figure 2: Comparison of the potential per N_c between N_c-baryon, k-baryon, and $(N_c + \overline{k})$-baryon for $k/N_c = 0.8$, $\overline{k_1}/N_c = 2/3$, and $\overline{k_2}/N_c = 2$ at temperature $T = 0.25$.

range between that of the deconfinement and the chiral phase transition. This is consistent, at least in a qualitative way, with the studies of the multibody bound states in the sQCD in the framework of the real QCD [23] mentioned in the previous section.

To actually understand the physics of deconfined QGP, it is thus crucial to investigate the thermodynamical properties of the holographic multiquark phase. In order to extract the thermodynamic potential from the gravity dual model, the path integral approach in quantum gravity [42] has been used. In this technique, the time direction is circled with period $\beta = 1/T$ in the same manner as the thermal circle in the finite temperature quantum field theory. As discussed in [43] based on the early works [44, 45], the grand canonical potential, or the Gibbs free energy, $\Omega(T, \mu)$ has the leading contribution from the classical Euclidean action of the bulk theory in the grand canonical ensemble, that is, $\Omega(T, \mu) \sim S_{\text{bulk}}^{\text{on-shell}}$. Similarly, the Helmholtz free energy $F(T, n_b)$ has the leading contribution from the Legendre transform with respect to the baryonic charge of the classical Euclidean action, that is, $F(T, n_b) \sim \widetilde{S}_{\text{bulk}}^{\text{on-shell}}$ in the canonical ensemble. If we are interested in the situation of nonfixed baryon number density but fixed chemical potential, the relevant thermodynamic potential is the grand canonical potential.

The deconfinement phase transition can be realized as the Hawking-Page transition due to the competition between the action of the background geometry corresponding to the confined phase and the action of the background corresponding to the deconfined phase [8]. Since the coloured multiquark matter can exist only in the deconfined phase (however, the colour-singlet multiquarks such as a baryon can also exist in the confined phase), its grand canonical potential in the Sakai-Sugimoto model is β times the combination of the classical action of the deconfining spacetime geometry and the configuration of flavour sector, which includes N_f D8-$\overline{\text{D8}}$-branes, the probe D4-brane vertex, and the radial strings. Note that the part of hanging strings, extending from the baryon vertex to the flavour branes, is neglected, and we assume that there is no distortion of the vertex due to the connecting strings (such distortion is discussed in [39, 40]). As a result, the baryon vertex is embedded into the flavour branes and becomes an instanton on them.

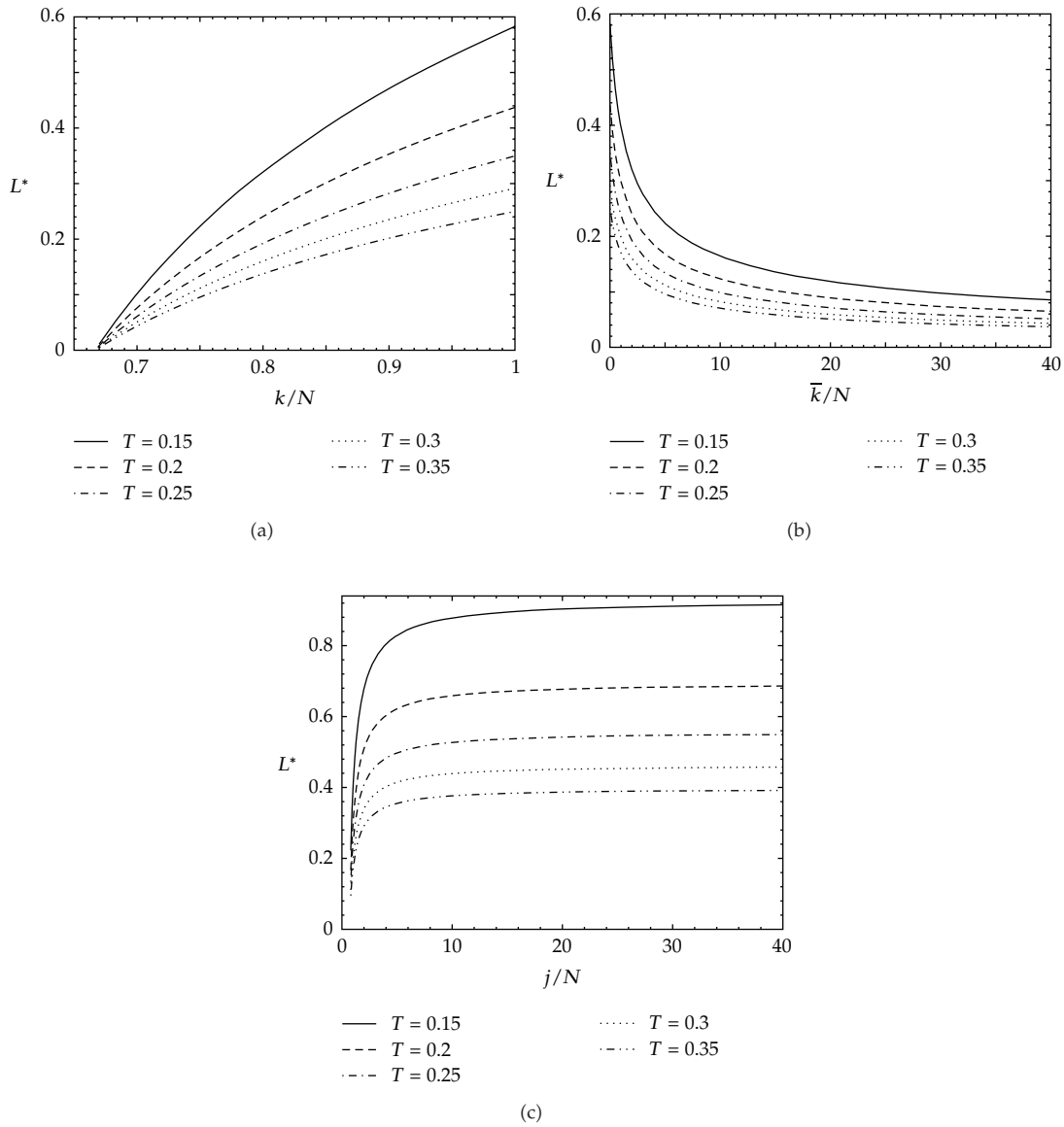

Figure 3: (a) the screening lengths of k-baryons with respect to k, (b) the screening lengths of $(N_c + \overline{k})$-baryons with respect to $\overline{k}$, and (c) the screening lengths of j-mesonance with respect to j for $T = 0.15 - 0.35$.

Intriguingly, whereas the deconfining spacetime geometry action (scales as N_c^2) dominates the action of the fundamental matter sector (scales as $N_c N_f$), the dominating part can be ignored in the consideration of the holographic phase transition in the deconfined phase. Above the deconfinement, the multiquarks phase competes with the vacuum phase and the chiral-symmetric quark-gluon plasma. In this section, we will explore the phase diagram of the deconfined nuclear matter especially the region of the parameter space where the multiquark phase is dominant. Then we will study the thermodynamics of the multiquark nuclear matter in the dilute and dense limits.

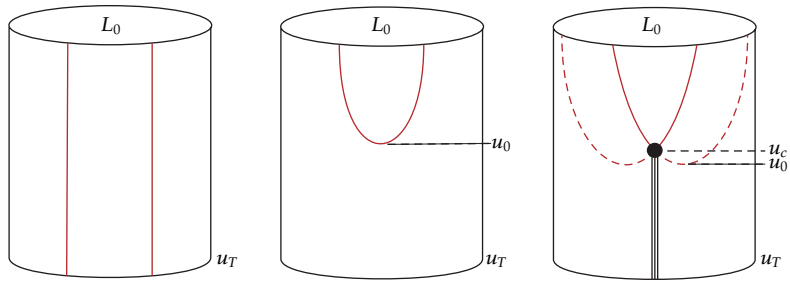

Figure 4: Configurations of χS-QGP (a) vacuum (b), and multiquark nuclear phase (c) in $x_4 - u$ projection.

3.1. Phase Diagram

In order to determine a phase diagram, we need to find which phase of nuclear matter is thermodynamically preferred to others in a particular region of the parameter space. For the grand canonical ensemble at a fixed μ, the thermodynamically preferred phase is the configuration with the grand canonical potential smaller than that of all other phases.

We will first determine the brane configuration in the presence of the external sources by minimizing the classical action. The position of the tip u_c of the D8-$\overline{\text{D8}}$ will be determined from the equilibrium condition at the tip. The resulting brane configuration corresponds to the multiquark nuclear phase. On the other hand, the vacuum phase corresponds to the configuration with zero sources and density, and the χS-QGP phase is dual to the brane configuration with parallel branes without a tip. The $x_4 - u$ projecion of the brane configuration for each deconfined phase is schematically shown in Figure 4. Then we will define the normalized grand canonical potential using the action of the D8-branes. The action of each brane configuration is divergent from the limit $u \to \infty$. By subtracting with the action of the vacuum configuration, we can regulate the grand canonical potential of each configuration. By comparing the grand canonical potential of each phase, we finally draw a phase diagram in (μ, T) parameter space.

Start with the DBI action of the D8-branes

$$S_{\text{D8}} = -\mu_8 \int d^9X e^{-\phi} \ \text{Tr}\sqrt{-\det\left(g_{MN} + 2\pi\alpha' \mathcal{F}_{MN}\right)}, \tag{3.1}$$

where g_{MN} is the induced metric of the D8-world volume and the field strength tensor of the gauge group $U(N_f)$ living in the N_f flavour branes is

$$\mathcal{F} = d\mathcal{A} + i\mathcal{A} \wedge \mathcal{A}. \tag{3.2}$$

While the full D8-brane world-volume gauge fields is

$$\mathcal{A} = \mathcal{A}_{SU(N_f)} + \frac{1}{\sqrt{2N_f}}\widehat{\mathcal{A}}, \tag{3.3}$$

we turn on only the time component of the diagonal subgroup $U(1)$ part, $\widehat{\mathcal{A}}/\sqrt{2N_f}$ in order to introduce the finite chemical potential, or equivalently finite baryon density [43, 46]. From the deconfining spacetime metric, (2.3), the DBI action of the D8-branes becomes

$$S_{\mathrm{D8}} = \mathcal{N}\int du\, u^4\sqrt{f(u)\left(x_4'(u)\right)^2 + u^{-3}\left(1-\left(\widehat{a}_0'(u)\right)^2\right)}, \tag{3.4}$$

where the factor $\mathcal{N}$ is defined to be

$$\mathcal{N} \equiv \frac{\mu_8\beta N_f\Omega_4 V_3 R^5}{g_s}, \tag{3.5}$$

as the result of integrating out all world-volume coordinates except the holographic direction u. And $\widehat{a}$ are defined as

$$\widehat{a} = \frac{2\pi\alpha'\widehat{\mathcal{A}}}{R\sqrt{2N_f}}. \tag{3.6}$$

The action does not depend on $\widehat{a}_0$, hence we can define a constant

$$d \equiv \frac{\delta S_{\mathrm{D8}}}{\delta\widehat{\mathcal{F}}_{0u}} \tag{3.7}$$

$$= \frac{u\widehat{a}_0'(u)}{\sqrt{f(u)\left(x_4'(u)\right)^2 + u^{-3}\left(1-\left(\widehat{a}_0'(u)\right)^2\right)}}, \tag{3.8}$$

which can be interpreted as the electric displacement field along the holographic direction. Similarly for the variation of action with respect to $x_4(u)$, we can define another constant of motion, says Γ, so that we can rearrange to obtain

$$\left(x_4'(u)\right)^2 = \frac{1}{u^3 f(u)}\left[\frac{f(u)\left(u^8+u^3d^2\right)}{\Gamma^2} - 1\right]^{-1}, \tag{3.9}$$

from which at large u

$$x_4(u) \approx \frac{L_0}{2} - \frac{2}{9}\frac{\Gamma}{u^{9/2}}, \tag{3.10}$$

where L_0 is the separation between D8 and $\overline{\mathrm{D8}}$ branes at $u \to \infty$ defined by

$$L_0 \equiv 2\int_{u_c}^{\infty} x_4'(u)du. \tag{3.11}$$

The parameter Γ can be thought of as the curvature of the D8-$\overline{\mathrm{D8}}$-branes around the cusp. It becomes zero when the flavour embedding is in the parallel configuration representing the chiral-symmetric QGP. According to [47], this means that it can be used as an order parameter of the nuclear matter/χS-QGP phase transition.

We will set $L_0 = 1$ to allow the possibility of the chiral symmetry restoration as separate phase transition from the deconfinement. Apply the equilibrium condition at the cusp u_c (see the appendix), we obtain Γ in terms of $x_4'(u_c)$,

$$\Gamma = \frac{f(u_c)\sqrt{u_c^8 + u_c^3 d^2}}{\sqrt{f(u_c)\left(x_4'(u_c)\right)^2 + u_c^{-3}}} x_4'(u_c) \tag{3.12}$$

$$= u_c^3 f(u_c)\left[\left(u_c^5 + d^2\right) - \frac{d^2\eta_c^2(T, n_s)}{9f(u_c)}\right], \tag{3.13}$$

where

$$\eta_c(T, n_s) \equiv 1 + \frac{1}{2}\left(\frac{u_T}{u_c}\right)^3 + 3n_s\sqrt{f(u_c)}. \tag{3.14}$$

Note that the formula of $x_4'(u_c)$ is derived from the variation of the total action, in which the D8-branes action has been transformed to possess the dynamical variable d rather than a_0',

$$\frac{\partial\widetilde{S}_{\text{total}}}{\partial u_c} = \frac{\partial\left(\widetilde{S}_{\text{D8}} + S_{\text{D4}} + \widetilde{S}_{\text{F1}}\right)}{\partial u_c} = 0. \tag{3.15}$$

This is reminiscent of the way we obtain the equilibrium condition of the multiquark vertex, (2.11), minimizing the surface terms with respect to u_c.

It is important to emphasize that the parameter n_s is the number of radial strings in the unit of N_c. Due to the zero length of the hanging strings, we cannot distinguish the different classes of multiquarks proposed in Section 2 for a particular value of n_s, but some possibilities, j-mesonance for example, can be ruled out by examining their thermodynamic stability. This will be shown in this subsection.

Before going further to calculate the classical action, let us comment about the electric displacement d. It has been shown in [48] that it is related to the baryon number density. The baryon number density corresponds to the number density of instantons, n_4, on the D8-branes. It also contributes to the Chern-Simons (CS) action of the flavour branes [13].

Beginning with the D8-brane CS term [49]

$$S_{\text{D8}}^{\text{CS}} = \frac{\mu_8}{3!}\int_{R^4\times R_+\times S^4} C_3 \wedge \text{Tr}\left(2\pi\alpha'\mathcal{F}\right)^3. \tag{3.16}$$

It is convenient to rescale the RR (Ramond-Ramond) field following the Appendix of [13] such that

$$\begin{aligned} S_{\text{D8}}^{\text{CS}} &= \frac{1}{48\pi^3}\int_{R^4\times R_+\times S^4} C_3 \wedge \text{Tr}\,\mathcal{F}^3 \\ &= \frac{1}{48\pi^3}\int_{R^4\times R_+\times S^4} F_4\ \omega_5(\mathcal{A}), \end{aligned} \tag{3.17}$$

where the last expression is obtained through the integration by part. $F_4 = dC_3$ is the RR 4-form field strength and $\omega_5(\mathcal{A})$ is the CS 5-form:

$$\omega_5(\mathcal{A}) = \mathrm{Tr}\left(\mathcal{A}\mathcal{F}^2 - \frac{1}{2}\mathcal{A}^3\mathcal{F} + \frac{1}{10}\mathcal{A}^5\right), \tag{3.18}$$

satisfying $d\omega_5 = \mathrm{Tr}\,\mathcal{F}^3$. Using the fact that integrating the F_4 flux over the S^4 in the N_c D4-branes background gives

$$\frac{1}{2\pi}\int_{S^4} F_4 = N_c, \tag{3.19}$$

and the relevant term is only the first term in the CS 5-form, (3.18), once turning on only the time-component of the diagonal $U(1)_V$ field, we obtain

$$S_{\mathrm{D8}}^{\mathrm{CS}} = \frac{N_c}{24\pi^2}\int_{R^4\times R_+}\frac{1}{\sqrt{2N_f}}\widehat{\mathcal{A}}_0 \wedge \mathrm{Tr}(\mathcal{F}\wedge\mathcal{F}). \tag{3.20}$$

Assuming a uniform distribution of D4-branes in $\mathbb{R}^3$ at $u = u_c$, we have [50]

$$\frac{1}{8\pi^2}\mathrm{Tr}(\mathcal{F}\wedge\mathcal{F}) = R^{-3}n_4\delta(u-u_c)d^3\mathbf{x}\,du, \tag{3.21}$$

where n_4 is defined to be the (dimensionless) number density of instantons, or the wrapped D4-branes, at $u = u_c$. From the viewpoint that the low-energy effective theory on the D8-brane includes the Skyrme model [13], it is natural to interpret n_4 as the baryon number density.

Using (3.6), (3.20), and (3.21), we obtain

$$S_{\mathrm{D8}}^{\mathrm{CS}} = \frac{n_4 N_c \beta V_3}{2\pi\alpha' R^2}\int_{u_c}^{\infty} du\ \widehat{a}_0(u)\ \delta(u-u_c). \tag{3.22}$$

From both the DBI and CS parts of D8-branes action, the equation of motion with respect to the $U(1)$ gauge field gives [48]

$$n_4 = \frac{2\pi\alpha' R^2\mathcal{N}}{\beta V_3 N_c}d. \tag{3.23}$$

Note that this reflects the one-dimensional electrostatic effect in which the point electric charges are put at u_c, generating constant electric field in the holographic direction.

The normalized grand canonical potential from the holographic model can be defined using the D-brane action as

$$\Omega(\mu) = \frac{1}{\mathcal{N}}S_{\mathrm{D8}}[x_4(u), \widehat{a}_0(u)]_{cl}. \tag{3.24}$$

Since the D-brane action diverges from the limit $u \to \infty$ of the integration, the grand canonical potential needs to be regulated by subtracting with the grand canonical potential of the vacuum phase at the same temperature.

Apart from the grand canonical potential, the chemical potential also needs to be holographically identified in the dual bulk theory. To this end, the time component of the $U(1)_V$ gauge field $\widehat{\mathcal{A}}_0$ is taken into account. From the field/operator matching scheme, a bulk field evaluated at $u \to \infty$, that is, the boundary of the spacetime background plays a role as the source of the dual operator in the generating function of correlation functions in quantum field theory. In other words, this nonnormalizable mode of the bulk field is dual to the coefficient of the field operator. Since the chemical potential is the coefficient of the charge density operator term, it can be holographically identified as $\widehat{\mathcal{A}}_0(\infty)$. By rescaling for convenience, we can write the dimensionless chemical potential as

$$\mu = \widehat{a}_0(\infty). \tag{3.25}$$

Similarly, the baryon number density in our normalization is given by

$$n_b = -\frac{\partial\Omega(T,\mu)}{\partial\mu} = d, \tag{3.26}$$

even though the true baryon number density is n_4 defined in (3.23). Consequently, d can then be used to denote the baryon number density.

Since the free energy in the canonical ensemble is the combination of the on-shell Legendre-transformed D8-brane action and the source term, it is convenient to obtain μ through

$$\mu = \frac{\partial\mathcal{F}_E(T,d)}{\partial d}, \tag{3.27}$$

where the free energy is holographically defined as the Legendre-transformed D8-brane action plus the source terms

$$\mathcal{F}_E(T,d) = \frac{1}{\mathcal{N}}\left(\widetilde{S}_{\mathrm{D8}}[T, x_4(u), d(u)]_{\text{on-shell}} + S_{\text{source}}(T,d,u_c)\right). \tag{3.28}$$

The Legendre-transformed action $\widetilde{S}_{\mathrm{D8}}$ is given by

$$\widetilde{S}_{\mathrm{D8}} = S_{\mathrm{D8}} + \mathcal{N}\int_{u_c}^{\infty} d(u)\widehat{a}_0^{V'}\,du, \tag{3.29}$$

$$= \mathcal{N}\int_{u_c}^{\infty} du\, u^4\sqrt{f(u)\left(x_4'(u)\right)^2 + u^{-3}}\sqrt{1+\frac{d^2}{u^5}} \tag{3.30}$$

The chemical potential can then be written as

$$\mu = \frac{1}{\mathcal{N}}\left\{\int_{u_c}^{\infty} du\left(\frac{\delta\widetilde{S}_{\mathrm{D8}}}{\delta d(u)} + \frac{\delta\widetilde{S}_{\mathrm{D8}}}{\delta x_4'}\frac{\partial x_4'}{\partial d}\right)\Bigg|_{T,L_0,u_c}^{\text{on-shell}} + \frac{\partial u_c}{\partial d}\Bigg|_{T,L_0}\left(\frac{\partial\widetilde{S}_{\mathrm{D8}}}{\partial u_c} + \frac{\partial S_{\text{source}}}{\partial u_c}\right)\Bigg|_{d,T,L_0}^{\text{on-shell}} + \frac{\partial S_{\text{source}}}{\partial d}\Bigg|_{T,L_0,u_c}\right\}. \tag{3.31}$$

The second, third, and fourth terms drop out. It is clear from (3.15) corresponding to the equilibrium at the cusp that the third and fourth terms vanish. For the second term, it is because $\delta\widetilde{S}_{\mathrm{D8}}/\delta x_4'(u)$ is constant as can be seen from (3.30) that $\widetilde{S}_{\mathrm{D8}}$ depends only on x_4'. Integrating over the remaining gives $\partial L_0/\partial d$, which is zero, due to the scale fixing condition $L_0 = 1$. Hence we obtain

$$\mu = \int_{uc}^{\infty} \widehat{a}_0'(u) + \frac{1}{\mathcal{N}}\frac{\partial S_{\text{source}}}{\partial d}\Bigg|_{T,L_0,u_c}. \tag{3.32}$$

Now, it is ready to express the grand canonical potential for the multiquark (baryon corresponds to $n_s = 0$) phase. Using (3.24), (3.4), (3.8), (3.9), we obtain the formulae of the grand canonical potential for the multiquark matter. The chemical potential can be calculated from (3.32) by eliminating a_0' via (3.8) and substituting (3.9). The grand canonical potential and the baryon chemical potential of the phases can be expressed as the following:

Nuclear (Including Exotics) Phase

$$\Omega_{\mathrm{nuc}} = \int_{u_c}^{\infty} du\left[1 - \frac{\Gamma^2}{f(u)(u^8 + u^3d^2)}\right]^{-1/2}\frac{u^5}{\sqrt{u^5 + d^2}}, \tag{3.33}$$

$$\mu_{\mathrm{nuc}} = \int_{u_c}^{\infty} du\left[1 - \frac{\Gamma^2}{f(u)(u^8 + u^3d^2)}\right]^{-1/2}\frac{d}{\sqrt{u^5 + d^2}} + \frac{1}{3}u_c\sqrt{f(u_c)} + n_s(u_c - u_T). \tag{3.34}$$

Recall that Γ depends on u_c, d, T and n_s according to (3.12) and (3.14). The last two terms in (3.34) come from the derivative of the source-term action with respect to d.

There are at least other two phases that compete with the multiquark phase: the vacuum phase and the chiral-symmetric QGP phase. From the above formula of Ω_{nuc} and μ_{nuc}, we can obtain the grand canonical potential and the chemical potential of the vacuum simply by (i) setting $d = 0$, (ii) dropping the source terms in (3.34), (iii) changing the lower bound of integration from u_c to u_0, and (iv) replacing Γ by the constant of motion in the vacuum configuration, from $\delta S_{\mathrm{D8}}/\delta x_4'$, $\Gamma_0 = f(u_0)u_0^8$. Thus we obtain

Vacuum Phase, $d = 0$

$$\Omega_{\mathrm{vac}} = \int_{u_0}^{\infty} du\left[1 - \frac{\Gamma_0^2}{f(u)u^8}\right]^{-1/2}u^{5/2}. \tag{3.35}$$

Similarly, the grand canonical potential and the chemical potential of the χS-QGP phase can be obtained by setting $x_4'(u) = 0$, reflecting its parallel configuration, and turning off the source terms. That is, setting $\Gamma = 0$ in (3.33) and (3.34), changing lower bound of integration to u_T and dropping the source terms in (3.34) give

χS-QGP Phase, $x_4'(u) = 0$

$$\Omega_{\text{qgp}} = \int_{u_T}^{\infty} du \frac{u^5}{\sqrt{u^5 + d^2}}, \tag{3.36}$$

$$\mu_{\text{qgp}} = \int_{u_T}^{\infty} du \frac{d}{\sqrt{u^5 + d^2}}. \tag{3.37}$$

The phase transition in the parameter space (μ, T) is obtained by comparing the grand canonical potential between two phases at a particular T and μ. Let us say the transition between phase 1 with the grand canonical potential Ω_1 and phase 2 with Ω_2. Phase 1 is thermodynamically preferred once $\Omega_1 < \Omega_2$ and vice versa. There is a first order phase transition when $\Omega_1 = \Omega_2$. This kind of phase transition can be seen in the transition between the vacuum and χS-QGP phases and the transition between the χS-QGP and the nuclear matter. However, the phase transition between the vacuum and nuclear matter phases is of the second-order as seen from (3.34). The density d is continuous near $\mu = \mu_{\text{onset}}$, which is $\mu_{\text{nuc}}(d = 0)$, and behaves as $d \sim (\mu_{\text{nuc}} - \mu_{\text{onset}})$. Note that this reflects the absence of the interactions between the multiquarks and baryons. As a result, the critical chemical potential defined to be the value, at which

$$\frac{\partial d}{\partial \mu} = -\frac{\partial^2 \Omega}{\partial \mu^2} \tag{3.38}$$

has a discontinuity, is given by μ_{onset}. By numerical calculations, the phase transition lines can be obtained as shown in Figure 5. The phase diagram between the chiral-broken vacuum and the chiral symmetric QGP phases was first obtained in [51]. The phase diagram of all 3 deconfined phases including the baryonic nuclear phase (without the multiquarks) is originally discussed in [48].

This phase diagram also shows the presence of the multiquark phase which can be mixed in the region of normal baryon phase (with $n_s = 0$), say B + C for $n_s = 0.1$, and C for $n_s = 0.3$. The multiquark matter with $0 < n_s < 0.5$ is less stable than the normal baryon due to the larger value of the grand canonical potential. Above $n_s = 0.3$, it can be shown that the multiquark phase is unstable to density fluctuations, that is, $\partial\mu/\partial d < 0$, in some regions of high T and certain range of μ. For approximately $n_s > 0.5$, the multiquark phase is unstable thermodynamically to density fluctuations for most of the temperatures.

If the multiquark matter can exist in the quark-gluon plasma, it should mix with the normal baryon states in thermal equilibrium with the populations following the Boltzmann factor

$$\exp\left(-\frac{E}{k_B T}\right), \tag{3.39}$$

where E is the binding energies for the states. It is interesting to explore more about the population of these multiquark states in the quark-gluon plasma potentially produced in the

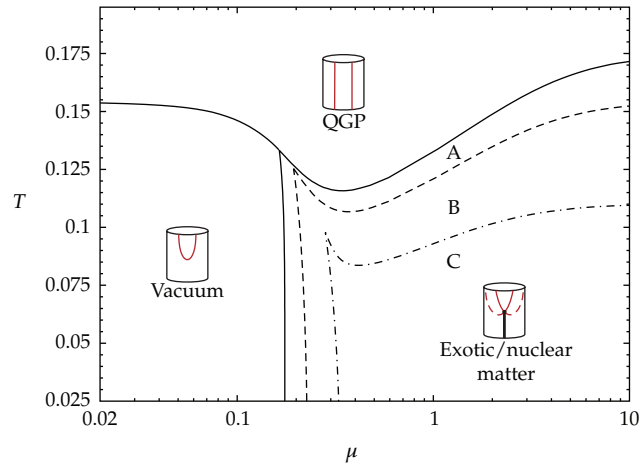

Figure 5: The phase diagram of deconfined nuclear matters in the Sakai-Sugimoto model. Multiquark phase is shown as the region on the lower right corner where it is divided into 3 parts according to the value of the colour strings n_s. A, B, C represent the region where multiquark phase with $n_s = 0$ (N_c-baryon), 0.1, 0.3 is the most thermodynamically preferred.

heavy-ion collision experiments such as the RHIC and the LHC. Existence of these multiquark states contribute significantly to the hydrodynamical and thermodynamical properties of the deconfined plasma.

3.2. Thermodynamic Relations

In the grand canonical ensemble, the grand canonical potential G_Ω is the function of the dynamical variables: the volume V, the temperature T, and the chemical potential μ. Its differential is

$$dG_\Omega = -PdV - SdT - Nd\mu, \tag{3.40}$$

where the coefficients P, S, and N are the pressure, entropy, and the total number of particles, respectively. It is better to understand the system of QGP in terms of volume density of extensive parameters. Let us define the volume density of G_Ω, S, and N to be Ω, s, and d, respectively. Hence, the pressure is

$$P = -\frac{G_\Omega}{V} \equiv -\Omega(T,\mu). \tag{3.41}$$

From (3.26) and (3.41), we use the chain rule to obtain

$$\left.\frac{\partial P}{\partial d}\right|_T = \left.\frac{\partial \mu}{\partial d}\right|_T d, \tag{3.42}$$

so that

$$P(d,T,n_s) = \mu(d,T,n_s)d - \int_0^d \mu(d',T,n_s)d(d'), \tag{3.43}$$

where we have assumed that the regulated pressure is zero when there is no nuclear matter, that is, $d = 0$.

While the equations of motion cannot be obtained analytically, we can find them in the limit of very small and very large density. Using (3.34) and (3.43), we take $d \approx 0$ and use the binomial expansion, then (see [52] for details)

$$P \simeq \frac{\alpha_0}{2} d^2 - \frac{3\beta_0(n_s)}{4} d^4, \tag{3.44}$$

where

$$\begin{aligned} \alpha_0 &\equiv \int_{u_0}^{\infty} du \, \frac{u^{-5/2}}{1 - f_0 u_0^8 / f u^8}, \\ \beta_0(n_s) &\equiv \int_{u_0}^{\infty} du \frac{u^{-5/2}}{2\sqrt{1 - f_0 u_0^8 / f u^8}} \left(\frac{f_0 u_0^3}{f u^8 - f_0 u_0^8} \left(1 - \frac{\eta_0^2}{9 f_0} - \frac{u_0^5}{u^5} \right) + \frac{1}{u^5} \right). \end{aligned} \tag{3.45}$$

Note that we have used the fact that η_c of (3.14) becomes $\eta_0 + \mathcal{O}(d)$, where η_0 is η_c with u_c replaced by u_0. Similarly, f_0 is defined to be $f(u)$ with $u = u_0$. On the other hand, for the limit of large d in (3.34), the pressure from (3.43) becomes [12]

$$P \simeq \frac{2}{35} \left(\frac{\Gamma(1/5)\Gamma(3/10)}{\Gamma(1/2)} \right) d^{7/5}. \tag{3.46}$$

Numerically, the relations between the pressure and the density of the multiquark matter for different values of n_s are plotted in Figure 6. This is consistent with the results of analytic calculations that $P \sim d^2$ for small d and $P \sim d^{7/5}$ for large d. Since the relations are not sensitive to the change of T, therefore we present only the plots at $T = 0.03$. The transition from small to large d is apparent at $d_c \simeq 0.072$. We can also see the dependence of pressure on n_s from the plots. The pressure of the multiquarks with larger n_s is smaller for small d. On the other hand, the pressure of the multiquarks with smaller n_s is merely slightly larger in the large d limit. Actually, the pressure is nearly insensitive to the changing of n_s for $d > d_c$ as is implied from (3.46).

From the differential of the free energy, the entropy density can be written as

$$s = -\frac{\partial \mathcal{F}_E}{\partial T}, \tag{3.47}$$

where $\mathcal{F}_E$ is the free energy density which relates to the grand potential density as $\mathcal{F}_E = \Omega + \mu d$. Using (3.41), the entropy density becomes

$$s = \frac{\partial P}{\partial T} - \left(\frac{\partial \mu}{\partial T} \right) d. \tag{3.48}$$

Since the pressure P and the contribution of D8-branes to the baryon chemical potential ($\mu - \mu_{\text{source}}$) are insensitive to the changing of the temperature, the entropy density is dominated by the derivative of μ_{source} with respect to T, That is,

$$s \simeq -\left(\frac{\partial \mu_{\text{source}}}{\partial T} \right) d. \tag{3.49}$$

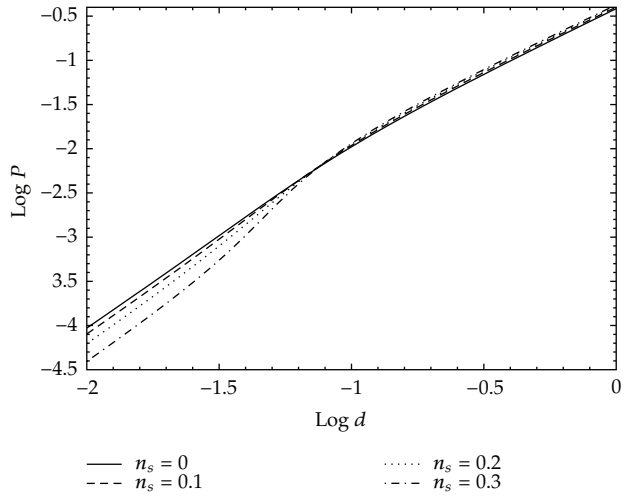

Figure 6: Pressure versus density of the multiquark phase in logarithmic scale at $T = 0.03$, zoomed in around the transition region.

It is found numerically in [52] that u_c is approximately constant with respect to the temperature range between the gluon deconfinement and the chiral symmetry restoration, we thus obtain

$$\begin{aligned}\frac{\partial \mu_{\text{source}}}{\partial T} &= \frac{\partial}{\partial T}\left(\frac{1}{3}u_c\sqrt{f(u_c)} + n_s(u_c - u_T)\right)\\ &\approx -\frac{\left(16\pi^2/9\right)^3 T^5}{u_0^2\sqrt{1-\left(u_T/u_0\right)^3}} - n_s\frac{32\pi^2 T}{9},\end{aligned} \tag{3.50}$$

such that

$$s \approx \frac{\left(16\pi^2/9\right)^3 T^5 d}{u_0^2\sqrt{1-\left(u_T/u_0\right)^3}} + n_s\frac{32\pi^2 T d}{9}. \tag{3.51}$$

The entropy density has the temperature dependence $\sim T^5$ for small n_s, whereas it is dominated by the colour term, that is, $s \propto n_s T$, for larger n_s. This agrees with the numerical results shown in Figure 7. We already know that the free quarks and gluons in the χS-QGP have the entropy density scales as T^6 [48]. Intriguingly, the presence of the colour charges of multiquarks implies that the multiquark matter in the sQGP behave less like free particles with the weaker temperature dependence $s \sim n_s T$. Also confirmed numerically in Figure 7 is the linear dependence of the entropy density to the density d.

From (3.43), it is important to note that the pressure is mainly contributed from the flavour D8-brane part since μ_{source} is mostly constant with respect to the density. This is because the constant part of μ with respect to the density will cancel out when substituted into (3.43). Conversely, the entropy density is mainly contributed from the source term, namely, the vertex and radial strings.

Lastly, the dependence of the baryon chemical potential μ on d is plotted in Figure 8. The $\mu - d$ relation is found to be mostly independent of the temperature. It is found that the

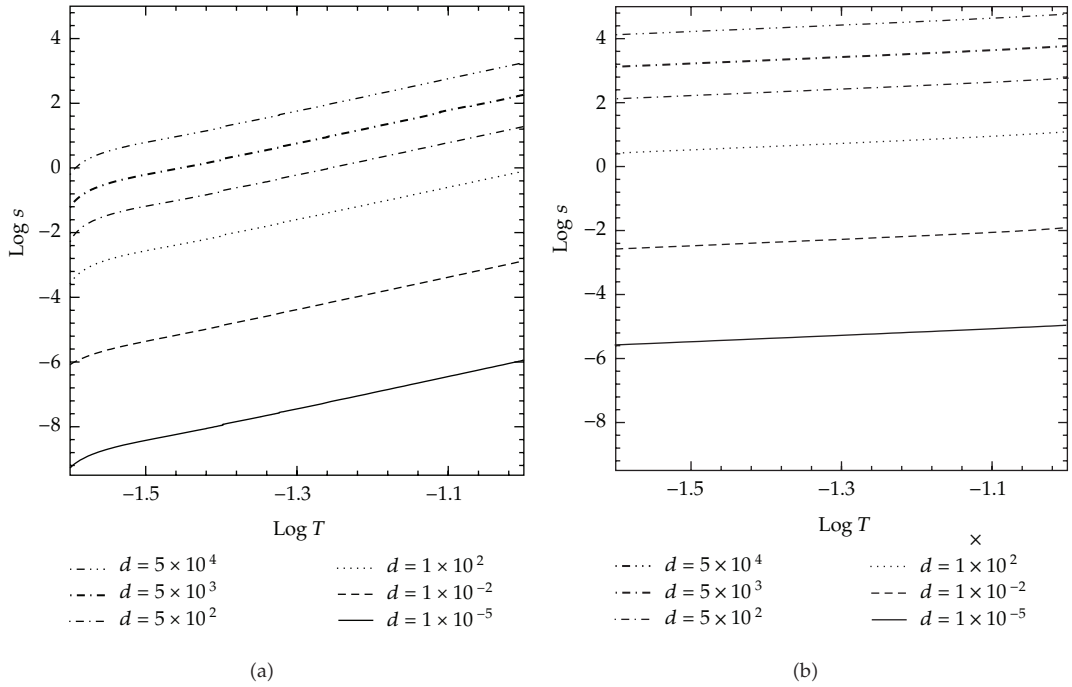

Figure 7: Entropy versus temperature of the multiquark phase in logarithmic scale for $n_s = 0$ (a), 0.3 (b).

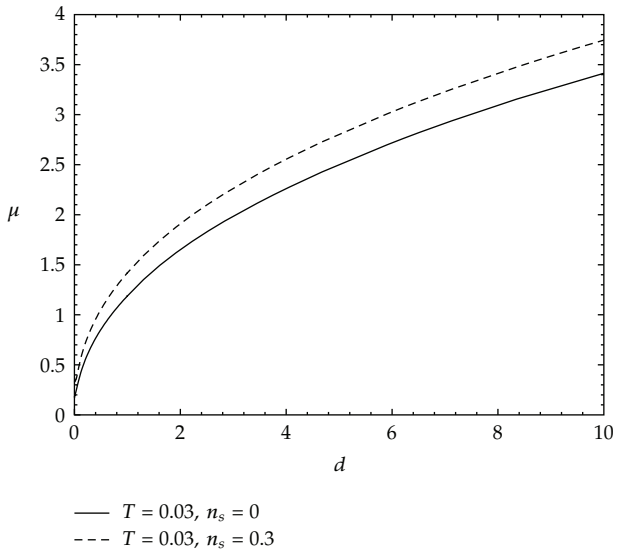

Figure 8: The baryon chemical potential versus number density of the multiquark phase at $T = 0.03$.

relation can be well approximated by the power law with $\mu \sim d$ for small density and $\mu \sim d^{2/5}$ for large density. The difference indicates that the behaviour of multiquark quasiparticles is more like fermions as a consequence of the DBI action [48].

4. Magnetic Properties of Holographic Multiquarks in the Quark-Gluon Plasma

In the deconfined SS model, the multiquark phase has been shown to be the most thermodynamically preferred in the extremely dense and warm condition (in the temperature range above the deconfinement but below the chiral symmetry restoration). It is possible that the real dense and warm QCD soup also energetically prefers the multiquark phase in such condition. In the early universe, during the electroweak phase transition, the Higgs mechanism could create enormous magnetic fields in the boundary region between two domains with different vacuum expectation values [53]. These gigantic fields could have crucial impact on the phase transitions of the warm nuclear soup at later epoch. Collision of energetic charged particles at the hadron and heavy ion colliders could produce extremely large magnetic fields in the vicinity of the collision point. At RHIC and LHC, it has been estimated that the induced local magnetic fields could be as large as $10^{14\text{-}15}$ Tesla [54]. Finally, magnetic fields of order of 10^{10} Tesla could be produced by the magnetars on the large astrophysical scale [55]. Therefore, it is interesting to investigate the effects of extremely strong magnetic fields to the multiquark phase above the deconfinement temperature.

To mimic behaviour of the strongly coupled nuclear matter in the presence of a uniform magnetic field, we turn on another component of the $U(1) \subset U(N_f)$ field denoted as a_3^V. The nonnormalizable modes of a_3^V are identified with the vector potential of the magnetic field B (not to be confused with B used in Section 2), defined in units of $1/2\pi\alpha'$. We choose the direction of the magnetic field so that

$$a_3^V = Bx_2. \tag{4.1}$$

As before, the baryon chemical potential μ of the corresponding gauge matter at the boundary is identified with the nonnormalizable mode of the DBI-gauge field by

$$\mu = a_0^V (u \longrightarrow \infty). \tag{4.2}$$

Additional sources of the baryonic charge in terms of the instanton and strings contribute the following action

$$\begin{aligned} S_{\text{source}} &= \mathcal{N} d(u_c) \left[\frac{1}{3} u_c \sqrt{f(u_c)} + n_s (u_c - \mathrm{u}_T) \right] \\ &\simeq \mathcal{N} d \mu_{\text{source}}, \end{aligned} \tag{4.3}$$

where $n_s = k_r/N_c$ is the number of radial strings in the unit of $1/N_c$ as in the zero magnetic field case. The electric displacement, $d(u_c) \equiv \partial L/\partial a_0^{V'}|_{u_c}$, representing the baryonic charge density from the D4 at u_c has been approximated to be d (the exact value is $d - (3/2)Ba_1^A(\infty)$). This action does not contain the gauge fields of the flavour branes and thus does not affect the equations of motion. However, it contributes tidal weight to the total configuration, pulling down the flavour branes closer to the horizon. The scale-fixing condition $L_0 = 1$ is determined by the equilibrium between this tidal weight of the additional sources (including the tension of the colour strings) and the tension of the flavour branes. The position u_c of the tip of the connecting branes determined from this condition will also depend on the magnetic field in presence.

The response of the flavour branes to the magnetic field is encoded in the axial a_1^A component of the $U(1)$ induced through the Chern-Simons action of the branes in the bulk. In the boundary gauge theory, this corresponds to the axial anomaly described by the Wess-Zumino-Witten action [56]. The non-normalizable mode of a_1^A at the boundary is identified with the response of the chiral condensate to the external magnetic field, $a_1^A(u \to \infty) \equiv \nabla\varphi$, which we will call the pion gradient.

The D-brane and the Chern-Simons action of the configuration can be calculated straightforwardly to be

$$S_{\mathrm{D8}} = \mathcal{N}\int_{u_c}^{\infty} du\, u^{5/2}\sqrt{1+\frac{B^2}{u^3}}\sqrt{1+f(u)\left(a_1'^A\right)^2-\left(a_0'^V\right)^2+f(u)u^3x_4'^2}, \tag{4.4}$$

$$S_{\mathrm{CS}} = -\frac{3}{2}\mathcal{N}\int_{u_c}^{\infty} du\left(\partial_2 a_3^V a_0^V a_1^{A'} - \partial_2 a_3^V a_0^{V'} a_1^A\right), \tag{4.5}$$

where $\mathcal{N} = N_c R_{\mathrm{D4}}^2/(6\pi^2(2\pi\alpha')^3)$ defines the brane tension. To preserve the gauge invariance of the total action in the situation where the gauge transformation does not vanish at the spatial infinity, addition of surface terms effectively results in the factor $3/2$ in the Chern-Simons action [57].

Appearance of horizon in the background spacetime connects classical behaviour of the bulk physics to the physics of the quantum gauge matter at the boundary in a holographic manner. The brane-bulk interaction provides a solid correspondence between bulk fields and operators of the gauge theory on the boundary. Classical solutions of the gauge fields on the D8-$\overline{\mathrm{D8}}$ probe as well as its geometric configuration will describe physics of the dense strongly coupled nuclear matter in the presence of the external magnetic field in a holographic manner.

By conventional variational method, the equations of motion with respect to the gauge field components are given by the Euler-Lagrange equation with respect to the gauge field component a_0^V, a_1^A,

$$\frac{\sqrt{u^5+B^2u^2}f(u)a_1'^A}{\sqrt{1+f(u)\left(a_1'^A\right)^2-\left(a_0'^V\right)^2+f(u)u^3x_4'^2}} = j_A - \frac{3}{2}B\mu + 3Ba_0^V, \tag{4.6}$$

$$\frac{\sqrt{u^5+B^2u^2}a_0'^V}{\sqrt{1+f(u)\left(a_1'^A\right)^2-\left(a_0'^V\right)^2+f(u)u^3x_4'^2}} = d - \frac{3}{2}Ba_1^A(\infty) + 3Ba_1^A. \tag{4.7}$$

Note that d, j_A are the baryon charge density and current density of the dual gauge matter at the boundary $(u \to \infty)$ given by

$$\begin{aligned} j^\mu(x, u \longrightarrow \infty) &\equiv \left.\frac{\delta S_{\mathrm{eom}}}{\delta A_\mu}\right|_{u\to\infty} \\ &\equiv \left(d, \vec{j}_A\right). \end{aligned} \tag{4.8}$$

They can be presented with the gauge fields as

$$d = \left.\frac{\sqrt{u^5 + B^2u^2}\,a_0'^V}{\sqrt{1 + f(u)\left(a_1'^A\right)^2 - \left(a_0'^V\right)^2 + f(u)u^3x_4'^2}}\right|_\infty - \frac{3}{2}Ba_1^A(\infty),$$
$$j_A = \left.\frac{\sqrt{u^5 + B^2u^2}\,f(u)a_1'^A}{\sqrt{1 + f(u)\left(a_1'^A\right)^2 - \left(a_0'^V\right)^2 + f(u)u^3x_4'^2}}\right|_\infty - \frac{3}{2}B\mu. \tag{4.9}$$

The action does not explicitly depend on x_4, consequently the associate constant of motion allows us to rewrite $x_4'(u)$ as the following:

$$\left(x_4'(u)\right)^2 = \frac{1}{u^3 f(u)}\left[\frac{u^3[f(u)(C(u) + D(u)^2) - \left(j_A - (3/2)B\mu + 3Ba_0^V\right)^2]}{F^2} - 1\right]^{-1}, \tag{4.10}$$

where

$$F = \frac{u_c^3\sqrt{f(u_c)}\sqrt{f(u_c)\left(C(u_c) + D(u_c)^2\right) - \left(j_A - (3/2)B\mu + 3Ba_0^V(u_c)\right)^2}\,x_4'(u_c)}{\sqrt{1 + f(u_c)u_c^3x_4'^2(u_c)}}, \tag{4.11}$$

and $C(u) \equiv u^5 + B^2u^2$, $D(u) \equiv d + 3Ba_1^A(u) - 3B\nabla\varphi/2$.

From the scale-fixing condition

$$L_0 = 2\int_{u_c}^{\infty} x_4'(u)du = 1, \tag{4.12}$$

the position of the tip u_c of the brane configuration is determined by the equilibrium of forces to be, (see the appendix),

$$\left(x_4'(u_c)\right)^2 = \frac{1}{f_cu_c^3}\left[\frac{9}{d^2}\frac{\left(f_c\left(C_c + D_c^2\right) - \left(j_A - (3/2)B\mu + 3Ba_0^V(u_c)\right)^2\right)}{\left(1 + (1/2)(u_T/u_c)^3 + 3n_s\sqrt{f_c}\right)^2} - 1\right]. \tag{4.13}$$

The introduction of the Chern-Simons interaction of the gauge fields to the magnetic field results in the dependence of x_4' on the gauge field a_0^V, a_1^A. It is consequently required to solve (4.6), (4.7), and (4.12) simultaneously. Since the physical parameters, $\mu, \nabla\varphi$, also depend on the gauge field components by $a_0^V(\infty) = \mu, a_1^A(\infty) = \nabla\varphi$, we need a triple-shooting algorithm to solve for the solutions numerically.

Under the boundary conditions $a_0^V(u_c) = \mu_{\text{source}}$, $a_1^A(u_c) = 0$, the values of $u_c, \mu, \nabla\varphi$ are chosen so that they solve the equations of motion and satisfy $a_0^V(\infty) = \mu$, $a_1^A(\infty) = \nabla\varphi$. If the solutions also satisfy the scale fixing condition (4.12), we keep the solutions, otherwise we adjust the value of u_c and repeat the shooting procedure.

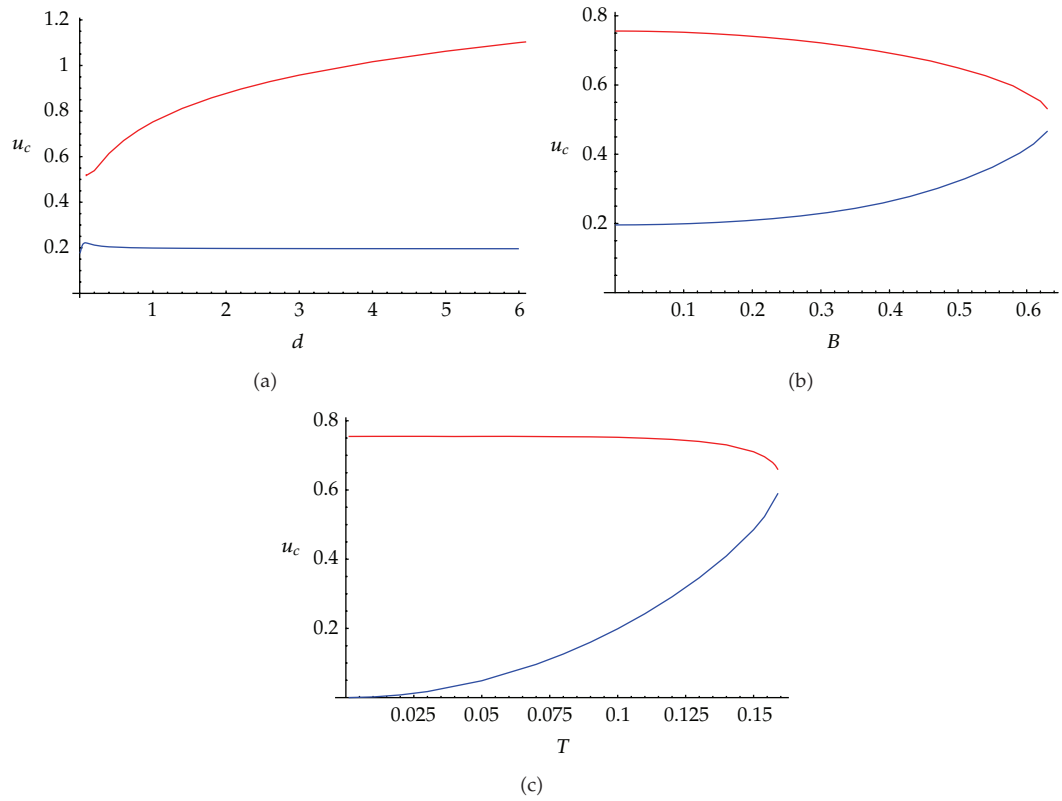

Figure 9: Position u_c of the vertex for $n_s = 0$ (normal baryon) and fixed $j_A = 0$ as a function of (a) d with fixed $B = 0.10$, $T = 0.10$, (b) B with fixed $d = 1$, $T = 0.10$, (c) T with fixed $B = 0.10$, $d = 1$. The lower (blue) line is the configuration **A** with u_c close to u_T, and the upper (red) line is the configuration **B** with large separation between u_c and u_T.

4.1. Two Multiquark Configurations and the Multiquark Merging

The numerical solutions obtained by the shooting algorithm reveal two possible multiquark configurations, one with small and one with large u_c. The small-u_c configuration (configuration **A**) has longer stretch in the u-direction, therefore it contains higher gluon content and larger energy. The free energy of this configuration is consequently larger than the large-u_c configuration (configuration **B**) and becomes less energetically favoured. The relationships between u_c and the baryonic density, the magnetic field, and the temperature are shown in Figure 9 (from [58]).

From Figure 9, the density dependence of the two configurations shows that as density increases, configurations **A** and **B** diverge from each other. They become two distinctive phases at large densities. On the other hand, the increase of magnetic field and temperature merges the two configurations together. At the critical field and/or temperature, configurations **A** and **B** merge and disappears (i.e., they do not satisfy the scale-fixing condition anymore).

In Figure 10, the chemical potential and the pion gradient response of the multiquark phase are plotted as functions of the magnetic field for the multiquark phase with the number of colour strings $n_s = 0$, 0.1, 0.2. Magnetic merging occurs at higher field for the multiquarks with smaller n_s. Interestingly, the less-preferred configuration **A** has a negative

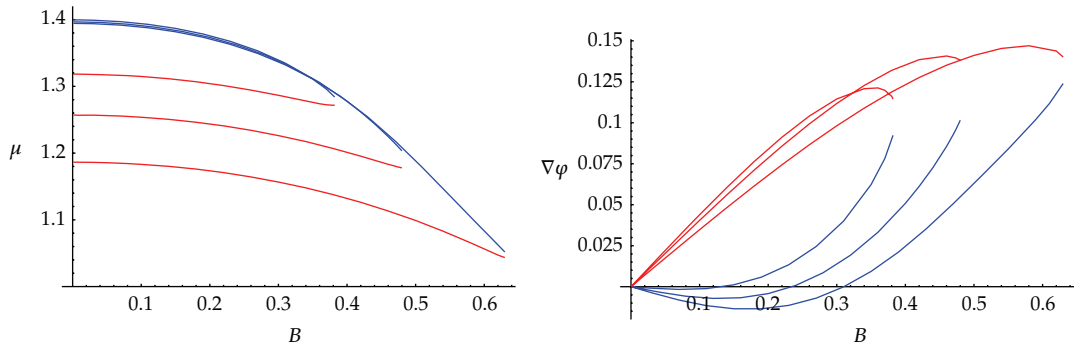

Figure 10: Comparison between the baryon chemical potential (a) and the pion gradient (b) as a function of B at fixed $j_A = 0$, $d = 1$, $T = 0.10$; for $n_s = 0$ (normal baryon), the bottom graph; $n_s = 0.10$, the middle graph; $n_s = 0.20$, the top graph. The blue lines are the configuration **A** with u_c close to u_T, and the red lines are the configuration **B** with large separation between u_c and u_T.

linear response $\nabla\varphi$ to the magnetic field for small fields. Thorough investigation in [58] reveals that both multiquark configuration **A**, **B** are more thermodynamically preferred than the magnetized vacuum, and each configuration is stable under density fluctuations since

$$\frac{\partial^2 \mathcal{F}_{\mathrm{E}}}{\partial d^2} = \frac{\partial \mu}{\partial d} > 0, \tag{4.14}$$

where the free energy $\mathcal{F}_{\mathrm{E}}$ will be defined in the next subsection.

We would like to emphasize that there are actually two possible multiquark phases for the deconfined nuclear matter at finite density. Even though phase **B** is more energetically preferred, both multiquark phases could coexist in general situation. Large magnetic field or high temperature could merge the two multiquark configurations into one. Remarkably once they merge, the multiquark can no longer exist since it does not satisfy the scale fixing condition. They would either turn into a multiquark configuration with larger density or a chiral-symmetric QGP. We will discuss more on the thermodynamic properties and phase diagram of the multiquark phases in the subsequent sections.

4.2. *Thermodynamic Properties of the MQ-$\nabla\varphi$ Phase*

The holographic principle conjectures that the partition function of the string theory in the bulk is equal to the partition function of the gauge theory on the boundary. The free energy of the gauge matter at the boundary is equivalent to the string action in the bulk, namely, the DBI action up to a periodicity factor [59]. The D8-brane action from (4.4) can be calculated to be

$$S_{\mathrm{D8}} = \mathcal{N} \int_{u_c}^{\infty} du\, C(u) \sqrt{\frac{f(u)\left(1 + f(u)u^3 x_4'^2\right)}{f(u)\left(C(u) + D(u)^2\right) - \left(j_A - (3/2)B\mu + 3Ba_0^V\right)^2}}. \tag{4.15}$$

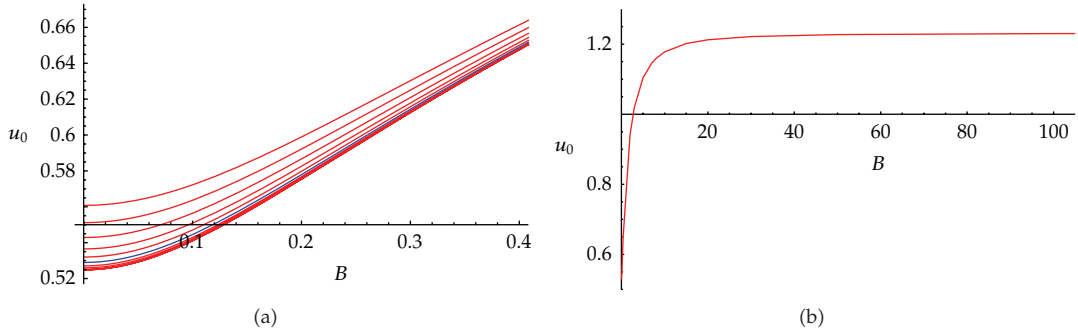

Figure 11: Relation between u_0 and external magnetic field B of the vacuum for (a) the temperature $T = 0.02$–0.15, the upper lines have higher temperatures, (b) u_0 saturates to the approximate value of 1.23 at large field for all temperatures (only $T = 0.10$ curve is shown here).

The action is divergent from the limit $u \to \infty$ and we need to regulate it using the action of the magnetized vacuum. For the magnetized vacuum, the field a_0^V, a_1^A, the baryon density, and chemical potential are set to zero giving

$$S[\text{magnetized vacuum}] = \int_{u_0}^{\infty} \sqrt{C(u)\left(1 + f(u)u^3 x_4'^2\right)}\Big|_{\text{vac}} du, \tag{4.16}$$

where

$$x_4'(u)\big|_{\text{vac}} = \frac{1}{\sqrt{f(u)u^3\left(f(u)u^3 C(u)/f(u_0)u_0^3 C(u_0) - 1\right)}}. \tag{4.17}$$

The position u_0 is the tip of the connecting brane configuration, since there is no source, $x_4'(u_0) \to \infty$ and the branes and antibranes connect smoothly. Figure 11 shows u_0 as a function of the magnetic field and temperature. The value of u_0 converges to approximately 1.23 for high fields for all temperatures.

The regulated free energy at fixed density is then defined to be

$$\mathcal{F}_{\text{E}}(d, B) \equiv \Omega(\mu, B) + \mu d, \tag{4.18}$$

where $\Omega(\mu, B) = S[a_0(u), a_1(u)](\text{e.o.m.}) - S[\text{magnetized vacuum}]$, and the total action $S[a_0(u), a_1(u)](\text{e.o.m.})$ is given by $S_{\text{D8}} + S_{\text{CS}}$.

The corresponding magnetization at fixed density is subsequently

$$M(d, B) = -\frac{\partial \mathcal{F}_{\text{E}}(d, B)}{\partial B}\bigg|_d. \tag{4.19}$$

For $n_s = 0, 0.1, 0.2$ we can plot the free energy and magnetization of the multiquark-$\nabla\varphi$ matter as a function of the magnetic field as shown in Figure 12. Configuration **A** has larger free energy and magnetization than configuration **B**. The magnetic merging is clearly visible at critical fields. The critical field for multiquark with higher number of colour strings n_s is smaller, reflecting less stability. The magnetization is approximately linear for small fields for

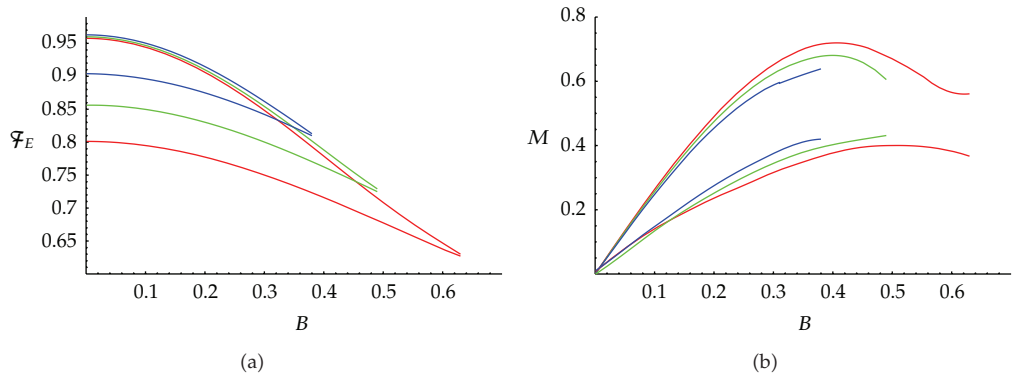

Figure 12: The free energy and magnetization of the multiquarks nuclear matter at fixed $j_A = 0$, $d = 1$, and $T = 0.10$ for $n_s = 0$ (red), 0.10 (green), 0.20 (blue). The upper lines are the configuration **A** with u_c close to u_T, and the lower lines are the configuration **B** with large separation between u_c and u_T.

both configurations. The free energy of configuration **A** is clearly larger than configuration **B**, implying that it is less energetically preferred. Here and henceforth, we will focus our consideration to the multiquarks in configuration **B**.

For moderate fields $B = 0.05$–0.15, we can study the temperature dependence of the baryon chemical potential and the free energy of the MQ-$\nabla\varphi$ phase as shown in Figure 13. Remarkably, they inherit the temperature dependence from the factor $\sqrt{f(u)} = \sqrt{1 - u_T^3/u^3}$ in the spacetime metric of the background SS model,

$$\mu = \mu_0(d, B)\sqrt{1 - \left(\frac{T}{T_0}\right)^6}, \tag{4.20}$$

$$F = F_0(d, B)\sqrt{1 - \left(\frac{T}{T_0}\right)^6}, \tag{4.21}$$

where for $d = 1$, $B = 0.10$, $\mu_0 = 1.1849$, $F_0 = 0.7976$, respectively. The best-fit values of T_0 for the chemical potential and the free energy are 0.269 and 0.233, respectively. Note that the characteristic temperature T_0 of the chemical potential is slightly larger than the value of the free energy due to the additional temperature dependence of the u_c in the free energy case [60]. It should be noted that the temperature dependence becomes significant for $T \gtrsim 0.10$.

When the magnetic field is applied to the multiquark phase, the chiral condensate responds to the field by developing the pion gradient $\nabla\varphi$ in the direction of the applied field. For moderate fields, the response is linear, $\nabla\varphi \propto B$, as we can see from Figure 10. The induced domain wall is stable among the multiquarks, carrying baryon density $d_{\nabla\varphi} = 3B\nabla\varphi/2$ [56].

Figure 14 shows the relationship between the pion gradient and the magnetic field in the temperature range $T = 0.02$–0.15. For $d = 1$, the slope m (or the linear response) of the response $\nabla\varphi$ to B depends on the temperature approximately as $m = m_0\sqrt{1 - (T/T_0)^6}$, and

$$\nabla\varphi \simeq Bm_0\sqrt{1 - \left(\frac{T}{T_0}\right)^6}, \tag{4.22}$$

where $m_0 = 0.347$, $T_0 = 0.177$.

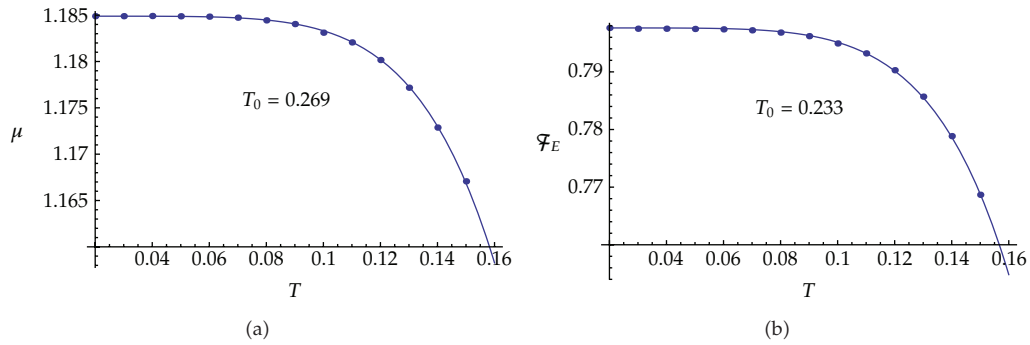

Figure 13: For $d = 1$, $B = 0.10$, (a) the baryon chemical potential as a function of T, the best-fit curve is in the form $\mu_0\sqrt{1-(T/T_0)^6}$ with $\mu_0 = 1.1849$, $T_0 = 0.269$; (b) the free energy as a function of T, the best-fit curve is in the form $F_0\sqrt{1-(T/T_0)^6}$ with $F_0 = 0.7976$, $T_0 = 0.233$. Other curves within the range $B = 0.05$–0.15 can also be fitted well with the same T_0.

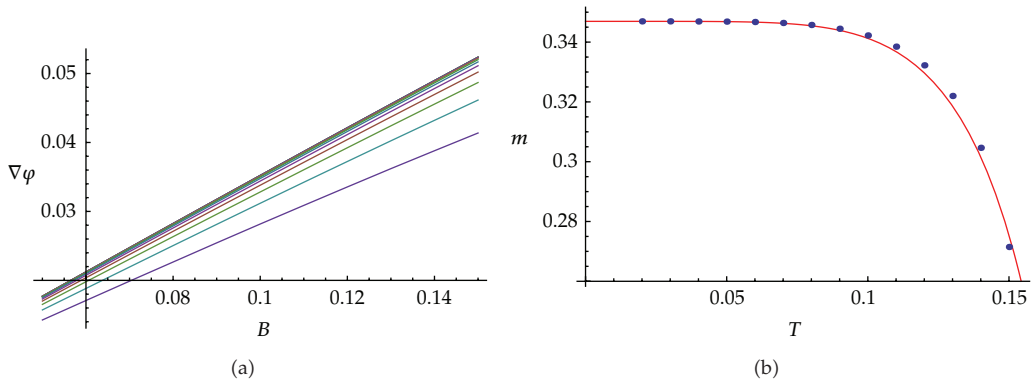

Figure 14: (a) The pion gradient versus magnetic field for $T = 0.02$–0.15 at $d = 1$, lower lines have higher temperatures. (b) The linear response or slope of the linear function between the pion gradient and the magnetic field as a function of the temperature for the range $B = 0.05$–0.15 and density $d = 1$. The red line is the best-fit curve in the form $m_0\sqrt{1-(T/T_0)^6}$ with $m_0 = 0.347$, $T_0 = 0.177$.

The pion gradient is induced naturally by the magnetic field as a result of axial anomaly in the boundary gauge theory. It can be described by the Wess-Zumino-Witten action in the chiral perturbation theory whilst the similar effect is represented by the Chern-Simons action of the string theory in the bulk [56]. The pion gradient forms a domain wall which also carries baryonic charge and contributes to the total baryon density of the gauge matter. However, the population of the baryon density from the domain wall in the MQ-$\nabla\varphi$ phase decreases as the total density grows. This is shown in Figure 15. The ratio $R_{\nabla\varphi} \equiv d_{\nabla\varphi}/d = 3B\nabla\varphi$ can be approximated by a power law of the density as

$$\begin{aligned} R_{\nabla\varphi} &\simeq (\text{const.})d^{-6/5}, \\ &\simeq \frac{3B^2 m_0}{2d}\sqrt{1-\left(\frac{T}{T_0}\right)^6}, \end{aligned} \tag{4.23}$$

as a result of (4.22).

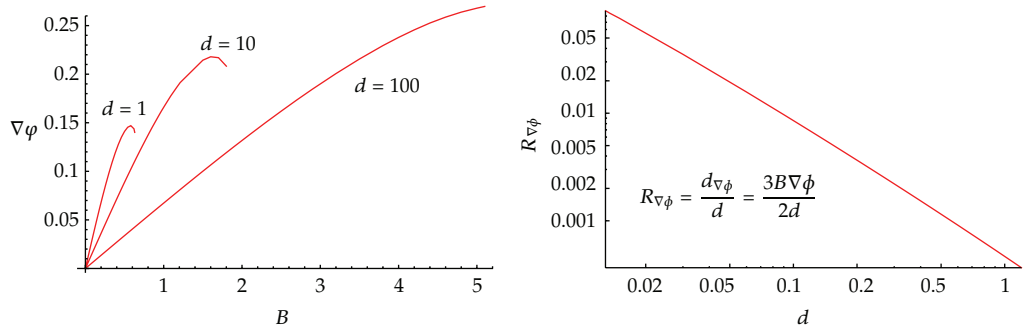

Figure 15: (a) The pion gradient as a function of B for density $d = 1, 10, 100$ at $T = 0.10$. (b) The density ratio of the pion gradient with respect to the total baryon density of the multiquark phase at $B = 0.10$ and $T = 0.10$ in the double-log scale.

As the nuclear matter gets denser, the linear response of the chiral condensate to the magnetic field becomes smaller. The multiquark contribution to the baryonic charge density becomes dominant. In the extremely dense situation, the dominating phase of the deconfined nuclear matter is the multiquark with tiny mixture of the pion gradient when the magnetic field is present.

The remaining important issue is whether the MQ-$\nabla\varphi$ phase is more thermodynamically preferred than other phases such as the pure pion gradient and the chiral-symmetric QGP. Under which circumstances that the MQ-$\nabla\varphi$ phase is the most preferred and what the phase diagram of the deconfined nuclear matter in the SS model looks like are to be discussed.

5. Comparison to Other Phases

In the presence of the magnetic field, there are 4 possible nuclear phases in the deconfined SS model. For zero baryonic charge density and currents, there is a brane configuration corresponding to a magnetized vacuum. For nonzero baryon density, there are 3 possible brane configurations corresponding to 3 different nuclear phases:

MQ-$\nabla\varphi$ Phase

$j_A = 0,\ \mu_{\text{source}} = a_0^V(u_c),\ \nabla\varphi = a_1^A(\infty),\ a_1^A(u_c) = 0,$

Pure Pion Gradient Phase

The same conditions with the MQ-$\nabla\varphi$ phase except, $\mu_{\text{source}} = 0,\ a_0^V(u_c) \neq 0,\ d = (3/2)B\nabla\varphi,\ x_4'(u_c) \to \infty,$

χS-QGP

$x_4'(u) = 0$ and $\nabla\varphi = a_1^A(\infty) = 0,\ \mu_{\text{source}} = a_0^V(u_c = u_T) = 0,\ j_A = (3/2)B\mu$ (in order to satisfy the equation of motion at u_T with $f(u_T) = 0$).

The pure pion gradient phase corresponds to the brane configuration with no instanton at the tip u_c, where D8 and $\overline{\text{D8}}$ connect and thus $\mu_{\text{source}} = 0$. The chiral condensate

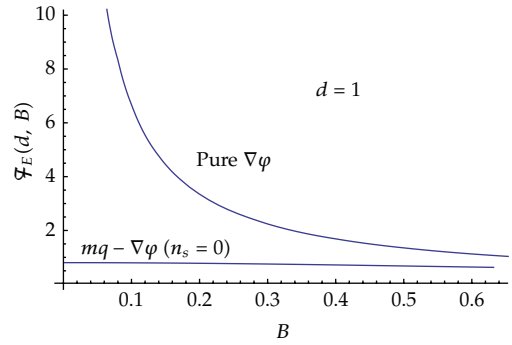

Figure 16: The free energy as a function of the density of the pure pion gradient phase compared to the multiquark-$\nabla\varphi$ phase at fixed $d = 1.0,\ T = 0$.

responds to the magnetic field by generating a gradient in the direction of the field. The induced domain wall carries baryonic charge density according to $d = 3B\nabla\varphi/2$ [56]. Since there is no instanton at the tip, the branes connect smoothly just like in the case of vacuum and $x_4'(u_c) \to \infty$.

The χS-QGP phase corresponds to the brane configuration with the D8 parallel to the $\overline{\text{D8}}$. Both branes never connect, and the distance between them in the direction x_4 is fixed to L_0. There is also no instanton source at the tip and $\mu_{\text{source}} = 0$. Chiral symmetry demands that $a_1^A(\infty) = \nabla\varphi = 0$. Remarkably, the equation of motion in the bulk automatically governs that the axial current is generated with $j_A = 3B\mu/2$, a linear response of the magnetic field [57].

In the following subsections, we will compare the MQ-$\nabla\varphi$ with the pure pion gradient phase and subsequently the χS-QGP phase. By using the free energy at fixed density, it will be demonstrated that the pure pion gradient is always less energetically preferred than the MQ-$\nabla\varphi$ for sufficiently large chemical potential. The second order phase transition lines between the 2 phases are drawn. The MQ-$\nabla\varphi$ phase is shown to be more preferred than the χS-QGP for moderate fields and temperatures. For very large field and temperature, the χS-QGP phase is the most thermodynamically preferred at a fixed density. Phase diagrams between the MQ-$\nabla\varphi$ and the χS-QGP for a fixed magnetic field and temperature are drawn and approximated with the power law.

5.1. Multiquark-Domain Wall versus Pure $\nabla\varphi$ Phase

The pure pion gradient phase has been explored in details in [56] using the effective field theory with the anomalous WZW action. The zero-temperature behaviour in the confined SS model and the bottom-up AdS/QCD model is studied in [47] and [61], respectively. Reference [62] compares the pure pion gradient phase with the χS-QGP by approximating $f(u) \simeq 1$ for the pure pion gradient phase. In this subsection, we will present the results from [63] where the full temperature dependence is taken into consideration.

Figure 16 shows the free energy at fixed density $d = 1$ of the pure $\nabla\varphi$ and the MQ-$\nabla\varphi$ phases as functions of the magnetic field. Apparently, the MQ-$\nabla\varphi$ is more energetically preferred than the pure pion gradient. At higher densities, since $\mu \sim d$ for the pure $\nabla\varphi$ [63] and $\mu \sim d^n, n < 1$ for the MQ-$\nabla\varphi$, the dominant term μd in the free energy will make the MQ-$\nabla\varphi$ phase even more energetically preferred (with smaller free energy). It has been confirmed

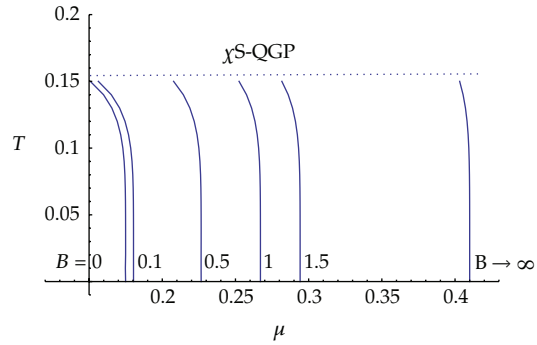

Figure 17: The onset chemical potential of the multiquark-$\nabla\varphi$ phase as a function of T, B (for $B \to \infty$, $u_0 = 1.23$ is used). These lines can be served as the transition lines between the $\nabla\varphi$ phase on the left and multiquark-$\nabla\varphi$ phase ($n_s = 0$) on the right. The dotted line represents schematic transition to the chiral-symmetric QGP phase.

numerically down to $d = 0.1$ that the MQ-$\nabla\varphi$ is always more thermodynamically preferred than the pure $\nabla\varphi$ phase.

However, in the region of the parameter space, where the baryon chemical potential is smaller than the onset chemical potential of the multiquarks, only pure $\nabla\varphi$ phase can exist. The curve of the onset chemical potential of the multiquarks can thus be served as the second order transition line between the two phases. It depends on both the temperature and magnetic field in presence given by

$$\mu_{\text{onset}} = \frac{1}{3}u_c\sqrt{f(u_c)} + n_s(u_c - u_T), \tag{5.1}$$

where u_c is a function of both B and T. The phase diagram (μ, T) between the pure $\nabla\varphi$ and MQ-$\nabla\varphi$ is shown in Figure 17.

The dotted line in the phase diagram represents a schematic transition from a chirally broken nuclear phases to the chiral-symmetric QGP phase. The transition from the pure $\nabla\varphi$ to the χS-QGP is investigated in [62]. Transition between the MQ-$\nabla\varphi$ and the χS-QGP will be discussed in the next subsection.

5.2. Multiquark-Domain Wall versus χS-QGP Phase

In this subsection, we explore the phase diagram of the MQ-$\nabla\varphi$ and the χS-QGP phases. For a fixed density, the baryon chemical potential and the free energy of each phase can be plotted as in Figure 18 [58, 60]. The MQ-$\nabla\varphi$ is energetically preferred for small and intermediate fields for a fixed density. As the field increases further, the chiral-symmetric QGP becomes more favourable. At even larger fields, the curve of the χS-QGP has a break signifying a phase transition to the lowest Landau level [62, 64].

The phase diagrams (d, B) for fixed temperature and (d, T) for fixed magnetic field are presented in Figure 19. At given magnetic field and temperature, the MQ-$\nabla\varphi$ phase is more energetically preferred for a sufficiently large density. Dense nuclear matter prefers to form multiquark states even in the presence of the magnetic field. Nevertheless, for a given density, sufficiently high field and temperature will make the MQ-$\nabla\varphi$ phase less preferred than the χS-QGP.

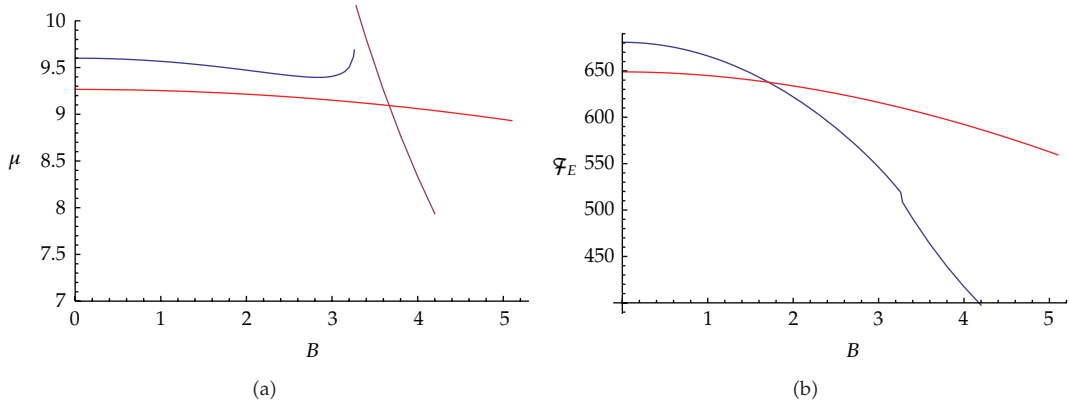

Figure 18: For the dense multiquark with $d = 100$, $T = 0.10$, (a) the chemical potential, (b) the free energy as a function of B. The multiquark curves in red are compared with the χS-QGP curves in blue for the chemical potential and the free energy.

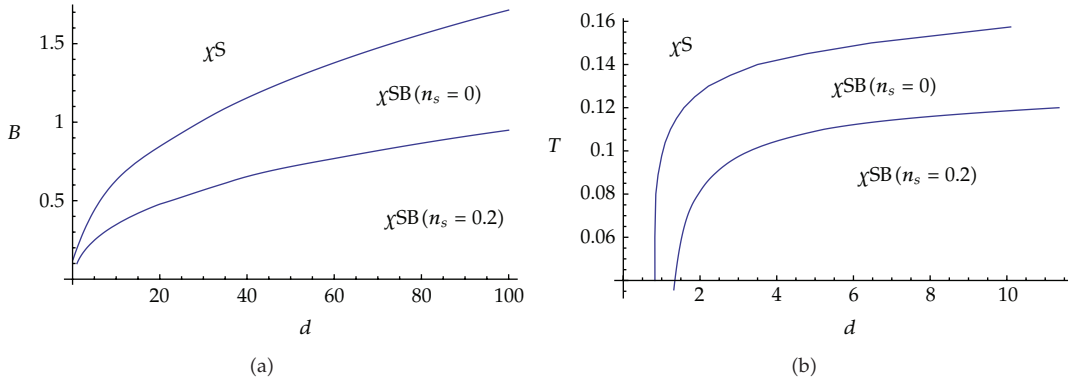

Figure 19: The phase diagram of the dense nuclear phases involving multiquarks when gluons are deconfined for (a) $T = 0.10$ and (b) $B = 0.20$. The chiral-symmetric quark-gluon plasma and the chirally broken MQ-$\nabla\varphi$ phase are represented by χS and χSB, respectively, n_s is the number of colour strings in fractions of $1/N_c$.

The transition lines between the χS-QGP and the MQ-$\nabla\varphi$ phases in the (d, B) phase diagram can be approximated with a power law,

$$B \sim d^{0.438(0.436)}, \tag{5.2}$$

for multiquarks with $n_S = 0(0.2)$ at $T = 0.10$. This is weaker than the power-law $B \sim d^{2/3}$ of the χS-QGP transition to the lowest Landau level studied in [64]. On the other hand, the transition line in the (d, T) phase diagram is weaker than a logarithm, yet still an increasing function of d.

6. Conclusions

In this paper, we review the development of the holographic multiquark states in the deconfined quark-gluon plasma. We discuss their physical properties such as the binding energy, the screening length, the thermodynamical properties and the equation of state. Using the Sakai-Sugimoto model, we also explore the possible phase diagram of the multiquark matter. The multiquark phase is the most energetically preferred when the density and/or the baryon chemical potential is sufficiently large and the temperature is not too high. Even though the multiquark states with colour degrees of freedom are less preferred than the colour-singlet baryons, they are more energetically favoured than the other phases in such dense condition.

The magnetic properties and the magnetic phase diagram of the multiquark matter are subsequently reviewed. There are 2 possible holographic multiquark configurations, both of them are stable under density fluctuations. High magnetic field and temperature merge the 2 configurations into one. Once they merge, they transit to the multiquark configurations with larger densities, or to the chiral-symmetric QGP phase. In the region of the parameter space with sufficiently large densities and moderate fields at a fixed temperature, the magnetized multiquark phase is the most thermodynamically preferred. For a fixed magnetic field, sufficiently high temperature will melt the multiquarks into quarks and gluons regardless of the density.

In the region of parameter space with small density and baryon chemical potential ($\mu < \mu_{\text{onset}}$ of the multiquarks), another magnetized nuclear phase called the pure pion gradient is dominant. When chiral symmetry is broken, an external strong magnetic field could induce a response of the chiral condensate in the direction of the applied field. The generated pion gradient also carries baryonic charge density and the corresponding chemical potential. However, once $\mu > \mu_{\text{onset}}$ of the multiquarks, the multiquark phase is always energetically preferred than the pure pion gradient. Inevitably, the pion gradient is also induced in the multiquark matter under the external field and render the multiquark matter in a mixed MQ-$\nabla\varphi$ phase. The population of the pion gradient in the mixed phase is found to be a decreasing function with respect to the baryon density.

Appendix

Force Condition of the Multiquark Configuration

The forces on the D4-brane in the flavour D8-branes are balanced among three forces from the tidal weight of the D4-brane, the force from the strings attached to the D4, and the force from the D8-branes. Varying the total action with respect to u_c gives the surface term. Together with the scale-fixing condition $2\int_{u_c}^{\infty} du x_4'(u) = L_0 = 1$, we obtain [48]

$$x_4'(u_c) = \left.\frac{\left(\widetilde{L}(u_c) - (\partial S_{\text{source}}/\partial u_c)\right)}{\partial \widetilde{S}/\partial x_4'}\right|_{u_c}, \tag{A.1}$$

as the condition on u_c.

The Legendre transformed action is given by

$$\begin{aligned}\widetilde{S} &= \int_{u_c}^{\infty} \widetilde{L}(x_4'(u), d)du \\ &= \mathcal{N}\int_{u_c}^{\infty} du\sqrt{\frac{1}{f(u)} + u^3 x_4'^2} \\ &\quad \times \sqrt{f(u)\Big(C(u) + D(u)^2\Big) - \left(j_A - \frac{3}{2}B\mu + 3Ba_0^V\right)^2},\end{aligned} \tag{A.2}$$

where $C(u) \equiv u^5 + B^2u^2$, $D(u) \equiv d + 3Ba_1^A(u) - 3B\nabla\varphi/2$. It is calculated by performing Legendre transformation with respect to $a_0^{V\prime}$ and $a_1^{A\prime}$, respectively. Note that the Chern-Simons action is also included in the total action during the transformations.

The Chern-Simons term with the derivatives $a^{V\prime}, a^{A\prime}$ eliminated is

$$S_{\mathrm{CS}} = -\mathcal{N}\frac{3}{2}B\int_{u_c}^{\infty} du\frac{\left(a_0^V\left(j_A - (3/2)B\mu + 3Ba_0^V\right) - f(u)D(u)a_1^A\right)\sqrt{1/f(u) + u^3x_4'^2}}{\sqrt{f(u)\Big(C(u) + D(u)^2\Big) - \left(j_A - (3/2)B\mu + 3Ba_0^V\right)^2}}. \tag{A.3}$$

Lastly, in order to compute $x_4'(u_c)$ we consider the source term [12]

$$S_{\mathrm{source}} = \mathcal{N}d(u_c)\left[\frac{1}{3}u_c\sqrt{f(u_c)} + n_s(u_c - u_T)\right] \tag{A.4}$$

$$\simeq \mathcal{N}d\mu_{\mathrm{source}}, \tag{A.5}$$

where $n_s = k_r/N_c$ is the number of radial strings in the unit of $1/N_c$. We have approximated the electric displacement at the position of the D4 brane source, $d(u_c) \equiv -\partial L/\partial a_0^{V'}|_{u_c} = d - (3/2)Ba_1^A(\infty)$ with d.

From (A.1), (A.2), (A.3), (A.5), and setting $a_0^V(u_c) = \mu_{\mathrm{source}}$, $a_1^A(u_c) = 0$ we can solve to obtain

$$\left(x_4'(u_c)\right)^2 = \frac{1}{f_c u_c^3}\left[\frac{9}{d^2}\frac{\left(f_c\left(C_c + D_c^2\right) - \left(j_A - (3/2)B\mu + 3Ba_0^V(u_c)\right)^2\right)}{\left(1 + (1/2)(u_T/u_c)^3 + 3n_s\sqrt{f_c}\right)^2} - 1\right], \tag{A.6}$$

where $f_c \equiv f(u_c)$, $C_c \equiv C(u_c)$, $D_c \equiv D(u_c)$.

When we fix the parameter n_s, the temperature T, the baryon density d, the axial current $j_A = 0$ (by minimizing the action with respect to $a_1^A(\infty)$), and setting $a_1^A(u_c) = 0, a_0^V(u_c) = \mu_{\mathrm{source}}$, then the position u_c of the D4-brane is completely determined as a function of the magnetic field B. Once the equations of motion are solved, the value of $\mu = a_0^V(\infty)$ and $a_1^A(\infty)$ are determined.

In the case of no magnetic field and finite baryon density, the force balance condition at the tip can be obtained simply by using (A.6). It can be done by setting all spatial components

of bulk $U(1)$ gauge fields to be zero, leaving only the time component nonvanishing. This results in $C_c = u_c^5$ and $D_c = d$. Therefore, we obtain

$$\left(x_4'(u_c)\right)^2 = \frac{1}{f_c u_c^3}\left[\frac{9}{d^2}\frac{f_c\left(u_c^5 + d^2\right)}{\left(1 + (1/2)(u_T/u_c)^3 + 3n_s\sqrt{f_c}\right)^2} - 1\right], \tag{A.7}$$

implying the force balance condition at the tip.

Acknowledgments

Ekapong Hirunsirisawat is supported in part by the Commission on Higher Education (CHE), Thailand, under the Program Strategic Scholarships for Frontier Research Network for the Thai Doctoral Degree Program for this research. Piyabut Burikham is supported in part by the Toray Science Foundation, Japan (TSF), the Thailand Research Fund (TRF), and Commission on Higher Education (CHE) under Grant RMU5380048 and also by the Thailand Center of Excellence in Physics (ThEP). Piyabut Burikham and Ekapong Hirunsirisawat are also supported in part by Research Strategic (A1B1), Research Funds from the Faculty of Science, Chulalongkorn University.

References

[1] V. Khachatryan, A. M. Sirunyan, A. Tumasyan et al., "Observation of long-range, near-side angular correlations in proton-proton collisions at the LHC," *Journal of High Energy Physics*, vol. 2010, no. 9, pp. 1–38, 2010.

[2] E. Laermann and O. Philipsen, "Lattice QCD at finite temperature," *Annual Review of Nuclear and Particle Science*, vol. 53, pp. 163–198, 2003.

[3] T. Umeda, R. Katayama, O. Miyamura, and H. Matsufuru, "The study of charmonia near the deconfining transition on an anisotropic lattice with O(a) improved quark action," *International Journal of Modern Physics A*, vol. 16, no. 12, pp. 2215–2241, 2001.

[4] M. Asakawa and T. Hatsuda, "J/ψ and ηc in the deconfined plasma from lattice QCD," *Physical Review Letters*, vol. 92, no. 1, Article ID 012001, 4 pages, 2004.

[5] H. Iida, T. Doi, N. Ishii, and H. Suganuma, "J/Psi at high temperatures in anisotropic lattice QCD," *POS*, vol. LAT2005, article 184, 2006.

[6] J. M. Maldacena, "The Large N limit of superconformal field theories and supergravity," *Advances in Theoretical and Mathematical Physics*, vol. 2, pp. 231–252, 1998.

[7] E. Witten, "Anti-de Sitter space and holography," *Advances in Theoretical and Mathematical Physics*, vol. 2, pp. 253–291, 1998.

[8] E. Witten, "Anti-de Sitter space, thermal phase transition, and confinement in gauge theories," *Advances in Theoretical and Mathematical Physics*, vol. 2, no. 3, pp. 505–532, 1998.

[9] E. Witten, "Baryons and branes in anti de Sitter space," *Journal of High Energy Physics*, vol. 2, no. 7, 1998.

[10] D. J. Gross and H. Ooguri, "Aspects of large N gauge theory dynamics as seen by string theory," *Physical Review D*, vol. 58, no. 10, Article ID 106002, 12 pages, 1998.

[11] A. Brandhuber, N. Itzhaki, J. Sonnenschein, and S. Yankielowicz, "Baryons from supergravity," *Journal of High Energy Physics*, vol. 2, no. 7, article 020, 1998.

[12] P. Burikham, A. Chatrabhuti, and E. Hirunsirisawat, "Exotic multi-quark states in the deconfined phase from gravity dual models," *Journal of High Energy Physics*, vol. 2009, no. 5, article 006, 2009.

[13] T. Sakai and S. Sugimoto, "Low energy hadron physics in holographic QCD," *Progress of Theoretical Physics*, vol. 113, no. 4, pp. 843–882, 2005.

[14] T. Sakai and S. Sugimoto, "More on a holographic dual of QCD," *Progress of Theoretical Physics*, vol. 114, no. 5, pp. 1083–1118, 2005.

[15] R. L. Jaffe, "Multiquark hadrons. II. Methods," *Physical Review D*, vol. 15, no. 1, pp. 281–289, 1977.

[16] R. L. Jaffe, "Multiquark hadrons. I. Phenomenology of $Q^2\overline{Q}^2$ mesons," *Physical Review D*, vol. 15, no. 1, pp. 267–280, 1977.

[17] R. L. Jaffe, "Perhaps a stable dihyperon," *Physical Review Letters*, vol. 38, no. 5, pp. 195–198, 1977.

[18] R. L. Jaffe, "Exotica," *Physics Reports*, vol. 409, no. 1, pp. 1–45, 2005.

[19] J. Adams, M. M. Aggarwal, Z. Ahammed et al., "Experimental and theoretical challenges in the search for the quark-gluon plasma: the STAR Collaboration's critical assessment of the evidence from RHIC collisions," *Nuclear Physics A*, vol. 757, no. 1-2, pp. 102–183, 2005.

[20] B. B. Back, M. D. Baker, M. Ballintijn et al., "The PHOBOS perspective on discoveries at RHIC," *Nuclear Physics A*, vol. 757, no. 1-2, pp. 28–101, 2005.

[21] K. Adcox, S. S. Adler, S. Afanasiev et al., "Formation of dense partonic matter in relativistic nucleus-nucleus collisions at RHIC: experimental evaluation by the PHENIX Collaboration," *Nuclear Physics A*, vol. 757, no. 1-2, pp. 184–283, 2005.

[22] I. Arsene, I. G. Bearden, D. Beavis et al., "Quark-gluon plasma and color glass condensate at RHIC? The perspective from the BRAHMS experiment," *Nuclear Physics A*, vol. 757, no. 1-2, pp. 1–27, 2005.

[23] J. Liao and E. V. Shuryak, "Polymer chains and baryons in a strongly coupled quark-gluon plasma," *Nuclear Physics A*, vol. 775, no. 3-4, pp. 224–234, 2006.

[24] E. V. Shuryak and I. Zahed, "Rethinking the properties of the quark-gluon plasma at Tc < T < 4Tc," *Physical Review C*, vol. 70, no. 2, Article ID 21901, pp. 1–4, 2004.

[25] E. V. Shuryak and I. Zahed, "Toward a theory of binary bound states in the quark-gluon plasma," *Physical Review D*, vol. 70, no. 5, Article ID 054507, 16 pages, 2004.

[26] Y. Imamura, "Baryon mass and phase transitions in large N gauge theory," *Progress of Theoretical Physics*, vol. 100, no. 6, pp. 1263–1272, 1998.

[27] K. Ghoroku and M. Ishihara, "Baryons with D5-brane vertex and k-quark states," *Physical Review D*, vol. 77, no. 8, Article ID 086003, 11 pages, 2008.

[28] K. Ghoroku, M. Ishihara, A. Nakamura, and F. Toyoda, "Multiquark baryons and color screening at finite temperature," *Physical Review D*, vol. 79, no. 6, 11 pages, 2009.

[29] M. Bando, T. Kugo, A. Sugamoto, and S. Terunuma, "Pentaquark baryons in string theory," *Progress of Theoretical Physics*, vol. 112, no. 2, pp. 325–355, 2004.

[30] W. Y. Wen, "Multi-quark potential from AdS/QCD," *International Journal of Modern Physics*, vol. 23, pp. 4533–4543, 2008.

[31] M. V. Carlucci, F. Giannuzzi, G. Nardulli, M. Pellicoro, and S. Stramaglia, "AdS-QCD quark-antiquark potential, meson spectrum and tetraquarks," *European Physical Journal C*, vol. 57, no. 3, pp. 569–578, 2008.

[32] H. Forkel, "Light scalar tetraquarks from a holographic perspective," *Physics Letters, Section B*, vol. 694, no. 3, pp. 252–257, 2010.

[33] K. Ghoroku, A. Nakamura, T. Taminato, and F. Toyoda, "Holographic penta and hepta quark state in confining gauge theories," *Journal of High Energy Physics*, vol. 2010, no. 8, article 007, 2010.

[34] J. Polchinski and M. J. Strassler, "The string dual of a confining four-dimensional gauge theory," http://arxiv.org/abs/hep-th/0003136.

[35] I. R. Klebanov and M. J. Strassler, "Supergravity and a confining gauge theory: duality cascades and χSB-resolution of naked singularities," *Journal of High Energy Physics*, vol. 4, no. 8, pp. 21–35, 2000.

[36] J. Maldacena and C. Nuñez, "Towards the large N limit of pure N = 1 super Yang-Mills theory," *Physical Review Letters*, vol. 86, no. 4, pp. 588–591, 2001.

[37] O. Aharony, J. Sonnenschein, and S. Yankielowicz, "A holographic model of deconfinement and chiral symmetry restoration," *Annals of Physics*, vol. 322, no. 6, pp. 1420–1443, 2007.

[38] K. Peeters and M. Zamaklar, "The string/gauge theory correspondence in QCD," *European Physical Journal*, vol. 152, no. 1, pp. 113–138, 2007.

[39] C. G. Callan, A. Güijosa, and K. G. Savvidy, "Baryons and string creation from the 5-brane world-volume action," *Nuclear Physics B*, vol. 547, no. 1-2, pp. 127–142, 1999.

[40] C. G. Callan, A. Güijosa, K. G. Savvidy, and O. Tafjord, "Baryons and flux tubes in confining gauge theories from brane actions," *Nuclear Physics B*, vol. 555, no. 1-2, pp. 183–200, 1999.

[41] J. Maldacena, "Wilson loops in large N field theories," *Physical Review Letters*, vol. 80, no. 22, pp. 4859–4862, 1998.

[42] S. W. Hawking, "The path integral approach to quantum gravity," in *General Relativity:An Einstein Centenary Survey*, S. W. Hawking and W. Israel, Eds., pp. 746–789, Cambridge University Press, New York, NY, USA, 1979.

[43] S. Kobayashi, D. Mateos, S. Matsuura, R. C. Myers, and R. M. Thomson, "Holographic phase transitions at finite baryon density," *Journal of High Energy Physics*, vol. 2007, no. 2, article 016, 2007.
[44] A. Chamblin, R. Emparan, C. V. Johnson, and R. C. Myers, "Charged AdS black holes and catastrophic holography," *Physical Review D*, vol. 60, no. 6, 17 pages, 1999.
[45] A. Chamblin, R. Emparan, C. V. Johnson, and R. C. Myers, "Holography, thermodynamics, and fluctuations of charged AdS black holes," *Physical Review D*, vol. 60, no. 10, pp. 1–20, 1999.
[46] D. Mateos, S. Matsuura, R. C. Myers, and R. M. Thomson, "Holographic phase transitions at finite chemical potential," *Journal of High Energy Physics*, vol. 2007, no. 11, article 085, 2007.
[47] O. Bergman, G. Lifschytz, and M. Lippert, "Response of holographic QCD to electric and magnetic fields," *Journal of High Energy Physics*, vol. 2008, no. 5, article 007, 2008.
[48] O. Bergman, M. Lippert, and G. Lifschytz, "Holographic nuclear physics," *Journal of High Energy Physics*, vol. 2007, no. 11, article 056, 2007.
[49] J. Polchinski, String Theory. Vol. 2: Superstring Theory and Beyond.
[50] M. R. Douglas, "Branes within branes," http://arxiv.org/abs/hep-th/9512077.
[51] N. Horigome and Y. Tanii, "Holographic chiral phase transition with chemical potential," *Journal of High Energy Physics*, vol. 2007, no. 1, article 072, 2007.
[52] P. Burikham, E. Hirunsirisawat, and S. Pinkanjanarod, "Thermodynamic properties of holographic multiquark and the multiquark star," *Journal of High Energy Physics*, vol. 2010, no. 6, article 040, 2010.
[53] T. Vachaspati, "Magnetic fields from cosmological phase transitions," *Physics Letters, Section B*, vol. 265, no. 3-4, pp. 258–261, 1991.
[54] D. E. Kharzeev, L. D. McLerran, and H. J. Warringa, "The effects of topological charge change in heavy ion collisions: 'Event by event P and CP violation'," *Nuclear Physics A*, vol. 803, no. 3-4, pp. 227–253, 2008.
[55] R. C. Duncan and C. Thompson, "Formation of very strongly magnetized neutron stars: implications for gamma-ray bursts," *Astrophysical Journal*, vol. 392, no. 1, pp. L9–L13, 1992.
[56] D. T. Son and M. A. Stephanov, "Axial anomaly and magnetism of nuclear and quark matter," *Physical Review D*, vol. 77, no. 1, Article ID 014021, 9 pages, 2008.
[57] O. Bergman, G. Lifschytz, and M. Lippert, "Magnetic properties of dense holographic QCD," *Physical Review D*, vol. 79, no. 10, 2009.
[58] P. Burikham, "Magnetic properties of holographic multiquarks in the quark-gluon plasma," *Journal of High Energy Physics*, vol. 2010, no. 4, article 045, 2010.
[59] O. Aharony, S. S. Gubser, J. Maldacena, H. Ooguri, and Y. Oz, "Large N field theories, string theory and gravity," *Physics Report*, vol. 323, no. 3-4, pp. 183–386, 2000.
[60] P. Burikham, "Magnetic phase diagram of dense holographic multiquarks in the quark-gluon plasma," *Journal of High Energy Physics*, vol. 2011, no. 5, article 121, 2011.
[61] E. G. Thompson and D. T. Son, "Magnetized baryonic matter in holographic QCD," *Physical Review D*, vol. 78, no. 6, Article ID 066007, 6 pages, 2008.
[62] F. Preis, A. Rebhan, and A. Schmitt, "Inverse magnetic catalysis in dense holographic matter," *Journal of High Energy Physics*, vol. 2011, no. 3, article 033, 2011.
[63] P. Burikham and T. Chullaphan, "Magnetized domain walls in the deconfined sakai-sugimoto model at finite baryon density," *Journal of High Energy Physics*, vol. 2011, article 026, 2011.
[64] G. Lifschytz and M. Lippert, "Holographic magnetic phase transition," *Physical Review D*, vol. 80, no. 6, Article ID 066007, 7 pages, 2009.

Published for SISSA by Springer

Received: March 13, 2012
Accepted: May 14, 2012
Published: June 4, 2012

Holographic magnetic star

Piyabut Burikham[a,b] **and Tossaporn Chullaphan**[a]

[a] *Theoretical High-Energy Physics and Cosmology Group, Department of Physics, Faculty of Science, Chulalongkorn University, Phyathai Road, Bangkok 10330, Thailand*

[b] *Thailand Center of Excellence in Physics, CHE, Ministry of Education, Bangkok 10400, Thailand*

E-mail: piyabut@gmail.com, chullaphan.t@gmail.com

Abstract: A warm fermionic AdS star under a homogeneous magnetic field is explored. We obtain the relativistic Landau levels by using Dirac equation and use the Tolman-Oppenheimer-Volkoff (TOV) equation to study the physical profiles of the star. Bulk properties such as sound speed, adiabatic index, and entropy density within the star are calculated analytically and numerically. Bulk temperature increases the mass limit of the AdS star but external magnetic field has the opposite effect. The results are partially interpreted in terms of the pre-thermalization process of the gauge matter at the AdS boundary after the mass injection. The entropy density is found to demonstrate similar temperature dependence as the magnetic black brane in the AdS in certain limits regardless of the different nature of the bulk and Hawking temperatures. Total entropy of the AdS star is also found to be an increasing function of the bulk temperature and a decreasing function of the magnetic field, similar behaviour to the mass limit. Since both total entropy and mass limit are global quantities, they could provide some hints to the value of entropy and energy of the dual gauge matter before and during the thermalization.

Keywords: Holography and quark-gluon plasmas, Gauge-gravity correspondence, AdS-CFT Correspondence

ArXiv ePrint: 1203.0883

doi:10.1007/JHEP06(2012)021

JHEP06(2012)021

Contents

JHEP06(2012)021

1 Introduction

Duality between gravity and gauge theory in spacetime with different dimensionalities has been discovered by Maldacena in 1998 [1]. The type-IIB string theory in $AdS_5 \times S_5$ is conjectured to be dual to a gauge theory in four dimensional Minkowski spacetime (M_4) at the boundary of the AdS space. The correspondence can be used as a complementary method to study the strongly coupled gauge theory in four dimensional Minkowski spacetime, a cousin of quantum chromodynamics, by avoiding the uncontrollable non-perturbative calculation via the application of weak-strong duality. We can deal with this problem by alternatively performing calculations in the tractable weakly interacting string theory in

five (plus five compact dimensions which provide details that are not relevant here) dimensional Anti de Sitter space (AdS_5). The duality is extended to a finite temperature situation by adding a horizon in the radial coordinate [2]. The string theory in an AdS space with black hole horizon in the radial direction is proposed to be dual to a gauge theory at finite temperature. The duality is made quantitative in the sense that the Hawking temperature in the bulk theory corresponds to the temperature of the gauge theory on the boundary. The AdS/CFT correspondence provides the first string-theoretic example of the underlying generic principle of the holographic duality (i.e. the holographic principle).

The idea of holographic duality was originally proposed by 't Hooft [3] in a generic quantum gravity situation involving a gravitational horizon. The precise string theoretic version was given by Susskind [4]. When an object falls into a black hole, it will be stretched, torn apart into bits and eventually the bits will be smeared out over the horizon. Consequently, all of the bulk information is spread over the horizonal surface resulting in an effective boundary description of the bulk theory. The bulk world is holographically encoded on the boundary. Connection between AdS space and holography was further clarified by Witten [5] after discovery of the AdS/CFT correspondence.

Given an AdS space, the weakly-coupled bulk gravity theory corresponds to a strongly-coupled boundary gauge theory. Adding a black hole to the AdS space, the dual gauge theory on the boundary becomes thermal with the temperature equal to the corresponding Hawking-Page temperature of the background [6]. It is thus interesting to investigate the intermediate situation where there exists a massive object before gravitational collapse into a black hole in the AdS space and search for the dual description in the gauge theory side. It is argued in ref. [7, 8] that the degenerate fermions in the AdS correspond to the composite multitrace operator constructed from product of single trace operators in the large central charge limit on the boundary. It is not unreasonable to think of this "free" fermionic operator as the conformal cousin of a QCD nucleon such as neutron and proton. These "free fermions", however, still interact with each other by the colour-singlet interaction of order $1/N$ assuming negligible in the large N limit. The colour-singlet (glueball) exchange on the boundary corresponds holographically to the gravitational interaction in the bulk. While gravity pulls the bulk mass together causing the gravitational collapse, the colour-singlet interaction should be responsible for the deconfinement phase transition of the injected mass in the dual picture.

Arguably, the gravitational collapse of the star in the AdS would correspond to a thermalization process of the dual gauge matter on the boundary [9–15]. Consideration of the mass limit of the fermionic star in the AdS bulk could reveal certain details of the pre-thermalization process in the dual gauge picture. The mass limit of the AdS star corresponds to the minimum amount of injected mass required in order for the boundary gauge matter to start the thermalization process (since the bulk gravitational collapse starts when injected mass exceeds the mass limit). Specifically, it is also interesting to ask what the dual object of the bulk temperature is on the boundary world before black hole formation? Should it correspond to some parameter characterizing the superheated phase of gauge matter before the start of the thermalization? Moreover, what is the exact nature of the colour-singlet (glueball exchange) interaction responsible for the deconfinement of

JHEP06(2012)021

the dual gauge matter into the thermalized deconfined plasma (which is the dual picture of the gravitational collapse caused by gravity)?

The heavy-ion collision experiments at RHIC and CERN's LHC (Large Hadron Collider) smash two charged ions at extreme energies, producing dense and hot nuclear matter with properties of the strongly coupled plasma. In the vicinity of the collision point, the induced magnetic field could be enormous [16]. Understanding the physics of dense hot nuclear plasma under such circumstances requires nonperturbative treatments of the strong interaction and the holographic method is one option. One holographic dual of the magnetized nuclear matter at finite temperature is proposed to be a magnetized black brane in the AdS space [17]. It was found that the entropy density of the magnetized brane in the AdS obeys the third law of thermodynamics with entropy $S \sim T$ (temperature) for small temperature.

In this article, we consider a fermionic star in the holographic AdS_5 background in the presence of external magnetic field at finite bulk temperature. The mass limit and other properties of the star is studied with respect to the changes in the magnetic field and bulk temperature. Even though there is no complete understanding of the dual description in the gauge theory side of this situation, we argue certain aspects of the duality. In section 2, the Tolman-Oppenheimer-Volkoff (TOV) equation [18, 19] in the background AdS_5 is calculated starting from the general dimensionality. The energy levels of the bulk charged fermions in the presence of the magnetic field are calculated in the flat space approximation. The pressure and density of the bulk fermions at finite field and temperature are subsequently derived. Section 3 presents analytic and numerical results for each case of finite temperature and field. The mass limits depend crucially on the field and bulk temperature. The mass-radius relations for each case are discussed in section 4. The bulk adiabatic index and sound speed of the fermions inside the AdS star are discussed in section 5. The entropy density and total entropy in the bulk are also computed. Section 6 investigates the dependence of mass limit on the AdS radius. Section 7 contains further discussions and summary of our results.

2 Holographic star under external magnetic field

The study of the magnetized star in the AdS space consists of two main calculations. First, the pressure and energy density need to be calculated for the system of charged fermions in the magnetic field at arbitrary temperature. The star will be assumed electrically neutral and we will focus only on the effect of magnetic field to the charged particles. At zero temperature, the energy states of the charged fermions in the magnetic field are separated naturally into Landau levels. The partition function in the macrocanonical ensemble of these energy levels will provide the generic expression for the pressure and energy density of the fermionic system at finite temperature. The pressure and energy density are subsequently used in the equation of state required by the TOV equation in the 5-dimensional AdS spacetime. Even though we will focus on interpreting the results of the bulk AdS star in terms of the dual gauge theory, the calculations in the bulk picture are self-consistent and satisfactorily describe a real magnetized fermionic star in the 5-dimensional AdS spacetime.

JHEP06(2012)021

2.1 The equations of hydrostatic equilibrium for a spherical symmetric star in d dimensions

In order to study the behaviour of a degenerate star in d-dimensional AdS spacetime, we derive the spherical symmetric TOV equation in d dimensions as given in appendix A. In the presence of external magnetic field, the pressure of the fermionic matter in the star is actually anisotropic due to the quantization of the energy levels. However, in the classical limit where the momentum in the direction of the magnetic field is much larger than the square root of the magnetic field, $< p_z^2 > /m^2c^2 \gg 2Be\hbar/m^2c^3$, the pressure becomes isotropic [20, 21] and the spherical symmetric TOV equation is applicable. The resulting equations of motion describing the AdS star in the spherical symmetric approximation are $T(r) = T_0\mu(r)/\mu_0$ for the temperature $T(r)$, and

$$M'(r) = \frac{2V_{d-2}}{(d-2)}\rho(r)\, r^{d-2}, \tag{2.1}$$

$$\mu'(r) = \mu(r)\left(\frac{B'(r)}{B(r)} - \frac{V_{d-2}C_{d-1}}{(d-2)}\left(\rho(r)\, c^2 + P_r(r)\right) r B^2(r)\right), \tag{2.2}$$

where $B(r) = (1 - \frac{MC_{d-1}}{r^{d-3}} + \frac{r^2}{l^2})^{-1/2}$, l is the AdS radius, V_{d-2} is the area of S^{d-2} and $C_{d-1} = \frac{16\pi G}{(d-2)V_{d-2}c^4}$. To solve the equations of motion, we need the equation of state or the explicit expression of $P(r), \rho(r)$ in terms of the chemical potential $\mu(r)$. Standard evaluation of the partition function requires the layout of energy states of the fermionic system which can be obtained in the following subsection.

2.2 Relativistic Landau energy level in 5 dimensions

We now solve the Dirac equation to find the relativistic energy level of a charged fermion in the presence of external magnetic field in the 5 dimensional spacetime. As an approximation, we will ignore the effect of curvature on the energy levels of the fermions. The effects of gravity and the AdS curvature will be considered only through the Einstein equations stated in the previous subsection. Starting from the Dirac equation in flat space

$$i\hbar\gamma^\mu\partial_\mu\psi - mc\psi = 0, \tag{2.3}$$

where m is the mass of the fermion. The gamma matrices are chosen to be in the Dirac representation as the following

$$\gamma^0 = \begin{pmatrix} \mathbf{1} & 0 \\ 0 & -\mathbf{1} \end{pmatrix}, \qquad \vec{\gamma} = \begin{pmatrix} 0 & \vec{\sigma} \\ -\vec{\sigma} & 0 \end{pmatrix}, \tag{2.4}$$

where $\mathbf{1}$ and $\vec{\sigma}$ are 2×2 identity matrix and Pauli matrices respectively. We will consider only the positive energy solution since we are interested in the particle not the antiparticle. The positive energy solution $\psi(x) = u(p)\, e^{-ipx} = u(p)\, e^{-iEt+i\vec{p}\cdot\vec{x}}$ satisfies the equation $(\gamma^\mu p_\mu - m)\, u(p) = 0$. Let $\hbar = 1$ and consider a particle in an external magnetic field, the effect of the magnetic field can be taken into account by adding the field momentum,

JHEP06(2012)021

$p_\mu \to p_\mu - qA_\mu$. We will choose the magnetic field to point in the z direction and uniformly distributed over the entire x, y, z space. The equation of motion of the fermion in 5 dimensional space becomes

$$\{p_x^2 + p_y^2 + p_z^2 + p_w^2 - 2qBxp_y + q^2B^2x^2 - qB\sigma_z\}\phi = \left(E^2 - m^2c^4\right)\phi. \tag{2.5}$$

The momentum component in the extra dimension is represented by p_w corresponding to the coordinate w. We have assumed the solution in the form $\phi = e^{i(p_y y + p_z z + p_w w)} f(x)$ and neglect the effect of the AdS curvature to the momentum component p_w. This is a good approximation as long as the AdS radius of curvature is large compared to the wavelength of the bulk fermions.

The energy condition from the equation of motion is given by

$$E_n^2 = m^2c^4 + p_z^2c^2 + p_w^2c^2 + (2n - \nu + 1)\, 2mc^2\mu_B B. \quad (n = 0, 1, 2, \ldots, \quad \nu = \pm 1)$$

If we let $j = n - \frac{\nu}{2}$, then we have

$$E_j^2 = m^2c^4 + p_z^2c^2 + p_w^2c^2 + \left(j + \frac{1}{2}\right) 4mc^2\mu_B B, \tag{2.6a}$$

$$= m^2c^4 + p_n^2c^2 + \left(j + \frac{1}{2}\right) 4mc^2\mu_B B. \qquad \left(p_n^2 = p_z^2 + p_w^2\right) \tag{2.6b}$$

From equation (2.6a) and (2.6b), energy is quantized in the $x-y$ plane and contains certain degeneracy of states, i.e., there are several states with the same one-particle energy. The number of states g_j of a discrete energy level j is

$$\begin{aligned} g_j &= \frac{g_s}{h^2}\int dp_x dp_y dx dy = \frac{g_s L_x L_y}{h^2} 2\pi \int_{p_j}^{p_{j+1}} pdp = \frac{g_s \pi L_x L_y}{h^2}\left(p_{j+1}^2 - p_j^2\right), \\ &= \frac{g_s \pi L_x L_y}{h^2}\left(4m\mu_B B\right). \qquad \left(\because p_j^2c^2 = \left(p_x^2 + p_y^2\right)c^2 = 4jmc^2\mu_B B\right) \end{aligned} \tag{2.7}$$

where $g_s(= 2s + 1)$ is a spin degeneracy independent of j. The degeneracy is proportional to the field and vanishes for $B \to 0$. The discrete energies from the degrees of freedom of the plane perpendicular to the magnetic field is called the Landau levels, characterizing the statistical properties of the fermionic system. Extension to finite temperature situation can be done by considering the corresponding partition function.

2.3 Pressure and energy density under magnetic field at finite temperature

Thermodynamical pressure and energy density of the magnetized fermion gas can be calculated from the grand canonical partition function given by

$$\begin{aligned} \ln Z &= \frac{1}{h^2}\int_{-\infty}^{\infty} dp_z dp_{\mathrm{AdS}} dz dx_{\mathrm{AdS}} \sum_{j=0}^{\infty} g_j \ln\left(1 + e^{-\frac{\left(E_j - \mu\right)}{k_B T}}\right), \\ &= \frac{g_s L_x L_y L_z L_{\mathrm{AdS}}}{h^4}\left(4\pi m\mu_B B\right)\int_{-\infty}^{\infty} dp_z dp_{\mathrm{AdS}} \sum_{j=0}^{\infty} \ln\left(1 + e^{-\frac{\left(E_j - \mu\right)}{k_B T}}\right), \\ &= \left(\frac{4g_s \pi m\mu_B BV}{h^4}\right)(2\pi)\int_0^{\infty} p_n dp_n \sum_{j=0}^{\infty} \ln\left(1 + e^{-\frac{\left(E_j - \mu\right)}{k_B T}}\right). \end{aligned} \tag{2.8}$$

Use the Euler-Maclaurin formula (see appendix B) and certain tricks of integration, we finally have the pressure in the asymptotically approximated form

$$
\begin{aligned}
P &= \frac{k_B T}{V} \ln Z = \frac{k_B T}{V} \left(\ln Z_0 + \ln Z_B \right), \\
&\simeq \left(\frac{g_s \pi^2}{2h^4} \right) \left[\int_{mc^2}^{\mu} \left(\frac{\epsilon^2}{c^2} - m^2 c^2 \right)^2 d\epsilon - k_B T \int_0^{\frac{\mu - mc^2}{k_B T}} \frac{\left(\frac{(\mu - k_B T y)^2}{c^2} - m^2 c^2 \right)^2}{e^y + 1} dy \right. \\
&\quad \left. + k_B T \int_0^{\infty} \frac{\left(\frac{(\mu + k_B T y)^2}{c^2} - m^2 c^2 \right)^2}{e^y + 1} dy \right] - \left(\frac{2\pi^2 m^2 \mu_B^2 B^2}{3h^4} \right) \left[(\mu - mc^2) \right. \\
&\quad \left. - k_B T \int_0^{\frac{\mu - mc^2}{k_B T}} \frac{dy}{e^y + 1} + k_B T \int_0^{\infty} \frac{dy}{e^y + 1} \right].
\end{aligned} \tag{2.9}
$$

Likewise the energy density is given by

$$
\begin{aligned}
U &= \frac{g_s}{h^2} \int_{-\infty}^{\infty} dp_z dp_{\mathrm{AdS}} dz dx_{\mathrm{AdS}} \sum_{j=0}^{\infty} g_j \frac{E_j}{z^{-1} e^{\frac{E_j}{k_B T}} + 1}, \\
&= \frac{g_s L_x L_y L_z L_{\mathrm{AdS}}}{h^4} \left(4\pi m \mu_B B \right) \int_{-\infty}^{\infty} dp_z dp_{\mathrm{AdS}} \sum_{j=0}^{\infty} \frac{E_j}{z^{-1} e^{\frac{E_j}{k_B T}} + 1}, \\
&= \left(\frac{8 g_s \pi^2 m \mu_B B V}{h^4} \right) \int_0^{\infty} p_n dp_n \sum_{j=0}^{\infty} \frac{E_j}{z^{-1} e^{\frac{E_j}{k_B T}} + 1}.
\end{aligned} \tag{2.10}
$$

Again, use the Euler-Maclaurin formula and tricks of integration, so that $\rho c^2 = \frac{U}{V} = \frac{U_0 + U_B}{V}$ becomes

$$
\begin{aligned}
\rho c^2 \simeq & \left(\frac{2 g_s \pi^2}{h^4 c^2} \right) \left[\int_{mc^2}^{\mu} \epsilon^2 \left(\frac{\epsilon^2}{c^2} - m^2 c^2 \right) d\epsilon - k_B T \int_0^{\frac{\mu - mc^2}{k_B T}} \frac{(\mu - k_B T y)^2 \left(\frac{(\mu - k_B T y)^2}{c^2} - m^2 c^2 \right)}{(e^y + 1)} dy \right. \\
& \left. + k_B T \int_0^{\infty} \frac{(\mu + k_B T y)^2 \left(\frac{(\mu + k_B T y)^2}{c^2} - m^2 c^2 \right)}{(e^y + 1)} dy \right] + \left(\frac{2 g_s \pi^2 m^2 \mu_B^2 B^2}{3h^4} \right) \left[(\mu - mc^2) \right. \\
& - k_B T \int_0^{\frac{\mu - mc^2}{k_B T}} \frac{dy}{(e^y + 1)} + k_B T \int_0^{\infty} \frac{dy}{(e^y + 1)} - \int_{mc^2}^{\mu} \frac{\epsilon e^{\frac{\epsilon - \mu}{k_B T}}}{k_B T} d\epsilon - 2 \int_0^{\frac{\mu - mc^2}{k_B T}} \frac{(\mu - k_B T y)\, e^{-y}}{(e^y + 1)} dy \\
& \left. + \int_0^{\frac{\mu - mc^2}{k_B T}} \frac{(\mu - k_B T y)\, e^{-y}}{(e^y + 1)^2} dy + \int_0^{\infty} \frac{(\mu + k_B T y)\, e^{y}}{(e^y + 1)^2} dy \right].
\end{aligned} \tag{2.11}
$$

Both expressions for the pressure and energy density are in the remarkable form with the dependence on B separated out in simple quadratic functions. The integrations can be cast into logarithmic and polylogarithmic functions depending only on the temperature (and not the field) as are shown in the next section.

3 Numerical results

In this section, the equations of motion, eq. (2.1), (2.2) will be solved numerically. To emphasize effects of both temperature and external magnetic field, the physical properties

JHEP06(2012)021

of the degenerate star in the AdS_5 under the influence of both temperature and external magnetic field are investigated by dividing into 4 cases; 1.) $T = 0, B = 0$, 2.) $B = 0, T > 0$, 3.) $B > 0, T = 0$, and 4.) $B, T > 0$. Before going into the details of each case, we integrate equations (2.9) and (2.11) to obtain

$$\begin{aligned} P = & \left(\frac{g_s\pi^2}{30c^4h^4}\right)\Bigg[3\mu(r)^5 - 10m^2c^4\mu(r)^3 + 15m^4c^8\mu(r) - 8m^5c^{10} - 10k_B^2T^2m^2c^4\pi^2\mu(r) \\ & + 7k_B^4T^4\pi^4\mu(r) + 10k_B^2T^2\pi^2\mu(r)^3 - 120k_B^3T^3m^2c^4Li_3\left(-e^{\frac{mc^2-\mu(r)}{k_BT}}\right) \\ & + 360k_B^4T^4mc^2Li_4\left(-e^{\frac{mc^2-\mu(r)}{k_BT}}\right) - 360k_B^5T^5Li_5\left(-e^{\frac{mc^2-\mu(r)}{k_BT}}\right) \\ & - 20k_BTm^2c^4\mu_B^2B^2\ln\left(1+e^{\frac{\mu(r)-mc^2}{k_BT}}\right)\Bigg], \end{aligned} \tag{3.1}$$

$$\begin{aligned} \rho c^2 = & \left(\frac{g_s2\pi^2}{15c^4h^4}\right)\Bigg[3\mu(r)^5 - 5m^2c^4\mu(r)^3 + 2m^5c^{10} - 5k_B^2T^2m^2c^4\pi^2\mu(r) + 7k_B^4T^4\pi^4\mu(r) \\ & + 10k_B^2T^2\pi^2\mu(r)^3 + 30k_B^2T^2m^3c^6Li_2\left(-e^{\frac{mc^2-\mu(r)}{k_BT}}\right) - 150k_B^3T^3m^2c^4Li_3\left(-e^{\frac{mc^2-\mu(r)}{k_BT}}\right) \\ & + 360k_B^4T^4mc^2Li_4\left(-e^{\frac{mc^2-\mu(r)}{k_BT}}\right) - 360k_B^5T^5Li_5\left(-e^{\frac{mc^2-\mu(r)}{k_BT}}\right)\Bigg] + \left(\frac{4m^2\pi^2\mu_B^2B^2}{3h^4}\right) \\ & \times\left[\frac{mc^2}{1+e^{\frac{\mu(r)-mc^2}{k_BT}}} - \mu(r) - k_BT\ln\left(1+e^{\frac{mc^2-\mu(r)}{k_BT}}\right) + k_BT\ln\left(1+e^{\frac{\mu(r)-mc^2}{k_BT}}\right)\right], \end{aligned} \tag{3.2}$$

where $Li_s(z) = \sum_{k=1}^{\infty}\frac{z^k}{k^s}$ is a polylogarithm function. For numerical analysis, we set $G_5 = Gl$, $G = c = \hbar = k_B = \mu_B = l = 1$, $m = 0.1$. We can transform the numerical results to the SI unit by using the table of dimensional translation given in appendix C. The coupled equations of motion between mass and chemical potential (eq. (2.1), (2.2)) are numerically solved to find the chemical potential and the accumulated mass within the star. The density and pressure profiles can be subsequently obtained. The boundary conditions at the center of star are chosen to be $M(r = 0) = 0$ and $\mu(r = 0) = e \simeq 2.718281828$ for every case.

3.1 Case I, zero temperature and zero magnetic field

This is the condition of degenerate star in AdS_5 considered in ref. [7]. The fermions degenerate into the lowest possible energy states filling the energy levels up until the Fermi energy in 5 dimensions. In this limit, the pressure and the energy density, eq. (3.1), (3.2), reduce to

$$P = \left(\frac{g_s\pi^2}{30c^4h^4}\right)\left(3\mu(r)^5 - 10m^2c^4\mu(r)^3 + 15m^4c^8\mu(r) - 8m^5c^{10}\right), \tag{3.3a}$$

$$\rho c^2 = \left(\frac{g_s2\pi^2}{15c^4h^4}\right)\left(3\mu(r)^5 - 5m^2c^4\mu(r)^3 + 2m^5c^{10}\right). \tag{3.3b}$$

First, the surface of the star can be defined at the radial distance, R, where the pressure becomes zero. Apparently from eq. (3.3a), the pressure is zero when $\mu(r = R) = mc^2$. On

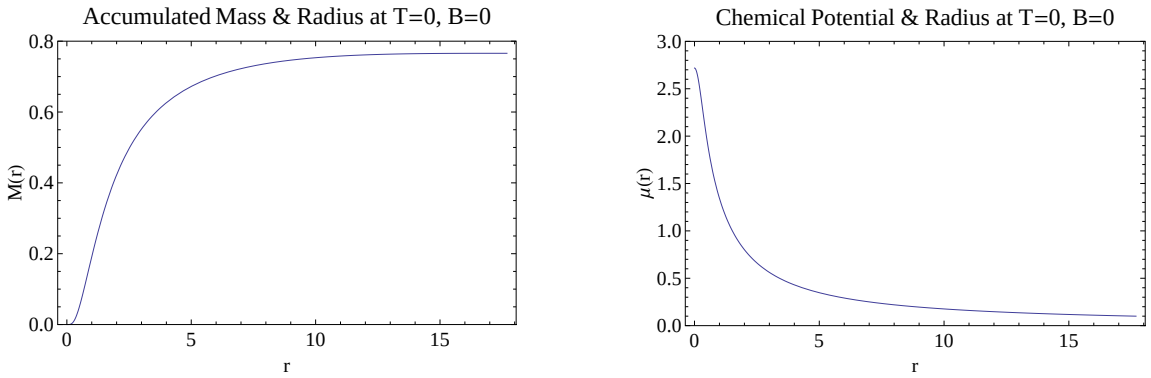

(a) (b)

Figure 1. The accumulated mass(a) and the chemical potential(b) distribution in the degenerate star at $T = 0$, $B = 0$.

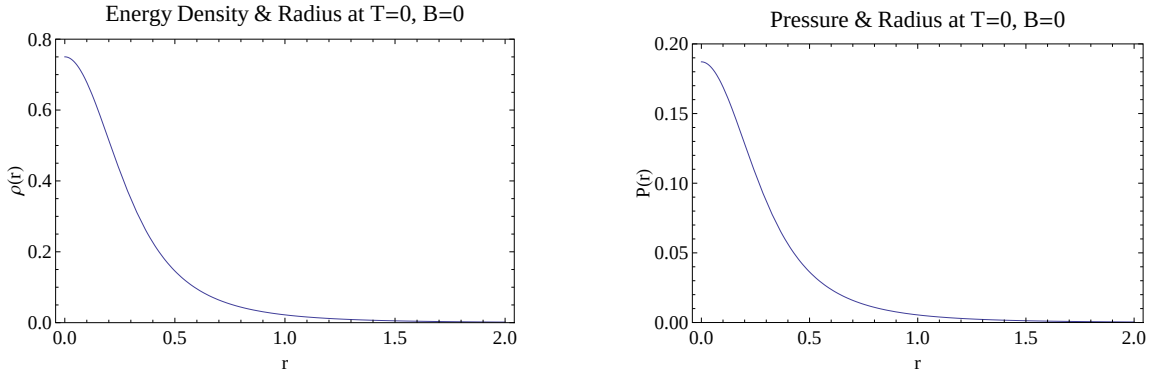

(a) (b)

Figure 2. The density(a) and the pressure(b) distribution in the degenerate star at $T = 0$, $B = 0$.

the other hand, from eq. (3.3b), the density vanishes when $\mu/mc^2 = -1.3848, 1$. Therefore in this case, both the pressure and energy density become zero at the radius R where $\mu(R) = mc^2$.

The accumulated mass, the chemical potential, the density and the pressure distribution of the star versus the radius are presented in figure 1 and 2. Relations between the total mass and the central chemical potential/density of the degenerate star are shown in figure 3.

From the numerical solution, the edge of the degenerate star is at $r = 17.6922$ where the pressure drops to zero. In figure 1(a), the accumulated mass grows rapidly, in particular for the interval between $r = 0$ and $r = 5$. Beyond the central region, the accumulated mass increases less rapidly and becomes steady. The behavior of the accumulated mass is determined by the density and the pressure distribution within the star. Initially, both the energy density and pressure in figure 2, decrease rapidly then they drop to zero more gradually at larger distance. The chemical potential also behaves similarly (figure 1(b)).

JHEP06(2012)021

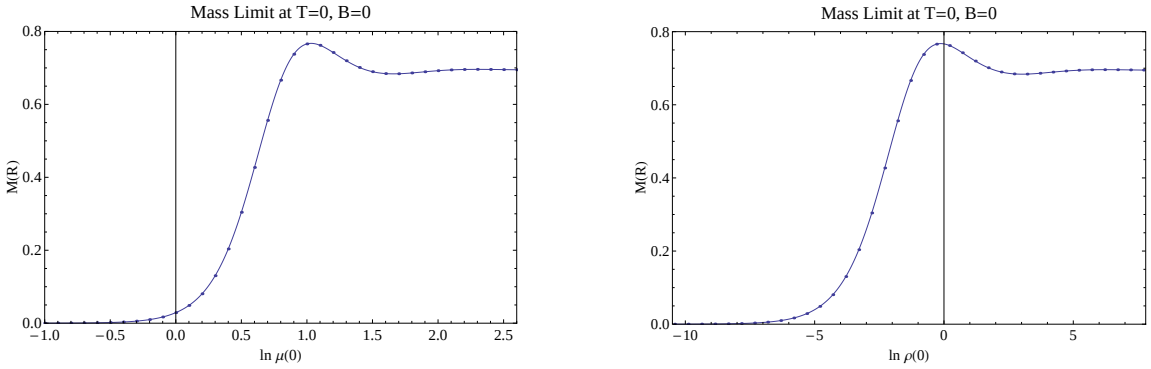

(a) (b)

Figure 3. The relation between mass and central chemical potential/density (in logarithmic scale) of the degenerate star at $T = 0$, $B = 0$.

It is clear that the matter in the star becomes extremely dense in the region near the core. Figure 3 shows the mass curve of the degenerate star as a function of the central chemical potential and density. From numerical analysis, the maximum mass is found to be $M_{\max} = 0.767302$ for the central chemical potential equal to $e^{1.033}$ or at the central energy density equal to $e^{-0.122306}$. This maximal mass can be interpreted to be the mass limit above which gravitational collapse occurs. A mass injection into an empty AdS space until the accumulated mass exceeds the mass limit would result in a gravitational collapse in the bulk. The collapse corresponds to a thermalization process to finite temperature of the dual gauge matter. Therefore, the mass limit corresponds to the minimum injected mass required by the dual gauge matter to start the thermalization process into the thermal equilibrium. After deconfinement thermalization, the dual gauge matter is in thermal equilibrium at the Hawking temperature at this mass limit, i.e. $T_{\text{gauge}} = T_H$ with [22]

$$T_H = \frac{1}{\pi\ell}\left(\frac{r_+}{\ell}\right) + \frac{1}{2\pi r_+}, \tag{3.4}$$

where the horizon radius $r_+ = \ell\left((\sqrt{1+4MC_4/\ell^2}-1)/2\right)^{1/2}$ for AdS_5. Note that the mass dependence of the Hawking-Page temperature in the limit of large ($r_+ \gg \ell$) and small ($r_+ \ll \ell$) black hole in the AdS is

$$T_H \simeq \frac{(MC_4)^{1/4}}{\pi\ell^{3/2}}, \frac{1}{2\pi\sqrt{MC_4}} \tag{3.5}$$

respectively.

It is interesting to note that for $r_+/\ell < \sqrt{1/2}$ (small black hole with negative specific heat after the gravitational collapse), the higher the mass limit, the smaller temperature the dual gauge matter would thermalize to. This corresponds to $M < 3\ell^2/4C_4 = 9\pi/32$ (for $\ell = 1$, approximately 0.8836). The mass limit of our AdS star for $T, B = 0$ is roughly 0.767 and therefore the black hole at the end of gravitational collapse for AdS star at this mass limit is a small black hole with small negative specific heat.

JHEP06(2012)021

3.2 Case II, zero temperature and finite magnetic field

For this case, the magnetic field is turned on and the mass limit and other properties at zero temperature are studied by comparing to the results of Case I. Since the changes from case I is small, we will present the results using the numerical differences between the two cases. Starting from the pressure and energy density for nonzero magnetic field

$$P = \left(\frac{g_s\pi^2}{30c^4h^4}\right)\left(3\mu(r)^5 - 10m^2c^4\mu(r)^3 + 15m^4c^8\mu(r) - 8m^5c^{10} - 20m^2c^4\mu_B^2B^2(\mu - mc^2)\right), \tag{3.6a}$$

$$\rho c^2 = \left(\frac{g_s 2\pi^2}{15c^4h^4}\right)\left(3\mu(r)^5 - 5m^2c^4\mu(r)^3 + 2m^5c^{10}\right) - mc^2\left(\frac{4m^2\pi^2\mu_B^2B^2}{3h^4}\right). \tag{3.6b}$$

Observe that the pressure of the star has almost the same form as the pressure in Case I. The correction term to the pressure from the magnetic field contains the factor $\mu - mc^2$. The density appears to be smaller due to the contribution from the term $-mc^2\left(\frac{4m^2\pi^2\mu_B^2B^2}{3h^4}\right)$.

Since the pressure vanishes at $\mu = mc^2$ as in case I, the surface of the star is defined in the similar way, at $\mu(R) = mc^2$. Interestingly at this radius, the density becomes negative

$$\rho(R) = -\frac{4m^3c^2\pi^2\mu_B^2B^2}{3h^4}, \tag{3.7}$$

due to the interaction energy between the fermion's magnetic moment and the external field. Interestingly, there is a critical field strength where the density becomes zero,

$$B_c = \frac{mc^2}{\mu_B}\sqrt{\frac{3u^5 - 5u^3 + 2}{5}}, \tag{3.8}$$

where $u \equiv \mu/mc^2$ is a rescaled chemical potential. For magnetic field stronger than this critical value, the energy density becomes negative and there is no star formation or black hole in the bulk. Since there is no horizon in the bulk, the dual gauge matter is at zero temperature under extremely strong magnetic field.

Likewise, there is a critical field where the pressure becomes zero,

$$B_c' = \frac{mc^2}{\mu_B}(u-1)\sqrt{\frac{1}{20}(3u^2 + 9u + 8)}. \tag{3.9}$$

For $u > 1$, B_c' is always smaller than B_c, therefore the pressure becomes negative before the density as the field is increased. At $u = 1$, both B_c and B_c' are zero.

For numerical study, the magnetic field strength is chosen to be 0.10 and 0.20 for our consideration. Figure 4 show that the mass limit, comparing to case I, decreases when the magnetic field increases. The maximum mass for $B = 0.2$ is appreciably smaller than the maximum mass at $B = 0.1$. Consider the equation of state in the energy density part (eq. (3.6b)). Since the coupled equations of motion between mass and chemical potential of the star (eq. (2.1) and (2.2)) involve the energy density, decreasing the energy density leads to the decrease of mass and the chemical potential of the star comparing to case I. The increase of the chemical potential subsequently leads to the decrease in the pressure of the star. Numerical analysis confirms these behaviour as are shown in figure 5. Note that

JHEP06(2012)021

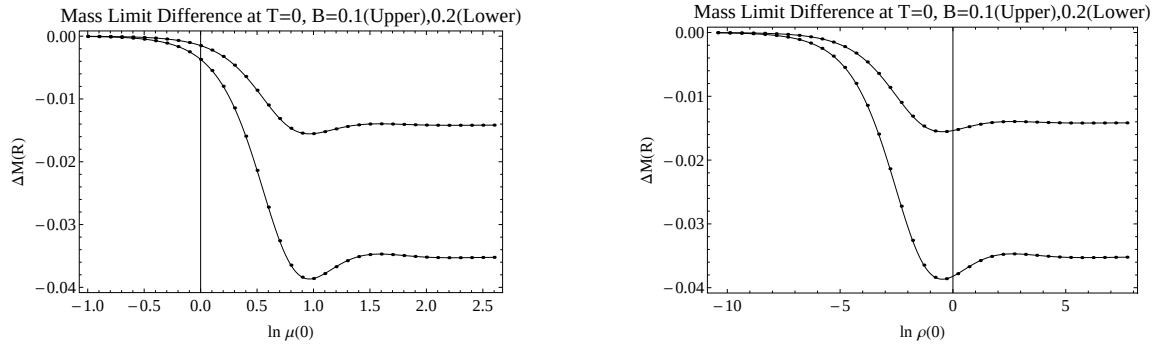

(a) **(b)**

Figure 4. The relation between mass and central chemical potential (a) and central density (b) of the degenerate star at $T = 0$, the mass difference between the nonzero magnetic field case and the $T, B = 0$ case is presented.

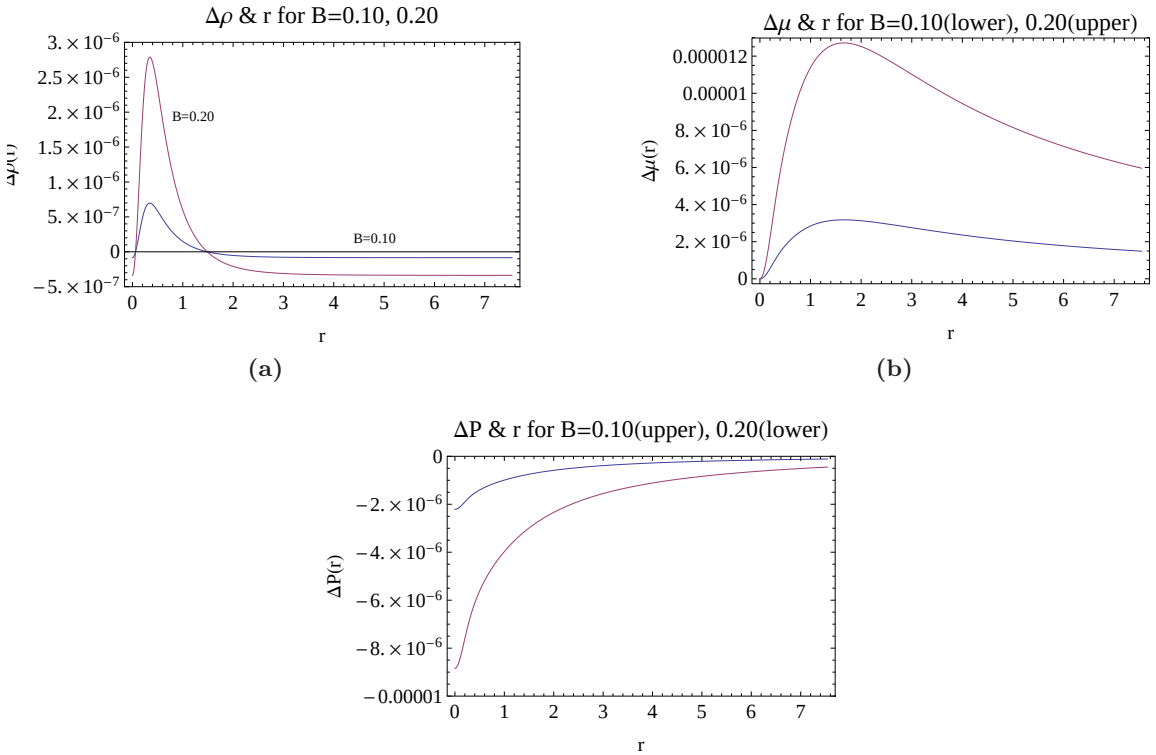

(a) **(b)**

(c)

Figure 5. The difference of the density (a), the chemical potential (b), the pressure (c), between finite and zero magnetic field cases for $T = 0$.

in the core region ($0 < r \lesssim 1.4$), the density increases due to the increase of the chemical potential. However, in the outer region of the star, the effect of the magnetic field becomes dominant resulting in the decrease of the density. Accumulated mass eventually becomes smaller than the mass in case I.

JHEP06(2012)021

The maximal mass or the mass limit of the AdS star when the magnetic field is turned on is smaller than the mass limit in case I. Therefore the dual gauge matter under magnetic field thermalizes to larger temperature when the accumulated mass exceeds the mass limit even though it requires smaller injected mass in order to start the thermalization. Gravitational collapse of an AdS star under strong magnetic field corresponds to thermalization of the magnetized gauge matter from zero to finite temperature. Remarkably, the thermalized temperature (at the mass limit) is *larger* than when the field is absent previously discussed in case I. The magnetized gauge matter thermalizes more easily by requiring smaller injected mass, and also becomes hotter after the deconfinement thermalization.

3.3 Case III, finite temperature and zero magnetic field

For finite bulk temperature, the bulk fermions become thermal in the AdS space. Since the kinetic energy of the particles increases, the pressure becomes larger and the star grows bigger. Again, we study the small changes in the mass limit and other properties of the star by comparing the results to the zero temperature case. The pressure and energy density, eq. (3.1), (3.2) in this case reduce to

$$\begin{aligned} P = & \left(\frac{g_s\pi^2}{30c^4h^4}\right)\Big[3\mu(r)^5 - 10m^2c^4\mu(r)^3 + 15m^4c^8\mu(r) - 8m^5c^{10} - 10k_B^2T^2m^2c^4\pi^2\mu(r) \\ & + 7k_B^4T^4\pi^4\mu(r) + 10k_B^2T^2\pi^2\mu(r)^3 - 120k_B^3T^3m^2c^4Li_3\left(-e^{\frac{mc^2-\mu(r)}{k_BT}}\right) \\ & + 360k_B^4T^4mc^2Li_4\left(-e^{\frac{mc^2-\mu(r)}{k_BT}}\right) - 360k_B^5T^5Li_5\left(-e^{\frac{mc^2-\mu(r)}{k_BT}}\right)\Big], \end{aligned} \tag{3.10}$$

$$\begin{aligned} \rho c^2 = & \left(\frac{g_s2\pi^2}{15c^4h^4}\right)\Big[3\mu(r)^5 - 5m^2c^4\mu(r)^3 + 2m^5c^{10} - 5k_B^2T^2m^2c^4\pi^2\mu(r) + 7k_B^4T^4\pi^4\mu(r) \\ & + 10k_B^2T^2\pi^2\mu(r)^3 + 30k_B^2T^2m^3c^6Li_2\left(-e^{\frac{mc^2-\mu(r)}{k_BT}}\right) - 150k_B^3T^3m^2c^4Li_3\left(-e^{\frac{mc^2-\mu(r)}{k_BT}}\right) \\ & + 360k_B^4T^4mc^2Li_4\left(-e^{\frac{mc^2-\mu(r)}{k_BT}}\right) - 360k_B^5T^5Li_5\left(-e^{\frac{mc^2-\mu(r)}{k_BT}}\right)\Big]. \end{aligned} \tag{3.11}$$

It is interesting to investigate the large temperature limit, $k_BT \gg mc^2, \mu$. In this limit, the polylogarithmic function becomes a zeta function $Li_s(-1) = -(1-2^{1-s})\zeta(s)$ and thus

$$P = \left(\frac{g_s\pi^2}{30c^4h^4}\right)\frac{675}{2}\zeta(5)(k_BT)^5, \qquad \text{for large} \quad k_BT. \tag{3.12}$$

If we assume the star to be in a uniform temperature, this implies that the thermal fermions are not confined within a finite-size star when the temperature is sufficiently large, i.e. $k_BT \gg mc^2, \mu$. The result is not surprising, any particles with sufficiently large kinetic energy will escape the gravitational influence of the star.

We set temperature values in the simulation unit to be $0 - 0.3$. Figure 6 show that temperature increasing hardly affects the mass limit. For this case, the surface of star is defined at $\mu(r = R) = mc^2$ since the density and pressure do not necessarily reduce to

JHEP06(2012)021

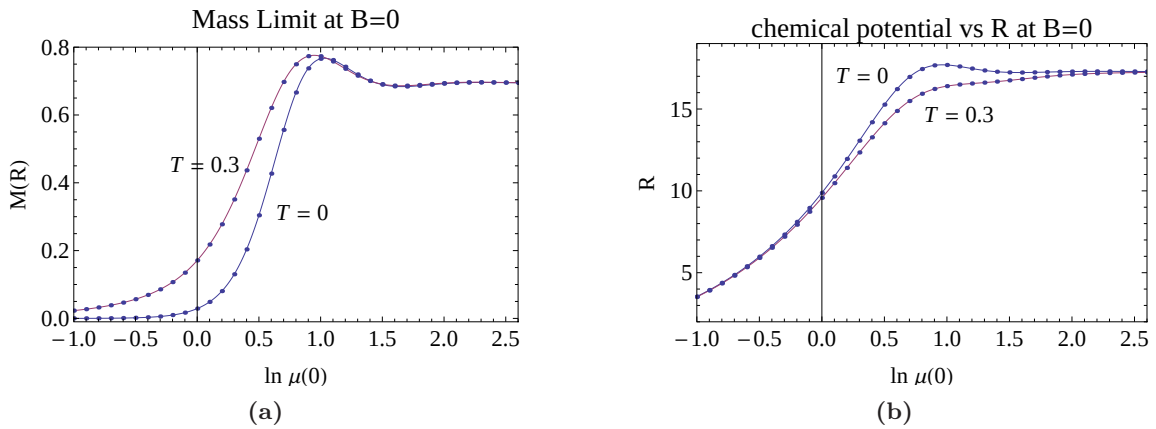

Figure 6. (a) The mass curves for $B = 0$ as a function of the central chemical potential. (b) The radius of the AdS star as a function of the central chemical potential for $B = 0$.

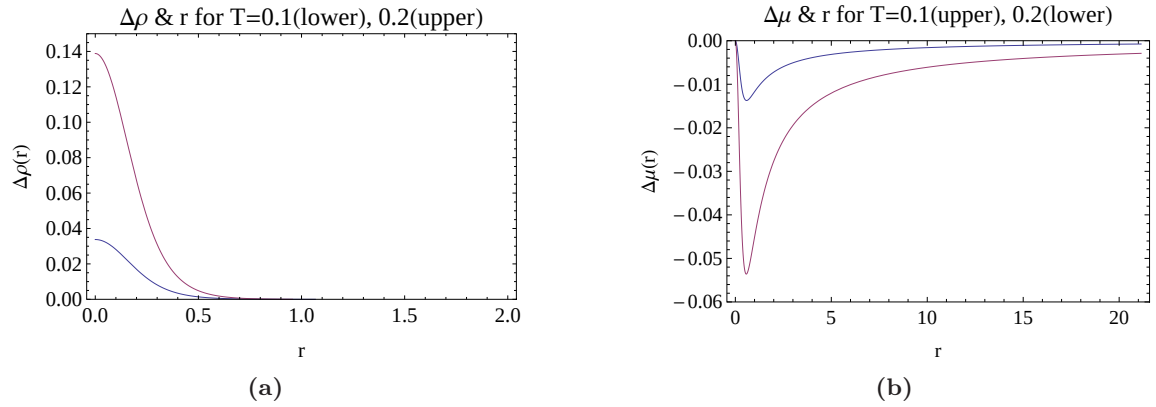

Figure 7. The difference of the density (a), and the chemical potential (b), between finite and zero temperature cases for $B = 0$.

zero. The maximum masses increase with the bulk temperature. This is because the small increase in the temperature affects the Fermi-Dirac distribution very slightly. Most particles are still in the same quantum states, mostly degenerate, and a very small part of the particles occupy higher energies than the Fermi energy and exert more pressure. Increasing temperature thus results in a small increase of pressure and energy density. Consequently, when temperature increases, the maximum mass also grows. For $T \gtrsim 0.1, 0.2$, the energy density and chemical potential reduce to zero at much larger radii as shown in figure 7. For sufficiently large temperature, even though the chemical potential reduces to mc^2 at smaller radii, the pressure does not reduce to zero. In other words, the thermal bulk fermions refuse to be confined within a finite-size star above a critical temperature.

To interpret the results in the dual gauge picture, caution has to be made regarding the bulk temperature. During the thermalization process corresponding to the gravitational

JHEP06(2012)021

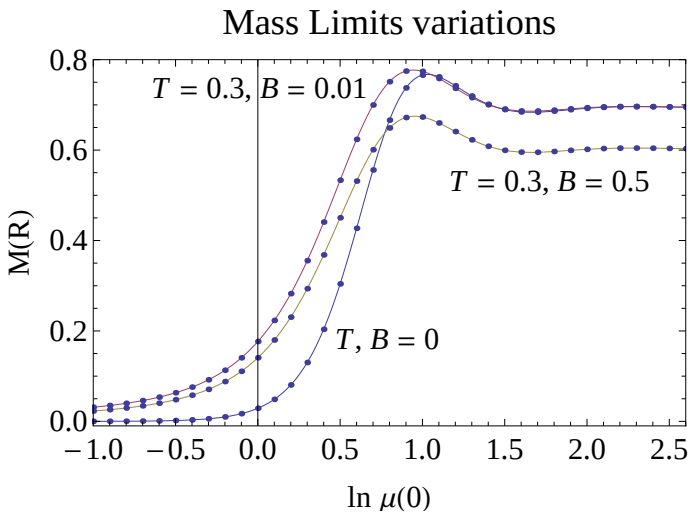

Figure 8. The mass limit curves for $T = 0.3, B = 0.01$ and $T = 0.3, B = 0.5$ in comparison to the mass limit curve at $T, B = 0$.

collapse in the gravity picture, the gauge matter is not in thermal equilibrium until a black hole is formed when the mass injection exceeds the mass limit. A zero-bulk-temperature AdS star collapsing into a black hole becomes thermal at nonzero Hawking temperature due to the emergence of a horizon. Therefore, the bulk temperature does not correspond to any sort of temperature of the gauge matter on the boundary world. One of the effects of the bulk temperature of the fermions in the AdS star is the increase of mass limit. Once a black hole is formed from gravitational collapse of the warm AdS star, the corresponding Hawking temperature is always smaller than the the zero bulk temperature case. After thermalization process, the dual gauge matter will be in thermal equilibrium at *lower* temperature than the case of zero bulk temperature collapse. However, the total injected energy is larger than the zero bulk temperature case. The bulk temperature thus serves as a parameter which delays the onset of the thermalization process as well as reducing the temperature of the resulting thermal equilibrium.

Certainly, the dual gauge matter at exactly the same temperature can be alternatively achieved by injecting mass into a black hole in AdS space, increasing its mass and reducing the corresponding Hawking temperature (however, if we keep increasing the black hole mass, it will finally become large black hole with positive specific heat and the temperature will start to increase with the mass). This choice would correspond to in-equilibrium thermalization where the gauge matter is always kept at thermal equilibrium as temperature decreases. The final thermal equilibrium at certain temperature can always be achieved by infinitely many different thermalization processes.

3.4 Case IV, finite temperature and finite magnetic field

We now consider effects from both the finite bulk temperature and nonzero magnetic field to the mass limit and other properties of the star. The equations of state have the full form according to eq. (3.1) and (3.2). Again, it is interesting to consider the extreme limit

JHEP06(2012)021

of large temperature in the presence of the magnetic field. For nonzero field, the pressure in this limit becomes

$$P = \left(\frac{g_s \pi^2}{30 c^4 h^4}\right)\left(\frac{675}{2}\zeta(5)(k_B T)^5 - 20 k_B T m^2 c^4 \mu_B^2 B^2 \ln 2\right), \text{ for } k_B T, \mu_B B \gg \mu, \quad (3.13)$$

provided that the field B is also comparably large. From eq. (3.13), the star will have definite surface at finite radius when $B \propto T^2$. Sufficiently hot star requires sufficiently strong field to confine its fermionic content.

We see the similar behaviour as in case II and III, temperature increase leads to the increase of the mass limit whereas the effect of the magnetic field is the opposite. In figure 8, when we set the field $B = 0.01$, the temperature $T = 0.3$ has stronger effect on the profile of the star. The mass limit becomes larger than the mass limit in the case of the zero temperature and magnetic field. Similar to case III, when the temperature increases, the mass limit grows larger (the upper line in the figure 8). However, if the magnetic field is enhanced further to $B = 0.5$, the mass limit becomes smaller than the zero-field zero-temperature mass limit. Namely, the influence of the magnetic field has overcome those of the temperature when it is sufficiently large.

Let us summarize implications for the thermalization of the dual gauge matter from the results in this mixed situation with $T, B > 0$. Generically, turning on the bulk temperature results in a larger mass limit in the AdS space while finite magnetic field leads to a smaller mass limit. If the injected mass exceeds the mass limit, gravitational collapse will occur and we end up with a black hole. The injected mass at the mass limit is also the minimum mass required for the dual gauge matter to start the thermalization. The Hawking temperature of the black hole can be identified with the temperature of the dual gauge matter at thermal equilibrium after the non-equilibrium thermalization process corresponding to the collapse, it is larger (smaller) for finite field (bulk temperature) than the collapse with $T, B = 0$. The field and the bulk temperature compete with opposite effects.

For zero-field finite temperature collapse, the final black hole has higher mass and thus corresponds to small temperature of the gauge matter. The final equilibrium at the same temperature can be achieved via in-equilibrium process by injecting mass into a black hole resulted from gravitational collapse of an AdS star with $T, B = 0$ (case I). On the contrary, when the field is turned on, we need to extract mass from a magnetized black hole, reducing its mass and increasing its Hawking temperature in order to achieve the thermal equilibrium at the same temperature and magnetic field.

The black hole immersed in the constant magnetic field in 4 dimensions was originally investigated in ref. [23]. Extension to the magnetized black hole in AdS_5 spacetime is required to fully understand the holographic description of the strongly coupled magnetized gauge matter, one such solution (magnetic brane) is discussed in ref. [17]. It is found that the entropy density of the black brane in AdS_5 is proportional to T for small T and has a T^3 dependence for higher temperatures. We will calculate the entropy density of the AdS star and compare to the case of magnetic brane in section 5. However, as stated above, we have assumed the field is not sufficiently strong that it affects the spacetime of the background and our analyses are thus limited to the moderate magnetic field situation.

JHEP06(2012)021

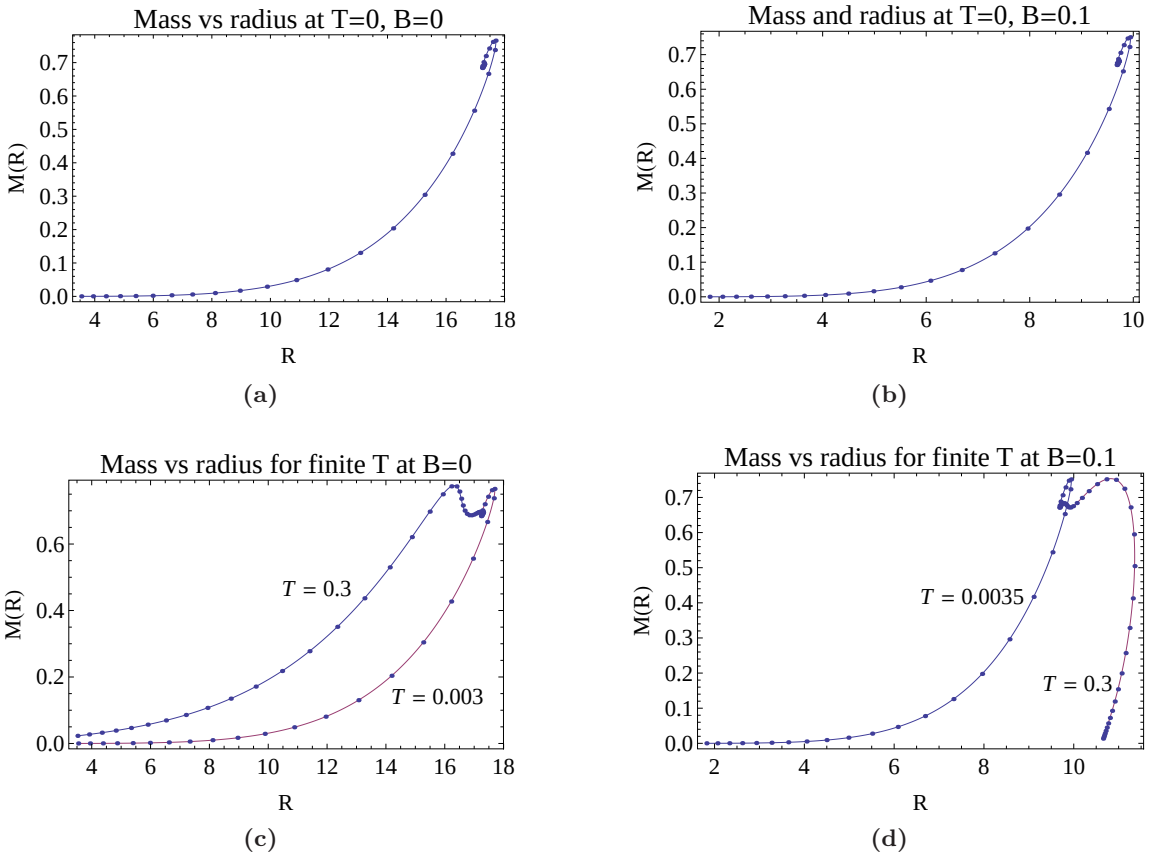

Figure 9. Relationships between mass and radius of the fermionic star.

4 Mass-radius relations

The mass sequences diagram of the AdS star for each case can be presented by the mass-radius plot of the star as shown in figure 9. Figure 9(a) is the mass-radius sequence for case I with zero temperature and zero magnetic field. The stars in this case have larger radius than case II (zero temperature, finite field) in figure 9(b) but smaller radius than case III (zero field, finite temperature) in figure 9(c). Interesting competition between temperature and magnetic field can be seen in figure 9(d), a sufficiently large field helps to confine the fermions within a finite-size star even for relatively higher temperatures comparing to case III.

For sufficiently high temperature, the mass-radius curve can change the way it spirals to the attractor fixed point at $\mu(0) \to \infty$. For $B = 0$ in figure 9(c), the curve with $T = 0.3$ "oscillates down" to the fixed point from the small radii instead of the typical anticlockwise spiralling. This is because at this temperature the radius of the star is an increasing function of $\mu(0)$ with no oscillation as we can see from figure 6(b). For $B = 0.1$ in figure 9(d), the curve with $T = 0.3$, "oscillates down" to the fixed point from the large radii without spiralling. It should be remarked that for case I and III (zero field), the mass at the attractor fixed point for $\mu(0) \to \infty$ is around 0.7. For case II and IV at $B = 0.1$,

JHEP06(2012)021

the fixed point mass for $\mu(0) \to \infty$ is around 0.68. The radius of the AdS star at the fixed point decreases with the field but does not depend very sensitively on the temperature.

5 The adiabatic index, sound speed, entropy density and total entropy of the AdS star

Many interesting physical properties of the fermions squeezed within the AdS star by its own gravity can be illustrated by certain thermodynamic and transport quantities. In this section, we consider two transport coefficients, the adiabatic index and sound speed of the AdS fermionic matter for each limiting case. The entropy density and total entropy of the AdS star are discussed subsequently.

Generically the adiabatic index, Γ, and the sound speed, c_s, of a medium are defined as

$$\begin{aligned} \Gamma &= \frac{\rho}{P}\frac{\partial P}{\partial \rho} = \frac{\rho}{P}c_s^2, \\ &= \frac{\rho}{P}\frac{\partial_\mu P}{\partial_\mu \rho} \end{aligned} \tag{5.1}$$

which can be calculated through the dependence on the chemical potential μ of both P and ρ. The general expressions for both quantities are very lengthy but they are simplified for the zero-temperature limit.

For $T = 0$, finite B,

$$\Gamma = \frac{3(u^2-1)^2 - 4v^2}{3u^2(u-1)^2(u+1)}\left(\frac{3u^5 - 5u^3 + 2 - 5v^2}{(3u^2+9u+8)(u-1)^2 - 20v^2}\right), \tag{5.2}$$

$$c_s = \frac{1}{2}\sqrt{\frac{(u^2-1)^2 - \frac{4}{3}v^2}{u^2(u^2-1)}}, \tag{5.3}$$

where $u \equiv \mu/mc^2$ is the rescaled chemical potential and $v \equiv \mu_B B/mc^2$ is the rescaled magnetic energy of the fermions.

For $T, B = 0$,

$$\Gamma = \left(\frac{1+u}{u^2}\right)\frac{3u^3 + 6u^2 + 4u + 2}{3u^2 + 9u + 8}, \tag{5.4}$$

$$c_s = \frac{1}{2}\sqrt{1 - \frac{1}{u^2}}. \tag{5.5}$$

A number of remarks are in order for the zero-temperature limit. From eq. (5.3) and (5.5), the sound speed for the nonzero field case ($v^2 > 0$) is shown to be larger than the case with $B = 0$. For $B = 0$ since $\mu \geq mc^2$ ($u \geq 1$), the sound speed is always real and the upper limit of c_s is always smaller than 1/2 or half the speed of light. For nonzero field, reality condition of c_s leads to the constraint $v \leq \sqrt{3}(u^2-1)/2$. Namely, for a given u, the upper limit on the magnetic field for ordinarily-compressible fermionic matter is

$$B_0 = \frac{\mu}{\mu_B}\frac{\sqrt{3}}{2}(u^2 - 1). \tag{5.6}$$

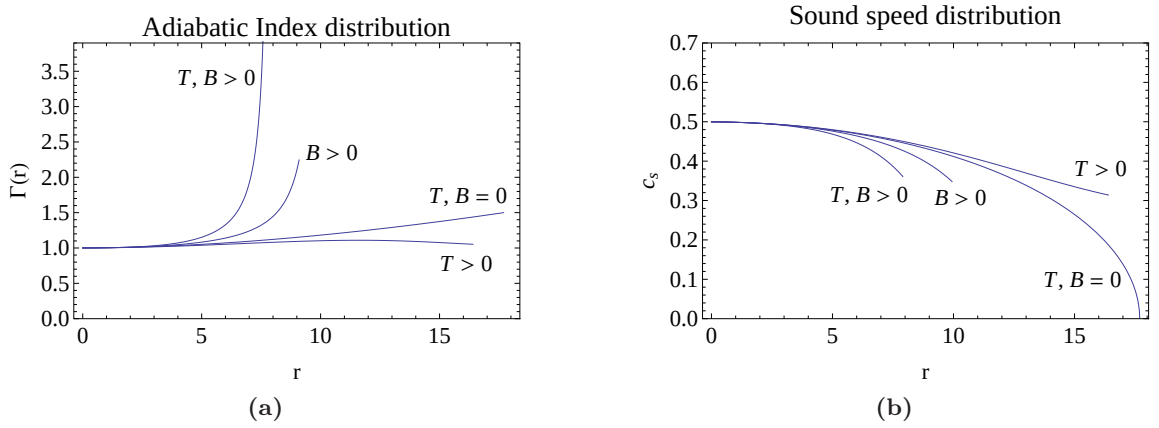

Figure 10. The adiabatic index and sound speed of the fermionic matter in the AdS star. The $T, B > 0$ label represents $T = 0.3, B = 0.2$ curve, the $T > 0$ and $B > 0$ label represents $T = 0.3, B = 0$ and $T = 0, B = 0.1$ curve respectively.

On the other hand, the upper limit from the light speed $c_s \leq 1$ is satisfied trivially for any value of B.

Numerical results for each case are presented in figure 10. The $B > 0$ and $T > 0$ label represents the curve with $T = 0, B = 0.1$ and $B = 0, T = 0.3$ respectively. The $T, B > 0$ label represents the curve with $T = 0.3, B = 0.2$.

When a thermodynamical system is injected with energy until it reaches a thermal equilibrium, the total energy density, pressure and number density are related to the entropy density by the relation $sT = P + \rho - \mu n$ where the entropy density in our case can be computed via

$$s = \left.\frac{\partial P}{\partial T}\right|_{\mu}, \tag{5.7}$$

from the Gibbs-Duhem relation. Using eq. (3.1), the entropy density of the fermionic content of the AdS star at finite temperature can be calculated to be

$$\begin{aligned} s = \frac{4\pi^2}{15c^4h^4}\Bigg[& \frac{5B^2c^4\mu_B^2m^2\left(\mu(r)-mc^2\right)e^{\frac{\mu(r)}{k_BT}}}{T\left(e^{\frac{c^2m}{k_BT}}+e^{\frac{\mu(r)}{k_BT}}\right)} - 5B^2c^4k_B\mu_B^2m^2\ln\left(e^{\frac{\mu(r)-c^2m}{k_BT}}+1\right) \\ & -450k_B^5T^4Li_5\left(-e^{\frac{c^2m-\mu(r)}{k_BT}}\right) + 360c^2k_B^4mT^3Li_4\left(-e^{\frac{c^2m-\mu(r)}{k_BT}}\right) \\ & +90k_B^4T^3\left(c^2m-\mu(r)\right)Li_4\left(-e^{\frac{c^2m-\mu(r)}{k_BT}}\right) - 90c^2k_B^3mT^2\left(c^2m-\mu(r)\right)Li_3\left(-e^{\frac{c^2m-\mu(r)}{k_BT}}\right) \\ & -90c^4k_B^3m^2T^2Li_3\left(-e^{\frac{c^2m-\mu(r)}{k_BT}}\right) + 30c^4k_B^2m^2T\left(c^2m-\mu(r)\right)Li_2\left(-e^{\frac{c^2m-\mu(r)}{k_BT}}\right) \\ & +7\pi^4k_B^4T^3\mu(r) + 5\pi^2k_B^2T\mu(r)\left(\mu(r)^2-(mc^2)^2\right)\Bigg]. \end{aligned} \tag{5.8}$$

JHEP06(2012)021

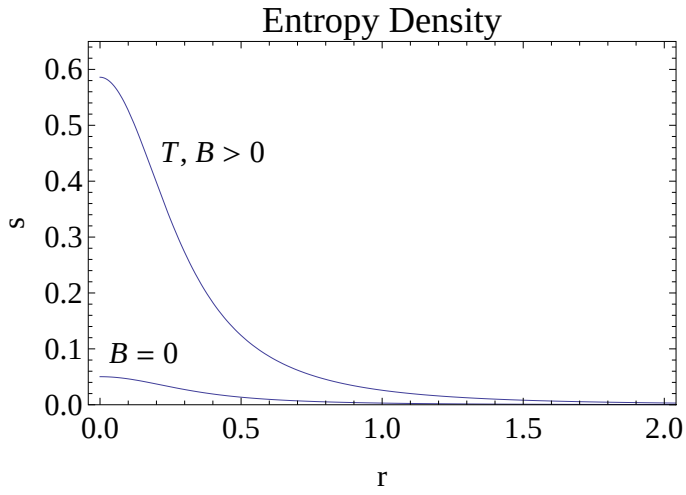

Figure 11. The entropy density of the fermionic matter in the AdS star. The $T, B > 0$ label represents $T = 0.3, B = 0.2$ curve and the $B = 0$ label represents $T = 0.03, B = 0$ curve respectively.

The entropy density of the fermion gas approaches zero as $T \to 0$, a typical behaviour from a quantum ensemble satisfying the third law of thermodynamics. In the low temperature limit, the last two terms of eq. (5.8) remain dominant and thus

$$s \simeq \frac{4\pi^4 k_B \mu(r)}{15(hc)^4} \left[5k_B T(\mu^2 - m^2c^4) + 7\pi^2(k_B T)^3\right]. \tag{5.9}$$

It is interesting to compare the T-dependence of our entropy density with the magnetized black hole studied in ref. [17] where $s \sim T$ for small temperatures and $s \sim T^3$ for larger temperatures. In our case of the fermions in the AdS star, the origin of the temperature dependence is the typical behaviour of free relativistic fermi gas persisting in any dimensions. For the magnetized AdS black hole, the entropy is determined from the central charge of the AdS_3 subspace of $AdS_3 \times T^2$ interpolating with the AdS_5. However, it must be aware that the bulk temperature of the AdS star and the Hawking temperature of the black hole are two distinct kinds of temperature. Only the latter corresponds to the temperature of dual gauge matter at a thermal equilibrium.

The entropy density of the magnetized fermion gas given by eq. (5.8) also depends on the magnetic field $s \sim B^2$. The dependence nevertheless vanishes in the $T \to 0$ limit. However, this formula is the result of the Euler-Maclaurin formula which is a good approximation for $k_B T \gg \mu_B B$, i.e. sufficiently high temperature. For smaller temperatures, starting with eq. (2.8), the zeroth mode becomes dominant and the field-dependence becomes $s \sim \partial_T \ln Z \sim B$. This is also similar to the behaviour of the magnetized black brane [17].

The entropy density from two numerical solutions are shown in figure 11. Since s is an increasing function of T, the star at relatively small temperatures will have smaller entropy density. For small temperatures or small entropy density, we can approximate $sT \ll P, \rho, \mu n$ leading to $P + \rho \simeq \mu n$.

Next we calculate the total entropy of the AdS star which should be equivalent to the entropy of the dual gauge matter before the thermalization. The total entropy of the star

JHEP06(2012)021

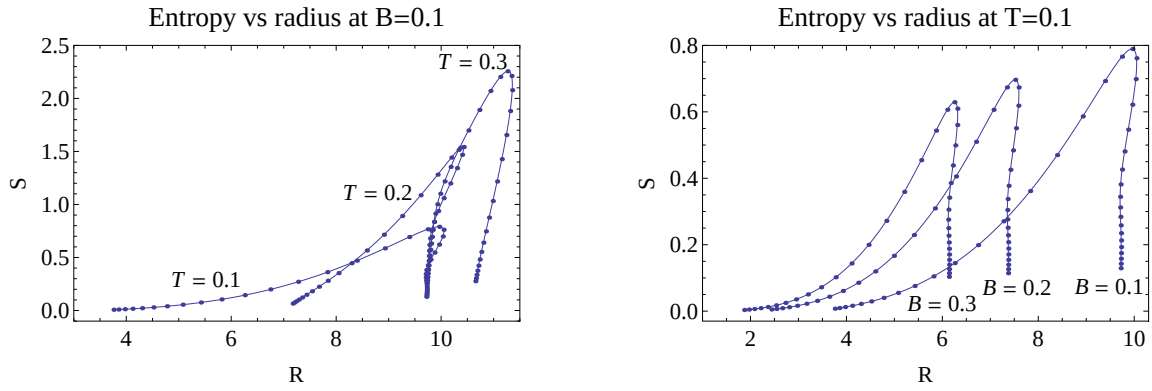

Figure 12. The total entropy as a function of radius of the AdS star for $B = 0.1; T = 0.1, 0.2, 0.3$ and $B = 0.1, 0.2, 0.3; T = 0.1$.

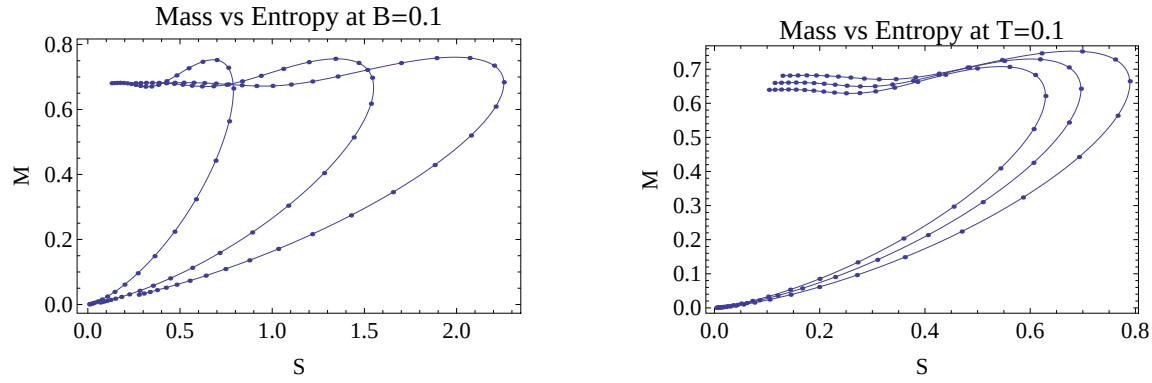

Figure 13. The total entropy as a function of mass of the AdS star for $B = 0.1; T = 0.1, 0.2, 0.3$ (from left to right) and $B = 0.1, 0.2, 0.3; T = 0.1$ (from right to left).

should be the lower bound of the total entropy of the black hole at the end of gravitational collapse when the mass of the AdS star exceeds the mass limit. This black hole entropy in turn corresponds to the total entropy of the dual gauge matter at the end of thermalization. In d dimensions, the total entropy is given by

$$S = \int_0^R s(r)\, \frac{2V_{d-2}}{d-2}\, r^{d-2}\, dr, \tag{5.10}$$

where the volume factor $2V_{d-2}r^{d-2}/(d-2)$ becomes $4\pi^2 r^3/3$ for $d = 5$.

Figure 12 shows the total entropy of the AdS star for $B = 0.1$ at temperature $T = 0.1, 0.2, 0.3$ and for $T = 0.1$ under field $B = 0.1, 0.2, 0.3$. The total entropy is an increasing function of the temperature and a decreasing function of the magnetic field. From small radii, the total entropy is an increasing function of the star radius. This is a similar behaviour to the accumulated mass which is also a global quantity. Remarkably, the total entropy converges to zero in the attractor fixed point $\mu(0) \to \infty$ limit. As the central density grows, the content of the AdS star concentrates more in the central region resulting in the decrease of total entropy towards zero (the volume weighing factor r^3 enhances contribution in the outer region in contrast to the core).

JHEP06(2012)021

The black hole at the end of gravitational collapse should possess at least the same amount of total entropy as the initial AdS star above the mass limit. The second law of thermodynamic demands that the entropy of the AdS star above the mass limit is always less than the black hole entropy after the collapse [25]. The entropy increase could continue until it reaches the maximum when a black hole is formed [26]. Unfortunately, the time evolution of the entropy during the gravitational collapse is not completely known. Partially because the thermal entropy is ill-defined during off-equilibrium processes and partially due to the geometric nature of black hole entropy at the end of the collapse. There are other kinds of entropy that can be assigned to the AdS star and the black hole. The entanglement entropy quantifies how much we do not know about the region behind the horizon and it is consistent with the geometric nature of the Bekenstein-Hawking entropy of the black hole. Entanglement entropy is found to increase in a different manner from the Kolmogorov-Sinai entropy [14, 15] during the collapse. However, all kinds of entropy are found to increase approximately linearly during the initial state of the gravitational collapse and saturate to a constant value at the end.

Each maximum of the M-S curve in figure 13 corresponds holographically to the entropy of the dual gauge matter at the beginning of the thermalization process. It is also proportional to entropy of the black hole after gravitational collapse assuming the linear progression to the saturated Bekenstein-Hawking entropy mentioned above. Arguably, the increase of entropy of the dual gauge matter from the injected mass state to the thermal equilibrium should also be the linear progression following by saturation as well. Note that the entropy is not maximal at the maximal mass nor the maximal radius as we can see from figure 12, 13.

6 Dependence of mass limit on the AdS radius

We vary the curvature radius of the AdS space, l, and study the changes in the profile of the star in this section. For simplicity, we will set the temperature and the external magnetic field to be zero. We let the curvature radius to be $1, 3, 5$ and 7, and observe considerable changes in the mass limit of the star as are shown in figure 14. The mass limit of the degenerate star increases evidently when we raise the curvature radius of the AdS space. Moreover, the peak of the mass limit curve shifts to the lower central density side. Note that increasing l corresponds to decreasing the bulk cosmological constant Λ. For $l = 3$, the maximum mass is $1.96473(r = 27.4029)$ for the central chemical potential $\mu(0) = e^{0.3825}$ or the central energy density $\rho(0) = e^{-3.38048}$. For $l = 5$, the maximum mass is $2.92023(r = 33.5921)$ for the central chemical potential $\mu(0) = e^{0.083}$ or the central energy density $\rho(0) = e^{-4.88441}$. For $l = 7$, the maximum mass is $3.71782(r = 38.4035)$ for the central chemical potential $\mu(0) = e^{-0.1115}$ or the central energy density $\rho(0) = e^{-5.86373}$.

7 Conclusions and discussions

In this work we have found that both temperature and external magnetic field affect the mass limit and other physical properties of the fermionic AdS star. The increase of bulk

JHEP06(2012)021

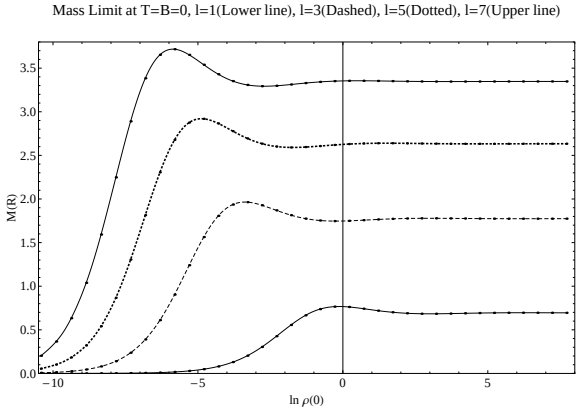

Figure 14. The relation between mass and central energy density (in logarithmic scale) of the degenerate star for varying AdS radius $l = 1 - 7$.

temperature enables the pressure and energy density of the star to increase. Consequently, the mass limit becomes slightly greater due to the larger pressure. This is the typical behavior of the Fermi gas at finite temperature. Too large temperature results in the the fermions refusing to be confined within a finite-size star, they will leak to the space inevitably.

In the presence of external magnetic field, the mass limit decreases when the magnetic field increases. As we can see from eq. (3.1) and (3.2), an increase in the magnetic field results in a smaller energy and pressure density as well as a smaller chemical potential. The mass limit becomes smaller naturally. There is an interesting competition between the temperature and the magnetic field to the density profile and mass limit of the star. Extremely strong magnetic field tends to make the bulk fermions stay in the Landau states with lower energies whilst the temperature causes the particles to flee the star.

The radius of curvature of the AdS space also affects the mass limit evidently. When the radius of curvature increases, the mass limit increases substantially as are shown in figure 14. Interestingly, the peak of the mass limit curve shifts to the lower central density side.

Gravitational collapse in the AdS space has holographic dual in terms of the non-equilibrium thermalization of the gauge matter on the boundary. Even though the Hawking temperature of the black hole at the end of the gravitational collapse can be matched with the temperature at thermal equilibrium of the gauge matter at the end of thermalization, the bulk temperature of the AdS star does not seem to have such a straightforward relationship with the dual gauge matter. The Hawking temperature of the resulting black hole is not directly related to the temperature of the fermionic star before the collapse but inversely proportional to the mass of the star. Therefore it is the mass limit studied in our work which corresponds to the temperature of the gauge matter at the thermal equilibrium after thermalization, i.e. $T_{\text{gauge}} \sim \sqrt{3/32\pi M_{\text{limit}}}$ (the black hole formed at our mass limit is small AdS black hole with negative specific heat, the precise relationship is given in eq. (3.4)), for a given mass injection M_{limit} in the dual gauge picture. The mass limit also plays the role of the minimum injected mass required for the dual gauge matter to undergo the thermalization into the thermal equilibrium. Larger mass limit means that it requires more injected energy to thermalize, and once it thermalizes, the gauge matter will be at lower Hawking temperature.

JHEP06(2012)021

It should be remarked that the AdS black holes formed at the end of the gravitational collapse of the AdS stars at our mass limits are small black holes with negative specific heat. They are previously thought to be less thermodynamically preferred than the AdS vacuum in the context of the AdS/CFT correspondence and only the large AdS black hole with positive specific heat was considered relevant for the dual of the thermal gauge matter. However, inevitable collapse at the mass limits corresponding to small AdS black holes suggest that there might exist the phase of thermal gauge matter with negative specific heat dual to these black holes at the end of the gravitational collapse. Injecting more mass would make these AdS black holes and their gauge duals eventually become thermodynamically stable with positive specific heat.

Entropy density of the AdS star under uniform magnetic field is found to show interesting behaviour; $s \sim T$ for small and $s \sim T^3$ for higher *bulk* temperatures. Such T-dependence is typical for free fermion gas (modulo the magnetic field existence) and it is amusingly similar to the T-dependence of the magnetic black brane entropy in the AdS [17] even though the latter is the Hawking-Page temperature of the brane, not the bulk temperature of the material making up the brane itself. Nevertheless, the correspondence between the bulk and boundary exists throughout the gravitational collapse as long as the background is the AdS. The holographic duality suggests that the Hilbert spaces of both the gravity and gauge theory as well as their partition functions are equivalent. A global probe for the number of degrees of freedom on both sides of the duality is the entropy. The total entropy of the AdS star above the mass limit, which indicates the lower bound of the black hole entropy at the end of gravitational collapse, should also be the lower bound of the total entropy of the gauge matter at the end of thermalization in the dual picture, $S_{\text{gauge}} \gtrsim S_{\text{AdS}}$. We found that the entropy (at the mass limit) of the AdS star is an increasing (decreasing) function of the temperature (magnetic field), similar behaviour to the mass limit.

The remaining unanswered question is the exact correspondence between the gravitational collapse in the bulk and non-equilibrium deconfinement thermalization of the dual gauge matter. If bulk gravity is dual to colour-singlet glueball interaction and it causes the gravitational collapse in the AdS, how could the glueball exchange describe the deconfinement thermalization in the dual gauge picture? Should there exist the critical glueball density corresponding to the mass limit in the bulk which determines the deconfinement phase transition on the gauge theory side? What is the boundary (CFT) gauge description of the TOV equation and more generically the Einstein equation in the (AdS) bulk? What are the duals of bulk temperature and other thermodynamic and transport quantities such as the adiabatic index and sound speed of the AdS star in the gauge theory side?

Acknowledgments

T.C. would like to thank Sirachak Panpanich for valuable helps. P.B. is supported in part by the Thailand Research Fund (TRF) and Commission on Higher Education (CHE) under grant RMU5380048 and also by the Thailand Center of Excellence in Physics (ThEP). T.C. is supported in part by the Thailand Research Fund (TRF) and Commission on Higher Education (CHE) under grant RMU5380048.

JHEP06(2012)021

A The equation of hydrostatic equilibrium for a spherical symmetric star in d dimensions

We solve the Einstein equation in d-dimensional spacetime in this section. Starting from the Einstein equation,

$$G^{\mu}{}_{\nu} = R^{\mu}{}_{\nu} - g^{\mu}{}_{\nu}\frac{R}{2} = V_{d-2}C_{d-1}T^{\mu}{}_{\nu}, \tag{A.1}$$

where $R^{\mu}{}_{\nu}$, $g^{\mu}{}_{\nu}$, R, $T^{\mu}{}_{\nu}$, V_{d-2}, C_{d-1} are Ricci tensor, metric tensor, Ricci scalar, energy-momentum tensor, the area of S^{d-2} and constant $\left(\frac{16\pi G}{(d-2)V_{d-2}c^4}\right)$ respectively. Assuming a perfect fluid, the energy-momentum tensor is given by

$$T^{\mu}{}_{\nu} = \begin{pmatrix} \rho c^2 & & & & \\ & -P_r & & & \\ & & -P_{\theta_1} & & \\ & & & \ddots & \\ & & & & -P_{\theta_{d-2}} \end{pmatrix}, \tag{A.2}$$

where we use a spherically symmetric metric in d dimensions in the polar coordinates [24]

$$\begin{aligned} ds^2 &= A(r)c^2dt^2 - B(r)dr^2 - r^2 d\Omega_{d-2}^2 \\ &= A(r)c^2dt^2 - B(r)dr^2 - r^2 d\theta_1^2 - r^2\sin^2\theta_1\left(d\theta_2^2 + \cdots + \prod_{i=2}^{d-3}\sin^2\theta_i d\theta_{d-2}^2\right) \\ &= A(r)c^2dt^2 - B(r)dr^2 - r^2 d\theta_1^2 - r^2\sin^2\theta_1\left(d\theta_2^2 + \sum_{j=3}^{d-2}\prod_{i=2}^{j-1}\sin^2\theta_i d\theta_j^2\right). \end{aligned} \tag{A.3}$$

The Lagrangian of this metric is then given by

$$L = A(r)c^2\dot{t}^2 - B(r)\dot{r}^2 - r^2\dot{\theta}_1^2 - r^2\sin^2\theta_1\left(\dot{\theta}_2^2 + \sum_{j=3}^{d-2}\prod_{i=2}^{j-1}\sin^2\theta_i\dot{\theta}_j^2\right). \tag{A.4}$$

We will use the Euler-Lagrange equation to find the equations of motion and read off the connections,

$$\partial_\tau\left(\frac{\partial L}{\partial\dot{q}}\right) = \frac{\partial L}{\partial q}. \tag{A.5}$$

Consider t component, the equation of motion is

$$\ddot{t} + \frac{A'}{A}\dot{r}\dot{t} = 0, \tag{A.6}$$

and the connections are

$$\Gamma^{t}{}_{rt} = \Gamma^{t}{}_{tr} = \frac{A'}{2A}. \tag{A.7}$$

The equation of motion in the r component reads

$$\ddot{r}+\frac{A'c^2}{2B}\dot{t}^2+\frac{B'}{2B}\dot{r}^2-\frac{r}{B}\dot{\theta}_1^2-\frac{r\sin^2\theta_1}{B}\left(\dot{\theta}_2^2+\sum_{j=3}^{d-2}\prod_{i=2}^{j-1}\sin^2\theta_i\dot{\theta}_j^2\right)=0, \tag{A.8}$$

and the connections in the r component are

$$\Gamma^r{}_{tt}=\frac{A'c^2}{2B},\Gamma^r{}_{rr}=\frac{B'}{2B},\Gamma^r{}_{\theta_1\theta_1}=\frac{-r}{B},\Gamma^r{}_{\theta_2\theta_2}=\frac{-r\sin^2\theta_1}{B},$$
$$\ldots,\Gamma^r{}_{\theta_j\theta_j}=\frac{-r\sin^2\theta_1}{B}\prod_{i=2}^{j-1}\sin^2\theta_i. \tag{A.9}$$

Likewise, the equation of motion in the θ_1 component is

$$\ddot{\theta_1}+\frac{2}{r}\dot{r}\dot{\theta_1}-\sin\theta_1\cos\theta_1\left(\dot{\theta}_2^2+\sum_{j=3}^{d-2}\prod_{i=2}^{j-1}\sin^2\theta_i\dot{\theta}_j^2\right)=0, \tag{A.10}$$

and the connections in the θ_1 component are

$$\Gamma^{\theta_1}{}_{r\theta_1}=\Gamma^{\theta_1}{}_{\theta_1 r}=\frac{1}{r},\Gamma^{\theta_1}{}_{\theta_2\theta_2}=-\sin\theta_1\cos\theta_1,$$
$$\ldots,\Gamma^{\theta_1}{}_{\theta_j\theta_j}=-\sin\theta_1\cos\theta_1\prod_{i=2}^{j-1}\sin^2\theta_i, \tag{A.11}$$

where $3\leqslant j\leqslant d-2$. Similarly, the equation of motion in the θ_2 component is

$$\ddot{\theta_2}+\frac{2}{r}\dot{r}\dot{\theta_2}+2\cot\theta_1\dot{\theta_1}\dot{\theta_2}-\sin\theta_2\cos\theta_2\sum_{j=4}^{d-2}\prod_{i=3}^{j-1}\sin^2\theta_i\dot{\theta}_j^2\ =0, \tag{A.12}$$

and the relevant connections are

$$\Gamma^{\theta_2}{}_{r\theta_2}=\Gamma^{\theta_2}{}_{\theta_2 r}=\frac{1}{r},\Gamma^{\theta_2}{}_{\theta_1\theta_2}=\Gamma^{\theta_2}{}_{\theta_2\theta_1}=\cot\theta_1,$$
$$\ldots,\Gamma^{\theta_2}{}_{\theta_j\theta_j}=-\sin\theta_2\cos\theta_2\prod_{i=3}^{j-1}\sin^2\theta_i, \tag{A.13}$$

where $4\leqslant j\leqslant d-2$. The equation of motion in the θ_j $(j\geqslant 3)$ component is

$$\ddot{\theta_j}+\frac{2}{r}\dot{r}\dot{\theta_j}+2\cot\theta_1\dot{\theta_1}\dot{\theta_j}+\frac{2\sum_{l=2}^{j-1}\prod_{\substack{i=2\\ i\neq l}}^{j-1}\sin\theta_l\cos\theta_l\sin^2\theta_i}{\prod_{i=2}^{j-1}\sin^2\theta_i}\dot{\theta}_l\dot{\theta}_j$$
$$-\sum_{k=j+1}^{d-2}\prod_{i=j+1}^{k-1}\sin\theta_j\cos\theta_j\sin^2\theta_i\dot{\theta}_k^2=0, \tag{A.14}$$

and the connections in θ_j component are

$$\Gamma^{\theta_j}{}_{r\theta_j}=\Gamma^{\theta_j}{}_{\theta_j r}=\frac{1}{r},\Gamma^{\theta_j}{}_{\theta_1\theta_j}=\Gamma^{\theta_j}{}_{\theta_j\theta_1}=\cot\theta_1,\Gamma^{\theta_j}{}_{\theta_l\theta_j}=\Gamma^{\theta_j}{}_{\theta_j\theta_l}$$

JHEP06(2012)021

$$= \frac{\prod_{\substack{i=2\\ i\neq l}}^{j-1} \sin\theta_l \cos\theta_l \sin^2\theta_i}{\prod_{i=2}^{j-1}\sin^2\theta_i} = \cot\theta_l, \Gamma^{\theta_j}{}_{\theta_k\theta_k} = -\sin\theta_j\cos\theta_j \prod_{i=j+1}^{k-1}\sin^2\theta_i, \tag{A.15}$$

where $2 \leqslant l \leqslant j-1$ and $j+1 \leqslant k \leqslant d-2$. The Ricci tensor and Ricci scalar can be calculated from

$$\begin{aligned} R^{\rho}{}_{\sigma\mu\nu} &= \partial_\mu \Gamma^{\rho}{}_{\nu\sigma} - \partial_\nu \Gamma^{\rho}{}_{\mu\sigma} + \Gamma^{\rho}{}_{\mu\lambda}\Gamma^{\lambda}{}_{\nu\sigma} - \Gamma^{\rho}{}_{\nu\lambda}\Gamma^{\lambda}{}_{\mu\sigma}, \\ R_{\mu\nu} &= R^{\lambda}{}_{\mu\lambda\nu}, \\ R &= R^{\mu}{}_{\mu} = g^{\mu\nu}R_{\mu\nu}. \end{aligned}$$

After some calculations, we have

$$\begin{aligned} R^{t}{}_{t} &= \frac{A''}{2AB} - \frac{A'B'}{4AB^2} - \frac{(A')^2}{4A^2B} + (d-2)\frac{A'}{2rAB}, \\ R^{r}{}_{r} &= \frac{A''}{2AB} - \frac{A'B'}{4AB^2} - \frac{(A')^2}{4A^2B} + (d-2)\frac{B'}{2rB^2}, \\ R^{\theta_1}{}_{\theta_1} &= \frac{A'}{2rAB} - \frac{B'}{2rB^2} - \frac{(d-3)}{r^2}\left(1-\frac{1}{B}\right), \\ R^{\theta_2}{}_{\theta_2} &= \frac{A'}{2rAB} - \frac{B'}{2rB^2} - \frac{(d-3)}{r^2}\left(1-\frac{1}{B}\right), \\ R^{\theta_i}{}_{\theta_i} &= \frac{A'}{2rAB} - \frac{B'}{2rB^2} - \frac{(d-3)}{r^2}\left(1-\frac{1}{B}\right). \end{aligned}$$

Consider $G^{t}{}_{t} = R^{t}{}_{t} - \frac{g^{t}_{t}}{2}\left(R^{t}{}_{t} + R^{r}{}_{r} + R^{\theta_1}{}_{\theta_1} + R^{\theta_2}{}_{\theta_2} + \ldots + R^{\theta_i}{}_{\theta_i} + \ldots + R^{\theta_{d-2}}{}_{\theta_{d-2}}\right) = V_{d-2}C_{d-1}T^{t}{}_{t} \to R^{t}{}_{t} - \left(R^{r}{}_{r} + \ldots + R^{\theta_{d-2}}{}_{\theta_{d-2}}\right) = 2V_{d-2}C_{d-1}\rho c^2$, then

$$(d-2)\frac{B'}{rB^2} + \frac{(d-2)(d-3)}{r^2}\left(1-\frac{1}{B}\right) = 2V_{d-2}C_{d-1}\rho c^2, \tag{A.17}$$

$$B' - \frac{(d-3)}{r}B = B^2\left(\frac{2rV_{d-2}C_{d-1}\rho c^2}{(d-2)} - \frac{(d-3)}{r}\right). \tag{A.18}$$

If we consider an AdS space(with a negative cosmological constant, Λ), then the Einstein equation reads

$$G^{\mu}{}_{\nu} + \Lambda g^{\mu}{}_{\nu} = V_{d-2}C_{d-1}T^{\mu}{}_{\nu}, \tag{A.19}$$

and equation (A.18) becomes

$$B' - \frac{(d-3)}{r}B = B^2\left(\frac{2rV_{d-2}C_{d-1}\rho c^2}{(d-2)} - \frac{(d-3)}{r} - \frac{2\Lambda r}{(d-2)}\right). \tag{A.20}$$

Change $B \to B^2$, so that

$$B' - \frac{(d-3)}{2r}B = B^3\left(\frac{rV_{d-2}C_{d-1}\rho c^2}{(d-2)} - \frac{(d-3)}{2r} - \frac{\Lambda r}{(d-2)}\right). \tag{A.21}$$

The solution to this equation is

$$B^2 = \frac{1}{1 - \frac{2c^2 V_{d-2} C_{d-1}}{(d-2) r^{d-3}} \int \rho r^{d-2} dr + \frac{2\Lambda r^2}{(d-2)(d-1)}}. \tag{A.22}$$

Let $\frac{2\Lambda}{(d-2)(d-1)} = \frac{1}{l^2}$, then

$$B^2 = \frac{1}{1 - \frac{2c^2 V_{d-2} C_{d-1}}{(d-2) r^{d-3}} \int \rho r^{d-2} dr + \frac{r^2}{l^2}} = \frac{1}{1 - \frac{M C_{d-1}}{r^{d-3}} + \frac{r^2}{l^2}}. \tag{A.23}$$

Also the accumulated mass can be defined to be

$$M(r) = \frac{2V_{d-2}}{(d-2)} \int \rho r^{d-2} dr. \tag{A.24}$$

Consider $G^r{}_r = R^r{}_r - \frac{g^r{}_r}{2}\left(R^t{}_t + R^r{}_r + R^{\theta_1}{}_{\theta_1} + R^{\theta_2}{}_{\theta_2} + \ldots + R^{\theta_i}{}_{\theta_i} + \ldots + R^{\theta_{d-2}}{}_{\theta_{d-2}}\right) = V_{d-2} C_{d-1} T^r{}_r \to R^r{}_r - \left(R^t{}_t + \ldots + R^{\theta_{d-2}}{}_{\theta_{d-2}}\right) = 2V_{d-2} C_{d-1} P_r$, then

$$\frac{(d-2) A'}{rAB} - \frac{(d-2)(d-3)}{r^2}\left(1 - \frac{1}{B}\right) = 2V_{d-2} C_{d-1} P_r.$$

Use equation (A.17) from $G^t{}_t$ and multiply by $rB/(d-2)$,

$$\frac{A'}{A} + \frac{B'}{B} = \frac{2V_{d-2} C_{d-1}}{(d-2)} rB\left(\rho c^2 + P_r\right). \tag{A.25}$$

Change $A \to A^2$, $B \to B^2$, equation (A.25) becomes

$$\frac{A'}{A} + \frac{B'}{B} = \frac{V_{d-2} C_{d-1} rB^2}{(d-2)}\left(\rho c^2 + P_r\right),$$

Solve this equation to find relations between A and B,

$$A^2(r) = \frac{e^{2\chi(r)}}{B^2(r)}, \tag{A.26}$$

where

$$\chi(r) = \frac{V_{d-2} C_{d-1}}{(d-2)} \int \left(\rho(r) c^2 + P_r(r)\right) rB^2(r)\, dr. \tag{A.27}$$

Finally we obtain the coupled equations of motion from equation (A.24) and (A.27)

$$M'(r) = \frac{2V_{d-2}}{(d-2)} \rho(r) r^{d-2}, \tag{A.28a}$$

$$\chi'(r) = \frac{V_{d-2} C_{d-1}}{(d-2)}\left(\rho(r) c^2 + P_r(r)\right) rB^2(r). \tag{A.28b}$$

Moreover, when we consider the energy momentum conservation $\nabla_\mu T^\mu{}_\nu = 0$ by letting $\nu = r$ and $P_r = P_{\theta_1} = \ldots = P_{\theta_i} = \ldots = P_{\theta_{d-2}} = P$, $A \to A^2$, it leads to the TOV equation in d-dimension,

$$\frac{dP}{dr} = -\left(\rho c^2 + P\right)\frac{A'}{A}.$$

JHEP06(2012)021

Next we want to rewrite this equation in the form containing thermodynamic quantities such as the chemical potential, the entropy, and the temperature of matter within the spherically symmetric star. From thermodynamic relations involving the entropy density s;

$$sT = P + \rho c^2 - \mu n, \tag{A.29}$$

$$s\ dT = dP - n\ d\mu, \tag{A.30}$$

the TOV equation can be rewritten as

$$s\left(T' + T\frac{A'}{A}\right) + n\left(\mu' + \mu\frac{A'}{A}\right) = 0, \tag{A.31}$$

implying two equations to be satisfied simultaneously

$$T' + T\frac{A'}{A} = \mu' + \mu\frac{A'}{A} = 0. \tag{A.32}$$

The temperature equation can be solved to obtain the redshifted temperature profile within the star $T = T_0/A(r)$ where $A(0) = 1$ and T_0 is the temperature at the star center. The chemical potential equation similarly gives

$$\mu(r) = \frac{\mu_0}{A(r)}. \tag{A.33}$$

The coupled equations of motion can then be written in terms of the accumulated mass and chemical potential as the following

$$M'(r) = \frac{2V_{d-2}}{(d-2)}\rho(r)\, r^{d-2}, \tag{A.34a}$$

$$\mu'(r) = \mu(r)\left(\frac{B'(r)}{B(r)} - \frac{V_{d-2}C_{d-1}}{(d-2)}\left(\rho(r)\, c^2 + P_r(r)\right) r B^2(r)\right). \tag{A.34b}$$

B Euler-Maclaurin formula

A slowly converging series can be evaluated effectively by using an integral as in the Euler-Maclaurin formula

$$\sum_{j=0}^{\infty} f\left(j + \frac{1}{2}\right) \approx \int_0^{\infty} f(x)\ dx + \frac{1}{24}(f'(0) - f'(\infty)) + O(x^3). \tag{B.1}$$

In this article, the partition function sum over Landau states is approximated using this conventional method by letting

$$f(x) = \ln\left(1 + \exp\left(\frac{\mu - \sqrt{m^2c^4 + p_n^2c^2 + 4xmc^2\mu_B B}}{k_B T}\right)\right), \tag{B.2}$$

where $x = j + 1/2$.

quantity	dimensionless variable	physical variable
density	ρ	$\rho_0\rho$
pressure	P	$\rho_0 P$
mass	M	$\left(\frac{c^{10}}{G^4\rho_0}\right)^{\frac{1}{3}} M$
radius	r	$\left(\frac{c^4}{G\rho_0}\right)^{\frac{1}{3}} r$
temperature	T	$\frac{\left(\rho_0 c^4\hbar^4\right)^{\frac{1}{5}}}{k_B} T$
magnetic field	B	$\frac{\left(\rho_0 c^4\hbar^4\right)^{\frac{1}{5}}}{\mu_B} B$

Table 1. Dimensional translation table of physical quantities, the rescale parameter $\rho_0 = \frac{\left(\frac{m_p}{m_s}c^2\right)^5}{c^4\hbar^4}$ where m_p and m_s are the rest mass of particles and the mass used in simulation, respectively.

C Dimensional translation table

$\rho_0 = \frac{\left(\frac{m_p}{m_s}c^2\right)^5}{c^4\hbar^4}$ where m_p and m_s are the rest mass of particles and the mass used in simulation, respectively.

References

[1] J.M. Maldacena, *The large-N limit of superconformal field theories and supergravity*, *Adv. Theor. Math. Phys.* **2** (1998) 231 [*Int. J. Theor. Phys.* **38** (1999) 1113] [hep-th/9711200] [INSPIRE].

[2] E. Witten, *Anti-de Sitter space, thermal phase transition and confinement in gauge theories*, *Adv. Theor. Math. Phys.* **2** (1998) 505 [hep-th/9803131] [INSPIRE].

[3] G. 't Hooft, *Dimensional reduction in quantum gravity*, gr-qc/9310026 [INSPIRE].

[4] L. Susskind, *The world as a hologram*, *J. Math. Phys.* **36** (1995) 6377 [hep-th/9409089] [INSPIRE].

[5] E. Witten, *Anti-de Sitter space and holography*, *Adv. Theor. Math. Phys.* **2** (1998) 253 [hep-th/9802150] [INSPIRE].

[6] S. Hawking and D.N. Page, *Thermodynamics of black holes in anti-de Sitter space*, *Commun. Math. Phys.* **87** (1983) 577 [INSPIRE].

[7] J. de Boer, K. Papadodimas and E. Verlinde, *Holographic neutron stars*, *JHEP* **10** (2010) 020 [arXiv:0907.2695] [INSPIRE].

[8] X. Arsiwalla, J. de Boer, K. Papadodimas and E. Verlinde, *Degenerate stars and gravitational collapse in AdS/CFT*, *JHEP* **01** (2011) 144 [arXiv:1010.5784] [INSPIRE].

[9] U.H. Danielsson, E. Keski-Vakkuri and M. Kruczenski, *Spherically collapsing matter in AdS, holography and shellons*, *Nucl. Phys.* **B 563** (1999) 279 [hep-th/9905227] [INSPIRE].

[10] E. Shuryak, S.-J. Sin and I. Zahed, *A gravity dual of RHIC collisions*, *J. Korean Phys. Soc.* **50** (2007) 384 [hep-th/0511199] [INSPIRE].

JHEP06(2012)021

[11] S. Lin and E. Shuryak, *Toward the AdS/CFT gravity dual for high energy collisions. 3. Gravitationally collapsing shell and quasiequilibrium*, *Phys. Rev.* **D 78** (2008) 125018 [arXiv:0808.0910] [INSPIRE].

[12] P.M. Chesler and L.G. Yaffe, *Horizon formation and far-from-equilibrium isotropization in supersymmetric Yang-Mills plasma*, *Phys. Rev. Lett.* **102** (2009) 211601 [arXiv:0812.2053] [INSPIRE].

[13] S. Bhattacharyya and S. Minwalla, *Weak field black hole formation in asymptotically AdS spacetimes*, *JHEP* **09** (2009) 034 [arXiv:0904.0464] [INSPIRE].

[14] V. Balasubramanian et al., *Thermalization of strongly coupled field theories*, *Phys. Rev. Lett.* **106** (2011) 191601 [arXiv:1012.4753] [INSPIRE].

[15] V. Balasubramanian et al., *Holographic thermalization*, *Phys. Rev.* **D 84** (2011) 026010 [arXiv:1103.2683] [INSPIRE].

[16] D.E. Kharzeev, L.D. McLerran and H.J. Warringa, *The effects of topological charge change in heavy ion collisions: 'Event by event P and CP-violation'*, *Nucl. Phys.* **A 803** (2008) 227 [arXiv:0711.0950] [INSPIRE].

[17] E. D'Hoker and P. Kraus, *Magnetic brane solutions in AdS*, *JHEP* **10** (2009) 088 [arXiv:0908.3875] [INSPIRE].

[18] R.C. Tolman, *Static solutions of Einstein's field equations for spheres of fluid*, *Phys. Rev.* **55** (1939) 364 [INSPIRE].

[19] J. Oppenheimer and G. Volkoff, *On massive neutron cores*, *Phys. Rev.* **55** (1939) 374 [INSPIRE].

[20] V. Canuto and H. Chiu, *Quantum theory of an electron gas in intense magnetic fields*, *Phys. Rev.* **173** (1968) 1210 [INSPIRE].

[21] V. Canuto and H. Chiu, *Thermodynamic properties of a magnetized Fermi gas*, *Phys. Rev.* **173** (1968) 1220 [INSPIRE].

[22] V.E. Hubeny, D. Marolf and M. Rangamani, *Hawking radiation from AdS black holes*, *Class. Quant. Grav.* **27** (2010) 095018 [arXiv:0911.4144] [INSPIRE].

[23] F.J. Ernst, *Black holes in magnetic universe*, *J. Math. Phys.* **17** (1976) 54.

[24] L.E. Blumenson, *A derivation of n-dimensional spherical coordinates*, *Amer. Math. Mon.* **67** (1960) 63.

[25] J.D. Bekenstein, *Entropy bounds and black hole remnants*, *Phys. Rev.* **D 49** (1994) 1912 [gr-qc/9307035] [INSPIRE].

[26] E. Greenwood, *Time evolution of entropy in gravitational collapse*, *JCAP* **06** (2009) 032 [arXiv:0811.0816] [INSPIRE].

JHEP06(2012)021

Published for SISSA by Springer

Received: *March 29, 2011*
Revised: *May 5, 2011*
Accepted: *May 17, 2011*
Published: *May 26, 2011*

Magnetic phase diagram of dense holographic multiquarks in the quark-gluon plasma

Piyabut Burikham

Theoretical High-Energy Physics and Cosmology Group, Department of Physics, Faculty of Science, Chulalongkorn University, Bangkok 10330, Thailand
Thailand Center of Excellence in Physics, CHE, Ministry of Education, Bangkok 10400, Thailand
Department of Physics, CERN Theory Division, CH-1211 Geneva 23, Switzerland

E-mail: piyabut@gmail.com

Abstract: We study phase diagram of the dense holographic gauge matter in the Sakai-Sugimoto model in the presence of the magnetic field above the deconfinement temperature. Even above the deconfinement, quarks could form colour bound states through the remaining strong interaction if the density is large. We demonstrate that in the presence of the magnetic field for a sufficiently large baryon density, the multiquark-pion gradient (MQ-$\bigtriangledown\varphi$) phase is more thermodynamically preferred than the chiral-symmetric quark-gluon plasma. The phase diagrams between the holographic multiquark and the chiral-symmetric quark-gluon plasma phase are obtained at finite temperature and magnetic field. In the mixed MQ-$\bigtriangledown\varphi$ phase, the pion gradient induced by the external magnetic field is found to be a linear response for small and moderate field strengths. Its population ratio decreases as the density is raised and thus the multiquarks dominate the phase. Temperature dependence of the baryon chemical potential, the free energy and the linear pion gradient response of the multiquark phase are well approximated by a simple analytic function $\sqrt{1-\frac{T^6}{T_0^6}}$ inherited from the metric of the holographic background.

Keywords: Holography and quark-gluon plasmas, Brane Dynamics in Gauge Theories, D-branes

ArXiv ePrint: 1103.4379

doi:10.1007/JHEP05(2011)121

JHEP05(2011)121

Contents

1 Introduction

Discovery of the AdS/CFT correspondence [1] and the generalization in terms of the holographic principle have provided us with alternative theoretical methods to explore the physics of strongly coupled gauge matter. Holographic models have been constructed to mimic behaviour of the strongly coupled gauge matter in various situations. The Sakai-Sugimoto (SS) model [2, 3] is a holographic model which contains chiral fermions in the fundamental representation of $U(N_c)$. Its low energy limit is the closest holographic model of the QCD so far. It can also accommodate distinctively the chiral symmetry restoration and the deconfinement phase transition in the non-antipodal case [4]. It provides interesting possibility of the existence of the exotic nuclear phase where quarks and gluons are deconfined but the chiral symmetry is still broken.

In the SS model, there are two background metrics describing a confined and a deconfined phase. The deconfined phase corresponds to the background metric with a black hole horizon. The Hawking temperature of the black hole is identified with the temperature of the dual "QCD" matter. When gluons are deconfined, the thermodynamical phase of the nuclear matter can be categorized into 3 phases, the vacuum phase, the chirally broken phase and the chiral-symmetric phase. In the deconfined phase, the interaction between quarks and gluons become the screened Coulomb potential. If the coupling is still strong, bound states of quarks could form (see ref. [5–10] for multiquark related studies). The phase diagram of the holographic nuclear matter in the SS model is studied in details in ref. [11] and extended to include multiquarks with colour charges in ref. [10]. It has certain similarity to the conventional QCD phase diagram speculated from other approaches e.g. the existence of critical temperature line above which chiral symmetry is restored. The phase diagram also shows the thermodynamic preference of the multiquark phase with broken chiral symmetry for moderate temperature in the situation when the density is sufficiently large. As an implication, it is thus highly likely that matters in the core of neutron stars are compressed into the multiquark nuclear phase. A thorough investigation on the

JHEP05(2011)121

multiquark star suggests higher mass limits of the neutron stars if they have multiquark cores [12].

When the magnetic field is turned on, the phase structure becomes more complicated. Magnetic field induces the pion gradient or a domain wall as a response of the chiral condensate of the chirally broken phase [13]. In the confined phase, this is distinctive [14]. However, it is demonstrated in ref. [15] that the pion gradient is subdominant to the contribution from the multiquarks in the chirally broken deconfined phase. It was also shown in ref. [15] that for sufficiently large density, the multiquark phase is more thermodynamically preferred than the chiral-symmetric quark-gluon plasma for small and moderate magnetic field strengths. Therefore it is interesting to explore the phase diagram of the deconfined nuclear matter in the presence of the external magnetic field. We establish two phase diagrams between the chirally broken multiquark (χSB) and the chiral-symmetric quark-gluon plasma (χS-QGP), one at fixed temperature, $T = 0.10$, and another at fixed field, $B = 0.20$. The magnetic phase diagram of the similar model for zero baryon density is investigated in ref. [16]. The phase diagram at finite density without instanton source is explored in ref. [17] with the approximation $f(u) \simeq 1$. We found that in the presence of the instanton for $T \gtrsim 0.10$, this approximation is no longer valid.

Our main results demonstrate that for a given magnetic field and moderate temperature, the most preferred nuclear phase in the SS holographic model is the multiquark-pion gradient (MQ-$\bigtriangledown\varphi$) phase provided that the density is sufficiently large. We also study the temperature dependence of the baryon chemical potential, the free energy, and the linear response of the pion gradient of the mixed MQ-$\bigtriangledown\varphi$ phase and show that they inherit the temperature dependence mostly from the SS background.

Extremely strong magnetic fields could have been produced in many situations. The Higgs mechanism in the cosmological electroweak phase transition could create enormous magnetic fields in the region between two different domains with different Higgs vacuum expectation values [18] which could play vital role in the phase transitions of the nuclear soup at later times. At the hadron and heavy ion colliders, colliding energetic charged particles could produce exceptional strong magnetic field locally. The local magnetic fields produced at RHIC and LHC are estimated to be in the order of 10^{14-15} Tesla [19]. On the astrophysical scale, certain types of neutron stars called the magnetars could produce magnetic fields as strong as 10^{10} Tesla [20].

This article is organized as the following. In section 2, the setup of the deconfined SS model with additional baryon vertex and string sources are discussed. Main results are elaborated in section 3. Section 4 concludes the article.

2 Holographic setup of the magnetized multiquark phase

The setup we will use is the same as in ref. [15], the Sakai-Sugomoto model with additional baryon vertex and strings (baryon vertex is introduced in ref. [21, 22]). Starting from a 10 dimensional type IIA string theory with one dimension compactified into a circle which we will label x^4. Two stacks of D8-branes and $\overline{\text{D8}}$-branes are then located at distance L from each other in the x^4 direction at the boundary. This separation will be fixed

JHEP05(2011)121

at the boundary and it will play the role of the fundamental scale of our holographic model. Open-string excitations with one end on the D8 and $\overline{\text{D8}}$ will represent quarks with different chiralities. In the background where the D8 and $\overline{\text{D8}}$ are parallel, excitations for each chirality are independent and there is a chiral symmetry in the background and at the boundary. For background with connecting D8 and $\overline{\text{D8}}$, chiral symmetry is broken and there is a chiral condensate. When the energy of the connecting configuration is minimal and there is no extra sources, we define the corresponding boundary gauge matter to be in a vacuum phase.

Since the partition function of the string theory in the bulk is conjectured to be equal to the partition function of the gauge theory on the boundary, the free energy of the boundary gauge matter is equivalent to the superstring action in the bulk (modulo a periodicity factor) [23]. We turn on non-normalizable modes of the gauge field a_3^V, a_1^A, a_0^V (defined in units of $R_{D4}/2\pi\alpha'$) in the D8-branes and identify them with the vector potential of the magnetic field, B (defined in units of $1/2\pi\alpha'$), the gradient of the chiral condensate, $\bigtriangledown\varphi$, and the baryon chemical potential, μ, at the boundary respectively. These curious holographic correspondence between the branes' fields and the thermodynamical quantities of the gauge matter at the boundary allows us to study physics of the strongly coupled non-Abelian gauge matter at finite density in the presence of the external magnetic field. Electric field can also be added using other components of the gauge field on the D8-branes [16, 24] but we will not consider such cases here.

The background spacetime of the Sakai-Sugimoto model is in the form

$$\begin{aligned} ds^2 &= \left(\frac{u}{R_{D4}}\right)^{3/2}\left(f(u)dt^2+\delta_{ij}dx^i dx^j+dx_4{}^2\right)+\left(\frac{R_{D4}}{u}\right)^{3/2}\left(u^2 d\Omega_4^2+\frac{du^2}{f(u)}\right) \quad (2.1)\\ F_{(4)} &= \frac{2\pi N}{V_4}\epsilon_4, \qquad e^{\phi}=g_s\left(\frac{u}{R_{D4}}\right)^{3/4}, \qquad R_{D4}^3\equiv\pi g_s N_c l_s^3, \end{aligned}$$

where $f(u)\equiv 1-u_T^3/u^3$, $u_T=16\pi^2R_{\rm D4}^3T^2/9$. V_4 is the volume of the unit four-sphere Ω_4 and ϵ_4 represents the volume 4-form. l_s and g_s are the string length scale and the string coupling respectively. R is the compactified radius of the x^4 coordinate. This radius is different from the curvature R_{D4} of the background in general. The dilaton field is denoted by ϕ which will be eliminated by the function of u as stated above.

The direction of the magnetic field is chosen so that the vector potential is

$$a_3^V = Bx_2. \quad (2.2)$$

The baryon chemical potential μ of the corresponding gauge matter is identified with the non-normalizable mode of the DBI gauge field at the boundary by

$$\mu = a_0^V(u\to\infty). \quad (2.3)$$

The five-dimensional Chern-Simon term of the D8-branes generates another axial part of the $U(1)$, a_1^A, by coupling it with B and a_0^V. In this way, the external magnetic field induces the axial current j_A associated with the axial field a_1^A. The non-normalizable mode of this field at the boundary corresponds to the response of the chiral condensate to the

JHEP05(2011)121

magnetic field which we call the pion gradient, $\bigtriangledown\varphi$. External field causes the condensate to form a domain wall which can be characterized by the gradient of the condensate with respect to the direction of the applied field. The pion gradient also acts as a source of the baryon density in our gauge matter.

Additional sources of the baryon density and the baryon chemical potential can be added to the configuration in the form of the baryon vertex and strings. The vertex appears as an instanton at the tip u_c of the brane configuration and the strings hang down from the vertex to the horizon u_T [10, 11].

$$S_{source} = \mathcal{N}d\Big[\frac{1}{3}u_c\sqrt{f(u_c)} + n_s(u_c - u_T)\Big], \tag{2.4}$$

$$= \mathcal{N}d\mu_{source} \tag{2.5}$$

where $n_s = k_r/N_c$ is the number of radial strings in the unit of $1/N_c$. Since the radial strings could merge with strings from other multiquark and generate a binding potential between the multiquarks, this number therefore represents the colour charges of the multiquark in the deconfined phase. It is interesting to note that when there is only string source representing quark matter, the quark matter becomes thermodynamically unstable under density fluctuations [11]. However, adding baryon vertex together with the strings makes the multiquark configuration stable under the density fluctuations [10]. The multiquark phase is even more thermodynamically preferred than the χS-QGP when the density is sufficiently large and the temperature is not too high.

With this setup, then the DBI and the Chern-Simon actions of the D8-branes configuration can be calculated to be

$$S_{D8} = \mathcal{N}\int_{u_c}^{\infty} du\ u^{5/2}\sqrt{1+\frac{B^2}{u^3}}\sqrt{1+f(u)(a_1'^A)^2-(a_0'^V)^2+f(u)u^3x_4'^2}, \tag{2.6}$$

$$S_{CS} = -\frac{3}{2}\mathcal{N}\int_{u_c}^{\infty} du\ (\partial_2 a_3^V a_0^V a_1^{A\prime} - \partial_2 a_3^V a_0^{V\prime} a_1^A), \tag{2.7}$$

where $\mathcal{N} = NR_{D4}^2/(6\pi^2(2\pi\alpha')^3)$ defines the brane tension. The factor 3/2 in the Chern-Simon action fixes the surface effect of the region with uniform magnetic field as explained in ref. [14]. We have to add extra surface terms to preserve the gauge invariance since the gauge transformation does not vanish at the boundary in this case.

We can write down the equations of motion with respect to each gauge field a_0^V, a_1^A as

$$\frac{\sqrt{u^5+B^2u^2}\ f(u)a_1'^A}{\sqrt{1+f(u)(a_1'^A)^2-(a_0'^V)^2+f(u)u^3x_4'^2}} = j_A - \frac{3}{2}B\mu + 3Ba_0^V, \tag{2.8}$$

$$\frac{\sqrt{u^5+B^2u^2}\ a_0'^V}{\sqrt{1+f(u)(a_1'^A)^2-(a_0'^V)^2+f(u)u^3x_4'^2}} = d - \frac{3}{2}Ba_1^A(\infty) + 3Ba_1^A. \tag{2.9}$$

d, j_A are the corresponding density and current density of the dual gauge matter at the boundary of the background ($u \to \infty$) given by

$$j^\mu(x, u\to\infty) \equiv \frac{\delta S_{eom}}{\delta A_\mu}\bigg|_{u\to\infty} \tag{2.10}$$

$$\equiv (d, \vec{j_A}). \tag{2.11}$$

JHEP05(2011)121

In terms of the gauge fields, they are

$$d = \frac{\sqrt{u^5 + B^2u^2}\ a_0'^V}{\sqrt{1 + f(u)(a_1'^A)^2 - (a_0'^V)^2 + f(u)u^3x_4'^2}}\Big|_\infty - \frac{3}{2}Ba_1^A(\infty), \tag{2.12}$$

$$j_A = \frac{\sqrt{u^5 + B^2u^2}\ f(u)a_1'^A}{\sqrt{1 + f(u)(a_1'^A)^2 - (a_0'^V)^2 + f(u)u^3x_4'^2}}\Big|_\infty - \frac{3}{2}B\mu. \tag{2.13}$$

In order to solve these equations, we need to specify the boundary conditions. Due to the holographic nature of the background spacetime, the boundary conditions correspond to physical requirement we impose to the gauge matter. If we want to address chirally broken phase of the gauge matter, we will take $a_1^A(\infty) \equiv \bigtriangledown\varphi$ to be an order parameter of the chiral symmetry breaking (also a response to the external magnetic field) and minimize the action with respect to it. This results in setting $j_A = 0$. On the other hand, if we want to study the chiral-symmetric gauge matter (or chiral-symmetric quark-gluon plasma for $N_c = 3$ case), x_4' and $a_1^A(\infty)$ will be set to zero. For vacuum phase, a_0^V, a_1^A and d, j_A will be set to zero.

In any cases, since the total action does not depend on $x_4(u)$ explicitly, the constant of motion gives

$$(x_4'(u))^2 = \frac{1}{u^3 f(u)}\Big[\frac{u^3[f(u)(C(u) + D(u)^2) - (j_A - \frac{3}{2}B\mu + 3Ba_0^V)^2]}{F^2} - 1\Big]^{-1}, \tag{2.14}$$

where

$$F = \frac{u_c^3\sqrt{f(u_c)}\sqrt{f(u_c)(C(u_c) + D(u_c)^2) - (j_A - \frac{3}{2}B\mu + 3Ba_0^V(u_c))^2}\ x_4'(u_c)}{\sqrt{1 + f(u_c)u_c^3\ x_4'^2(u_c)}} \tag{2.15}$$

and $C(u) \equiv u^5 + B^2u^2, D(u) \equiv d + 3Ba_1^A(u) - 3B\bigtriangledown\varphi/2$. The constant of motion with respect to $x_4(u)$ relates the slope x_4' at arbitrary u to the value at u_c,

$$(x_4'(u_c))^2 = \frac{1}{f_c u_c^3}\Big[\frac{9}{d^2}\frac{(f_c(C_c + D_c^2) - (j_A - \frac{3}{2}B\mu + 3Ba_0^V(u_c))^2)}{(1 + \frac{1}{2}(\frac{u_T}{u_c})^3 + 3n_s\sqrt{f_c})^2} - 1\Big].$$

The calculation of $x_4'(u_c)$ is described in the appendix as a result from the equilibrium and scale fixing condition

$$L_0 = 2\int_{u_c}^{\infty} x_4'(u)\ du = 1. \tag{2.16}$$

The equations of motion eq. (2.8), (2.9) can be solved numerically under the constraint (2.16). The value of $\mu, \bigtriangledown\varphi, u_c$ and the initial values of $a_0^V(u_c), a_1^A(u_c)$ are chosen so that $a_0^V(\infty) = \mu, a_1^A(\infty) = \bigtriangledown\varphi$ and $L_0 = 1$ are satisfied simultaneously. Since there are 3 conditions to be satisfied in finding the physical solutions numerically, we need the use the shooting algorithm for 3 targets at once.

JHEP05(2011)121

3 Magnetic phase diagram of the dense nuclear phase

Generically, the action (2.6) and (2.7) are divergent from the $u \to \infty$ limit of the integration and we need to regulate it using the action of the vacuum which is also divergent. The contribution from the region $u \to \infty$ is divergent even when the magnetic field is turned off and it is intrinsic to the DBI action in this background. The divergence can be understood as the infinite zero-point energy of the system and thus could be systematically removed by regularisation.

Therefore the regulated free energy is given by

$$\mathcal{F}_{\rm E} = \Omega(\mu, B) + \mu d, \tag{3.1}$$

where $\Omega(\mu, B) = S[a_0(u), a_1(u)](e.o.m.) - S[\text{magnetized vacuum}]$. Note that we need to Legendre transform the DBI and the Chern-Simon action to obtain the bulk action as a function of the non-normalizable modes a_0^V, a_1^A in order to identify it with the free energy of the gauge matter at the boundary. In terms of the free energy at the boundary, this is equivalent to the Legendre transform of the grand canonical with respect to μ and d.

We can calculate the total action satisfying the equation of motion $S[a_0(u), a_1(u)](e.o.m.) = S_{D8} + S_{CS}$ to be

$$S_{D8} = \mathcal{N} \int_{u_c}^{\infty} du\, C(u) \sqrt{\frac{f(u)(1 + f(u)u^3 x_4'^2)}{f(u)(C(u) + D(u)^2) - (j_A - \frac{3}{2}B\mu + 3Ba_0^V)^2}}, \tag{3.2}$$

$$S_{CS} = -\mathcal{N}\frac{3}{2}B \int_{u_c}^{\infty} du\, \frac{\left(a_0^V (j_A - \frac{3}{2}B\mu + 3Ba_0^V) - f(u)D(u)a_1^A\right)\sqrt{\frac{1}{f(u)} + u^3 x_4'^2}}{\sqrt{f(u)(C(u) + D(u)^2) - \left(j_A - \frac{3}{2}B\mu + 3Ba_0^V\right)^2}}. \tag{3.3}$$

The three nuclear phases above the deconfinement temperature are governed by the same equations of motion, each with specific boundary conditions as the following,

magnetized vacuum phase: $a_0^V, a_1^A = 0; d, j_A = 0$,

multiquark-pion gradient phase: $a_0^V(u_c) = \mu_{source}, a_1^A(u_c) = 0, a_1^A(\infty) = \bigtriangledown\varphi, j_A = 0$,

χS-QGP phase: $x_4'(u) = 0, a_0^V(u_c = u_T) = 0, a_1^A(\infty) = 0, j_A = \frac{3}{2}B\mu$.

We will demonstrate later that in the mixed phase, the pion gradient is generically dominated by the multiquark when the chiral symmetry is broken. In ref. [15], it is shown that the pure pion gradient phase is always less preferred thermodynamically than the mixed phase of MQ-$\bigtriangledown\varphi$. It is interesting to note that for the pure pion gradient phase, a large magnetic field is required in order to stabilize the generated domain wall [13]. This critical field is determined by the mass of the pion in the condensate, $B_{crit} \sim m_\pi^2/e$. In ref. [15], this critical behaviour is confirmed in the holographic SS model (the zero-temperature situation is studied in ref. [25]). More investigation of the pure pion gradient phase in the holographic model should be conducted especially when the field is large since the distinctive feature of physics from the DBI action becomes apparent in this limit. We will leave this task for future work and focus our attention to the mixed MQ-$\bigtriangledown\varphi$ phase in this article.

JHEP05(2011)121

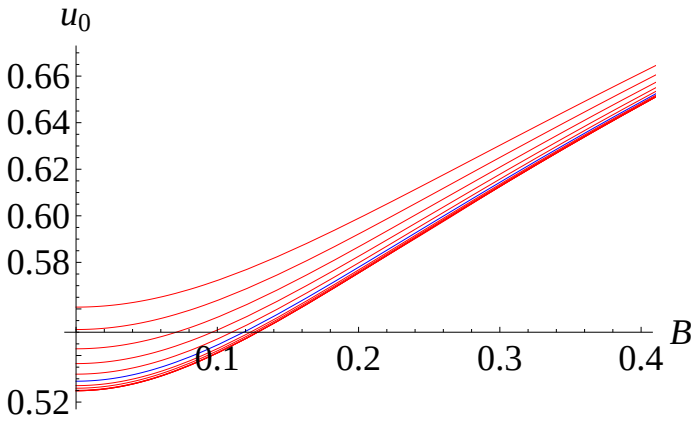

Figure 1. The position u_0 of the connected D8-$\overline{\text{D8}}$ vacuum configuration as a function of B for $T = 0.02 - 0.15$. The upper lines have higher temperatures.

The action of the magnetized vacuum when we set $a_0^V, a_1^A = 0$ and $d, j_A = 0$ is

$$S[\text{magnetized vacuum}] = \int_{u_0}^{\infty} \sqrt{C(u)(1 + f(u)u^3 x_4'^2)}\Big|_{vac} du,$$

where

$$x_4'(u)|_{vac} = \frac{1}{\sqrt{f(u)u^3\left(\frac{f(u)u^3 C(u)}{f(u_0)u_0^3 C(u_0)} - 1\right)}}. \tag{3.4}$$

The position u_0 where $x_4' \to \infty$ is the tip of the brane configuration of the magnetized vacuum. It increases slightly with temperature as is shown in figure 1. The difference between each temperature decreases as the magnetic field gets larger and all curves converge to the same saturated value $u_0 = 1.23$ in the large field limit.

We can study the temperature dependence of the magnetized multiquark nuclear matter by considering its baryon chemical potential and the free energy as shown in figure 2. Both the chemical potential and the free energy decrease steadily as the temperature rises, regardless of the magnetic field. This is originated from the temperature dependence of $f(u) = 1 - \frac{u_T^3}{u^3}$ of the SS background in the deconfined phase. The temperature dependence could be fit very closely with the function $\sqrt{1 - \left(\frac{T}{T_0}\right)^6}$ as the following

$$\mu = \mu_0(d, B)\sqrt{1 - \left(\frac{T}{T_0}\right)^6}, \tag{3.5}$$

$$F = F_0(d, B)\sqrt{1 - \left(\frac{T}{T_0}\right)^6}. \tag{3.6}$$

where for $d = 1, B = 0.10$; $\mu_0 = 1.1849, F_0 = 0.7976$ respectively. For the baryon chemical potential (free energy), the best-fit value of T_0 is 0.269 (0.233). The fittings are shown in figure 3. This could be explained by noting that the regulated free energy is given by

JHEP05(2011)121

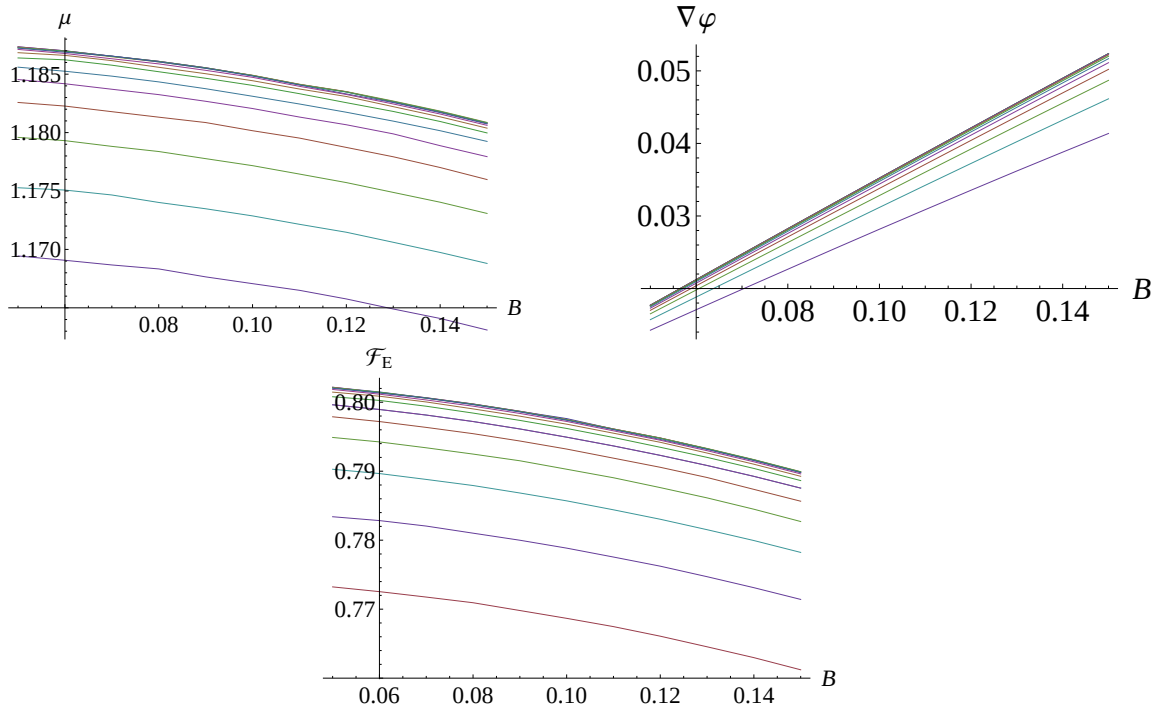

Figure 2. The chemical potential (a), the pion gradient (b), and the free energy (c) of the multiquark phase with baryon density $d = 1$ as a function of B for temperature $T = 0.02 - 0.15$. The lower curves represent multiquark at higher temperatures.

$\mu d + \Omega(\mu, B)$. The contribution from the first term is dominant therefore the free energy has almost the same temperature dependence as the chemical potential. However, there is a minor contribution from $S_{\rm D8}+S_{\rm CS}$ containing $f(u_c) = 1-\frac{u_T^3}{u_c^3}$ which for small temperature fractions modifies the temperature function in the following manner,

$$C_1\sqrt{1-\frac{T^6}{T_1^6}}+C_2\sqrt{1-\frac{T^6}{T_2^6}} \simeq C_0\sqrt{1-\frac{T^6}{T_0^6}}, \tag{3.7}$$

where $C_{1,2}$ are some arbitrary constants and C_0, T_0 are given by

$$C_0 = C_1 + C_2, \tag{3.8}$$

$$\frac{1}{T_0^6} = \frac{1}{C_1+C_2}\left(\frac{C_1}{T_1^6}+\frac{C_2}{T_2^6}\right). \tag{3.9}$$

It should be noted from figure 3 that the temperature dependence is significant for $T \gtrsim 0.10$ and the approximation $f(u) \simeq 1$ is not accurate for temperature in this range. The characteristic temperatures we found here are consistent with the phase diagram of the multiquark in figure 7.

In the multiquark phase when the magnetic field is turned on, the pion gradient is induced by the field in addition to the multiquark. The multiquark phase thus contained the mixed content of multiquarks and the pion gradient. For moderate fields (not too large), the response is linear $\bigtriangledown\varphi \propto B$. In contrast to the case of pure pion gradient phase,

JHEP05(2011)121

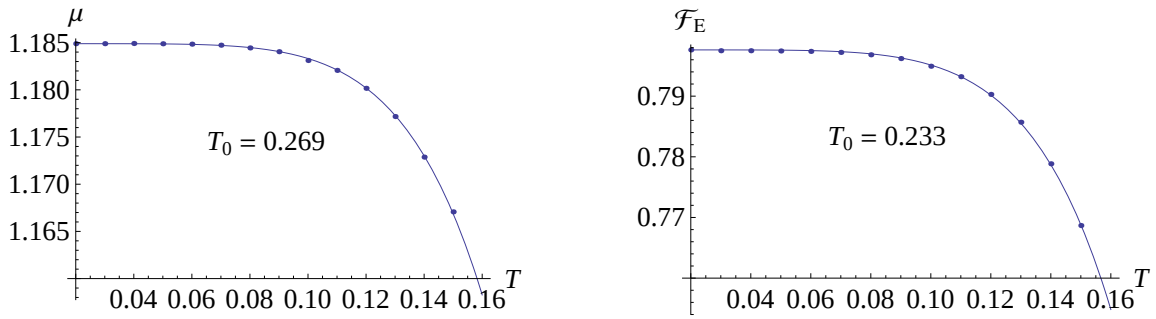

Figure 3. For $d = 1, B = 0.10$,(a) the baryon chemical potential as a function of T, the best-fit curve is in the form $\mu_0\sqrt{1-(\frac{T}{T_0})^6}$ with $\mu_0 = 1.1849, T_0 = 0.269$; (b) the free energy as a function of T, the best-fit curve is in the form $F_0\sqrt{1-(\frac{T}{T_0})^6}$ with $F_0 = 0.7976, T_0 = 0.233$. Other curves within the range $B = 0.05 - 0.15$ can also be fitted well with the same T_0.

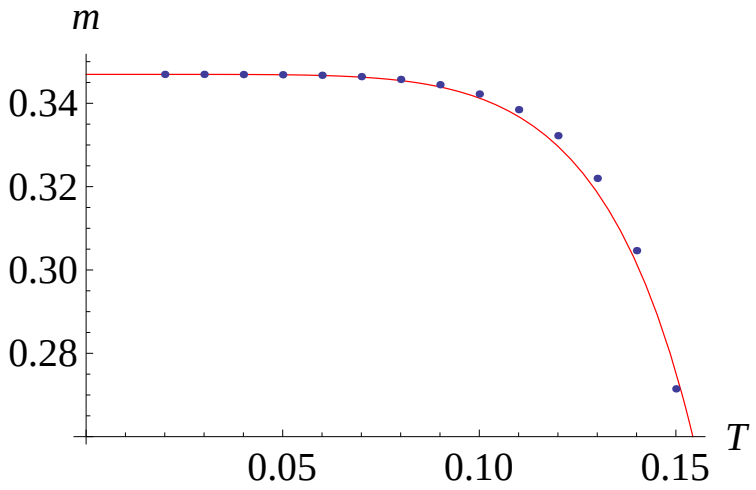

Figure 4. The linear response or slope of the linear function between the pion gradient and the magnetic field as a function of the temperature for the range $B = 0.05 - 0.15$ and density $d = 1$. The red line is the best-fit curve in the form $m_0\sqrt{1-(\frac{T}{T_0})^6}$ with $m_0 = 0.347, T_0 = 0.177$.

the domain wall in the mixed MQ-$\bigtriangledown\varphi$ phase is stable among the surrounding multiquarks even for small field. The critical magnetic field to stabilize the domain wall in the case of pure pion gradient is not required in the mixed phase.

Figure 2 (b) shows a linear relation between the pion gradient and the magnetic field which is valid up to moderate fields. For $d = 1$, we found that the slope, m (or the linear response), of this linear function depends on the temperature approximately as $m = m_0\sqrt{1-(\frac{T}{T_0})^6}$, and

$$\bigtriangledown\varphi \simeq Bm_0\sqrt{1-\left(\frac{T}{T_0}\right)^6}, \tag{3.10}$$

where $m_0 = 0.347, T_0 = 0.177$. The curve fitting is shown in figure 4. The density depen-

JHEP05(2011)121

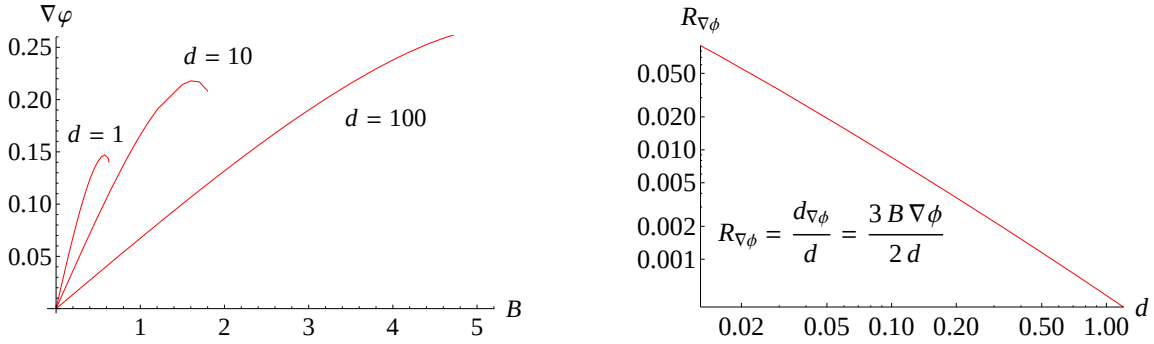

Figure 5. (a) The pion gradient as a function of B for density $d = 1, 10, 100$ at $T = 0.10$. (b) The density ratio of the pion gradient with respect to the total baryon density of the multiquark phase at $B = 0.10, T = 0.10$ in the double-log scale.

dence is encoded in $m_0 = m_0(d), T_0 = T_0(d)$. As the density increases, the slope of the linear response of the pion gradient becomes smaller as is shown in figure 5. The ratio of the pion gradient density and the total baryonic density $R_{\bigtriangledown\varphi} \equiv d_{\bigtriangledown\varphi}/d = 3B\bigtriangledown\varphi/2d$ [14] for $B = 0.10, T = 0.10$ is plotted in the log-scale in figure 5 (b). It could be well approximated by

$$R_{\bigtriangledown\varphi} \simeq (\text{const.})d^{-6/5}, \tag{3.11}$$

$$\simeq \frac{3B^2 m_0}{2d}\sqrt{1-\left(\frac{T}{T_0}\right)^6}, \tag{3.12}$$

from eq. (3.10). This implies that the multiquark states are more preferred than the pion gradient in the presence of the magnetic field, the denser the nuclear matter, the more stable the multiquarks become and the lesser the population of the pion gradient.

Finally we compare the free energy of the MQ-$\bigtriangledown\varphi$ phase and the chiral-symmetric quark-gluon plasma phase. For high density, $d = 100$, this is shown in figure 6. For a given density, the multiquark phase is more thermodynamically preferred than the χS-QGP for small and moderate fields. As the magnetic field gets larger, the χS-QGP becomes more thermodynamically preferred. When the field becomes very strong, the transition into the lowest Landau level finally occurs [26]. For a fixed density, increasing magnetic field inevitably results in the chiral symmetry restoration. The phase transition between the MQ-$\bigtriangledown\varphi$ and the χS-QGP is a first order since the free energy is continuous at the transition and the slope has a discontinuity. It implies that the magnetization, $M(d, B) = -\frac{\partial \mathcal{F}_{\rm E}}{\partial B}$, of the nuclear matter abruptly changes at the transition.

On the other hand, for a fixed field and the moderate temperature, the increase in the baryon density could make the multiquark phase more stable than the χS-QGP. This is shown in the phase diagram in figure 7. At a given magnetic field, the multiquark phase could become the most preferred magnetized nuclear phase provided that the density is made sufficiently large and the temperature is not too high. In contrast, the effect of the temperature is the most dominant for chiral-symmetry restoration even when the field is turned on. Sufficiently large temperature will induce chiral-symmetry restoration for

JHEP05(2011)121

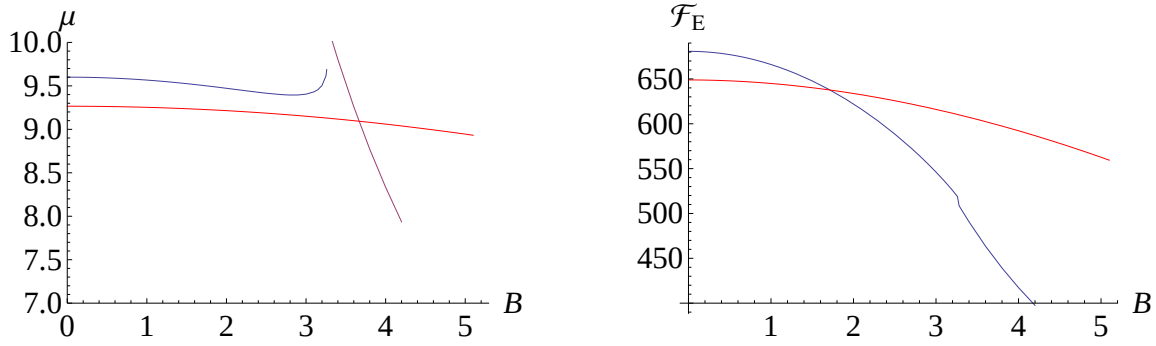

Figure 6. For the dense multiquark with $d = 100, T = 0.10$, (a) the chemical potential, (b) the free energy as a function of B. The multiquark curves in red are compared with the χS-QGP curves in blue for the chemical potential and the free energy.

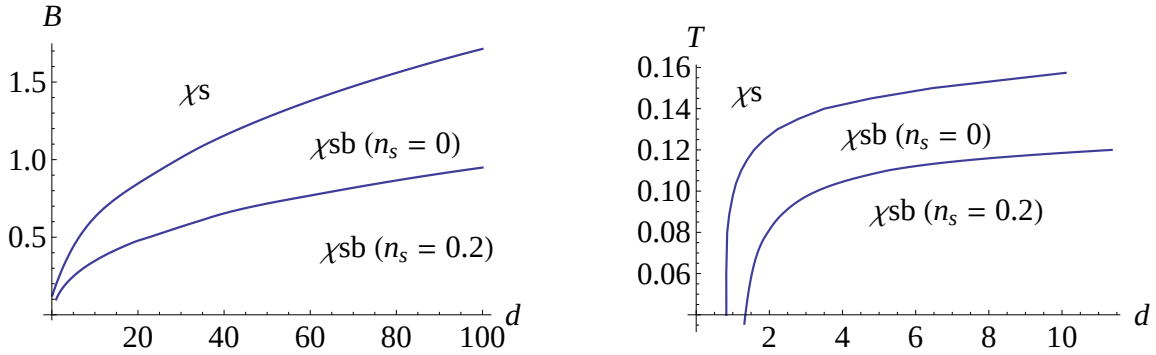

Figure 7. The phase diagram of the dense nuclear phases involving multiquarks when gluons are deconfined for (a) $T = 0.10$ and (b) $B = 0.20$. The chiral-symmetric quark-gluon plasma and the chirallly broken MQ-$\bigtriangledown\varphi$ phase are represented by χS and χSB respectively, n_s is the number of colour strings in fractions of $1/N_c$.

most densities as is shown the figure 7(b). Nevertheless, theoretically we can always find sufficiently large density above which the multiquark phase is more preferred.

The transition line between the MQ-$\bigtriangledown\varphi$ and the χS-QGP phases in the (d, B) phase diagram can be approximated by a power-law

$$B \sim d^{0.438\ (0.436)} \tag{3.13}$$

for the multiquark with $n_s = 0$ (0.2). This power-law is weaker than the transition line of the χS-QGP to the lowest Landau level studied in ref. [26] for the antipodal SS model ($B \sim d^{2/3}$). The multiquarks with more colour charges ($n_s > 0$) are less preferred thermodynamically but they require higher densities. On the other hand, the transition line in the (d, T) phase diagram is an increasing function of d but weaker than the logarithmic of the density. Nevertheless, theoretically for a fixed B, T, we can always find sufficiently large density above which the MQ-$\bigtriangledown\varphi$ phase is preferred. The high density region is actually dominated by the multiquark phase indeed.

JHEP05(2011)121

4 Conclusion

We explore the properties of the miltiquark-domain wall (MQ-$\bigtriangledown\varphi$) solution of the SS model above the deconfinement temperature. The temperature dependence of the baryon chemical potential, the pion gradient linear response (m), and the free energy of the MQ-$\bigtriangledown\varphi$ phase has been studied and fitted with a simple function, $\sqrt{1-\frac{T^6}{T_0^6}}$, inherited from the deconfined SS background. Their characteristic temperatures, T_0, are different from one another depending on other parameters such as u_c, the position of the baryon vertex. Remarkably, they do not depend on the field for moderate field strength $B = 0.05 - 0.15$.

For chirally broken deconfined nuclear matter in the presence of the magnetic field, the nuclear matter with finite baryon density and chemical potential could respond to the magnetic field by inducing a pion gradient or a domain wall of the chiral condensate. This pion gradient response is found to be a linear function of the field for moderate fields at any density. However, we demonstrate further that the population ratio of the pion gradient decreases as the density increases. The other sources of the baryon charge namely the multiquarks finally dominate the chirally broken nuclear phase and most of the baryon density is in the form of the multiquark at high density.

Magnetic phase diagram of the dense gauge matter have been explored in the deconfined SS model. At fixed magnetic field and moderate temperature, the MQ-$\bigtriangledown\varphi$ phase are more preferred than the χS-QGP for the high density region. The transition line in the (d, B) phase diagram at $T = 0.10$ can be fitted closely with the power-law $B \sim d^{0.438\ (0.436)}$ for the multiquark with $n_s = 0$ (0.2). On the other hand, the transition line in the (d, T) phase diagram is weaker than the logarithmic of the density but nevertheless it is an increasing function with respect to the density. These imply that for sufficiently large density, the chirally broken multiquark phase is the most preferred nuclear phase even in the presence of the external magnetic field.

The situation when density becomes extremely large and being dominant occurs in the core of dense star such as the neutron star. Therefore it is very likely that the core of dense warm star composes primarily of the multiquark nuclear matter even when an enormous magnetic field is present such as in the core of the magnetars. It is possible that a large population of the warm magnetars has multiquark cores. These warm dense objects could be relatively more massive than typical neutron stars.

Acknowledgments

I would like to thank CERN Theory Division for the warm hospitality during my visit where this work is completed. P.B. is supported in part by the Thailand Research Fund (TRF) and Commission on Higher Education (CHE) under grant RMU5380048 and Thailand Center of Excellence in Physics (ThEP).

A Force condition of the multiquark configuration

Fixing the characteristic scale L_0 to 1 for the brane configuration requires balancing three forces in the gravity picture. The D8-brane tension must be in equilibrium with the tidal

JHEP05(2011)121

weight of the D4 source and the string tension of the colour strings. The derivation of the $x_4'(u_c)$ presented here is the same as in ref. [15], it is included for completeness.

We vary the total action with respect to u_c to obtain the surface term. Imposing the scale-fixing condition $2\int_{u_c}^{\infty} dux_4'(u) = L_0 = 1$, we found that [11]

$$x_4'(u_c) = \left(\tilde{L}(u_c) - \frac{\partial S_{source}}{\partial u_c}\right) \Bigg/ \left.\frac{\partial \tilde{S}}{\partial x_4'}\right|_{u_c}, \tag{A.1}$$

as the condition on u_c.

We perform the Legendre transformed action with respect to $a_0^{V\prime}$ and $a_1^{A\prime}$ to obtain

$$\begin{aligned}\tilde{S} &= \int_{u_c}^{\infty} \tilde{L}(x_4'(u), d)\, du, \\ &= \mathcal{N}\int_{u_c}^{\infty} du \sqrt{\frac{1}{f(u)} + u^3 x_4'^2} \\ &\quad \times\sqrt{f(u)(C(u)+D(u)^2) - \left(j_A - \frac{3}{2}B\mu + 3Ba_0^V\right)^2},\end{aligned} \tag{A.2}$$

where $C(u) \equiv u^5 + B^2u^2, D(u) \equiv d + 3Ba_1^A(u) - 3B\bigtriangledown\varphi/2$. Note that the Chern-Simon action are included in the total action during the transformations.

The Chern-Simon term with the derivatives $a^{V\prime}, a^{A\prime}$ eliminated is

$$S_{CS} = -\mathcal{N}\frac{3}{2}B\int_{u_c}^{\infty} du\, \frac{\left(a_0^V(j_A - \frac{3}{2}B\mu + 3Ba_0^V) - f(u)D(u)a_1^A\right)\sqrt{\frac{1}{f(u)} + u^3x_4'^2}}{\sqrt{f(u)(C(u)+D(u)^2) - \left(j_A - \frac{3}{2}B\mu + 3Ba_0^V\right)^2}}. \tag{A.3}$$

From eq. (A.1), (A.2), (A.3), (2.5), and the boundary conditions, $a_0^V(u_c) = \mu_{source}, a_1^A(u_c) = 0$, we can solve to obtain the condition for the static equilibrium

$$(x_4'(u_c))^2 = \frac{1}{f_c u_c^3}\left[\frac{9}{d^2}\frac{(f_c(C_c + D_c^2) - (j_A - \frac{3}{2}B\mu + 3Ba_0^V(u_c))^2)}{(1 + \frac{1}{2}(\frac{u_T}{u_c})^3 + 3n_s\sqrt{f_c})^2} - 1\right],$$

where $f_c \equiv f(u_c), C_c \equiv C(u_c), D_c \equiv D(u_c)$.

References

[1] J.M. Maldacena, *The large-N limit of superconformal field theories and supergravity*, *Int. J. Theor. Phys.* **38** (1999) 1113 [*Adv. Theor. Math. Phys.* **2** (1998) 231] [hep-th/9711200] [SPIRES].

[2] T. Sakai and S. Sugimoto, *Low energy hadron physics in holographic QCD*, *Prog. Theor. Phys.* **113** (2005) 843 [hep-th/0412141] [SPIRES].

JHEP05(2011)121

[3] T. Sakai and S. Sugimoto, *More on a holographic dual of QCD*, *Prog. Theor. Phys.* **114** (2005) 1083 [hep-th/0507073] [SPIRES].

[4] O. Aharony, J. Sonnenschein and S. Yankielowicz, *A holographic model of deconfinement and chiral symmetry restoration*, *Annals Phys.* **322** (2007) 1420 [hep-th/0604161] [SPIRES].

[5] A. Brandhuber, N. Itzhaki, J. Sonnenschein and S. Yankielowicz, *Baryons from supergravity*, *JHEP* **07** (1998) 020 [hep-th/9806158] [SPIRES].

[6] K. Ghoroku, M. Ishihara, A. Nakamura and F. Toyoda, *Multi-quark baryons and color screening at finite temperature*, *Phys. Rev.* **D 79** (2009) 066009 [arXiv:0806.0195] [SPIRES].

[7] K. Ghoroku and M. Ishihara, *Baryons with D5 Brane Vertex and k-Quarks*, *Phys. Rev.* **D 77** (2008) 086003 [arXiv:0801.4216] [SPIRES].

[8] M.V. Carlucci, F. Giannuzzi, G. Nardulli, M. Pellicoro and S. Stramaglia, *AdS-QCD quark-antiquark potential, meson spectrum and tetraquarks*, *Eur. Phys. J.* **C 57** (2008) 569 [arXiv:0711.2014] [SPIRES].

[9] W.-Y. Wen, *Multi-quark potential from AdS/QCD*, *Int. J. Mod. Phys.* **A 23** (2008) 4533 [arXiv:0708.2123] [SPIRES].

[10] P. Burikham, A. Chatrabhuti and E. Hirunsirisawat, *Exotic Multi-quark States in the Deconfined Phase from Gravity Dual Models*, *JHEP* **05** (2009) 006 [arXiv:0811.0243] [SPIRES].

[11] O. Bergman, G. Lifschytz and M. Lippert, *Holographic Nuclear Physics*, *JHEP* **11** (2007) 056 [arXiv:0708.0326] [SPIRES].

[12] P. Burikham, E. Hirunsirisawat and S. Pinkanjanarod, *Thermodynamic Properties of Holographic Multiquark and the Multiquark Star*, *JHEP* **06** (2010) 040 [arXiv:1003.5470] [SPIRES].

[13] D.T. Son and M.A. Stephanov, *Axial anomaly and magnetism of nuclear and quark matter*, *Phys. Rev.* **D 77** (2008) 014021 [arXiv:0710.1084] [SPIRES].

[14] O. Bergman, G. Lifschytz and M. Lippert, *Magnetic properties of dense holographic QCD*, *Phys. Rev.* **D 79** (2009) 105024 [arXiv:0806.0366] [SPIRES].

[15] P. Burikham, *Magnetic properties of holographic multiquarks in the quark-gluon plasma*, *JHEP* **04** (2010) 045 [arXiv:0909.0614] [SPIRES].

[16] C.V. Johnson and A. Kundu, *External Fields and Chiral Symmetry Breaking in the Sakai-Sugimoto Model*, *JHEP* **12** (2008) 053 [arXiv:0803.0038] [SPIRES].

[17] F. Preis, A. Rebhan and A. Schmitt, *Inverse magnetic catalysis in dense holographic matter*, *JHEP* **03** (2011) 033 [arXiv:1012.4785] [SPIRES].

[18] T. Vachaspati, *Magnetic fields from cosmological phase transitions*, *Phys. Lett.* **B 265** (1991) 258 [SPIRES].

[19] D.E. Kharzeev, L.D. McLerran and H.J. Warringa, *The effects of topological charge change in heavy ion collisions: 'Event by event P and CP-violation'*, *Nucl. Phys.* **A 803** (2008) 227 [arXiv:0711.0950] [SPIRES].

[20] R.C. Duncan and C. Thompson, *Formation of very strongly magnetized neutron stars - implications for gamma-ray bursts*, *Astrophys. J.* **392** (1992) L9 [SPIRES].

JHEP05(2011)121

[21] E. Witten, *Baryons and branes in anti de Sitter space*, *JHEP* **07** (1998) 006 [hep-th/9805112] [SPIRES].

[22] D.J. Gross and H. Ooguri, *Aspects of large-N gauge theory dynamics as seen by string theory*, *Phys. Rev.* **D 58** (1998) 106002 [hep-th/9805129] [SPIRES].

[23] O. Aharony, S.S. Gubser, J.M. Maldacena, H. Ooguri and Y. Oz, *Large-N field theories, string theory and gravity*, *Phys. Rept.* **323** (2000) 183 [hep-th/9905111] [SPIRES].

[24] O. Bergman, G. Lifschytz and M. Lippert, *Response of Holographic QCD to Electric and Magnetic Fields*, *JHEP* **05** (2008) 007 [arXiv:0802.3720] [SPIRES].

[25] E.G. Thompson and D.T. Son, *Magnetized baryonic matter in holographic QCD*, *Phys. Rev.* **D 78** (2008) 066007 [arXiv:0806.0367] [SPIRES].

[26] G. Lifschytz and M. Lippert, *Holographic Magnetic Phase Transition*, *Phys. Rev.* **D 80** (2009) 066007 [arXiv:0906.3892] [SPIRES].

JHEP05(2011)121

Published for SISSA by Springer

Received: *May 22, 2011*
Revised: *July 7, 2011*
Accepted: *July 14, 2011*
Published: *August 5, 2011*

Magnetized domain walls in the deconfined Sakai-Sugimoto model at finite Baryon density

Piyabut Burikham[a,b,c] **and Tossaporn Chullaphan**[a]

[a] *Theoretical High-Energy Physics and Cosmology Group, Department of Physics, Faculty of Science, Chulalongkorn University, Phyathai Road, Bangkok 10330, Thailand*

[b] *Thailand Center of Excellence in Physics, CHE, Ministry of Education, Bangkok 10400, Thailand*

[c] *Department of Physics, CERN Theory Division, CH-1211 Geneva 23, Switzerland*

E-mail: piyabut@gmail.com, chullaphan.t@gmail.com

Abstract: The magnetized pure pion gradient ($\bigtriangledown\varphi$) phase in the deconfined Sakai-Sugimoto model is explored at zero and finite temperature. We found that the temperature has very small effects on the phase. The thermodynamical properties of the phase show that the excitations behave like scalar solitonic free particles. By comparing the free energy of the pion gradient phase to the competing multiquark-pion gradient (MQ-$\bigtriangledown\varphi$) phase, it becomes apparent that the pure pion gradient is less thermodynamically preferred than the MQ-$\bigtriangledown\varphi$ phase. However, in the parameter space where the baryonic chemical potential is smaller than the onset value of the multiquark, the dominating magnetized nuclear matter is the pion gradient phase.

Keywords: Holography and quark-gluon plasmas, Brane Dynamics in Gauge Theories, D-branes

ArXiv ePrint: 1105.2729

Open Access

doi:10.1007/JHEP08(2011)026

Contents

1 Introduction

Physics of dense nuclear matter is one of the most challenging area due to the lack of appropriate theoretical modeling. On one hand, the entities in the nuclear matter strongly couple to one another and therefore the perturbative treatment cannot be applied in a straightforward manner. On the other hand, the lattice approach to the Quantum Chromodynamics (QCD) can be applied to the situations of hot nuclear matter. The lattice results predict the deconfinement phase transition at temperature around 175 MeV for the dilute nuclear matter. However, this approach also faces difficulty in describing the nuclear matter with finite density due to the fermion sign problem.

An alternative and complementary approach is the application of the holographic principle or the AdS/CFT correspondence [1–3] to study the properties of the nuclear matter. The Sakai-Sugimoto (SS) model [4, 5] is a holographic model which could approximate the QCD at low energy most accurately. Starting with a type IIA string background with D4-branes as the source. Take the near-horizon limit and add the black hole horizon to generate Hawking-Page temperature to be identified with the temperature of the dual gauge matter. Since we need an approximately 4 dimensional QCD, one of the 5 dimensional subspace is compactified into a circle whose radius is chosen so small that the Kaluza-Klein states are much heavier than the relevant energy scales and temperatures.

The quarks and antiquarks are introduced as open-string excitations on the stack of N_f flavour D8 and $\overline{\text{D8}}$ branes located at fixed separation distance in the compactified coordinate. The boundary conditions of the sparticles in the circle are chosen to be antisymmetric at the location of the flavour branes and the zeroth modes are thus eliminated. Consequently, the gauge theory at the flavour branes is a SUSY-broken 5 dimensional Yang-Mills theory with quarks and antiquarks in the fundamental representation. The effective theory has the same particle content as the QCD. Using the AdS/CFT correspondence, the bulk theory of this brane configuration is conjectured to be dual to the QCD-like gauge theory at the boundary. The striking feature of the SS model is that it provides a natural geometric realization of the chiral symmetry breaking. When the D8 and $\overline{\text{D8}}$ merge at certain location

JHEP08(2011)026

in the radial coordinate, the quarks and antiquarks do not transform independently under the chiral transformation and therefore the chiral symmetry is broken in the connected brane configuration. A chiral symmetric configuration occurs when the two flavour branes are parallel and the dual gauge matter will be in the chiral symmetric phase.

Subsequent investigation reveals that the SS model accommodates the exotic possibility that the chiral symmetry restoration and the deconfinement can occur separately [6] when the distance between the D8 and $\overline{\text{D8}}$ branes in the compactified dimension is not too large. The deconfinement could occur at relatively low temperature while the chiral symmetry would be restored at larger temperature. Even though both the chiral symmetry breaking and the confinement are results of the strong coupling of the gauge theory, they are independent of one another as far as we know. It is thus possible that the real QCD also has distinctive chiral symmetry restoration and deconfinement.

Chiral condensate of the QCD-like dense matter is explored in ref. [7] using the Wess-Zumino-Witten induced anomalous term in the chiral perturbation theory and in ref. [8] using the bottom-up AdS/QCD based on the confined SS model. When the magnetic field is applied, the condensate will respond by developing a gradient in the direction of the applied field. This gradient also carries the baryonic charge density proportional to the applied field and the gradient of the condensate. Holographic studies of the chiral condensate response to the magnetic field is investigated in ref. [9] for the confined SS model. In ref. [10], the pure pion gradient phase is explored and compared with the chiral symmetric quark-gluon plasma phase in the zero temperature approximation of the deconfined SS model. In ref. [11], it is roughly compared with the mixed phase of the multiquark-pion gradient (MQ-$\bigtriangledown\varphi$) using a zero-instanton limit of the multiquark configuration. The preliminary results suggest that the pure pion gradient phase might be thermodynamically less preferred than the MQ-$\bigtriangledown\varphi$ phase. In this article, we perform a thorough investigation into the pure pion gradient phase at finite temperature as well as its thermodynamical comparison to the MQ-$\bigtriangledown\varphi$ in order to obtain a more definitive quantitative result. It is found that the pure pion gradient phase is insensitive to the change of temperature in the range $T = 0 - 0.16$. It is also shown that the pure pion gradient phase is generically less preferred than the MQ-$\bigtriangledown\varphi$ phase except when the baryon chemical potential is smaller than the onset value of the multiquarks. In that region of the phase diagram, the dominating phase is the pure pion gradient.

The article is organized as the following. In section 2, we setup the holographic model of the magnetized chirally broken nuclear phase without an instanton. A zero temperature solution is obtained and relevant dual physical quantities as well as their relationships are discussed. Thermodynamical properties of the pure pion gradient phase at finite temperature and the comparison with the multiquark phase are discussed in section 3. Section 4 concludes the article.

2 Holographic setup of the magnetized chirally broken phase

In the non-antipodal SS model, a stack of N_c D4-branes generates a curved 10 dimensional spacetime in type IIA string theory. The near-horizon limit of this background is then

JHEP08(2011)026

taken and the black hole horizon is added by introducing the factor $f(u)$ [3, 12] into the background. The x^4 direction is compactified with certain radius to obtain an effective $(1+3)$ dimensional subspace in the low energy limit. The resulting spacetime of the Sakai-Sugimoto model is in the form

$$ds^2 = \left(\frac{u}{R_{D4}}\right)^{3/2}\left(f(u)dt^2 + \delta_{ij}dx^i dx^j + {dx_4}^2\right) + \left(\frac{R_{D4}}{u}\right)^{3/2}\left(u^2 d\Omega_4^2 + \frac{du^2}{f(u)}\right)$$
$$e^{\phi} = g_s\left(\frac{u}{R_{D4}}\right)^{3/4}, \qquad R_{D4}^3 \equiv \pi g_s N_c l_s^3,$$

where $f(u) \equiv 1 - u_T^3/u^3$, $u_T = 16\pi^2 R_{\rm D4}^3 T^2/9$. T is the Hawking-Page temperature of the black hole which is identified with the temperature of the dual gauge matter at the boundary. R_{D4} is the curvature of the background which is generically different from the compactified radius R of the x^4 coordinate. ϕ is the dilaton field, a function of u in this background.

We then introduce stacks of N_f D8 and $\overline{\rm D8}$ flavour branes with separation L_0 on the circle of compactified x^4 at the boundary $u \to \infty$. Open string excitations with one end on these branes behave like chiral "quarks" and "antiquarks" in the fundamental representation of the $\mathrm{U}(N_f)$. In the brane configuration where D8 and $\overline{\rm D8}$ are parallel, open-string excitations on each stack of branes transform independently under the chiral transformation and thus we have a chiral symmetric background. The dual gauge matter will be in the chiral symmetric phase. On the other hand, in the connecting brane configuration, chiral symmetry is broken at the tip and the corresponding gauge matter will be in the chirally broken phase [6].

To add the baryonic density to the boundary gauge matter, the non-normalizable mode of the a_0^V component of the $\mathrm{U}(1) \subset \mathrm{U}(N_f)$ field is turned on. The baryon chemical potential μ of the corresponding gauge matter is identified with the non-normalizable mode of the DBI gauge field at the boundary by [13]

$$\mu = a_0^V(u \to \infty). \tag{2.1}$$

To turn on the magnetic field, another component a_3^V is used as the vector potential generating the magnetic field. The direction of the magnetic field is chosen so that the vector potential is

$$a_3^V = Bx_2. \tag{2.2}$$

The Chern-Simons action in the background couples these two components to the third component a_1^A of the U(1), generating the response to the external magnetic field. The response appears as the gradient of the chiral condensate along the direction of B at the boundary which is defined to be $a_1^A(u \to \infty) \equiv \bigtriangledown\varphi$. Here and henceforth, we will call $\bigtriangledown\varphi$ a pion gradient.

JHEP08(2011)026

The DBI and the Chern-Simons actions are then given by

$$S_{D8} = \mathcal{N}\int_{u_c}^{\infty} du\ u^{5/2}\sqrt{1+\frac{B^2}{u^3}}\sqrt{1+f(u)(a_1'^A)^2-(a_0'^V)^2+f(u)u^3x_4'^2}, \tag{2.3}$$

$$S_{CS} = -\frac{3}{2}\mathcal{N}\int_{u_c}^{\infty} du\ (\partial_2 a_3^V a_0^V a_1^{A\prime} - \partial_2 a_3^V a_0^{V\prime} a_1^A), \tag{2.4}$$

where $\mathcal{N} = N_c R_{D4}^2/(6\pi^2(2\pi\alpha')^3)$ defines the brane tension. The factor 3/2 in the Chern-Simons action comes from addition of surface term in order to maintain the gauge invariance of the total action in the situation when the gauge transformation does not vanish at the boundary (see ref. [9] for details). The integration limit u_c is the position of the tip of the D8-branes where it connects with the $\overline{\text{D8}}$.

Consequently, the equations of motion with respect to each gauge field a_0^V, a_1^A are

$$\frac{\sqrt{u^5+B^2u^2}\ f(u)a_1'^A}{\sqrt{1+f(u)(a_1'^A)^2-(a_0'^V)^2+f(u)u^3x_4'^2}} = j_A - \frac{3}{2}B\mu + 3Ba_0^V, \tag{2.5}$$

$$\frac{\sqrt{u^5+B^2u^2}\ a_0'^V}{\sqrt{1+f(u)(a_1'^A)^2-(a_0'^V)^2+f(u)u^3x_4'^2}} = d - \frac{3}{2}Ba_1^A(\infty) + 3Ba_1^A. \tag{2.6}$$

The corresponding density and current density, d, j_A, at the boundary($u\to\infty$) are defined as

$$j^\mu(x, u\to\infty) \equiv \left.\frac{\delta S_{eom}}{\delta A_\mu}\right|_{u\to\infty} \tag{2.7}$$

$$\equiv (d, \vec{j_A}). \tag{2.8}$$

They are related to the components of the U(1) gauge field by

$$d = \left.\frac{\sqrt{u^5+B^2u^2}\ a_0'^V}{\sqrt{1+f(u)(a_1'^A)^2-(a_0'^V)^2+f(u)u^3x_4'^2}}\right|_\infty - \frac{3}{2}Ba_1^A(\infty), \tag{2.9}$$

$$j_A = \left.\frac{\sqrt{u^5+B^2u^2}\ f(u)a_1'^A}{\sqrt{1+f(u)(a_1'^A)^2-(a_0'^V)^2+f(u)u^3x_4'^2}}\right|_\infty - \frac{3}{2}B\mu. \tag{2.10}$$

For the phase of pure pion gradient where chiral symmetry is broken, the axial current j_A is set to zero and the density $d = \frac{3}{2}B\bigtriangledown\varphi$ is the definition adapted from the Wess-Zumino-Witten action of the boundary gauge theory [7].

The constant of motion with respect to $x_4(u)$ for the pure pion gradient phase yields

$$(x_4'(u))^2 = \frac{1}{u^3 f(u)}\left[\frac{u^3\left[f(u)(C(u)+D(u)^2) - 9B^2\left(a_0^V-\frac{\mu}{2}\right)^2\right]}{F^2} - 1\right]^{-1}, \tag{2.11}$$

where

$$F = \frac{u_c^3\sqrt{f(u_c)}\sqrt{f(u_c)(C(u_c)+D(u_c)^2) - 9B^2\left(a_0^V(u_c)-\frac{\mu}{2}\right)^2}\; x_4'(u_c)}{\sqrt{1+f(u_c)u_c^3\; x_4'^2(u_c)}} \tag{2.12}$$

$$= u_c^{3/2}\sqrt{f(u_c)C(u_c) - 9B^2\left(a_0^V(u_c)-\frac{\mu}{2}\right)^2}, \tag{2.13}$$

with $C(u) \equiv u^5 + B^2u^2, D(u) \equiv d - 3B\bigtriangledown\varphi/2 + 3Ba_1^A(u)$. u_c is the position where the D8 and $\overline{\text{D8}}$ branes connect. Since there is no instanton in this case, the branes connect smoothly at u_c. We also have $D(u_c) = 0$ from $a_1^A(u_c) = 0$, and $x_4'(u_c) = \infty$.

Since the DBI action, eq. (2.3), is divergent from the limit $u \to \infty$, we would need the action of the magnetized vacuum for the regularization. For the magnetized vacuum, we can let the non-normalizable modes, $a_0^V, a_1^A = 0$ and $d, j_A = 0$. The vacuum action then takes the following form

$$S[\text{magnetized vacuum}] = \int_{u_0}^{\infty} \sqrt{C(u)(1+f(u)u^3x_4'^2)}\Big|_{vac} du,$$

where

$$x_4'(u)|_{vac} = \frac{1}{\sqrt{f(u)u^3\left(\frac{f(u)u^3C(u)}{f(u_0)u_0^3C(u_0)}-1\right)}}. \tag{2.14}$$

Again, the position of the tip of the brane configuration is denoted by u_0. The temperature and field dependence of the position u_0 are given in figure 1 of ref. [14]. It saturates approximately at 1.23 for all temperatures at high magnetic field. The action of the vacuum will be used to regulate the infinity of the DBI action from the limit $u \to \infty$ when we calculate the free energy of the dual gauge matter in the subsequent section.

2.1 Zero temperature approximation $f(u) \simeq 1$

We can numerically solve the equations of motion, eq. (2.5), (2.6) by using the shooting algorithm. However, it is illustrative to consider first the limiting case of zero temperature approximation where $f(u) \simeq 1$ and the equations of motion are sufficiently simplified that they yield exact analytic solutions. Later on we will actually find from the numerical solutions that most physical properties of the pion gradient phase are insensitive to the change of temperature. Interestingly, the bulk theory becomes dual to the Nambu-Jona-Lasinio (NJL) type model in the zero-temperature limit [15].

Starting from the equations of motion, eq. (2.5), (2.6), can be rewritten as

$$a_0'^V(a_0^V - \frac{\mu}{2}) = f(u)a_1^A a_1'^A \tag{2.15}$$

$$f(u)a_0'^V a_1'^A = \frac{9B^2a_1^A(a_0^V-\frac{\mu}{2})}{u^5+B^2u^2}(1+fu^3x_4'^2 + fa_1'^{A2} - a_0'^{V2}). \tag{2.16}$$

From eq. (2.15), for $f = 1$ we can solve to obtain

$$\left(a_0^V - \frac{\mu}{2}\right)^2 - \left(\frac{\mu}{2}\right)^2 = a_1^{A2} - (\bigtriangledown\varphi)^2. \tag{2.17}$$

JHEP08(2011)026

Using eq. (2.16), direct integration leads to

$$a_0^V = \frac{\mu}{2} + \sqrt{\left(\frac{\mu}{2}\right)^2 - (\bigtriangledown\varphi)^2}\ \cosh I(u) \tag{2.18}$$

$$a_1^A = \sqrt{\left(\frac{\mu}{2}\right)^2 - (\bigtriangledown\varphi)^2}\ \sinh I(u), \tag{2.19}$$

where

$$I(u) \equiv \int_{u_c}^{u} du \sqrt{g(u,u_c,B)\left[\frac{C(u)}{9B^2} - \left(\left(\frac{\mu}{2}\right)^2 - (\bigtriangledown\varphi)^2\right)\right]^{-1}}, \tag{2.20}$$

$$g(u,u_c,B) \equiv 1 + u^3 x_4'^2 \tag{2.21}$$

$$= 1 + \left[\frac{u^3(C(u) - 9B^2((\frac{\mu}{2})^2 - (\bigtriangledown\varphi)^2))}{u_c^3(C(u_c) - 9B^2((\frac{\mu}{2})^2 - (\bigtriangledown\varphi)^2))} - 1\right]^{-1}, \tag{2.22}$$

by using the boundary conditions $a_1^A(u_c) = 0$ and eq. (2.17) at u_c. Additionally, there are two constraints which need to be satisfied,

$$\cosh I_\infty = \frac{\mu}{2}\frac{1}{\sqrt{(\frac{\mu}{2})^2 - (\bigtriangledown\varphi)^2}}, \tag{2.23}$$

$$L_0 = 1 = 2\int_{u_c}^{\infty} du\ x_4'(u), \tag{2.24}$$

where $I_\infty \equiv I(u \to \infty)$. In the zero temperature case x_4' is given by

$$x_4'(u) = \left[u^3\left(\frac{u^3(C(u) - 9B^2((\frac{\mu}{2})^2 - (\bigtriangledown\varphi)^2))}{u_c^3(C(u_c) - 9B^2((\frac{\mu}{2})^2 - (\bigtriangledown\varphi)^2))} - 1\right)\right]^{-1/2}. \tag{2.25}$$

The pion gradient is thus

$$\bigtriangledown\varphi = \frac{\mu}{2}\tanh I_\infty. \tag{2.26}$$

In order to obtain the solutions, we numerically solve for u_c from the constraints eq. (2.23) and eq. (2.24) simultaneously by fixing two parameters among $(B, d, \bigtriangledown\varphi, \mu)$. The solutions always have $\frac{\mu}{2} > \bigtriangledown\varphi$ as a reality condition.

As is found in ref. [10] for the pure pion gradient and ref. [11, 16] for the model with instantons, there are 2 possible brane configurations satisfying the scale fixing condition $L_0 = 1$, one with small and one with large u_c. The brane configuration with small u_c has longer stretch in the u-direction and therefore has higher energy than the configuration with large u_c. The excess energy makes this configuration less preferred thermodynamically. For the pure pion gradient phase, there is also the small-u_c configuration (for sufficiently large μ and small B) which we found to be less preferred thermodynamically even than the vacuum. Therefore this configuration will not be considered in this article.

The solutions can be explored by slicing through the plane in the parameter space at fixed magnetic field (B), fixed density (d), and fixed chemical potential (μ) respectively. At fixed B, the solutions are shown in figure 1 for the position u_c and the chemical potential

JHEP08(2011)026

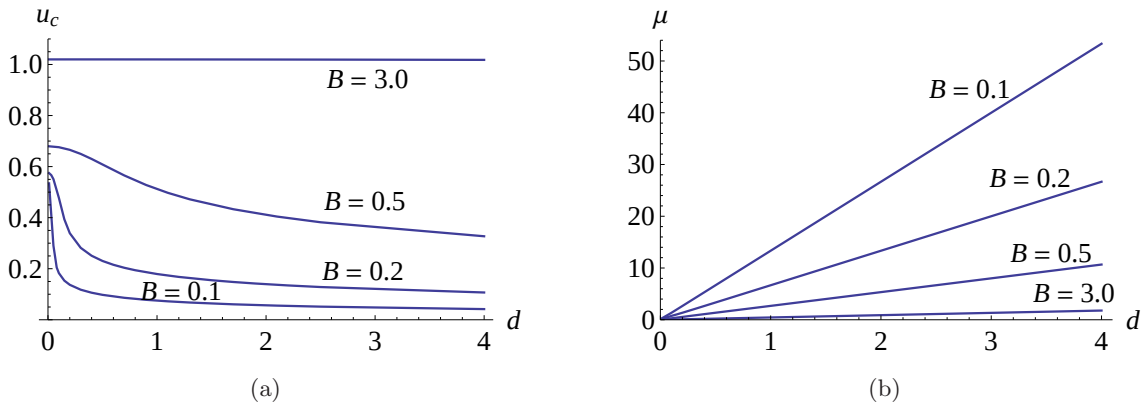

Figure 1. The position u_c (a) and the chemical potential (b) as a function of the density at fixed magnetic field B in the zero temperature limit.

as a function of the density. For small B, the position u_c has certain variation with respect to the density. As B increases, u_c saturates to an almost constant curve with a slight density dependence. The chemical potential at fixed $B(\geq 0.1)$ is found to be an exact linear function of the density. The slope of the linear function is inversely proportional to B. The relation can be summarized into the following simple form

$$\mu = \frac{4}{3}\frac{d}{B} \qquad \text{for } B \geq 0.1. \tag{2.27}$$

This implies from $d = 3B\bigtriangledown\varphi/2$ that $\mu = 2\bigtriangledown\varphi$ for $B \geq 0.1$. The linear relation between μ and d can be interpreted as the absence of self-interaction among the pion gradient excitations. Each pion gradient excitation seems to behave as free entity for $B \geq 0.1$. For small $B < 0.1$, we also find the linear relation between μ and d. It will be shown subsequently that $\mu \sim d/B^2$ for small B in the analysis at fixed μ.

For fixed d, the position u_c and the chemical potential are shown as functions of B in figure 2, 3 for $d = 1.0$. Solutions exist for the entire range of B, down to $u_c(B = 0) = 0$. The chemical potential μ is found to be inversely proportional to B as is shown in figure 3. This is consistent with eq. (2.27).

For fixed μ, figure 4 shows interesting transition between 2 regions of the parameter space. In figure 5, the relation between d and B is shown to be approximately quadratic for $B \leq 0.2$ and linear for $B \gtrsim 0.2$. From $d = 3B\bigtriangledown\varphi/2$, this implies that $\bigtriangledown\varphi$ is a linear function of B for $B \leq 0.2$ and a constant function for $B \gtrsim 0.2$. Figure 4(b) confirms the behaviour. Since the saturation at large B occurs around $\bigtriangledown\varphi = \mu/2$, the slope of the linear region, $B \leq 0.2$, is therefore proportional to μ. Consequently, for small B, $\bigtriangledown\varphi \sim \mu B$. The behaviour at small B is similar to the behaviour found in ref. [7, 9] for the confined phase. The result in the deconfined phase of the SS model in the zero temperature limit was first obtained in ref. [10].

It should be noted that the nonlinear effects of the DBI action become apparent for $B \gtrsim 0.2$ where $\bigtriangledown\varphi \simeq \mu/2$. From eq. (2.20), (2.26) since $I_\infty \to \infty$ as $B \to \infty$, the saturation always occurs at $\bigtriangledown\varphi \simeq \mu/2$ for any μ. As B increases, the pion gradient does not change

JHEP08(2011)026

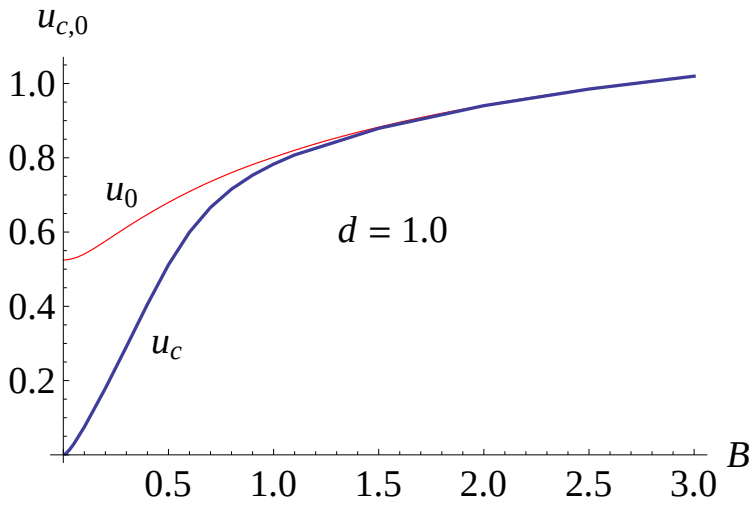

Figure 2. Position u_c as a function of B at a fixed density $d = 1.0$ in the zero temperature limit, the position u_0 of the magnetized vacuum is shown for comparison.

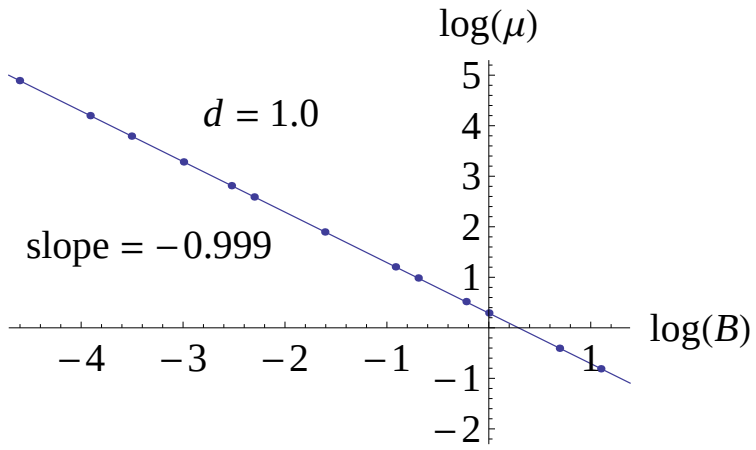

Figure 3. Chemical potential as a function of B at $d = 1.0, T = 0$ in the logarithmic scale.

but its baryonic density increases linearly with the field. This $\bigtriangledown\varphi$-saturation is a new effect observed only in the theory with DBI gauge interaction.

3 Thermodynamical properties of the pure pion gradient phase

In the pure pion gradient phase, since $x_4' \to \infty$ at u_c, the integrand of the action diverges at u_c in addition to the limit $u \to \infty$. This also occurs with the magnetized vacuum where x_4' is divergent at u_0. However, the limit which makes the integral and consequently the action divergent comes only from $u \to \infty$ (the divergences at $u_{0,c}$ are weaker than a simple pole and thus finite over integration). We can therefore regulate the action by subtracting the total action with the action of the magnetized vacuum in the usual manner.

JHEP08(2011)026

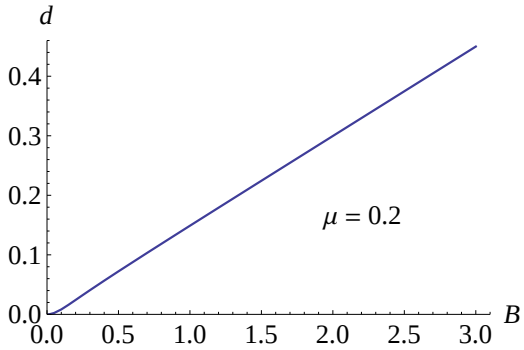

(a)

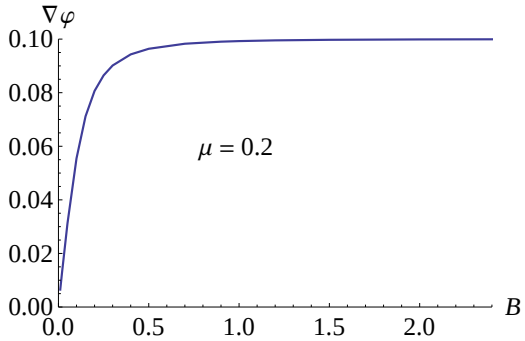

(b)

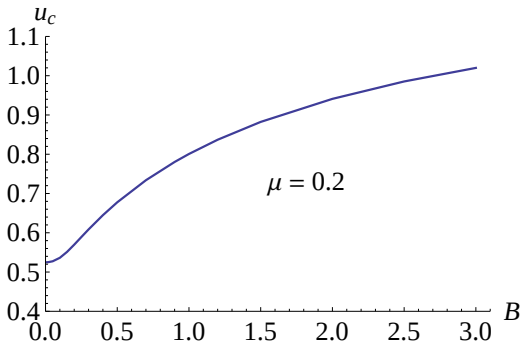

(c)

Figure 4. The density (a), the pion gradient (b), and the position u_c (c) as a function of B at fixed $\mu = 0.2, T = 0$.

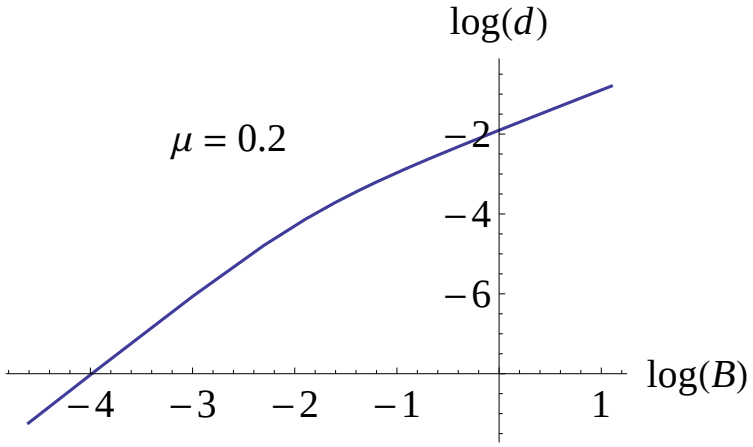

Figure 5. The density as a function of B at $\mu = 0.2, T = 0$ in the logarithmic scale.

Generically, the free energy can be defined at fixed density (in the canonical ensemble) or fixed chemical potential (in the grand canonical ensemble), they are related by the Legendre transform. In the holographic model, the free energy of the dual gauge matter at a fixed chemical potential is proportional to action of the D8-branes. Therefore, the

JHEP08(2011)026

regulated free energy in the canonical ensemble (Helmholtz free energy) is given by

$$\mathcal{F}_E(d,B) = \Omega(\mu,B) + \mu d, \tag{3.1}$$

where $\Omega(\mu,B) = S[a_0(u),a_1(u)](e.o.m.) - S[\text{magnetized vacuum}] \equiv \mathcal{F}(\mu,B)$, the free energy in the grand canonical ensemble (also known as the grand potential or Landau free energy).

We can calculate the total action satisfying the equation of motion $S[a_0(u),a_1(u)](e.o.m.) = S_{D8} + S_{CS}$ to be

$$S_{D8} = \mathcal{N}\int_{u_c}^{\infty} du\; C(u)\sqrt{\frac{f(u)(1+f(u)u^3x_4'^2)}{f(u)(C(u)+D(u)^2) - 9B^2\left(a_0^V - \frac{\mu}{2}\right)^2}}, \tag{3.2}$$

$$S_{CS} = -\mathcal{N}\frac{3}{2}B\int_{u_c}^{\infty} du\; \frac{\left(3Ba_0^V(a_0^V - \frac{\mu}{2}) - f(u)D(u)a_1^A\right)\sqrt{\frac{1}{f(u)} + u^3x_4'^2}}{\sqrt{f(u)(C(u)+D(u)^2) - 9B^2\left(a_0^V - \frac{\mu}{2}\right)^2}}. \tag{3.3}$$

For zero temperature the total action reduces to

$$S_{e.o.m.} = \mathcal{N}\int_{u_c}^{\infty} du\sqrt{\frac{g(u,u_c,B)}{C(u) - 9B^2((\frac{\mu}{2})^2 - (\bigtriangledown\varphi)^2)}}\left(C(u) - \frac{9B^2}{2}\left(\frac{\mu}{2}a_0^V(u) - (\bigtriangledown\varphi)^2\right)\right).$$

We can compute this action by substituting eq. (2.18) into the expression. The free energy at fixed chemical potential $\mathcal{F}(\mu,B)$ of the pure pion gradient phase at zero temperature is shown in figure 6. Once $d,\mu > 0$, the free energy becomes smaller than the free energy of the magnetized vacuum (being negative) and thus thermodynamically preferred than the vacuum phase. The magnetization at fixed chemical potential $\mathcal{M}(\mu,B) = -\frac{\partial\mathcal{F}(\mu,B)}{\partial B}$ therefore increases from zero and becomes constant $M(\mu = 0.2,B) \simeq 0.0152$ at large field ($B > 0.2$) as we can see from the slope of figure 6. On the other hand, the magnetization at fixed $d = 1.0$, $M(d,B) = -\frac{\partial\mathcal{F}_E(d,B)}{\partial B}$, of the pure pion gradient phase is a rapidly decreasing function of B as is shown in figure 7.

The pressure of the pure pion gradient as a function of the density can be calculated using eq. (2.27) and $d = \frac{\partial P}{\partial\mu}$ (see ref. [17]),

$$P(d,B) = \mu(d,B)d - \int_0^d \mu(d',B)\; d(d'), \tag{3.4}$$

$$= \frac{1}{2}k(B)d^2, \tag{3.5}$$

where $k(B) = 4/3B$ for $B \geq 0.1$. The quadratic dependence of the pressure on the density without higher order term reveals that the pion gradient excitations behave like free particles without either repulsive or attractive interaction among themselves.

For the parameter space in the region $d \ll 1, B \ll 1$ such as the regions shown in figure 4, 5, since $\bigtriangledown\varphi \sim \mu B, d = 3B\bigtriangledown\varphi/2$, we have $d = \alpha\mu B^2$ for some constant α. In this case, the linear relations between μ and d is still valid and the equation of state is again given by eq. (3.5) with $k(B) = 1/\alpha B^2$ (for $\mu = 0.2, \alpha \simeq 4.634$). This behaviour is similar

JHEP08(2011)026

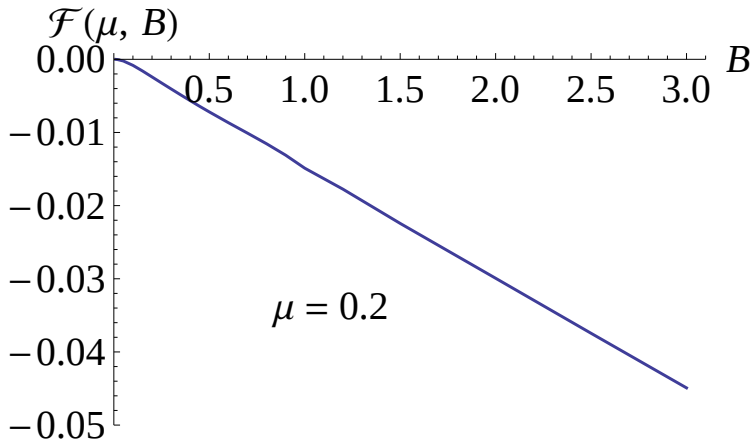

Figure 6. The Landau free energy as a function of B at fixed $\mu = 0.2, T = 0$.

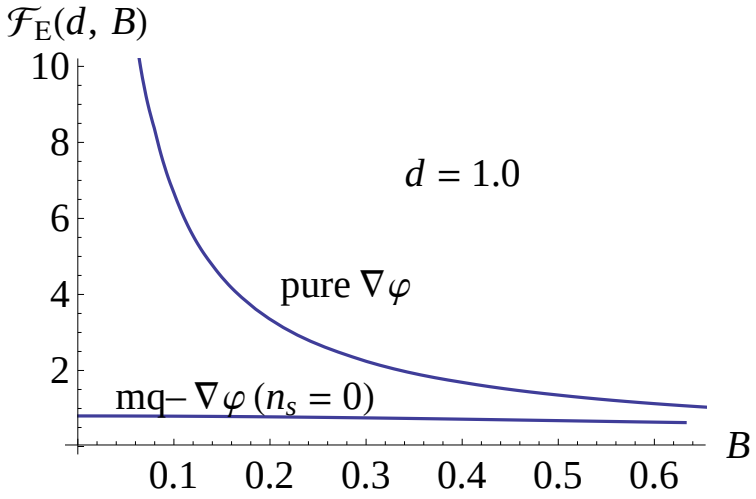

Figure 7. The Helmholtz free energy as a function of the density of the pure pion gradient phase compared with the multiquark-$\bigtriangledown\varphi$ phase at fixed $d = 1.0, T = 0$. The number of colour strings n_s represents the colour charges of the multiquark in unit of $1/N_c$. Baryon corresponds to multiquark with $n_s = 0$.

to what found in ref. [7] using the Wess-Zumino-Witten term in the boundary theory and in ref. [9, 10] for the confined and deconfined SS model at zero temperature.

The energy density can be calculated straightforwardly

$$\rho = \int_0^d \mu(\eta, B)\, d\eta, \tag{3.6}$$

$$= \frac{1}{2} k(B) d^2, \tag{3.7}$$

where $k(B) = 1/\alpha B^2, 4/3B$ for small and large B respectively. The results are remarkably similar to the results from the bottom-up AdS/QCD model considered in ref. [8]. The equation of state then becomes simply $P = \rho$ representing free gas of the solitonic excita-

JHEP08(2011)026

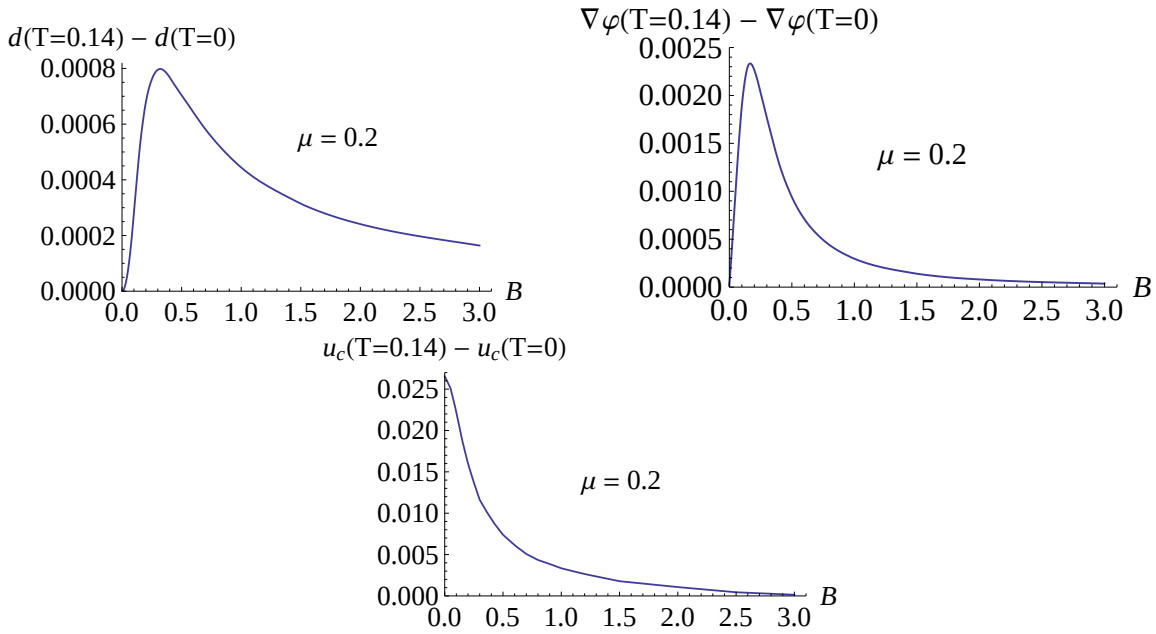

Figure 8. The difference between the density, the pion gradient, and the position u_c of the $\bigtriangledown\varphi$ phase at $T = 0.14$ and $T = 0$ as a function of B for $\mu = 0.2$.

tions of the the pion gradient. The adiabatic index, Γ, and the sound speed, c_s, are then calculated to be

$$\Gamma \equiv \frac{\rho}{P}\frac{\partial P}{\partial \rho} = \frac{\rho}{P}c_s^2 = 1, \tag{3.8}$$

$$c_s = 1, \tag{3.9}$$

the typical behaviour of the free gas.

For nonzero temperature, the full equations of motion, eq. (2.5), (2.6) can be solved numerically by double shooting algorithm aiming for two conditions to be satisfied at once: $a_1^A(u_c) = 0, L_0 = 1$ (with x_4' from eq. (2.11)) while fixing B, μ and d (and consequently $\bigtriangledown\varphi$). The boundary conditions, $a_0^V(\infty) = \mu, a_1^A(\infty) = \bigtriangledown\varphi$, are adjusted until we hit the target conditions. It is found that the temperature dependence of every physical quantity of the pure pion gradient is very weak. Figure 8 shows the *difference* of the density, the pion gradient, and the position u_c at fixed $\mu = 0.2$ between $T = 0.14$ and $T = 0$. Observe that the difference in the temperature dependence of the density and the pion gradient are the most distinctive in the transition region when the magnetic field changes from small to large values.

3.1 Comparison to the multiquark-$\bigtriangledown\varphi$ phase

We would like to consider whether the pure pion gradient phase is thermodynamically preferred than the other nuclear phases in certain regions of the parameter space. In the deconfined SS model in the presence of the magnetic field, there are generically 3 possible phases in addition to the vacuum; the chiral symmetric QGP phase, the chirally

JHEP08(2011)026

broken phase of multiquark-$\bigtriangledown\varphi$ (MQ-$\bigtriangledown\varphi$), and the pure pion gradient ($\bigtriangledown\varphi$) phase. The multiquark nuclear phase has been studied in ref. [11, 14, 18] and found to be the most preferred phase for the dense deconfined nuclear matter under moderate external magnetic fields. The multiquark phase actually has certain mixture of the pion gradient as the source for the baryon density. This is inevitable since the response of the nuclear matter to the external magnetic field is in the form of the spatial variation of the chiral condensate in the direction of the applied field which we call the pion gradient.

However, the ratio of the pion gradient population with respect to the multiquark decreases as d grows [14]. It is thus suggestive that the multiquark phase is likely to be more thermodynamically preferred than the pion gradient phase. In this subsection we directly compare the two phases at zero temperature using the free energy at fixed density $d = 1.0$. The MQ-$\bigtriangledown\varphi$ phase imposes the boundary conditions (see ref. [11, 14] for details);

$$j_A = 0,\ a_1^A(u_c) = 0,\ a_0^V(u_c) = \frac{1}{3}u_c\sqrt{f(u_c)} + n_s(u_c - u_T),$$

where n_s is the number of colour strings (hanging from the baryon vertex down to the horizon) in fractions of $1/N_c$.

The result is shown in figure 7. Clearly, the multiquark-pion gradient (MQ-$\bigtriangledown\varphi$) phase is more preferred than the pure pion gradient phase. Similar behaviours are confirmed for small $d \simeq 0.1$ and large $d \gg 1$. Especially at large densities, since the baryon chemical potential of the MQ-$\bigtriangledown\varphi$ phase increases slower than a linear function [11] whilst it is linear for the $\bigtriangledown\varphi$ phase, the dominant term μd in the free energy for the MQ-$\bigtriangledown\varphi$ phase becomes much smaller and thus more stable thermodynamically.

However, there is a region of parameter space where the $\bigtriangledown\varphi$ phase is dominant. When the baryon chemical potential $\mu < \mu_{\rm onset} \equiv \mu(d = 0) = \frac{1}{3}u_0\sqrt{f(u_0)} + n_s(u_0 - u_T)$ of the multiquark, the multiquarks cease to exist and the pion gradient which can be constructed at arbitrarily small μ (since $\mu \sim d$) will be dominating. The corresponding transition line in the (μ, T) diagram for $B = 0$ is shown in figure 8 of ref. [18]. For $B > 0$, dependence of u_0 on B affects the transition line accordingly as shown in figure 9. The dotted line represents schematic transition to the chiral symmetric quark-gluon plasma (χS-QGP) phase. The chiral symmetry restoration between the magnetized vacuum and the χS-QGP has been studied in ref. [19]. The transition between the pure pion gradient phase and the χS-QGP has been explored in ref. [10] with $f = 1$ approximation for the pure pion gradient. Since we found that the $\bigtriangledown\varphi$ phase is insensitive to the change of temperature, the results in ref. [10] should be justified to be a good approximated phase diagram. The chiral symmetry restoration between the MQ-$\bigtriangledown\varphi$ phase and the χS-QGP phase has been investigated in ref. [14].

4 Conclusions and discussions

The behaviour of the chirally broken pure pion gradient phase in the deconfined SS model is studied in the zero temperature limit and subsequently at finite temperature. The magnetic response of the chirally broken phase is linear $\bigtriangledown\varphi \sim \mu B$ for small field and saturates to constant value $\bigtriangledown\varphi \sim \mu/2$ for large field.

JHEP08(2011)026

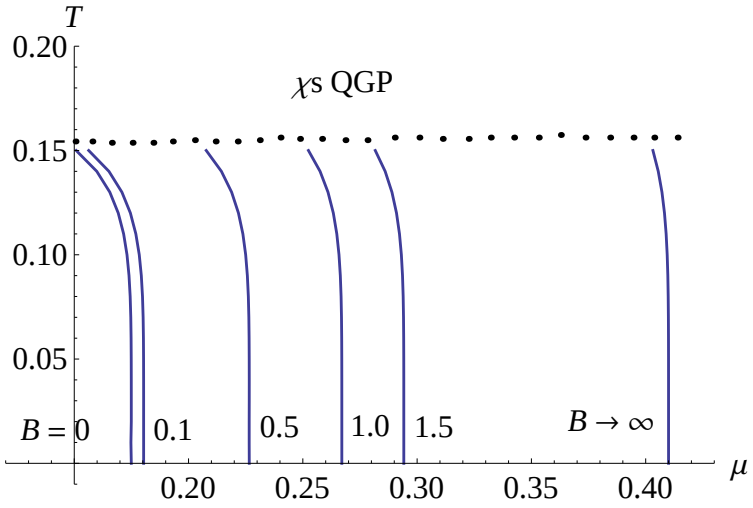

Figure 9. The onset chemical potential of the multiquark-$\bigtriangledown\varphi$ phase as a function of T, B (for $B \to \infty, u_0 = 1.23$ is used). These lines can be served as the transition lines between the $\bigtriangledown\varphi$ phase on the left and multiquark-$\bigtriangledown\varphi$ phase ($n_s = 0$) on the right. The dotted line represents schematic transition to the chiral symmetric QGP phase.

Relationship between μ and d is also linear $\mu = k(B)d$ where $k(B) \sim 1/B^2, 1/B$ for small and large B respectively. This implies that the excitations of the pion gradient behave like a free gas with no interaction among each other. The equation of state is thus simply $P = \rho$ with the sound speed equal to the speed of light. The free energies at fixed μ and d are obtained numerically. Magnetization at fixed μ increases with B for small field and drops to constant value for large field. Magnetization at fixed d is a decreasing function with respect to the magnetic field.

Using the free energy at fixed density, we show that the pure $\bigtriangledown\varphi$ phase is less preferred thermodynamically than the MQ-$\bigtriangledown\varphi$ phase at zero temperature. The configuration of the pure pion gradient phase is found to be insensitive to the change of temperature, the difference of the free energy at fixed μ for $T = 0$ and $T = 0.14$ is minimal, only about $\lesssim 2 \times 10^{-4}$. On the other hand, the free energy of the MQ-$\bigtriangledown\varphi$ phase is a decreasing function in the temperature [14]. Therefore, we can conclude that the pure pion gradient phase is generically less preferred than the MQ-$\bigtriangledown\varphi$ for general situation.

However, there is an exception for small chemical potential, $\mu \simeq 0.175 - 0.41$. When $\mu < \mu_{\rm onset}$ of the multiquarks, the multiquarks simply cannot exist while the pion gradient can be induced at arbitrarily small μ. Therefore, in this region of the parameter space, the pure pion gradient phase is dominating over any other phases. The transition lines are given by $\mu = \mu_{\rm onset}$ in the (μ, T) plane. The interior of certain classes of the dense astrophysical objects such as the magnetars [20] would have the corresponding regions where the chemical potential (and the density) and temperature fall into this range. In those regions, the dominating nuclear phase which governs physics of the stars would be the pure pion gradient.

Finally, the conversion factors to the corresponding physical quantities in the natural unit ($\hbar = c = 1$) are the following (see e.g. ref. [9], we have set $R_{D4} = 1$ in this article):

JHEP08(2011)026

$1/2\pi\alpha'$ for B, $R_{D4}/2\pi\alpha'$ for μ, $2\pi\alpha'\mathcal{N}/R_{D4}$ for d, and $R_{D4}^2 f_\pi/2\pi\alpha'$ for $\bigtriangledown\varphi$ where f_π is the pion decay constant. For the magnetic field, the conversion factor $1/2\pi\alpha'$ with $\alpha'^{-1} = 0.2\,\mathrm{GeV}^2$ corresponds to approximately 5.37×10^{14} Tesla in the SI unit.

Acknowledgments

P.B. would like to thank CERN Theoretical Physics Division for the warm hospitality during my visit where this work is completed. P.B. is supported in part by the Thailand Research Fund (TRF) and Commission on Higher Education (CHE) under grant RMU5380048, the Toray Science Foundation, Japan (TSF) and Thailand Center of Excellence in Physics (ThEP). P.B. and T.C. are supported in part by the 90th Year Chulalongkorn Scholarship.

References

[1] J.M. Maldacena, *The large-N limit of superconformal field theories and supergravity*, *Int. J. Theor. Phys.* **38** (1999) 1113 [*Adv. Theor. Math. Phys.* **2** (1998) 231] [hep-th/9711200] [SPIRES].

[2] E. Witten, *Anti-de Sitter space and holography*, *Adv. Theor. Math. Phys.* **2** (1998) 253 [hep-th/9802150] [SPIRES].

[3] O. Aharony, S.S. Gubser, J.M. Maldacena, H. Ooguri and Y. Oz, *Large-N field theories, string theory and gravity*, *Phys. Rept.* **323** (2000) 183 [hep-th/9905111] [SPIRES].

[4] T. Sakai and S. Sugimoto, *Low energy hadron physics in holographic QCD*, *Prog. Theor. Phys.* **113** (2005) 843 [hep-th/0412141] [SPIRES].

[5] T. Sakai and S. Sugimoto, *More on a holographic dual of QCD*, *Prog. Theor. Phys.* **114** (2005) 1083 [hep-th/0507073] [SPIRES].

[6] O. Aharony, J. Sonnenschein and S. Yankielowicz, *A holographic model of deconfinement and chiral symmetry restoration*, *Annals Phys.* **322** (2007) 1420 [hep-th/0604161] [SPIRES].

[7] D.T. Son and M.A. Stephanov, *Axial anomaly and magnetism of nuclear and quark matter*, *Phys. Rev.* **D 77** (2008) 014021 [arXiv:0710.1084] [SPIRES].

[8] E.G. Thompson and D.T. Son, *Magnetized baryonic matter in holographic QCD*, *Phys. Rev.* **D 78** (2008) 066007 [arXiv:0806.0367] [SPIRES].

[9] O. Bergman, G. Lifschytz and M. Lippert, *Magnetic properties of dense holographic QCD*, *Phys. Rev.* **D 79** (2009) 105024 [arXiv:0806.0366] [SPIRES].

[10] F. Preis, A. Rebhan and A. Schmitt, *Inverse magnetic catalysis in dense holographic matter*, *JHEP* **03** (2011) 033 [arXiv:1012.4785] [SPIRES].

[11] P. Burikham, *Magnetic properties of holographic multiquarks in the quark-gluon plasma*, *JHEP* **04** (2010) 045 [arXiv:0909.0614] [SPIRES].

JHEP08(2011)026

[12] E. Witten, *Anti-de Sitter space, thermal phase transition and confinement in gauge theories*, *Adv. Theor. Math. Phys.* **2** (1998) 505 [hep-th/9803131] [SPIRES].

[13] K.-Y. Kim, S.-J. Sin and I. Zahed, *Dense hadronic matter in holographic QCD*, hep-th/0608046 [SPIRES].

[14] P. Burikham, *Magnetic Phase Diagram of Dense Holographic Multiquarks in the quark-gluon Plasma*, *JHEP* **05** (2011) 121 [arXiv:1103.4379] [SPIRES].

[15] E. Antonyan, J.A. Harvey, S. Jensen and D. Kutasov, *NJL and QCD from string theory*, hep-th/0604017 [SPIRES].

[16] O. Bergman, G. Lifschytz and M. Lippert, *Holographic Nuclear Physics*, *JHEP* **11** (2007) 056 [arXiv:0708.0326] [SPIRES].

[17] P. Burikham, E. Hirunsirisawat and S. Pinkanjanarod, *Thermodynamic Properties of Holographic Multiquark and the Multiquark Star*, *JHEP* **06** (2010) 040 [arXiv:1003.5470] [SPIRES].

[18] P. Burikham, A. Chatrabhuti and E. Hirunsirisawat, *Exotic Multi-quark States in the Deconfined Phase from Gravity Dual Models*, *JHEP* **05** (2009) 006 [arXiv:0811.0243] [SPIRES].

[19] C.V. Johnson and A. Kundu, *External Fields and Chiral Symmetry Breaking in the Sakai-Sugimoto Model*, *JHEP* **12** (2008) 053 [arXiv:0803.0038] [SPIRES].

[20] R.C. Duncan and C. Thompson, *Formation of very strongly magnetized neutron stars-implications for gamma-ray bursts*, *Astrophys. J.* **392** (1992) L9 [SPIRES].

JHEP08(2011)026